R-10-73

Detailed analysis of selected hydraulic interference tests and review of new test analysis methods

Jan-Erik Ludvigson, Calle Hjerne

Geosigma AB

December 2014

Svensk Kärnbränslehantering AB
Swedish Nuclear Fuel
and Waste Management Co

Box 250, SE-101 24 Stockholm
Phone +46 8 459 84 00

ISSN 1402-3091
SKB R-10-73
ID 1450818

Detailed analysis of selected hydraulic interference tests and review of new test analysis methods

Jan-Erik Ludvigson, Calle Hjerne

Geosigma AB

December 2014

Keywords: Interference tests, Cross-hole tests, Pumping tests, Transmissivity, Storativity, Hydraulic conductivity, Specific storativity, Hydraulic tomography, Heterogeneous rock.

This report concerns a study which was conducted for SKB. The conclusions and viewpoints presented in the report are those of the authors. SKB may draw modified conclusions, based on additional literature sources and/or expert opinions.

A pdf version of this document can be downloaded from www.skb.se.

Preface

The detailed analysis of the selected hydraulic interference tests presented in this report was completed in 2010. This report consists of two parts. In Part A, the detailed analysis of the test results reflecting the hydraulic connectivity of the observation sections to the active borehole together with a review of a new test analysis method (hydraulic tomography) is presented. In Part B, a proposal of suitable data sets from previous interference tests to test the new method is presented. The report was finalised in 2014. However, despite the elapsed time to publication, the report does not reflect work and results beyond 2010. We do not foresee that the results of this investigation affect or in any way alter the conclusions of site assessment activities that supported site selection and/or licensing.

December 2014

Calle Hjerne
Geosigma AB

Abstract

Analysis of hydraulic interference tests in heterogeneous media (e.g. fractured rock) is commonly made using standard methods based on radial flow in equivalent homogeneous porous media. It may be assumed that these methods provide effective mean values of transmissivity and storativity for a large volume of rock bounded by the radius of influence. The accuracy and representativity of estimated hydraulic parameters from standard methods may thus not be sufficient in e.g. detailed contaminant studies in heterogeneous media, e.g. fractured rock with its individual structural constituents.

Therefore, alternative methods which can provide more detailed spatial distributions of the hydraulic parameters are needed for improved analysis of interference tests in heterogeneous media. Part A of this report includes a focussed literature review to reveal the meaning of hydraulic parameters obtained from standard analysis in heterogeneous media and to identify possible new analysis methods for interference tests in such media with the above capabilities. The literature study was mainly limited to papers appearing in the most common scientific journals on hydrogeology, published during the last c. 3–5 years (which in this case corresponds to 2005 to 2010).

Furthermore, in Part A, compilation and synthesis of estimated hydraulic parameter values from four selected large-scale interference tests at the sites Laxemar and Forsmark using standard methods was made. Scatter plots of estimated hydraulic parameters from the interference tests were prepared and analysed. As seen from the scatter plots the estimated transmissivity values of observation sections generally exhibit less variability than the estimated transmissivity from previous single-hole tests in the same sections. However, estimated storativity values (and thus hydraulic diffusivity T/S) from interference tests generally exhibit larger variability than transmissivity. The estimated hydraulic diffusivity is assumed to merely reflect the connectivity between the pumping borehole and the observation sections.

A clear (inverse) correlation was demonstrated between estimated storativity of the observation sections and the connectivity (in terms of pressure response time normalized for distance) of the sections to the pumping borehole. Thus, contrary to transmissivity, estimated (inverse) storativity in heterogeneous media is likely to better represent the connectivity between the observation section and the pumping borehole than the hydraulic properties of the media. As a consequence, a clear (positive) correlation between estimated hydraulic diffusivity and connectivity was also observed. These above conclusions from the diagnostic scatter plots for the selected interference tests at Laxemar and Forsmark are consistent with the findings in the referenced papers in the literature review.

The diagnostic scatter plots of estimated hydraulic parameters also indicated some general differences between the estimated parameter values at the two sites. However, the present data material is too limited to make any firm conclusions of the results. The estimated transmissivities from the two interference tests at Forsmark were generally slightly higher than those from Laxemar, and also showing lower variability. In addition, the deviations between the estimated transmissivity of the observation sections from the interference tests and that established from previous single-hole tests respectively were slightly lower at Forsmark. Slightly lower, apparent storativities and higher apparent hydraulic diffusivities were estimated from Forsmark results.

When comparing the results from the two sites, it should be remembered that the selection and number of observation sections for transient analysis are different. In addition, the hydrogeological conditions differ at the two sites. In particular, the estimated values from Forsmark are likely to be reflected by the superficial high-transmissive sub-horizontal deformation zones at this site. In addition, the inherent hydraulic properties of the actual rock volumes tested during the selected interference tests may be different.

Finally, an alternative, new method (hydraulic tomography) for design and analysis of interference tests in heterogeneous media is proposed and briefly described together with selected case studies. In Part B, a proposal of relevant test data from previous interference tests for hydraulic tomography analysis on different test scales is presented.

Sammanfattning

Analys av hydrauliska interferenstester i heterogena media (t.ex. sprickigt berg) görs vanligen med standardmetoder baserade på radiellt flöde i ekvivalenta homogena media. Det kan antas att dessa metoder ger effektiva medelvärden för transmissivitet och storativitet för en stor bergvolym inom influensradien. Precisionen för skattade hydrauliska parametrar från standardmetoder kan således inte vara tillräcklig vid t ex detaljerade föroreningsundersökningar i heterogena media, exempelvis sprickigt berg.

Därför behövs alternativa metoder som kan ge mer detaljerade rumsliga bestämningar av de hydrauliska parametrarna i heterogena media. Del A av denna rapport inkluderar en fokuserad litteraturstudie för att undersöka betydelsen av hydrauliska parametrar från standardanalys i heterogena media och för att identifiera möjliga nya analysmetoder för analys av interferenstester i sådana media med ovanstående kapacitet. Litteraturstudien var begränsad till publikationer i de mest vanliga vetenskapliga tidskrifter inom hydrogeologi, publicerade under de senaste c:a 3–5 åren.

Vidare gjordes en sammanställning och syntes av skattade hydrauliska parametervärden från fyra utvalda storskaliga interferenstester inom platserna Laxemar och Forsmark. Punktdiagram av skattade hydrauliska parametrar från interferenstesterna togs fram och diskuterades. De skattade transmissivitetsvärdena från observationssektioner uppvisade vanligen mindre spridning än skattade transmissiviteter från tidigare enhålstester i samma observationssektioner. Skattade storativitetsvärden (och därmed även hydraulisk diffusivitet T/S) från interferenstester uppvisar dock vanligen större spridning än transmissiviteten. Den skattade hydrauliska diffusiviteten antas avspegla konnektiviteten mellan pumphålet och observationssektionerna.

En tydlig (omvänd) korrelation konstaterades mellan skattad storativitet för observationssektionerna och sektionernas konnektivitet med pumphålet. Således, i motsats till transmissiviteten, antas skattad (invers) storativitet i heterogena media mer avspegla konnektiviteten mellan observationssektionen och pumphålet än de hydrauliska egenskaperna av media. Följaktligen observerades också en tydlig (positiv) korrelation mellan skattad hydraulisk diffusivitet och konnektivitet. Det föreslås därför att skattad storativitet och hydraulisk diffusivitet från standardanalys i heterogena media benämns *skenbar* storativitet respektive *skenbar* hydraulisk diffusivitet. Ovanstående slutsatser från de diagnostiska punktdiagrammen från de utvalda interferenstesterna i Laxemar och Forsmark överensstämmer med resultaten i de refererade publikationerna i litteraturstudien.

De diagnostiska punktdiagrammen för skattade hydrauliska parametrar indikerade också vissa generella skillnader för de skattade parametervärdena på de två platserna. Föreliggande datamaterial är dock alltför begränsat för att dra några säkra slutsatser om dessa resultat. De skattade transmissiviteterna från de båda interferenstesterna i Forsmark var generellt något högre än för Laxemar och visade också mindre spridning. Vidare var avvikelserna mellan skattad transmissivitet för observationssektionerna från interferenstesterna och tidigare enhålstester något lägre i Forsmark. Något lägre skenbara storativiteter och högre skenbara hydrauliska diffusiviteter skattades också för Forsmark.

Vid jämförelse av resultaten från de två platserna bör det hållas i minnet att urvalet av och antalet observationssektioner för transient analys är olika. Vidare skiljer sig de hydrogeologiska förhållandena åt på de två platserna. De skattade värdena från Forsmark avspeglas troligen av de högtransmissiva sub-horisontella deformationszonerna på denna plats. Vidare kan de specifika hydrauliska egenskaperna för de testade bergvolymerna under de valda interferenstesterna vara olika.

Slutligen föreslås en alternativ ny metod (hydraulisk tomografi) för analys av interferenstester i heterogena media och beskrivs översiktligt tillsammans med utvalda fallstudier. I del B av denna rapport presenteras förslag på lämpliga testdata på olika testskalor för hydraulisk tomografi.

PART A

Detailed analysis of results from selected hydraulic interference tests at Forsmark and Laxemar – review of new test analysis methods applicable to heterogeneous media

Contents

1 Introduction

SKB has carried out a large number of hydraulic interference tests in fractured crystalline rock in several projects including both surface boreholes and boreholes in underground facilities. In most cases, the interference tests have been combined with other measurements, e.g. tracer tests and groundwater flow measurements. It is anticipated that interference tests will also be an important source of information in future SKB projects.

The analysis of the interference tests have generally been made by standard methods for radial flow in equivalent homogeneous media. It is assumed that these methods provide effective mean values of transmissivity and storativity for a large volume of rock within the radius of influence. For example, estimated transmissivity values from observation sections from interference tests generally seem to exhibit much less variability than the estimated transmissivity from preceding single-hole tests in the same borehole sections. Estimated storativity values from interference tests generally seem to exhibit larger variability than transmissivity.

Estimated hydraulic diffusivity values from interference tests are assumed to be strongly correlated to the speed of propagation of the induced pressure disturbance from the pumping borehole. The rate of pressure propagation is reflected by the ratio of the observed time lag of the pressure response in the observation sections and their distance to the pumping borehole. This ratio is (inversely) correlated to the hydraulic diffusivity T/S of the observation sections. Thus, the hydraulic diffusivity is assumed to reflect the connectivity between the pumping borehole and the observation sections.

Estimated hydraulic parameters from standard methods may thus not be sufficient for e.g. detailed contaminant studies in heterogeneous media, e.g. fractured rock. Therefore, alternative methods which can provide more detailed description of spatial distributions of the hydraulic parameters are needed for analysis of interference tests in heterogeneous media. This report (Part A) therefore includes a focussed literature review to reveal the meaning of hydraulic parameters in heterogeneous media as obtained from standard analysis and to identify possible new analysis methods with improved capabilities for application to interference tests in such media. The literature study was limited to papers appearing in the most common scientific journals on hydrogeology, published during the last c. 3–5 years, i.e. in this case in 2005–2010.

Furthermore, in Part A a compilation and detailed analysis of estimated hydraulic parameters from four selected large-scale interference tests performed at the sites Laxemar and Forsmark is made as a basis for further conclusions regarding the results. Diagnostic scatter plots of the estimated hydraulic parameters from the interference tests are prepared, analysed and discussed. The estimated transmissivities were compared with the corresponding transmissivities obtained from previous single-hole tests in the same sections. The results of the scatter plots are discussed and compared with the findings of the literature review. Finally, any notable differences between the interference tests from Laxemar and Forsmark are discussed.

Only the results of the hydraulic (flow and pressure) analysis of the interference tests are presented and discussed in this report, i.e. not associated tracer tests and groundwater dilution measurements during the tests.

2 Implications of standard well test analysis applied to heterogeneous formations

2.1 Background

Several field studies have shown that standard analysis of hydraulic interference tests in heterogeneous media often result in rather constant ("effective") transmissivity values as estimated from observation boreholes. However, estimated storativity values generally show much more variability. A relevant question is therefore what the estimated values of the hydraulic parameters from standard well test analysis methods actually represent in heterogeneous formations.

The main results of a focussed literature study regarding the meaning of estimated hydraulic parameters (T, S and hydraulic diffusivity T/S) by standard well test methods (e.g. Jacob's method) together with hydraulic connectivity in heterogeneous aquifers and new analysis methods are summarized below. A new method (hydraulic tomography) for analysis of interference tests in heterogeneous media, as proposed in recent papers, is reviewed. Hydraulic tomography is an analysis method, but the method is dependent on data sampling in a specific way and certain quality to be useful.

The review of new methods is mainly based on studies documented in selected, recent papers of well testing published in common hydrogeology scientific journals during the last c. 5 years, i.e. in this case in 2005–2010. Results of a new method as presented in several papers are mainly based on simulated interference tests in synthetic, heterogeneous aquifers. Only a few studies are based on results from in situ field hydraulic interference tests in formations showing natural heterogeneity, e.g. crystalline rock.

As a background of the review of test analysis methods in heterogeneous media, Butler and Liu (1993) derived an analytical solution for pumping tests in a uniform aquifer including a disc-shaped feature with deviating T and S-values. They found that the drawdown was sensitive to the hydraulic properties of such a feature, but only for a limited duration of the test. They concluded that constant rate pumping tests are not sufficient to characterize the hydraulic properties of such non-uniformities. They proposed tests with a stepwise variable flow rate. However, although such tests are more sensitive to non-uniformities in the aquifer, they are probably not sufficient to characterize the hydraulic properties in real heterogeneous aquifers exhibiting large variability.

Oliver (1993) found that a small-scale feature with deviating T and S near the pumping well may influence the late-time drawdown at distant observation wells, depending on the location of the non-uniformity. He concluded that the analysis of the drawdown curve may be difficult since the effect of a small-scale feature close to the pumping well on the drawdown curve is similar to the effect of a large-scale non-uniformity at larger distance.

More recently, Meier et al. (1998) simulated pumping tests in synthetic 2D horizontal aquifers with spatially varying transmissivity but constant storativity. Sánchez-Vila et al. (1999) simulated well tests in synthetic heterogeneous aquifers with spatially varying transmissivity but with a constant storativity. Knudby and Carrera (2006) made numerical simulations regarding the possible relationship between connectivity and apparent hydraulic diffusivity in heterogeneous media, see Section 2.3.

Butler (2008) made a review of the results and presents state of the art of the evaluation of hydraulic interference tests in heterogeneous formations and meaning of results from standard well test analysis methods in such media. Wu et al. (2005) made a similar study also including numerical simulations. Yeh and Lee (2007) proposed new procedures s to collect and analyse data from interference tests in heterogeneous media. The meaning and implications of certain hydraulic parameters estimated from standard well test analysis methods for porous media applied to heterogeneous media, based on the more recent references, are summarized below.

2.2 Transmissivity and storativity

In standard analysis of interference tests applied to heterogeneous media, the equivalent porous media transmissivity T_o and storativity S_o of observation sections may be estimated by e.g. Cooper-Jacob's method (see e.g. Kruseman and de Ridder 1990) according to Equation 2-1 and Equation 2-2,

respectively for constant rate tests. Estimations of hydraulic parameters by this method should be made for times before any effects of hydraulic boundaries, leakage etc. have affected the drawdown responses.

$T_o = 2.3 \cdot Q/4\Pi - \Delta s$ (Equation 2-1)

$S_o = 2.25\ T_o\ t_0/r^2$ (Equation 2-2)

Q = pumping flow rate (m^3/s)

Δs = change in drawdown during a logarithmic cycle (m)

t_0 = intersection of semi-log straight line by the time axis (s)

r = radial distance between pumping and observation well (m)

In synthetic heterogeneous media, Meier et al. (1998) found that transmissivity values estimated from observation wells at different distances from the pumping well using Cooper-Jacob's method according to Equation 2-1 were close to the *effective* transmissivity (T_{eff}) of the heterogeneous media for uniform flow conditions. The effective transmissivity was determined from a permeameter-type approach based on the steady-state flow and head gradient through the media. The estimated transmissivity values by Cooper-Jacob's method were virtually independent of the location of the observation wells in the heterogeneous media.

Similarly, Sánchez-Vila et al. (1999) also found that estimated transmissivity values by Cooper-Jacob's method from different observation points tended to converge to the effective transmissivity (T_{eff}) for the heterogeneous media under the assumption of mean uniform flow conditions. This conclusion thus applies to comparisons of individual transmissivity values from the observation sections. They also found that estimated storativity values by Cooper-Jacob's method displayed higher variability than transmissivity and that the geometric mean of the storativity values could be used as an estimator of (("effective") storativity of the heterogeneous aquifer.

Butler (2008) also concluded that the estimated transmissivity from standard analysis methods (e.g. Cooper-Jacob's method) represents a large-scale volumetric average (effective) value in heterogeneous media. The storativity is then estimated by assuming that this large volumetric average value of the effective transmissivity (see Equation 2-3) is also representative of the specific hydraulic properties of the flow paths between the pumping and observation wells (which is not always the case). Thus, local variations in the transmissivity between these wells can lead to errors in the estimated storativity values by standard methods, i.e non-representative values for the specific flow paths between the wells. For example, this could be the case if the transmissivity of these flow paths is much lower (or higher) than the effective transmissivity of the media. On the other hand, the estimated hydraulic diffusivity by standard methods is assumed to primarily be a function of the specific hydraulic conditions (connections) between the pumping and observation wells, see below.

As discussed by Butler (2008) and Knudby and Carrera (2006), several studies have indicated that the storativity estimated by standard methods (e.g. Cooper-Jacob's method) may more represent the *degree of hydraulic connection* between the pumping borehole and the observation borehole (section). The estimated storativity from observation wells located in high-transmissivity zones were found to be lower than those estimated from observation wells located in low-transmissivity zones, i.e. zones of lower connectivity to the pumping borehole. According to Knudby and Carrera (2006), heterogeneity entails that estimated storativity values from Cooper-Jacob's method are different from their actual formation values and should therefore be referred to as *apparent* storativity S_a.

From numerical simulations, Wu et al. (2005) concluded that a heterogeneous aquifer may under certain assumptions be represented by an equivalent, spatially homogeneous medium with uniform, effective parameters of transmissivity and storativity (i.e. an equivalent homogeneous medium aquifer). They also found that both the effective transmissivity and storativity and the principal directions of transmissivity in the heterogeneous aquifer vary with test times. The effective transmissivity approached the geometric mean of the local transmissivity values at large times while the storativity approached the *arithmetic* mean of the local storativity values of the synthetic aquifer at large times.

From the simulated interference tests, Wu et al. (2005) concluded that the estimated transmissivity and storativity at early times changed with time and deviated significantly from the geometric mean

values of the synthetic fields. The estimated storativityvalues stabilized rather rapidly at a certain value dominated by the hydrogeological conditions between the pumping well and observation well. At late times, the estimated T-values approached (but did not coincide with) the *geometric* mean and were, furthermore, influenced by the location, size and degree of heterogeneity as the cone of depression developed over time.

According to Wu et al. (2005), the hydraulic head observed in a well at large test times is, to a certain degree, sensitive to the heterogeneity within the area of influence during a pumping test although it is more sensitive to the local heterogeneity near the pumping and the observation wells respectively. The early portion of the transient hydraulic head evolution at an observation well is highly influenced by the specific storage of a limited rock volume or area between the observation and the pumping well and is only weakly related to the hydraulic conductivity in the same area. In other words, the steady-state or late time head information is dependent of the hydraulic conductivity distribution over the entire area of influence while the transient head information at early times depends on a much smaller area and is also a strong function of specific storage (S_s).

Finally, Wu et al. (2005) concluded that the meaning of estimated transmissivity and storativity by standard well test methods (Theis, Cooper-Jacob etc.) may be difficult to interpret in heterogeneous aquifers. At large times, the estimated transmissivity may be close to (but not coincide with) some mean value of the aquifer properties. On the other hand, the estimated storativity is found to be dominated by the local, average S between the pumping well and the observation well.

In Chapter 4, a further discussion of the correlation between estimated transmissivity and storativity from standard analysis of selected interference tests at Forsmark and Laxemar to other parameters is presented.

2.3 Hydraulic diffusivity and connectivity

The connectivity of high-transmissive flow paths is considered to be important for both flow and transport in heterogeneous media. Knudby and Carrera (2006) found that the estimated hydraulic diffusivity T_o/S_o according to Equation 2-3 from standard analysis of hydraulic tests (e.g. Cooper-Jacob's method) correlated well to both early tracer arrival time and also to the product of a flow connectivity indicator, CF and a transport connectivity indicator, CT in a heterogeneous medium. They suggested denoting the estimated storativity and hydraulic diffusivity from standard analysis to *apparent* storativity S_a and *apparent* hydraulic diffusivity D_a, respectively in heterogeneous media. This indicates that the apparent hydraulic diffusivity accounts for both the average connectivity, related to the effective medium properties, as well as for the detailed connectivity not related to the effective properties of the medium.

According to Knudby and Carrera (2006) the apparent hydraulic diffusivity D_a is calculated according to Equation 2-3 for an equivalent porous medium and the actual heterogeneous medium respectively.

$$D_a = T_o/S_o = T_{eff}/S_a \qquad \text{(Equation 2-3)}$$

T_o = transmissivity from standard analysis for an equivalent homogeneous mediumT_{eff} = effective transmissivity for the heterogeneous medium studied S_o = storativity from standard analysis for an equivalent homogeneous medium S_a = apparent storativity for the heterogeneous medium studied.

The flow and transport connectivity indicators CF and CT, respectively are defined according to Equation 2-4 and Equation 2-5 for a heterogeneous medium.

$$CF = T_{eff}/T_G \qquad \text{(Equation 2-4)}$$

T_G = geometric mean of local, individual transmissivities of the synthetic heterogeneous medium.

$$CF = t_{AVE}/t_5 \qquad \text{(Equation 2-5)}$$

t_{AVE} = average arrival time of tracer solute from realisations of heterogeneous fields.
t_5 = time at which 5 % of the tracer solute has arrived from realisations of heterogeneous fields.

Knudby and Carrera (2006) also found that the flow connectivity depends more on the continuity of fast flow paths whereas transport connectivity seems to depend more on the width (aperture or channel width) of connected features. They concluded that hydraulic response (lag) times and early arrival times of tracers can be expected to be strongly correlated. This is supported by Hjerne et al. (2010) where a positive correlation between mean residence time and pressure response time was found for tracer tests carried out within SKB programmes. Furthermore, they suggested that it is reasonable to assume that estimated apparent storativity and apparent hydraulic diffusivity from e.g. Cooper-Jacob's method can be useful indicators of flow and/or transport connectivity in heterogeneous media.

In Chapter 4, a further discussion of the correlation between the estimated, apparent hydraulic diffusivity and other parameters estimated from standard analysis of the interference tests at Forsmark and Laxemar is presented.

2.4 Proposed analysis method in heterogeneous media

For detailed predictions of contaminant movement, a large volumetric average of transmissivity as obtained from standard analysis may be of limited value. Instead, information of the spatial variations in transmissivity or hydraulic conductivity is needed to predict contaminant movement in detail. However, as discussed above, such spatial variations in hydraulic parameters cannot be characterized using conventional analysis of pumping tests (e.g. Butler 2008), so other approaches must be explored.

Several authors (e.g. Wu et al. 2005, Yeh and Lee 2007, Butler 2008) have proposed hydraulic tomography (HT) as a method to improve the information on the spatial variations of the hydraulic parameters from interference tests in heterogeneous media.

During recent years, several studies of hydraulic tomography, both using data from synthetic aquifers and data from field tests, have been carried out to further test the capability of the method to provide inference of the spatial variations of hydraulic parameters from interference (cross-hole) tests in heterogeneous media. A short description of this method together with selected hydraulic tomography case studies is briefly reviewed in Chapter 5.

3 Summary of selected interference tests from Laxemar and Forsmark

3.1 General

In this chapter, a summary of the results of four large-scale hydraulic interference tests in fractured crystalline rock at the repository candidate sites Laxemar and Forsmark in Sweden is presented. The interference tests were combined with tracer tests and groundwater flow measurements in selected sections (combined interference tests). However, only the results of the analysis of the pressure interferences are summarized here. The primary objectives of the combined hydraulic interference and tracer tests were to verify the hydrogeological models of the candidate sites and secondly, if possible, determine transport properties for some of major flow paths in the investigated area.

Most of the interference tests were carried out by pumping in an open, rather shallow percussion borehole in the rock during several months (Table 3-1) and monitoring the pressure interferences in a large number of cored boreholes and percussion boreholes in the rock. This implies that mainly the shallow rock and hydraulic structures in the pumping boreholes are activated during the tests. However, the test in KFM02B was performed by pumping from an isolated deep section of the cored borehole. All pumping boreholes were inclined. During some tests, hydraulic head observations were also made in short pipes in the overlying soil layers.

All boreholes involved in the interference tests at the two sites are drilled from the surface. The distances between the pumping borehole and the observation boreholes range from less than c. 100 m to 1–2 km or more during the different interference tests. Both sub-vertical and inclined boreholes exist at the two sites. Most boreholes at both sites are connected to common site-specific hydro-monitoring systems (HMS) for pressure registration.

All boreholes at the two sites are located in fractured crystalline rock including deformation zones with increased transmissivity and less fractured rock (or matrix rock) between the zones. This means that the (local) variability in transmissivity of the different observation sections as determined from previous single-hole pumping tests and difference flow logging in these borehole sections is generally very high. At the Forsmark site, shallow sub-horizontal deformation zones dominate in the upper part of the bedrock with more low-transmissive rock in deeper parts. At the Laxemar site, sub-vertical deformation zones dominate.

The cored boreholes (prefix K-) are c. 700–800 m long and are divided in 5–10 observation sections by inflatable packers. Most of the percussion boreholes (prefix H-, c. 100–200 m long) are divided in 2–3 observation sections by means of packers. The cored boreholes have 76 mm diameter while most of the percussion boreholes have a diameter of c. 140 mm. All boreholes are cased at the top through the soil layers. At the Forsmark site, most cored boreholes are reamed to a larger diameter and cased to c. 100 m length.

In the combined interference tests, pumping was made in two continuous steps with rather constant flow rate during each step due to the combined tracer tests, see Table 3-1. In the interference test in HFM14 at Forsmark a constant flow rate was however used during the entire flow period. The configuration, flow rate, final drawdown at stop of pumping and estimated transmissivities of the pumping boreholes together with the duration of the flow period of the interference tests and additional measurements during the tests are shown in Table 3-1.

Most of the interference tests were performed by pumping in rather high-transmissive deformation zones to obtain high flow rates and significant drawdowns in the observation boreholes. The tests in HLX28 and HFM14 were carried out by pumping in significant deformation zones with large lateral extensions whereas the tests in HLX27 and KFM02B were carried out in more local zones. Pressure observations were made in a large number of observation sections in boreholes intersecting the pumped deformation zone as well as in sections of the less fractured rock outside these zones. In cored boreholes at least one, or possibly several, observation section(s) is located in a deformation zone with increased transmissivity while the remainder is located in less fractured rock. Some of the percussion boreholes are also intersected by deformation zones.

Table 3-1. Configuration, flow rate, final drawdown together with the estimated transmissivity T of the pumping boreholes and the duration of the interference tests at Forsmark and Laxemar. All interference tests were combined with tracer tests and groundwater flow measurements.

Site	Pumping borehole	Config. of pumping borehole	Pumped interval/bh inclin. [1] (m)	Flow rate (L/min)	Duration[2] (days)	Final drawd.[3] (m)	T [4] (m^2/s)
Laxemar	HLX28	Open hole	6.0–154.2 (–59.49)	350→300	c. 126	c. 36	$3 \cdot 10^{-4}$
Laxemar	HLX27	Open hole	6.0–164.7 (–59.41)	50→75	c. 90	c. 22	$3–5 \cdot 10^{-5}$
Forsmark	KFM02B	Isolated section	408.5–434.0 (?)	20→25	c. 55	c. 10	$3 \cdot 10^{-5}$
Forsmark	HFM14	Open hole	6.0–150.5 (–59.81)	349	c. 105	c. 12	$5 \cdot 10^{-4}$

[1] Interval below casing in percussion boreholes. Borehole inclination below horizintal.
[2] Duration of the pumping period.
[3] Final drawdown at stop of pumping.
[4] Determined from transient evaluation of single-hole pumping tests.

In several of the observation sections included in the interference tests, the hydraulic head was displaying an oscillating behaviour. This is caused by so called tidal fluctuations and earth tides in combination with changes of the sea water level. These phenomena have, to some extent, been investigated previously in Ludvigson et al. (2004). During several of the interference tests, precipitation (rainfall) affected the head registrations during certain periods, causing the heads to increase temporarily. Furthermore, during some of the tests, apparent no-flow boundary effects affected the head data at longer times.

During the interference tests, the barometric pressure, precipitation and the sea water level were measured. During some of the interference tests a persistent, naturally decreasing head trend was observed during the test periods. In such cases, linear corrections for the natural head trend were applied to the measured head in the observation sections. No other corrections of the measured head data due to e.g. precipitation, tidal effects, sea level changes were made.

3.2 Test analysis methods

3.2.1 General

Standard methods for constant flow rate interference tests in an equivalent porous medium were used for evaluation of the responses in the observation test sections in accordance with the methodology description for interference tests (SKB MD 330.003 v2.0). The transient analysis was performed using the software AQTESOLV Pro v. 4.0 that enables both manual and automatic type curve matching. The transient evaluation was carried out as an iterative process of manual type curve matching and by employing automatic non-linear regression.

The transient evaluation of the hydraulic parameters of the observation sections (mainly transmissivity and storativity) is normally based on the identified pseudo-radial flow regime and associated flow regimes during the tests, as identified by the diagnostic test analysis. The transient evaluation was made before any effects of outer hydraulic boundaries had affected the data.

As a first step in the diagnostic analysis all data were examined in linear pressure versus time diagrams to identify the responding sections to the pumping and disturbing effects, such as effects of precipitation, tidal effects and other noise in the data. All pressure data from the observation boreholes have, prior to evaluation, been corrected automatically in the HMS (Hydro Monitoring System) for atmospheric pressure changes by subtracting the latter pressure from the measured (absolute) pressure.

In addition, a response analysis was made to obtain an overview and classification of the drawdown responses. Finally, the apparent hydraulic diffusivity T/S was estimated from the response time lags to assess the hydraulic connectivity between the pumping section and the responding observation sections, to be compared with the estimated hydraulic diffusivity from the transient test analysis.

3.2.2 Diagnostics and transient analysis of observation sections

In the primary diagnostic analysis, data from all observation borehole sections included in the interference tests were examined in linear pressure versus time diagrams to identify the responding sections to the pumping. Corresponding diagrams of precipitation, tidal effects, sea water level etc. were also used in this process. Subsequently, a classification of the strength and response times (time lags) of the responses in the observation sections was made.

The evaluation of the dominant transient flow regimes during the tests, i.e. pseudo-linear (PLF), pseudo-radial (PRF) and pseudo-spherical (leaky) flow (PSF), respectively together with outer hydraulic boundary conditions was mainly based on the drawdown responses, including the drawdown derivative, in logarithmic diagrams. In particular, pseudo-radial flow is reflected by a constant (horizontal) derivative in such diagrams, whereas no-flow- (NFB) and constant head boundaries (CHB) are characterized by an increase and decrease of the derivative, respectively. Based on the qualitative evaluation, relevant theoretical models and data intervals were selected for transient evaluation of the responses.

In the transient evaluation, only observation sections with clear drawdown responses to the pumping were analysed with standard transient methods for radial flow in an equivalent homogeneous porous aquifer. The equivalent porous media transmissivity T_o and storativity S_o and, for responses indicating leaky flow, also the leakage coefficient $(K'/b')_o$, e.g. Hantush and Jacob (1955), Theis (1935), Kruseman and de Ridder (1990) were estimated. The responses were analysed according to the actual flow rate record (constant or variable) in the pumping borehole and identified flow regimes. Observation borehole sections with very weak and/or uncertain responses were only analysed qualitatively.

Different criteria were used for the selection of observation sections for subsequent transient analysis for the different interference tests. In case of the two confirmatory interference tests in HLX27 and HLX28 at Laxemar, most of the responding observation sections in the rock (drawdown > 0.1 m) were selected for transient analysis, see Table 3-2. Also in the confirmatory interference test in borehole KFM02B at Forsmark, most of the responding observations sections in the rock were analysed using transient methods. For observation sections with too weak and/or uncertain responses no transient analysis was made. Such sections explain the difference between the number of responding and analysed sections in Table 3-2.

However, in case of the interference test in borehole HFM14 only a few (6) observation sections were selected for transient analysis. Most of these sections were assumed to be located in sub-horizontal deformation zones with increased transmissivity and with a presumed good hydraulic connection with the pumping borehole.

Table 3-2. Total number of observation sections, number of responding observation sections together with number of analysed observation sections during the selected interference tests at Forsmark and Laxemar.

Site	Pumping borehole	Number of observation sections	Number of responding sections	Number of analysed sections*	Comments
Laxemar	HLX28	266	62	61	Only 1 observation section was not analysed (missing data).
Laxemar	HLX27	75	32	25	Only observation sections with clear responses were analysed.
Forsmark	KFM02B	115	25	18	Only observation sections with clear responses were analysed.
Forsmark	HFM14	185	109	6	Only a few observation sections with good connectivity were analysed.

* number of observation sections selected for transient analysis of T_o and S_o.

3.2.3 Diagnostics and transient analysis of pumping sections

Transient analysis was also performed of the responses in the pumping boreholes by standard models for radial flow, also accounting for wellbore storage and skin, e.g. Dougherty and Babu (1984) and Moench (1985) according to the flow regimes identified.

3.2.4 Response analysis

For all responding observation sections, their response time lags and distances to the pumping borehole section were determined. From these parameters two (normalised) response indices, defined below, were calculated. The connectivity Index 1 is defined by Equation 3-1 and Index 2-new by Equation 3-2. Index 1 is directly related to the hydraulic diffusivity of the section whereas Index 2-new reflects the strength of the drawdown response in relation to the flow rate in the pumping borehole.

The distance r_s is the 3D Euclidian (shortest) distance between the pumping section and the observation section. The response time lag, dt_L, is defined as the time lag after start of pumping until a specified drawdown was observed in the actual observation section. In general, a drawdown criterion of s = 0.1 m is used. However, for some tests at Forsmark, a drawdown criterion of s = 0.01 m was used for the estimation of dt_L. The maximum drawdown, s_p, in Equation 3-2 corresponds in most cases to the actual drawdown at the maximum time used by the transient evaluation of the test, before any effects of e.g. long drought periods or apparent hydraulic boundaries are observed in the drawdown curves. The flow rate Q_p corresponds to the flow rate at the time when s_p is defined.

The pumping flow rate Q_p, in combination with the time lags dt_L, distances r_s and drawdown s_p, were used to calculate the normalised response indices according to Equation 3-1 and Equation 3-2 as follows:

Index 1:

Distance r_s relative the response time dt_L [m^2/s].

$$Index\ 1 = \frac{r_s^2}{dt_L} \qquad \text{Equation 3-1}$$

Index 2 new:

Drawdown s_p relative the pumping rate Q_p, using the distance r_s as a weighting factor (assuming r_0 = 1 m) [s/m^2].

$$Index\ 2\ new = \frac{s_p}{Q_p} \cdot \ln\left(\frac{r_s}{r_0}\right) \qquad \text{Equation 3-2}$$

The classification of the response indices 1 and 2-new is shown in Table 3-3. From the estimated indices, cross plots of Index 2-new and Index 1 were prepared for each interference test to obtain an overview of the strength and speed of the responses in the observation sections. From these cross plots, observation sections for transient analysis are generally selected. In addition, the cross plots could be used in assessing the conformity of the responses with established hydro-structural models of deformation zones at the sites.

Table 3-3. Limits and classification of response indices. The response lag time dt_L in the observation sections is based on a drawdown criteria of s = 0.1 m.

	Limits	Classification	Colour code
Index 1 r_s^2/dt_L	$r_s^2/dt_L > 100$ m^2/s	Excellent	Red
	$10 < r_s^2/dt_L \leq 100$ m^2/s	High	Yellow
	$1 < r_s^2/dt_L \leq 10$ m^2/s	Medium	Green
	$r_s^2/dt_L \leq 1$ m^2/s	Low	Blue
Index 2 new $s_p/Q_p \cdot \ln(r_s/r_0)$	$(s_p/Q_p)\cdot\ln(r_s/r_0) > 5\cdot10^5$ s/m^2	Excellent	Red
	$5\cdot10^4 < (s_p/Q_p)\cdot\ln(r_s/r_0) \leq 5\cdot10^5$ s/m^2	High	Yellow
	$5\cdot10^3 < (s_p/Q_p)\cdot\ln(r_s/r_0) \leq 5\cdot10^4$ s/m^2	Medium	Green
	$(s_p/Q_p)\cdot\ln(r_s/r_0) \leq 5\cdot10^3$ s/m^2	Low	Blue
	$s_p < 0.1$ m	No response	Grey

In general, all data from observation sections are influenced by natural fluctuations of the groundwater level such as tidal effects and long term (seasonal) trends to a varying degree. These background variations of pressure may sometimes make it difficult to estimate the response time lag in the observation sections. The pressure changes due to tidal effects are different for the various observation boreholes and sections.

3.2.5 Estimation of apparent hydraulic diffusivity

The apparent hydraulic diffusivity of the responding observation sections was estimated in two ways, firstly as the ratio of estimated transmissivity and storativity T_o/S_o from the transient analysis of drawdown and secondly, from the estimated lag times in the observation sections. In general, good agreement was obtained between these two ways of estimating the apparent hydraulic diffusivity for most of the interference tests.

The calculation of the apparent hydraulic diffusivity T/S from the lag times and distances is based on radial flow according to Streltsova (1988) as described in the actual interference test reports. The time lag dt_L, used to estimate the hydraulic diffusivity by Streltsova (1988), is generally defined as the time when the pressure response in an observation section is 0.01 m. These estimates of the apparent hydraulic diffusivity should be seen as approximate and could be compared with the apparent hydraulic diffusivity calculated as the ratio of T_o/S_o from the transient evaluation of the observation sections from the drawdown curves.

3.2.6 Estmation of transmissivity of observation sections from previous single-hole tests

For observation sections in which transient analysis of is made from the interference tests, their transmissivity was also estimated from previous single-hole tests for comparison. In most cases, single-hole test data from difference flow logging (PFL) in cored boreholes and from single-hole pumping tests (HTHB) in percussion boreholes were used in this report. For a few cored boreholes, data from hydraulic injection tests (PSS) in 5 m sections were used.

Using the PFL method, described in the methodology report by Ludvigson et al. (2002) and test report by e.g. Rouhiainen and Sokolnicki (2005), it is possible to identify the position and estimate the transmissivity of conductive, single fractures along boreholes in fractured rock with a high resolution of borehole length (c. 0.1 m). For description of the methodology of hydraulic tests with HTHB in percussion boreholes and PSS tests in cored boreholes, refer to e.g. the test reports by Walger et al. (2007) and Harrström et al. (2007) respectively and the methodology reports by Ludvigson et al. (2007) and Enachescu and Rahm (2007) for the Forsmark and Laxemar sites, respectively.

3.3 Summary of the selected interference tests

In this section, a summary is presented for each of the selected interference test regarding the location of the boreholes, test periods, number of responding sections, disturbing effects on test data and details of the transient evaluation of the tests. The results of the selected tests are presented in Section 3.4 in unified diagrams. Only relevant pressure and flow rate data during the interference tests are presented (no tracer test data).

3.3.1 Interference test in HLX28 at Laxemar

The confirmatory hydraulic interference test and tracer test in HLX28 at Laxemar is reported by Thur et al. (2009). The aims of the tests were to verify parts of the hydrogeological model of the Laxemar area and, if possible, to determine transport properties for some major flow paths in the area.

The locations of the boreholes in the Laxemar area, including the pumping borehole HLX28, are shown in Figure 3-1. The flow period of the interference test lasted from 2009-01-20 to 2009-05-26. The flow rate and drawdown in the pumping borehole by the end of the flow period are shown in Table 3-1. The subsequent recovery period was recorded but not analysed in this case.

Heavy precipitation occurred 2009-02-21 to 2009-02-22 and later on which temporarily caused approximate steady-state groundwater head conditions in the observation boreholes. Subsequently, a drought period, starting at about 2009-04-01, caused a natural trend of decreasing groundwater levels in the area. This trend was interrupted by heavy rainfall at the end of April. Finally, by the end of the flow period, the head decreased significantly due to apparent outer no-flow boundary conditions in combination with the naturally decreasing head trend.

Diagnostic analyses of the responses were made for all cored boreholes and percussion boreholes in rock in the Laxemar area (monitored in the HMS) as well as in all soil monitoring wells within a radius of 1 km from HLX28, cf. Figure 3-1. A classification of the strength of the responses in the observation borehole sections was made from visual inspection of the pressure responses in the observation sections in linear diagrams, see Table 3-4.

The transient evaluation of the flow period was based on responses before 2009-02-06 (c. 25,000 min). After this time, drought periods, precipitation and effects of apparent no-flow boundaries affected the head. During the period up to 25,000 min, minor precipitation occurred and no significant effects of naturally declining groundwater levels or apparent hydraulic boundaries were observed. No corrections of the head data were therefore considered necessary during this time interval.

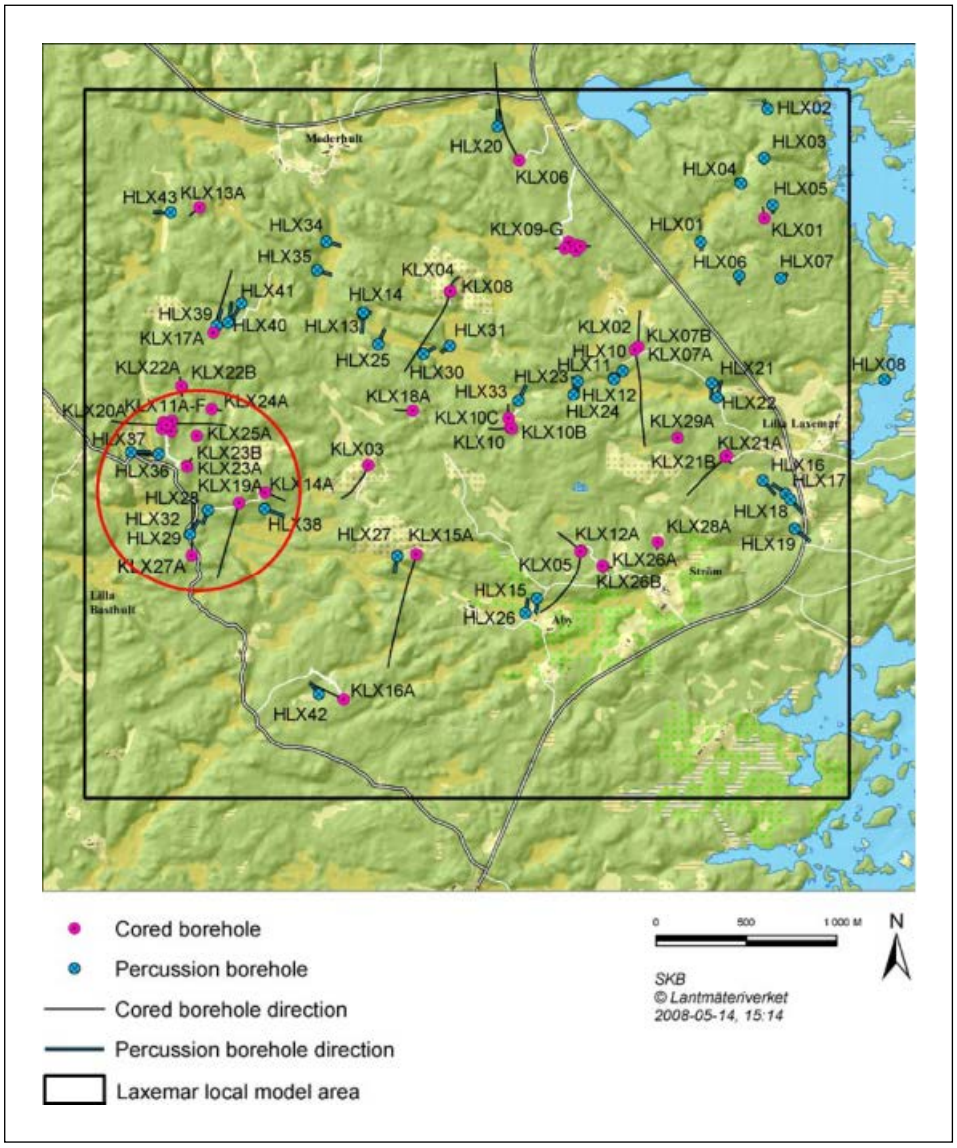

Figure 3-1. *The Laxemar site investigation area and the boreholes involved in the interference tests. The pumping borehole HLX28 is located in the south-western part of the area. From Thur et al. (2009).*

Table 3-4. Classification of the responses in the observation sections during the interference test in HLX28 at Laxemar.

Total number of responding sections (clear+weak)	Classification of the responses during interference test in HLX28			
	Clear = 1	Weak = 2	Uncertain = 3	No response = 4
63	53	10	1	202

The estimated hydraulic parameters from the first part of the flow period (0–25,000 min) were selected as being representative for the test. No transient evaluation was made for the recovery period. The estimated transmissivity from the intermediate response in the pumping borehole HLX28 is shown in Figure A1-1 in Appendix 1. As shown in the latter figure, the response in the pumping borehole indicated a dual-permeability system with a higher transmissivity at early times and lower at intermediate times. As an example of transient evaluation in an observation borehole section, the analysis in section HLX37:2, located 501 m from the pumping borehole, is shown in Figure A1-2 in Appendix 1.

The basic results of the transient evaluation of the interference test in HLX28 are presented in Section 2.4.

3.3.2 Interference test in HLX27 at Laxemar

The confirmatory hydraulic interference test and tracer test in HLX27 in Laxemar is reported by Lindquist et al. (2008a). The objectives of the combined interference test and tracer test in HLX27 were to partially verify the hydrogeological model of the Laxemar area and to verify transport characteristics that previously have been determined through laboratory tests on drill cores and other investigations.

The locations of the boreholes in the Laxemar area, including the pumping borehole HLX27, are shown in Figure 3-1. HLX27 are located to the south-east of HLX28, which was pumped in the preceding interference test presented above. The flow period of the interference test in HLX27 lasted from 2008-03-26 to 2008-06-26. The subsequent recovery period ended 2008-07-20. The flow rate and total drawdown in the pumping borehole HLX27 by the end of the flow period are shown in Table 3-1.

A classification of the responses in the observation borehole sections was made from visual inspection of the pressure responses in the observation sections in linear diagrams, see Table 3-5. Transient evaluation was only made of those sections showing clear responses. Eight of the observation sections were considered as being unaffected by the pumping during the interference test. Finally, in as many as 35 sections it cannot be confirmed if the sections were affected by the pumping or not. The reasons for this are small drawdowns at long distances in combination with superimposed natural disturbances (e.g. precipitation, tidal effects), external disturbances (e.g. other pumping or drilling activities) or defect or missing data.

During the interference test period (c. 4 months), a total precipitation of c. 125 mm (of which c. 50 mm during the flow period) was reported at two stations in the vicinity of the test area. The rain that fell just before stop of pumping and during the recovery period may have influenced the pressure in some of the observation boreholes and thus complicated the identification of responding sections at long distances as discussed above.

In addition, there were strong indications of a natural trend of decreasing groundwater levels during the entire interference test period. At the end of the recovery period analysed, the pressure in most observation sections had not returned to the levels that prevailed prior to start of pumping and the decreasing natural trend continued at the end of this period. Individual, linear trend corrections for the naturally decreasing head trend were applied to all observation sections before carrying out the transient analysis as well as the response analysis. No other corrections of the measured drawdown due to e.g. precipitation, tidal effects, seawater level et.c. were made.

Table 3-5. Classification of the pressure responses in the observation sections during the interference test in HLX27 at Laxemar.

Total # of observation sections	Total # of responding sections (clear+weak)	Classification of the responses during the interference test in HLX27			
		Clear	Weak	Uncertain	No response
75	32	25	7	35	8

The transient responses in the observation boreholes were rather complex during the flow period due to precipitation, the step increase of flow rate and several pump stops in the pumping borehole at longer times. The transient responses in the observation borehole sections were divided in two groups, i.e. sections with distinct and those with more subdued responses, respectively. Examples of such responses are shown in Figures A1-3 and A1-4 respectively together with the drawdown response in the pumping borehole in Appendix 1.

The most distinct responses occurred in the uppermost sections in the observation boreholes whereas more delayed responses occurred in deeper sections. In sections with distinct responses the effects of the flow rate change can be clearly seen but in sections with subdued responses these effects may not be readily observed.

In sections with the most distinct responses, a pseudo-spherical (leaky) flow regime dominated during early to intermediate times, before the onset of the disturbing effects discussed above. In some sections this flow regime was preceded by a short period of pseudo-radial flow. After the increase of flow rate at c. 37,000 min a transition towards new flow conditions, reflected by an apparent late pseudo-radial flow regime was indicated, eventually followed by a new pseudo-spherical (leaky) flow regime at longer times.

Due to the changed flow conditions after the flow rate change it was not possible to make a complete transient evaluation of the entire flow period with uniform values on the hydraulic (and leakage) parameters (even if variable flow rates were accounted for). Thus, the transient evaluation of the flow period was in most cases based on the first part of the flow period before the change of flow rate and before the disturbing effects, using a leaky aquifer model. In sections with subdued and delayed responses transient evaluation could, however, be performed on the entire drawdown curve with uniform parameters. The parameter values estimated from the early part are assumed to be representative for the complete flow period.

In addition, in some of the sections with the most distinct responses a separate transient evaluation was made on the later part of the flow period after the increase of flow rate. The estimated transmissivities from the later part of the flow period were higher than those estimated from the early part, possibly representing major large-scale hydraulic structures within the radius of influence of the test.

During the recovery period, most observation sections exhibited a dominant pseudo-spherical (leaky) flow regime, preceded by a short period of pseudo-radial flow in sections with the most distinct responses. Transient evaluation of the entire recovery period was in most cases readily made using a leaky aquifer model with uniform parameters. The agreement in evaluated parameter values estimated from the first part of the flow period and from the recovery period was generally good. The estimated hydraulic parameters from the recovery period were selected as being representative for the test.

As for the preceding interference test, the estimated transmissivities from the observation sections during the interference test in HLX27 were, in general, significantly higher than those estimated from previous single-hole tests in these observation sections. This fact is assumed to be due to the inherent differences between single-hole tests and interference tests regarding test scale, duration of pumping and investigated volume of rock etc. In this case, the estimated transmissivities of the observation sections are assumed to be dominated by the transmissivity of hydraulic structures intersecting the pumping borehole and nearby hydraulic structures. The estimated transmissivity of the pumping borehole HLX27 ranged from $2–4 \cdot 10^{-5}$ m^2/s.The basic results of the transient evaluation of the interference test in HLX27 are presented in Section 3.4.

3.3.3 Interference test in KFM02B at Forsmark

The confirmatory hydraulic interference test and tracer test in the pumping borehole section KFM02B:408.5–434.0 m at Forsmark is reported by Lindquist et al. (2008b). The objectives of this combined interference test and tracer test was to partially verify the hydrogeological model of the Forsmark candidate area and to verify the transport characteristics that previously had been determined through laboratory tests of drill cores.

The locations of the boreholes in the Forsmark area, including the pumping borehole KFM02B, are shown in Figure 3-2. All observation boreholes in bedrock included in the interference test and their approximate distances to the pumping section in borehole KFM02B are marked in Figure 3-2. The flow rate and drawdown by the end of the flow period in the pumping borehole KFM02B are shown in Table 3-1.

During the interference test approximately 50 mm of total precipitation (of which c. 20 mm during the flow period) was reported at two stations in the vicinity of the boreholes included in the test. The rain that fell just before stop of pumping and during the recovery period may in some boreholes have influenced the pressure in the observation boreholes and thus introduced some uncertainty in the interpretation of the responses.

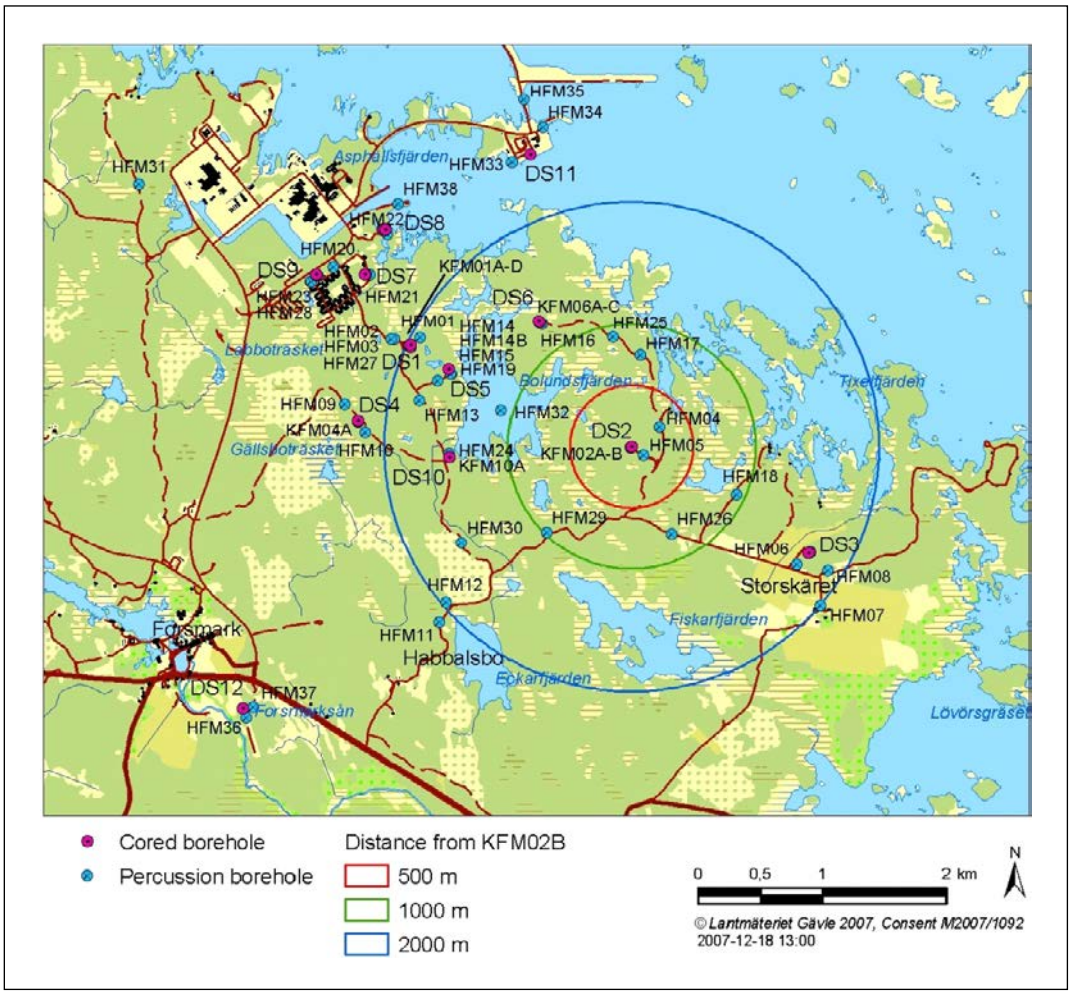

Figure 3-2. *Locations of boreholes and drill sites in the Forsmark investigation area. The pumping borehole KFM02B is located in the centre of the inner circle. The outer circles represent distances of 500 m, 1,000 m and 2,000 m, respectively, from the pumping borehole. From Lindquist et al. (2008b).*

There are strong indications of a superimposed natural trend of decreasing groundwater levels during the entire interference test period. At the end of the recovery period, the levels in many observation sections had not returned to the levels that prevailed prior to start of pumping. In some boreholes the decreasing natural trend continued at the end of the recovery period. The hydraulic head data were corrected prior to the transient analysis and the response analysis, based on an assumed naturally decreasing linear trend. The natural trend was, in general different in each observation section.

A classification of the type of responses in the observation borehole sections was made from visual inspection of the pressure responses in linear diagrams, see Table 3-6. Significant responses were registered in 25 of the 115 observation sections included in the interference test. Transient evaluation was performed for the clearest responses (18). In total, 90 of the sections were apparently unaffected by the pumping but 9 of these were considered as uncertain and it cannot be decided whether they were affected by the pumping or not. The relatively low number of responding sections may be due to the relatively low flow rate used in the pumping borehole section, see Table 3-1.

Complete transient evaluations were made for observation sections with clear responses during the entire flow period as well as during the recovery period. It was accounted for the variable flow in the pumping borehole section during the flow period. Pseudo-radial flow transitioning to pseudo-spherical (leaky) flow dominated the responses in most sections during both the flow and recovery periods. Thus, the leaky aquifer model by Hantush and Jacob (1955) was used for the transient evaluation. The transient evaluation of the pumping borehole section KFM02B:408.5–434.0 m and in observation section KFM02A:6 are shown in Figure A1-5 and A1-6 respectively in Appendix 1.

The basic results of the transient evaluation of the interference test in KFM02B are presented in Section 3.4.The agreement between the estimated hydraulic parameters from the flow period and recovery period was acceptable for most observation sections. The parameters from the flow period were selected as being representative for the test.

3.3.4 Interference test in HFM14 at Forsmark

The hydraulic interference test in HFM14 in Forsmark is reported by Gokall-Norman and Ludvigson (2008). The tracer test performed in conjunction with the hydraulic interference test is reported by Lindquist et al. (2008c). The main purpose of the interference test was to characterize different deformation zones, to quantify their hydraulic properties and to clarify whether there are any hydraulic boundaries in the area.

The locations of the boreholes in the Forsmark area, including the pumping borehole HFM14, are shown in Figure 3-3. Start and stop of the pumping occurred on 2007-06-28 and 2007-10-08, respectively. The recovery was measured until 2007-10-15. The flow rate and drawdown in the pumping borehole by the end of the flow period are shown in Table 3-1. During the interference test the pressure was registered in a large number of instrumented cored boreholes and percussion boreholes in the rock.

All pressure data were corrected for atmospheric pressure changes by subtracting the latter pressure from the measured (absolute) pressure. No further corrections of the measured drawdown have been made, e.g. due to natural trends, precipitation, tidal effects etc. During the interference test, there was quite a large amount of distributed precipitation events reported from two stations in the vicinity of the test area. A classification of the type of responses in the observation borehole sections was made from visual inspection of the pressure responses in the observation sections in linear diagrams, see Table 3-7.

The pressure was monitored in a total of 185 observation sections. In total, 109 observation sections were judged to be affected by the pumping. Approximately 50% of these sections had a final drawdown of more than 0.5 m. The remaining 76 sections were judged to be virtually unaffected by the pumping or had a too weak or uncertain response. Several of these sections were located at large distances (more than c. 1 km) from the pumping borehole. In addition, natural disturbances (e.g. precipitation, tidal effects), external disturbances (e.g. other pumping or drilling activities) made it difficult to deduce whether the sections were affected by the pumping in HFM14 or not.

Table 3-6. Classification of the responses in the observation sections during the interference test in KFM02B at Forsmark.

Classification of the responses during the interference test in KFM02B:408.5–434.0 m			
Total # of observation sections	**Total number of responding obs-sections (clear+weak)***	**Uncertain response**	**No response**
115	25	9	81

* no division in clear and weak responses was made in this case.

Table 3-7. Classification of the responses in the observation sections during the interference test in HFM14 at Forsmark.

Classification of the responses during interference test in HFM14		
Total number of observation sections	**Responding sections**	**Non-responding sections**
185	109	76

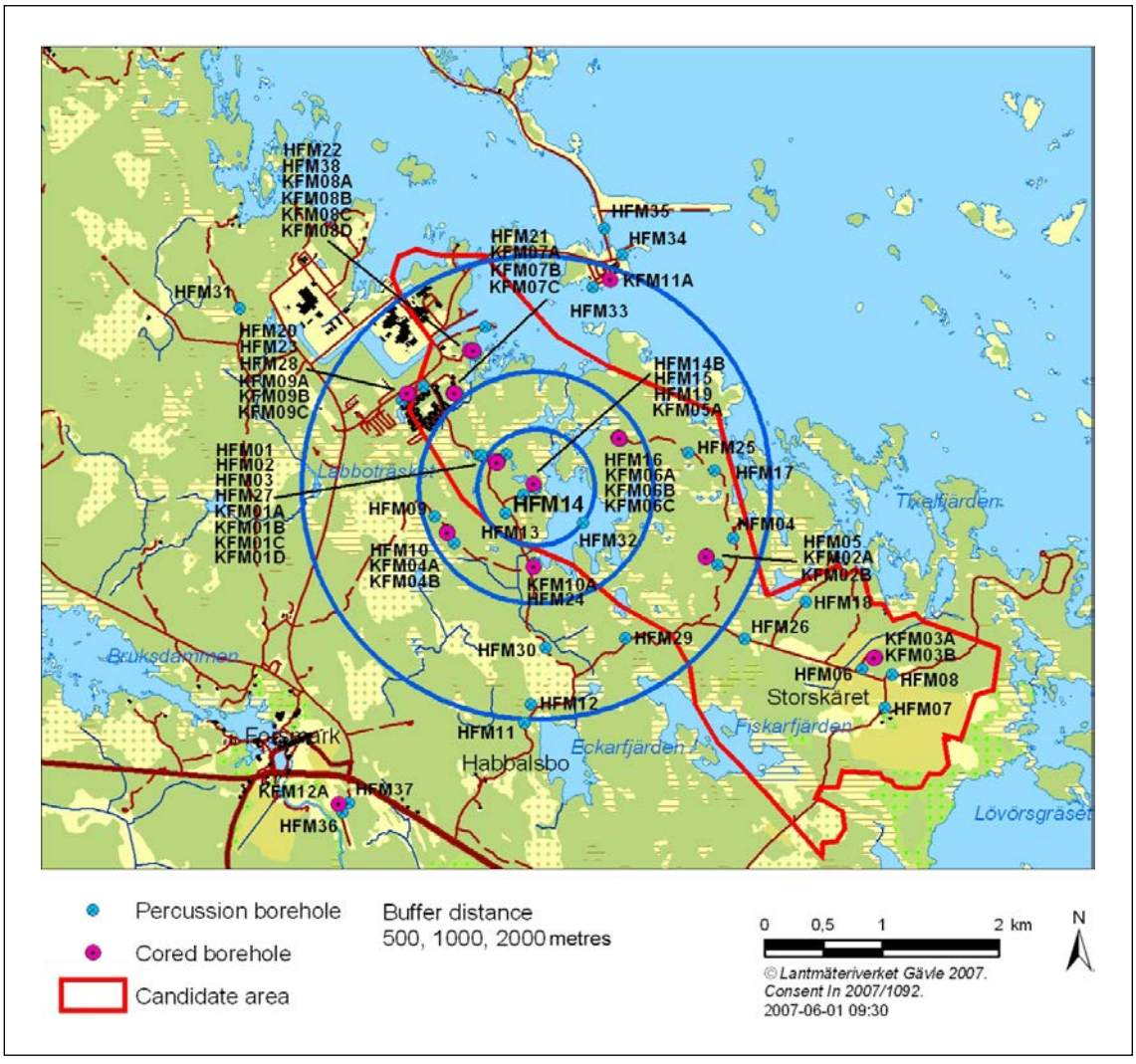

Figure 3-3. *The investigation area at Forsmark including part of the candidate area selected for more detailed investigations. The positions of the boreholes included in the interference test in HFM14 are displayed as well as the areas corresponding to radii of 500 m, 1,000 m and 2,000 m from HFM14, respectively. From Gokall-Norman and Ludvigson (2008).*

Transient evaluation was only applied to six (6) selected observation sections at locations of particular interest during the interference test in HFM14. The flow rate was stable during the entire flow period except some minor fluctuations at the very beginning of the flow period. The transient evaluation in the pumping borehole and in the observation section KFM10A:2 are shown in Figure A1-7 and A1-8 respectively in Appendix 1.

From diagnostic analysis of the responses in the selected observation sections, pseudo-radial flow during intermediate times transitioning to pseudo-spherical (leaky) flow at the end were dominating during both the flow and recovery periods of the test. The transient evaluation was performed using the Hantush-Jacob model (Hantush and Jacob 1955) for confined leaky aquifers.

The basic results of the transient evaluation of the interference test in HFM14 are presented in Section 3.4. The results from the transient evaluation of the flow and recovery periods were in good agreement. Results from the transient evaluation of the flow period were chosen as being representative for the test and the tested rock.

3.4 Comparison of results of the selected interference tests

In this section, comparisons of the basic results from standard evaluation of the selected interference tests in HLX27, HXL28, KFM02B and HFM14 are presented in unified scatter plots. The type of figures presented in this section may also be found in the primary data reports from the actual tests but here the results from the different tests are plotted jointly. For further details about the interference test results, e.g. responses in specific sections, it is referred to the primary data reports. Only results from the evaluation of pressure and flow rate data during the interference tests are presented (no tracer test results).

It should be observed that the data in the following plots only represent observation sections for which transient evaluations were made. As indicated in Table 3-2 and discussed in Section 3.2.2, all responding sections were not included in the transient evaluation which should be kept in mind when analysing the results below. This is particularly true for the interference test in HFM14 in Forsmark.

In Figure 3-4, a response diagram with *Index 2-new* versus *Index 1* for observation sections selected for transient evaluation is presented for the selected interference tests. *Index 2-new* represents the normalized drawdown with respect to flow rate (with a weighting factor for distance) and *Index 1* is assumed to reflect the connectivity (and hydraulic diffusivity) between the pumping borehole and the observation sections as reflected by their lag times. *Index 1* is based on the lag times of the pressure responses in the observation sections in relation to their distances to the pumping borehole. In all figures below, the drawdown s_p and flow rate Q_p correspond to the end of the time interval selected for transient evaluation, c.f, Section 3.3.

Observation sections with strong and fast responses should thus be located towards the upper right corner of the response diagram (yellow-red class limits on the X- and Y-axes according to Table 3-3). Weak and small responses should be located towards the lower left corner (blue class limits). Figure 3-4 indicates that rather strong (normalized) drawdown responses occur in several observation sections during the large-scale interference test in HLX28 for varying degree of connectivity to the pumping borehole. This fact may possibly reflect the presence of a dominant deformation zone hydraulically connected to, a variable degree, to several of the observation borehole sections.

Some observation sections, during the interference test in HLX27, and one section, during the test in KFM02B, also exhibit relatively strong normalized responses. These sections show good connectivity to the pumping borehole. Most of the selected observation sections during the interference test in HFM14 show fast but not very strong normalized responses. The interference test in HLX28 shows the largest variations of both the normalized responses as well as the assumed connectivity to the pumping borehole. Several observation sections show low (normalized) responses during the test in HLX28.

Figure 3-5 shows the normalized drawdown with respect to flow rate (s_p/Q_p) versus the distance from the pumping borehole (r_s) in a log-lin diagram for the selected interference tests. Also included are the (logarithmic) regression lines for Laxemar (based on tests HLX28 and HLX27) and Forsmark (based on tests KFM02B and HFM14). In addition, the normalized drawdowns in the pumping boreholes are indicated as dashed lines for comparison.

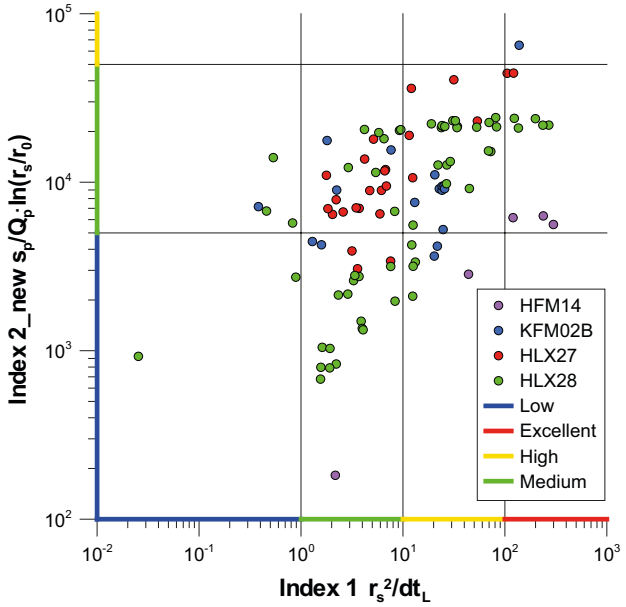

Figure 3-4. *Response diagram showing the drawdown responses in selected observation sections during the different interference tests. Response Index 2_new is plotted versus Index 1. The classification of the two indices is also shown on the axes of the diagram. The lag time dt_L is based on a drawdown of 0.1 m. The definitions of the indices are presented in Section 3.2.3.*

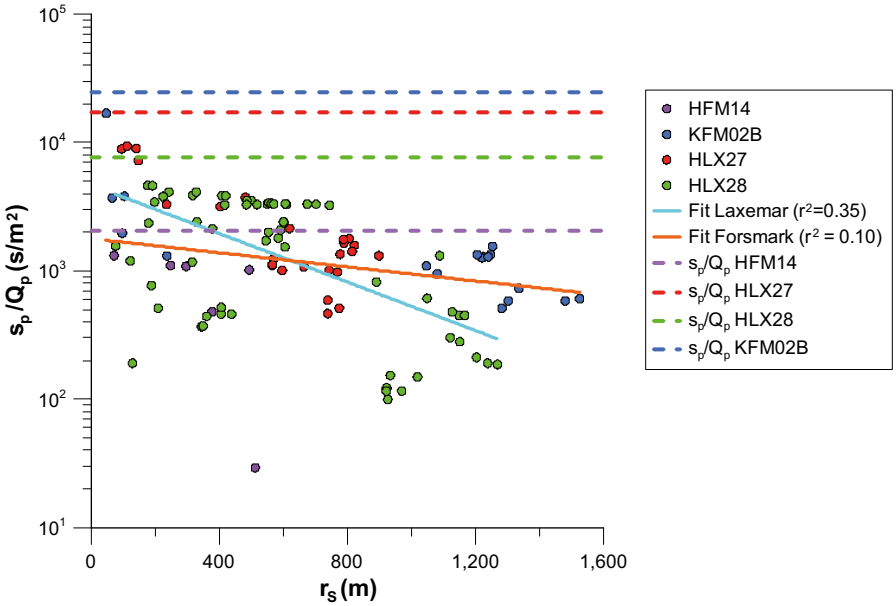

Figure 3-5. *Normalized drawdown with respect to flow rate (s_p/Q_p) versus distance from pumping borehole (r_s) for the selected interference tests. The regression lines for the tests at Laxemar and Forsmark are also shown together with the normalized drawdown in the corresponding pumping boreholes.*

Figure 3-5 shows that drawdown responses also occur at long distances from the pumping boreholes (c. 1,500 m). Secondly, the figure indicates a large variation in the normalized drawdown with distance during the interference tests, indicating a strongly heterogeneous rock. For the tests at Forsmark, only a minor decrease of s_p/Q_p with distance from the pumping borehole is indicated, possibly reflecting the presence of major sub-horizontal deformation zones at this site. The decrease of s_p/Q_p with distance is more pronounced for the tests at Laxemar.

The large-scale interference test in HLX28 shows the smallest deviation between the normalized drawdowns in observation sections and the drawdown in the pumping borehole, also in sections at long distances (c. 800 m). As discussed above, this fact may possibly reflect the presence of a dominating fracture zone in the area. The normalized drawdowns in most of the selected observation sections during the interference test in HFM14 are also only slightly less than the drawdown in the pumping borehole, indicating the presence of a dominant (sub-horizontal) deformation zone in the area. During the tests in KFM02B and HLX27 the normalized drawdowns in the observation sections are significantly lower than for the corresponding pumping boreholes.

Figure 3-6 shows the estimated transmissivity (T_o) versus estimated storativity (S_o) from transient evaluation of the selected observation sections. The horizontal lines indicate the estimated transmissivity for the corresponding pumping borehole sections. Figure 3-6 indicates that the estimated transmissivity of the majority of the observation sections fall within the narrow range of $1 \cdot 10^{-5}$ to $1 \cdot 10^{-3}$ m^2/s. This fact indicates that T_o generally reflects some kind of (effective) transmissivity of the entire rock volume, including deformation zones, within the radius of influence, but, in general, with a preference towards the estimated transmissivity of the pumping borehole section. Observation sections with similar transmissivity as the pumping boreholes may be assumed to be located in the same deformation zone.

The variability of the estimated storativities is slightly higher than that observed for the estimated transmissivity, ranging from $S_o = 2 \cdot 10^{-6}$ to $2 \cdot 10^{-3}$, cf. Figure 3-6. The observation section with an apparently high estimated $S_o = 2 \cdot 10^{-1}$ and high transmissivity corresponds to the uppermost section (with a free water table) with low connectivity to the pumping borehole HLX28 and is therefore considered as highly uncertain and not comparable with values from isolated borehole sections. Finally, there is no obvious correlation between the estimated transmissivity and estimated storativity of the observation sections for any of the tests.

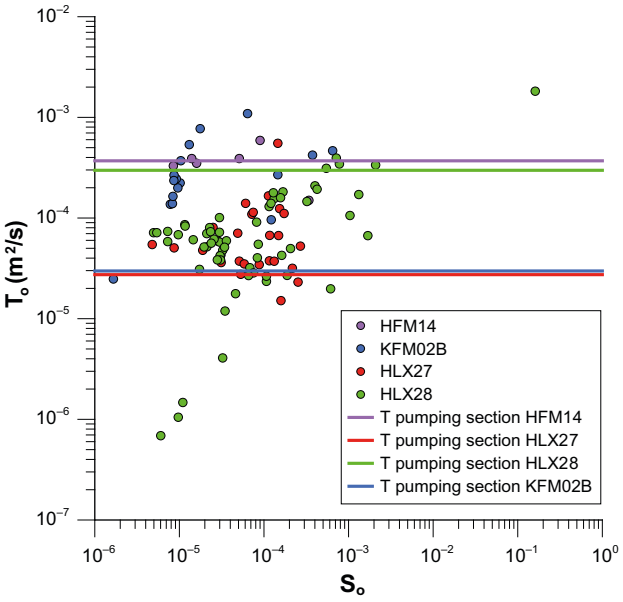

Figure 3-6. *Estimated transmissivity (To) versus estimated storativity (So) for the selected observation sections. The horizontal lines indicate the estimated transmissivity for the corresponding pumping borehole sections.*

In Figure 3-7 the estimated hydraulic diffusivity (T/S-Streltsova) from the response time lags versus the estimated hydraulic diffusivity (T_o/S_o) as a from the transient test evaluation for the observation sections of the selected interference tests is shown. Also shown are the estimated regression lines for the tests at Forsmark and Laxemar together with the 1:1 line of hydraulic diffusivity. Figure 3-7 generally indicates a good correlation between the estimated hydraulic diffusivities (except for the test in KFM02B). The diffusivities (T_o/S_o) estimated from the transient test evaluation are generally slightly higher than those estimated from the time lags.

Finally, Figure 3-7 shows that the estimated hydraulic diffusivities from the selected interference tests at Forsmark are higher than those from Laxemar**.** This fact may be an effect of the sub horizontal deformation zone and the otherwise more fractured and conductive upper 200 m of the rock at Forsmark.

Further discussion of the results of the standard evaluation of the interference tests is made in Chapter 4.

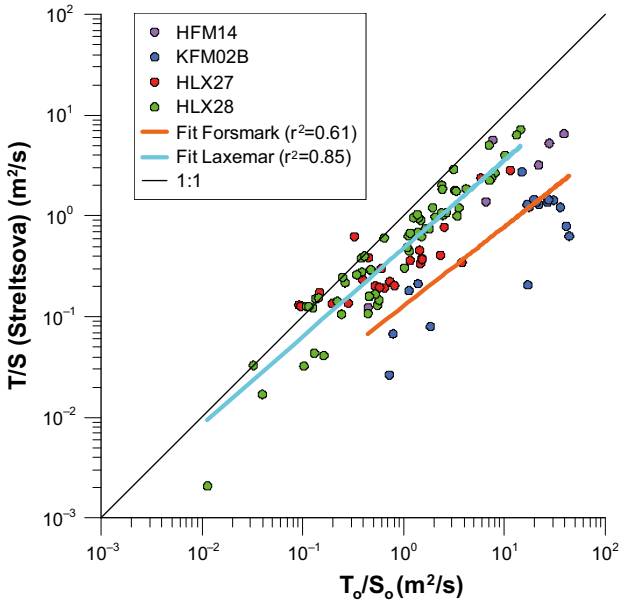

Figure 3-7. *Apparent hydraulic diffusivity estimated from the response time lags (T/S) according to Streltsova (1988) versus estimated apparent hydraulic diffusivity from transient test evaluation (T_o/S_o) for the different interference tests. Also shown are the estimated regression lines for the tests at the sites Forsmark and Laxemar together with the 1:1 line.*

4 Detailed analysis of hydraulic parameters estimated from selected interference tests at Forsmark and Laxemar

4.1 General

In this chapter, a detailed analysis of the results from standard evaluation of the interference tests previously performed in Laxemar and Forsmark, presented in Chapter 3, is made in various diagnostic scatter plots of estimated hydraulic parameters. The main aim of the detailed analysis is to identify and discuss possible implications of using standard analysis methods of interference tests in heterogeneous, crystalline rock and to compare with the observations made in the literature review in Section 2.

As mentioned above, the number of observation sections selected for transient analysis varied from test to test, depending on the principal objectives of the tests. This fact is important to recognize when interpreting the plots. The pumping boreholes, total number of observation sections included, number of responding observation sections and number of analysed observation sections in the different interference tests are shown in Table 3-2.

According to Table 2-2, T_o and S_o were estimated from a total of 86 observation sections (out of 94 responding observation sections) in the two Laxemar interference tests while only 24 sections (out of 134 responding sections) were analysed for these parameters in the two Forsmark tests. As discussed above, the observation sections in the Forsmark tests selected for transient analysis are likely to contain a higher percentage of sections located in interpreted deformation zones compared to the tests in Laxemar.

Furthermore, the main hydrogeological conditions are different at the two sites. In Forsmark, several high-transmissive sub-horizontal deformation zones occur with sparsely fractured rock in between. The Laxemar site is more dominated by sub-vertical deformation zones separated by less fractured rock. This implies that (observation) boreholes in Forsmark may more frequently penetrate interconnecting sub-horizontal, extensive deformation zones, also at long distances from the pumping borehole. The above facts should be born in mind when interpreting the diagnostic diagrams presented below.

In all scatter plots, a (logarithmic) regression line for all the data at each site is included although the correlation coefficient is low in some cases. The parameter denotations used in the diagnostic plots and their definitions are described below. As discussed in Section 2.2, the estimated transmissivity T_o from standard test analyses generally represents the effective transmissivity in heterogeneous media. The estimated storativity S_o and hydraulic diffusivity T_o/S_o from standard analysis are denoted *apparent* storativity and *apparent* hydraulic diffusivity respectively for heterogeneous media.

T_o = estimated (effective) transmissivity of observation section from interference tests.

T_{osh} = estimated (cumulative) transmissivity of observation section from single-hole tests.

S_o = estimated (apparent)storativity of observation section from interference test.

T_o/S_o = estimated (apparent) hydraulic diffusivity of observation section from interference test.

Index 1 = response Index 1 based on the estimated time lags in the observation sections, see Equation 3-1. Index 1 is assumed to indicate the connectivity between the pumping borehole and the actual observation section.

r_s = 3D (Euclidian) distance between the (midpoints of) pumping borehole and observation section.

4.2 Transmissivity plots

4.2.1 Estimated transmissivity of observation sections from interference tests and single-hole tests

Figure 4-1 shows the correlation of estimated transmissivity T_o of observation sections versus the corresponding (cumulative) transmissivity T_{osh} of the same sections as determined from previous single-hole tests. The results fromthe selected interference tests at Forsmark and Laxemar (test data are separated by different colours) are shown in a log-log diagram. Although the match length-wise between the observation sections from the interference tests and single-hole tests it not always identical all high-transmissive features are consistent.

Figure 4-1 (especially the single-hole tests) clearly demonstrates the strong heterogeneity of the rock (large tansmissiity range) at both sites although the data from Forsmark may be more biased to observation sections in (sub-horizontal) deformation zones implying a more uniform nature. For ideal hydraulic tests in a perfectly homogeneous and isotropic formation the data points should fall on a straight line with a slope of 1:1. However, in this case the slope of the estimated (logarithmic) regression lines is rather flat with approximately the same slope for both Forsmark and Laxemar data, indicating heterogeneity.

While the range of most T_o values on the Y-scale generally is c. 2 orders of magnitude (except a few outliers) the total range of the T_{osh} values on the X-axis is c. 6 orders of magnitude. The lower measurement limit for the single-hole tests is c. $3 \cdot 10^{-9}$ m^2/s which means that some of the T_{osh}-values are at, or below, this limit, see Section 2.2.5. Thus, for a lower measurement limit of these values, the lower values of T_{osh} along the X-axis might have been lower.

As discussed above, data from the interference tests in Forsmark and Laxemar represent different populations regarding the selection of observation sections for transient analysis. The estimated transmissivities from the interference tests in Forsmark may in many cases be dominated by sub-horizontal deformation zones with increased and more uniform transmissivity.

Regarding the estimated transmissivities from the two tests at Laxemar (HLX27 and HLX28), most of the T_o-values (except 4 data points) from the observation sections are within c. 1–2 orders of magnitude while the range for the T_{osh} values from single-hole tests is c. 6 orders of magnitude. The latter circumstance demonstrates the strong heterogeneity of the rock. The estimated transmissivities from the Forsmark tests (HFM14 and KFM02B) are probably biased towards higher values with more narrow range for the reasons discussed above. Most T_o values in Forsmark (except the two most extreme values) are within 1 order of magnitude while the T_{osh}-values are within c. 3 orders of magnitude.

Figure 4-1 also indicates that the estimated T_o values from the respective interference test represent some kind of average (effective) transmissivity values of the entire rock volume within the radius of influence. On the other hand, the transmissivity values from single-hole tests are assumed to represent more local values adjacent to the actual sections. These observations are in good agreement with the results of e.g. Wu et al. (2005) regarding the effective transmissivity in a heterogeneous aquifer as discussed in Chapter 3.

It is important to recall that estimated transmissivity values of observation sections from standard methods for interference tests are based on the assumption that the flow rate to the pumping borehole is evenly (radially) distributed throughout the homogeneous media. Thus, with this assumption, the transmissivities of the observation sections estimated from standard analysis may be expected to be rather uniform. However, in heterogeneous media this assumption of flow rate may not be valid. Due to th assumption of uniform flow rate, the variability of estimated transmissivity from standard methods will (apparently) be relatively small for interference tests in heterogeneous media. This fact is evident for the selected interference tests in Forsmark and Laxemar.

4.2.2 Transmissivity ratio T_o/T_{osh} versus connectivity Index 1

Figure 4-2 shows the transmissivity ratio T_o/T_{osh} for the same observation sections as shown in Figure 4-1 versus estimated connectivity Index 1 defined by Equation (2-1). The transmissivity ratio represents the deviation (order of magnitude) between the estimated transmissivity of the observation sections from the interference tests and the corresponding transmissivity from single-hole tests, respectively. As

discussed above, the connectivity Index 1 is based on the estimated response (lag) times after start of pumping until a certain response (s = 0.1 m) is observed in the actual observation sections. Connectivity Index 1 is directly related to the hydraulic diffusivity (T/S) of the sections, see Section 2.2.3.

Figure 4-2 shows that the transmissivity ratio T_o/T_{osh} ranges more than 5 orders of magnitude but most values are within 4 orders (1–10,000). Most values are above 1 (a ratio of 1 would correspond to ideal tests in a perfect homogeneous aquifer with $T_o = T_{osh}$) but a few values are below 1 for sections with estimated, high single-hole transmissivities with some uncertainty. These observations again indicate that T_o in general, represents some kind of increased, effective volume- averaged transmissivity of the rock volume within the entire radius of influence rather than the local transmissivity of the rock near the actual observation section (or the specific flow paths between the pumping borehole and observation borehole) due to the assumption of a homogeneous aquifer and evenly distributed flow rate by standard analysis methods. However, if an observation borehole section is located within the same deformation zone as the pumping borehole the estimated values on T_o and T_{osh} will be close, (more homogeneous test conditions).

Figure 4-2 (weakly) indicates that the calculated transmissivity ratio tends to be higher for observation sections with weak hydraulic connection (low Index 1) to the pumping borehole (and vice versa), both for the Forsmark and Laxemar sites. This tendency, which probably would have been even more emphasized if transient evaluation also was performed for a higher number of responding sections with weaker responses (cf. Table 2-2), most likely depends on the application of standard well test analysis methods (e.g uniform flow) for tests in heterogeneous (crystalline) rock as discussed above. For observation sections with good hydraulic connection to the pumping borehole (high values on connectivity Index 1), the regression lines seem to approach $T_o/T_{osh} = 1$ for both sites, as would be expected in a perfectly homogeneous formation.

Figure 4-2 also shows that the deviation between T_o and T_{osh} is higher at the Laxemar site (higher ratio) which may, at least partly, be due to the different criteria used by the selection of observation sections for transient analysis at the two sites as discussed above (c.f. Table 2-2) and the overall differences in hydrogeological conditions at the two sites. For example, most of the selected sections (6) from the interference test in HFM14 in Forsmark have rather high values on connectivity Index 1 and thus lower deviations of transmissivity, possibly reflecting the presence of high-transmissive subhorizontal deformation zones at Forsmark with increased connectivity. The slopes of the (logarithmic) regression lines are however rather similar for both sites.

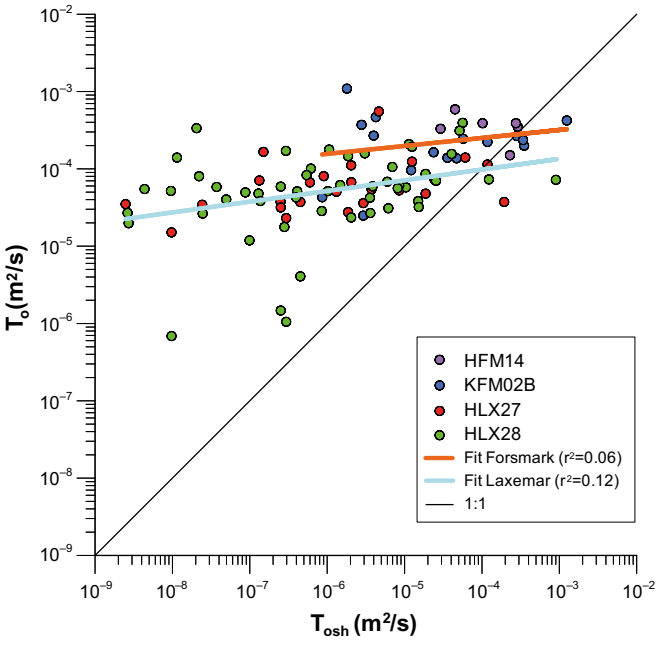

Figure 4-1. *Scatter plot of transmissivity estimated from observation sections (T_o) of the four selected interference tests in Laxemar and Forsmark versus the estimated (cumulative) transmissivity from single-hole tests (T_{osh}) in the corresponding sections . The calculated regression lines for the tests at Forsmark and Laxemar together with the 1:1 correlation line are also shown.*

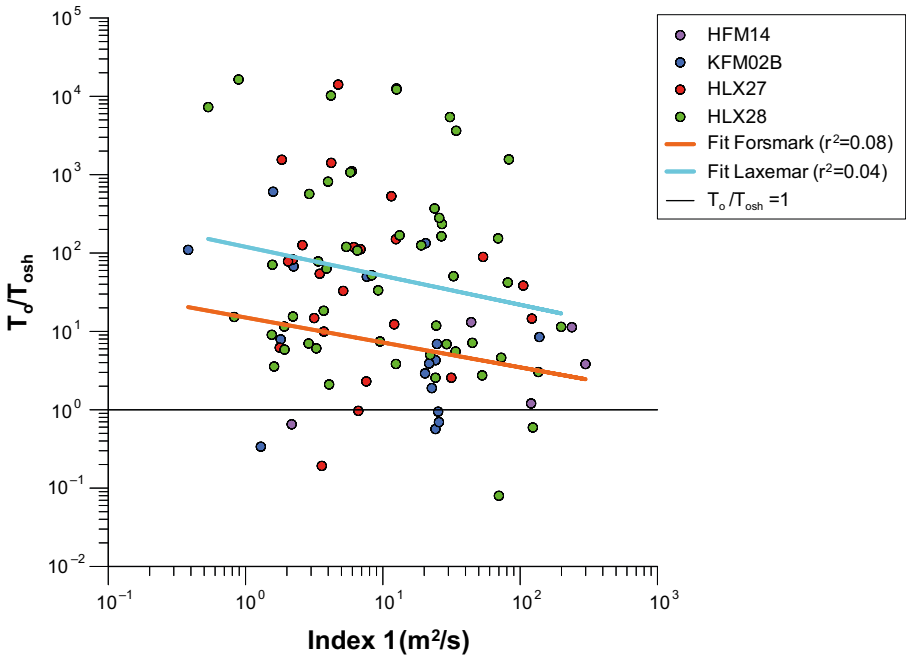

Figure 4-2. *Scatter plot of the calculated ratio of transmissivity for observation sections (T_o) from interference tests and single-hole tests (T_{osh}), respectively versus connectivity Index 1 from the four selected interference tests together with fitted regression lines for the tests at Laxemar and Forsmark, respectively, and the limiting line representing $T_o = T_{osh}$..*

4.2.3 Transmissivity ratio T_o/T_{osh} versus distance r_s

In Figure 4-3, the transmissivity ratio T_o/T_{osh} for the same observation sections as in Figure 4-1 and Figure 4-2 is plotted versus the Euclidian (3D) distance between the pumping borehole and the observation sections. The purpose is to see if the deviation between estimated transmissivities from the interference tests and single-hole tests, possibly, may be reflected by their distances from the pumping borehole.

Figure 4-3 indicates no clear correlation between the ratio T_o/T_{osh} and distance for the actual tests although there is a weakly increasing trend for the tests in Laxemar indicating a slight increase of the transmissivity ratio with distance. Although this indication is very uncertain, it may be due to the fact that a larger number of observation sections was analysed at Laxemar, also at long distances which may be less hydraulically connected to the pumping borehole, e.g. due to the absence of sub-horizontal zones. On the other hand, the presence of sub-horizontal zones in Forsmark may increase the hydraulic connection at longer distances in this site.

The variability of T_o/T_{osh} is very high (especially in Laxemar) and most distances to the pumping boreholes are concentrated within slightly more than one order of magnitude (100–1,000 m). However, as discussed above, a more clear tendency to increasing values of T_o/T_{osh} with distance (higher deviation of transmissivity) could possibly develop if all responding sections (i.e. also sections with weaker responses at long distances) are included in the transient evaluation of the tests, cf. Table 2.2.

4.2.4 T_o versus distance r_s

In Figure 4-4, the estimated transmissivities T_o for the analysed observation sections from the interference tests are plotted versus the Euclidian (3D) distance between the pumping borehole and the observation sections. This plot is similar to the plot in the previous figure. The purpose is to see whether the magnitude of the estimated transmissivity values of the sections possibly may be reflected by their associated distances from the pumping borehole, e.g. due to effects of heterogeneity.

Figure 4-4 indicates a weak, apparent decrease with distance for the data from Laxemar but the correlation coefficient is low and the variability of the estimated transmissivity is high. In particular, a few low transmissivity values related to the test in HLX28 seem to have a large impact on the correlation. In addition, most of the recorded distances are concentrated within slightly more than one order of magnitude (c. 100–1,000 m).

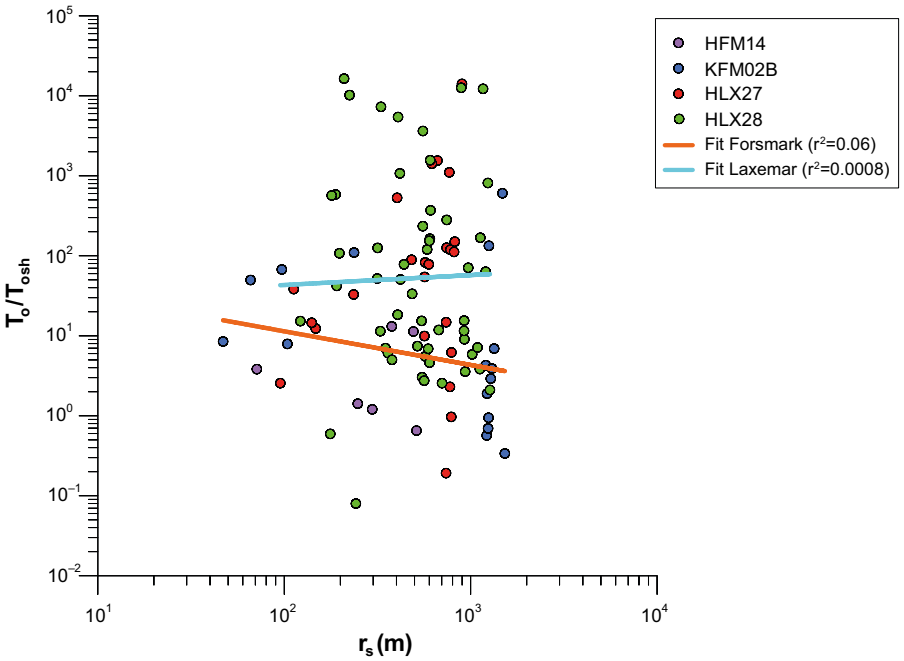

Figure 4-3. *Scatter plot of the estimated ratio of transmissivity for observation sections (T_o) and single-hole tests (T_{osh}), respectively versus distance from the pumping borehole for the selected interference tests together with fitted regression lines for the tests at Laxemar and Forsmark.*

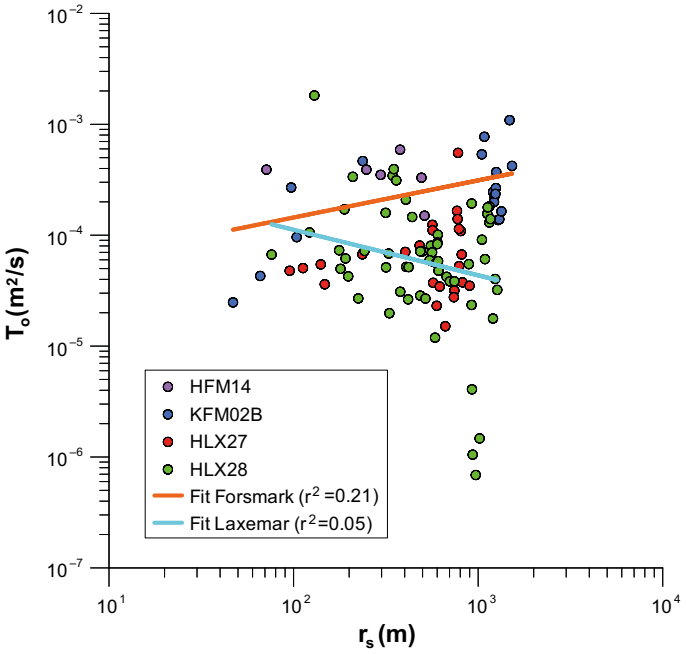

Figure 4-4. *Scatter plot of the estimated transmissivity for observation sections (T_o) versus distance from observation section to the pumping borehole for the four selected interference tests together with fitted regression lines for the tests at Laxemar and Forsmark.*

For the tests in Forsmark, the regression line indicates slightly increasing transmissivities with distance which may possibly reflect the presence of the extensive, high-transmissivity sub-horizontal deformation zones at this site. However, the population from Forsmark is dominated by data from the test in KFM02B which may not be representative in this respect. In addition, the regression lines at both sites may be affected by uncertainties in the transient evaluations, particularly for observation sections at long distances (small drawdown in combination with tidal effects). Consequently, the variability of estimated T_o is quite high at long distances which makes the regressions very uncertain.

4.3 Storativity plots

4.3.1 Storativity S_o versus connectivity Index 1

In the figures below, the estimated storativity and hydraulic diffusivity of the analysed observation sections from the selected interference tests are denoted apparent storativity and apparent hydraulic diffusivity as discussed in Section 3.2. In Figure 4-5 the estimated storativity S_o from the analysed interference tests for the same observation sections as in Figure 4-1 through Figure 4-4 are plotted versus connectivity Index 1. As before, this index is assumed to reflect the hydraulic connection (and hydraulic diffusivity) between the pumping borehole and observation sections. Increasing values of connectivity Index 1 correspond to increased hydraulic connection.

Figure 4-5 shows a clear (inverse) correlation between S_o and connectivity Index 1, both for Forsmark and Laxemar data. The apparent storativity decreases with increasing Index 1, i.e. increasing hydraulic connectivity between the pumping borehole and the observation sections. Thus, the apparent storativity seems to reflect the hydraulic connection between the boreholes. This fact is in agreement with the results of e.g. Wu et al. (2005) and Knudby and Carrera (2006) as discussed above.

Finally, the total variability of S_o is c. 3 orders of magnitude, ranging from c. $1 \cdot 10^{-3}$ to $1 \cdot 10^{-6}$ (with the exception of one outlier). The variability of estimated S_o seems to be higher than that observed for the (effective) transmissivity T_o in Figure 4-1. Thus, the estimated storativity seems to be more affected by heterogeneity than transmissivity. This is also in good agreement with the above two references.

Finally, the regression lines for S_o versus Index 1 indicate slightly lower apparent storativities at Forsmark, probably reflecting the hydrogeological conditions (e.g. high-transmissive deformation zones with improved hydraulic connection and lower apparent storativity) at this site.

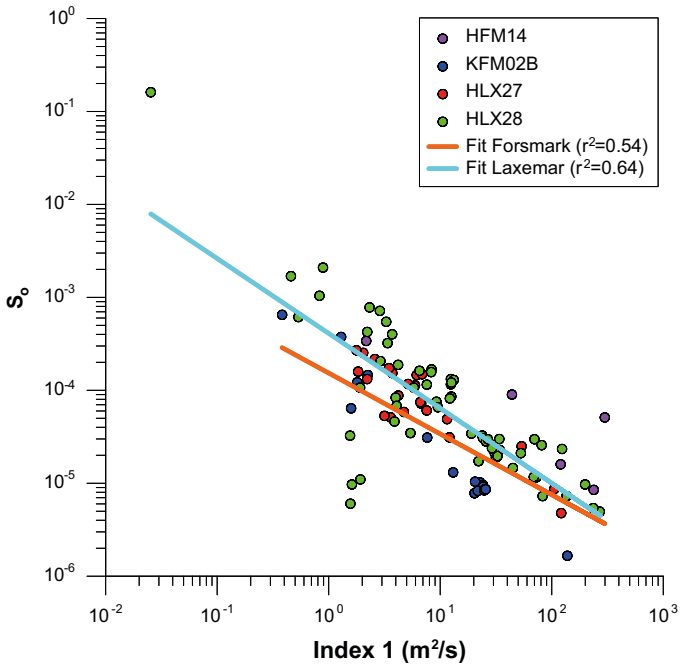

Figure 4-5. *Scatter plot of the estimated storativity for observation sections (S_o) versus connectivity Index 1 for the four selected interference tests together with fitted regression lines for the tests at Laxemar and Forsmark.*

4.3.2 Storativity S_o versus single-hole transmissivity T_{osh}

In Figure 4-6, the estimated (apparent)storativity S_o from the selected interference tests for the same observation sections as shown in Figure 4-5 is plotted versus T_{osh}, i.e. the estimated (cumulative) transmissivity of the same observation sections determined from previous single-hole tests. The single-hole transmissivity is assumed to represent the local properties of the rock close to the observation sections.

As might be expected, Figure 4-6 indicates that there is virtually no correlation at all between S_o and $T_{osh.}$ This means that estimated S_o of the observation sections from the interference tests depends very little on the magnitude of the local transmissivity of the observation sections. This fact strengthens the results from Figure 4-5, i.e. S_o depends much more on the hydraulic connection between the pumping borehole and the observation sections than on the local transmissivities of these sections. Moreover, as indicated in Figure 4-5, the regression lines indicate slightly lower apparent storativities for the tests at Forsmark than for the tests at Laxemar.

4.3.3 Storativity S_o versus distance r_s

In Figure 4-7 the estimated apparent storativity S_o for the same observation sections as in Figure 4-6 are plotted versus the Euclidian (3D) distance between the pumping borehole and the observation sections. The purpose is to see if the estimated apparent storativity values of the sections possibly may be reflected by their distances from the pumping borehole.

Figure 4-7 indicates a weak decrease with distance for the data for the selected interference tests from both Forsmark and Laxemar but the correlation coefficient is low and the variability of the apparent storativity is high. In addition, the distances are concentrated to within slightly more than one order of magnitude (c. 100–1,000 m). As before, the regression lines indicate that the apparent storativity is lower for the tests in Forsmark than in Laxemar.

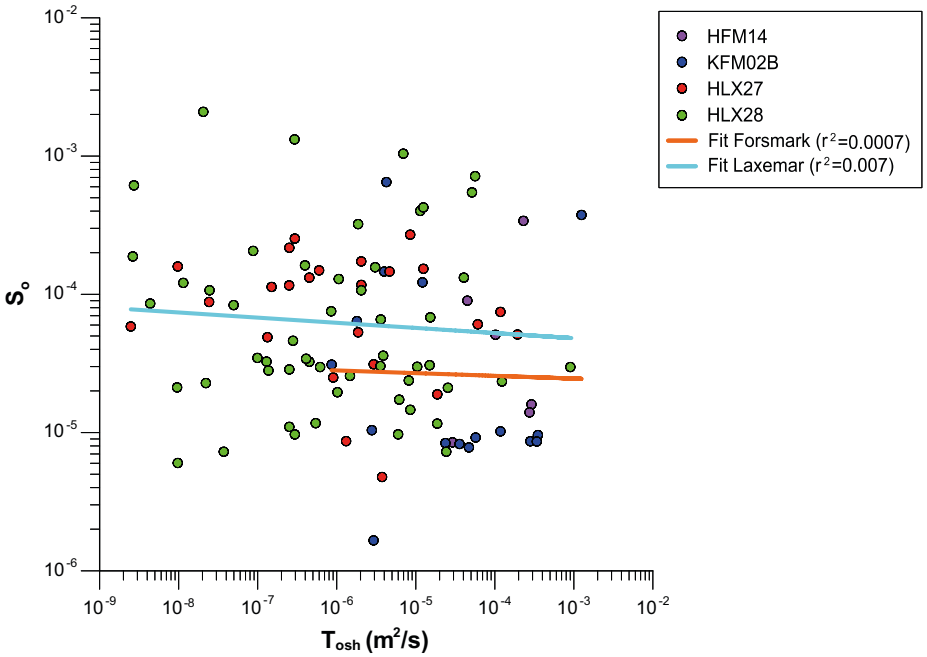

Figure 4-6. *Scatter plot of the estimated storativity for observation sections (S_o) versus estimated transmissivity of the sections from single-hole tests (T_{osh}) for the four selected interference tests together with fitted regression lines for the tests at Laxemar and Forsmark.*

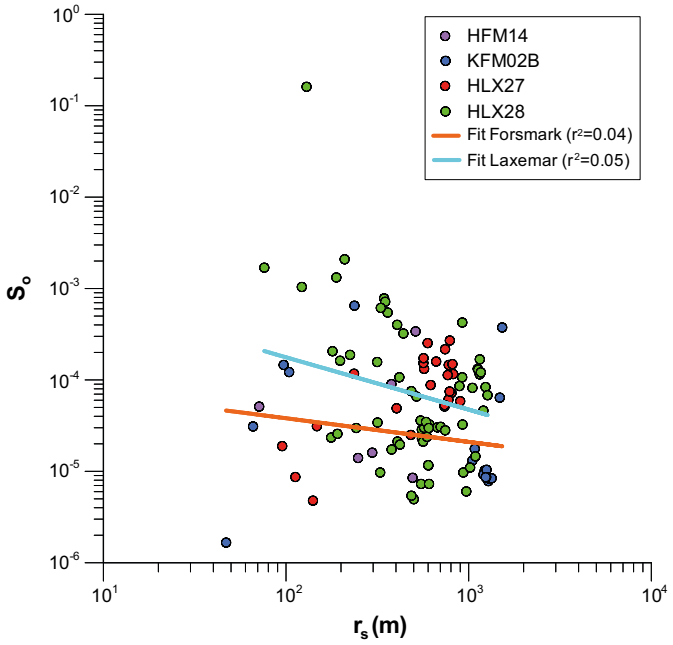

Figure 4-7. *Scatter plot of the estimated apparent storativity for observation sections (S_o) versus the distance from the pumping borehole from the four selected interference tests together with fitted regression lines for the tests at Laxemar and Forsmark.*

4.4 Hydraulic diffusivity plots

4.4.1 Hydraulic diffusivity T_o/S_o versus connectivity Index 1

In Figure 4-8, the estimated, (apparent) hydraulic diffusivity T_o/S_o for the selected interference tests for the same observation sections as in analysed preceding sections is plotted versus connectivity Index 1. As before, this index is assumed to reflect the hydraulic connection (and hydraulic diffusivity) between the pumping borehole and observation sections.

As expected, Figure 4-8 shows a clear (positive) correlation between T_o/S_o and connectivity Index 1, both for the tests at Forsmark and Laxemar. The apparent hydraulic diffusivity increases with increasing Index 1, i.e. increased hydraulic connectivity between the pumping borehole and the observation sections. Thus, the estimated, apparent hydraulic diffusivity seems to be a good indicator of the hydraulic connection between the pumping and observation boreholes. This conclusion is in good agreement with the findings by e.g. Knudby and Carrera (2006) as discussed in Section 3.3. This fact also implies that S_o is well (inversely) correlated to connectivity Index 1 (see Figure 4-6) and thus also inversely correlated to the apparent hydraulic diffusivity, see Figure 4-9. This fact is in agreement with the results of e.g. Meier et al. (1998) and Wu et al. (2005). Thus, it is concluded that Index 1 seems to be a good indicator of the hydraulic connectivity between the pumping borehole and observation sections.

As discussed above, the regression lines indicate higher apparent hydraulic diffusivity (a result of lower estimated storativity) for the tests in Forsmark. In particular, the estimated hydraulic diffusivity T_o/S_o from the interference test in KFM02B in Forsmark is significantly higher than for the other interference tests. This fact may possibly be due to that this test was performed in a closed borehole section in the pumping borehole as opposite to all other tests which may lead to improved hydraulic connection to the analysed observation borehole sections.

Finally, the variability of T_o/S_o is lower in Forsmark (range c.0.5–50 m^2/s). At Laxemar, T_o/S_o ranges between c. 0.01 to c. 10 m^2/s. The number of analysed observations was however higher from Laxemar. See Table 2-2.

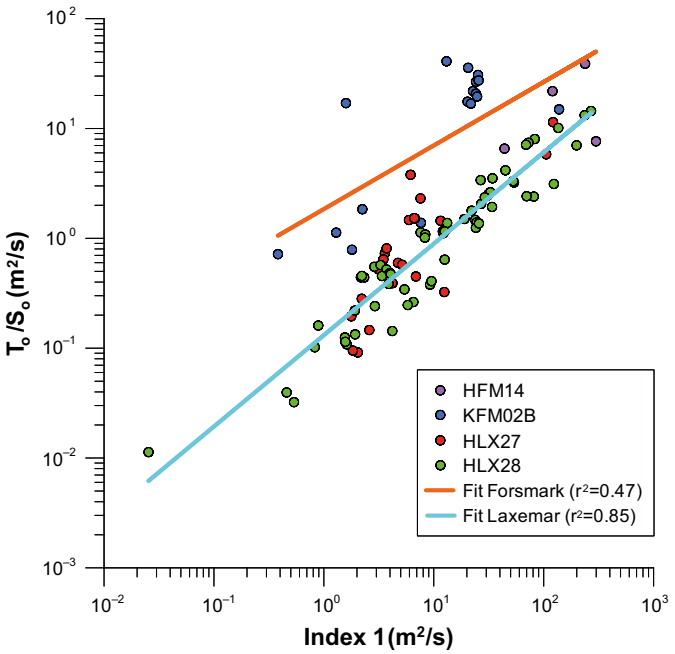

Figure 4-8. *Scatter plot of the estimated apparent hydraulic diffusivity for observation sections (T_o/ S_o) versus connectivity Index 1 for the four selected interference tests together with fitted regression lines for the tests at Laxemar and Forsmark.*

4.4.2 Hydraulic diffusivity T_o/S_o versus storativity S_o

In Figure 4-9, the estimated, (apparent) hydraulic diffusivity T_o/S_o from the same observation sections as above is plotted versus the apparent storativity S_o. As found in previous diagrams, a clear correlation exists between the apparent hydraulic diffusivity and S_o. The apparent hydraulic diffusivity is inversely correlated to S_o (and thus directly correlated to $1/S_o$). These results are consistent with the previous observations in Figure 4-5 and Figure 4-8.

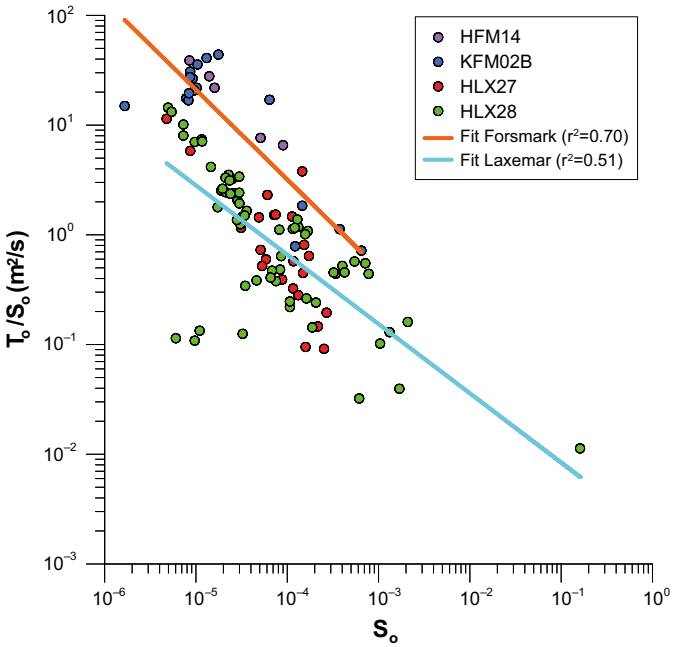

Figure 4-9. *Scatter plot of the estimated apparent hydraulic diffusivity for observation sections (T_o/ S_o) versus apparent storativity (S_o) for the four selected interference tests together with fitted regression lines for the tests at Laxemar and Forsmark.*

5 Hydraulic tomography for interference tests in heterogeneous media and selected case studies

5.1 General

According to the current literature review on analysis of hydraulic interference tests in heterogeneous media, hydraulic tomography was proposed in Chapter 2. No alternative method with the same potential was identified in the literature review. In this chapter a brief introduction of the basic principles behind hydraulic tomography is presented. Selected case studies on the application of hydraulic tomography in synthetic and real heterogeneous media are presented in Appendix A2. Finally, some guidelines for cost-effective hydraulic tomography are presented. For more details on the theory behind hydraulic tomography is referred to Yeh and Liu (2000) and Zhu and Yeh (2005) and other referenced papers in this report.

In the following, the term hydraulic tomography is mainly used for the analysis effort of hydraulic interference tests. However, the analysis requires that the interference tests are performed within the same array of boreholes by sequentially switching the sink/source sections within the same observation network.

The main advantage of hydraulic tomography compared to standard methods is that it is possible to estimate the spatial distribution of the hydraulic parameters of heterogeneous media. A series of hydraulic interference tests in the same array of boreholes and test sections, preferably combined with supporting data from other tests or measurements, e.g. single-hole tests, tracer tests, dilution tests, geophysical surveys etc, are needed for a complete hydraulic tomography survey. In addition, the reciprocity of the tested system may also be investigated. i.e. comparison of mutual responses between a certain pair of interchanged sink-source sections in two boreholes.

The performance and subsequent hydraulic tomography analysis of the interference tests thus need to be compatible. However, it is also quite possible to perform enhanced hydraulic tomography analysis (HT) of suitable, previously performed hydraulic interference tests and associated tests. For example, such subsequent analysis may be relevant in underground excavations in which a large number of short-time interference tests have been performed in the same array of borehole sections in combination with other kind of supporting tests.

5.2 Brief description of the methodology

Hydraulic tomography is, in the most simplified terms, analysis of a series of hydraulic cross-hole (interference) tests. A heterogeneous aquifer is stressed by pumping water from or injecting water into a well, and monitoring the pressure responses at other boreholes. A set of pressure responses yields an independent set of equations. Sequentially switching the pumping or injection locations, without installing additional wells, results in a large number of responses caused by stresses at different locations and, in turn, a large number of independent sets of equations. This large number of sets of equations makes the inverse problem (i.e. using aquifer stress and associated responses to estimate the spatial distribution of hydraulic parameters) better posed. Thus, the subsequent estimates of hydraulic parameters of a heterogeneous aquifer will more approach reality in comparison to standard test analysis methods for a homogeneous aquifer.

Hydraulic tomography (HT) thus utilizes data from sequential cross-hole hydraulic tests (series of cross-hole tests), followed by numerical inversion of all test data simultaneously (or sequentially) in order to estimate the spatial distribution of the hydraulic properties of heterogeneous media. With the HT method, data from multiple observation intervals in a number of wells or boreholes may be analysed but the wells/boreholes may also be open without isolated intervals. Sequential tests are conducted at selected intervals (sections) within the observation network. Water is withdrawn or injected, in general with a constant flow rate, from/to a selected active interval or borehole. Pressure responses are monitored in other intervals in this well and in other observation wells or boreholes, thus producing a set of pressure response data.

In essence, a set of pressure data from one pressure disturbance during a certain test corresponds to an x-ray snapshot of subsurface heterogeneity at the disturbance location. Repeating the test using different active test intervals is the same as taking additional x-ray snapshots of heterogeneity at different locations and in different directions. The geostatistical (inverse) model is an algorithm that synthesizes all the snapshots to estimate the three-dimensional distribution of a certain hydraulic parameter (e.g. hydraulic conductivity and specific storativity) within the studied area and rock volume. A compilation of different geostatistical models used for HT analysis is presented in Table 5.1.

According to Wu et al. (2005), a heterogeneous aquifer can under certain assumptions be treated as a spatially homogeneous medium with uniform "effective" values of transmissivity and storativity for the equivalent homogeneous aquifer. This concept is applied in hydraulic tomography analysis together with the classic principles of flow based on the diffusivity equation.

Yeh et al. (1995) developed a successive linear estimator (SLE) which is essentially based on cokriging. Yeh and Liu (2000) developed a sequential inverse method, which is refered to as the Sequential Successive Linear Estimator (SSLE) which is an extension of the SLE. This approach can be applied in hydraulic tomography for the interpretation of cross-hole pumping tests under *steady-state* conditions. The inverse model assumes a steady flow field and Ln(K) is treated as a stationary stochastic process. The model also assumes that the mean, variance and correlation structure of the K field is known a priori. This approach combines the traditional geostatistical approach and general governing flow principles to interpolate and extrapolate at locations where samples are not available. As a consequence, the SSLE yields more realistic K-estimates than kriging (which does not consider general principles of flow) and deterministic/zone-based or stochastic inverse modelling approaches that use only one pumping or injection data set at a time.

The SSLE inverse model algorithm is essentially composed of two parts. Firstly, the SLE is used for analysis of each cross-hole test. The estimator begins by cokriging the initial estimate of the effective K and observed heads in one test to create a cokriged map of Ln(K). A linear estimator, based on the differences between simulated and observed head values, is then successively used to improve the estimated map. Secondly, the hydraulic head data sets from each successive test are used sequentially (one by one) instead of including them simultaneously in the inverse model (SSLE). The sequential approach uses the estimated K field and covariances, conditioned on previous data sets as prior information for the next estimation based on a new data set. This process continues until all data sets are fully utilized.

According toYeh and Liu (2000), the main advantage of sequentially including cross-hole test data is its computational efficiency. Theyshowed that accurate hydraulic conductivity distributions can be obtained by hydraulic tomography by data sets from numerically simulated cross-hole tests in synthetic heterogeneous aquifers. Zhu and Yeh (2005) extended this method to allow analysis of cross-hole tests under *transient* conditions (time series of head data) which made it possible to estimate both the transmissivity T- (or K) and the storativity S- (or specific storativity S_s) fields from hydraulic tomography.

According to Wu et al. (2005), steady-state hydraulic tomography produces many non-overlapping equations and the SSLE effectively solves the system of equations. In addition, interpretation of steady-state HT (using the estimator SSLE) is faster than that of transient HT. The difference between steady-state HT and transient HT was found to vary with sampling time and simulation time step. But steady-state head information is always influenced by boundary conditions that may be uncertain in many is situ situations (Illman et al. 2007). Therefore, the answer to the question regarding which data set is more effective may vary depending on the given situation.

Table 5-1. Different geostatistical estimators used for hydraulic tomography of cross-hole tests together with actual data sets.

Geostatistical estimator	Data set(s) used	Head conditions	Reference
SLE	A single cross-hole test	Steady-state	Yeh et al. (1995)
SSLE	Several cross-hole tests used in sequence	Steady-state	Yeh and Liu (2000)
		Transient	Zhu and Yeh (2005)
SimSLE	Several cross-hole tests used simultaneously	Transient	Xiang et al. (2009)

Recently, Xiang et al. (2009) developed an alternative estimator (SimSLE) for hydraulic tomography. Instead of incorporating data sequentially into the estimation as is done in SSLE, a simultaneous successive linear stochastic estimator (SimSLE) is developed to include all drawdown data from different cross-hole tests during a HT survey simultaneously to estimate hydraulic properties of aquifers. Simultaneous inclusion of the data offers some advantages over the SSLE approach but requires large computational efforts (see the actual case study below).

5.3 Case studies of hydraulic tomography

In Appendix 2, short reviews of selected general papers of hydraulic tomography are firstly presented. Secondly, a few selected case studies of special interest (mainly field tests) and studies describing the methodology of hydraulic tomography studies are presented in more detail. In Table 5-, a summary of the case studies of hydraulic tomography described in Appendix 2 is presented. The case studies are labelled by the title of the associated reference.

Table 5-2. Summary of selected case studies of hydraulic tomography (HT).

Case study	Type of data used	Type of heterogeneous aquifer	Type of HT/estimator	Performance assessment of HT analysis	Reference
1	Field data	2D alluvium aquifer	Steady-state and transient/SSLE	The estimated K fields were compared with results from a tracer test, single-hole permeameter tests and cross-hole borehole radar.	Bohling et al. (2007)
2	Synthetic	2D	Steady-state/SSLE	Scatter plot of simulated and observed heads in sandbox from simulated, independent pumping test. Statistical measures L1 and L2.	Illman et al. (2008)
3	Field data from 6 pumping tests	2D alluvial aquifer	Transient/SSLE	Estimated T and S-fields were compared with assumed in-homogeneities and geological evaluations of the aquifer.	Straface et al. (2007)
4	Synthetic	2D cross section with fracture zones	Transient/SSLE	Statistical measures L1, L2 and correlation. Similarity analysis. Visual comparison of estimated K and Ss-fields.	Hao et al. (2008)
5	Field data from 2 cross-hole tests	3D in fractured granite in underground research site	Transient/SSLE	Scatter plot of estimated and measured heads, comparison to known fault zones and induced groundwater level responses during earth quakes.	Illman et al. (2009).
6	Synthetic and laboratory data	2D confined and laboratory sandbox	Transient/SimSLE	Statistical measures L1, L2 and correlation. Similarity analysis. Scatter plot of estimated and measured heads.	Xiang et al. (2009)
7	Synthetic	2D confined (cross section)	Steady-state/SSLE	Statistical measures L1, L2 and correlation. Scatter plots of true K and estimated K-fields.	Ni et al. (2009)

6 Summary and suggestions for further studies

The results of the literature survey of possible alternatives to well test analysis in heterogeneous media together with the case studies presented above suggest that hydraulic tomography is a promising new analysis method for hydraulic interference tests in heterogeneous media, as an alternative to standard analysis methods based on an equivalent homogeneous medium. However, more testing of the method in heterogeneous media with large variations and contrasts of the hydraulic parameters is probably needed. Some of the conclusions made by the authors of the selected, case studies of hydraulic tomography (HT) are summarized below. In additions, some conclusions are also drawn from the detailed analysis of the interference tests in Forsmark and Laxemar discussed in Chapter 4.

6.1 Conclusions from the case studies of hydraulic tomography

- Hydraulic tomography reveals detailed hydraulic heterogeneity of aquifers, which can be used to better predict different flow (and solute transport) scenarios in contrast to standard analysis of pumping tests based on effective hydraulic parameters of an equivalent homogeneous aquifer.
- Simultaneous use of all drawdown curves from observation wells during pumping tests in the analysis (SimSLE) constitutes some advantages over the previous sequential approach (SSLE) but suffers from the need for large computational resources.
- If the head data are affected by noise, the SNR (Signal-to-Noise Ratio) is a useful measure of the quality of the data in the HT analysis. Wavelet de-noising is recommended to correct the data from such noise. In addition, use of a stop convergence criterion in SimSLE avoids over-interpretation of noisy data.
- Estimated hydraulic conductivity and specific storage fields from hydraulic tomography have indicated that the classic diffusivity equation for groundwater flow may accurately predict the temporal and spatial distributions of drawdown induced by an independent pumping event in the aquifer. On the other hand, the classic diffusivity equation for groundwater flow may yield less satisfactory results when equivalent homogeneous properties of the aquifer are used.

Numerical assessments on the cross-hole test strategy showed that more pumping events (cross-hole tests) will generally lead to more accurate estimations of K fields of the aquifer. However, with a sufficient number of direct K-measurements (from single-hole tests in the observation sections) included as supporting data, more pumping events had relatively little impact on the final K estimation from HT.

Pumping locations which provided higher head changes (higher pumping rates) resulted in more accurate estimation of K fields. Thus, the pumping locations should be located in high K zones in the aquifer to maximize the head information from observation wells.

From the case study by Ni et al. (2009) it was concluded that the optimal number of pumping events (interference tests) for the synthetic 2D aquifer is 2 to 3, located in high K zones. This conclusion is however maybe not valid in general and for 3D hydraulic tomography. Finally, the appropriate distances from the pumping hole to observation boreholes are suggested to be less than one-third of the ln(K) correlation length in the X-direction.

6.2 Conclusions from the interference tests in Forsmark and Laxemar

The diagnostic scatter plots of estimated hydraulic parameters, based on standard analysis, from the selected interference tests from Forsmark and Laxemar showed that the range of the estimated transmissivities from the interference tests in general, varied within c. 2 orders of magnitude while the corresponding range of transmissivity from single-hole tests was c. 6 orders of magnitude. This fact

clearly demonstrates the strong degree of heterogeneity of the rock tested. The transmissivities estimated from the interference tests represent some kind of mean (effective) transmissivity for the rock volume within the radius of influence of the tests. This fact is consistent with the results of the literature review of tests in heterogeneous media. In most cases, the estimated, effective transmissivity of the observation sections is higher than the transmissivity of the sections from single-hole tests. There is a tendency that the deviation between the two mentioned transmissivities increases for observation sections with decreased hydraulic connection to the pumping borehole which fact is assumed to reflect the heterogeneity of the rock.

A clear (inverse) correlation was demonstrated between the estimated apparent storativity of the observation sections and the connectivity of the sections to the pumping borehole. For example, for geometrically interconnected sections along the same deformation zones, low apparent storativities were generally estimated. Thus, contrary to estimated transmissivity, the estimated apparent storativity in heterogeneous media is likely to more represent the connectivity between the observation section and the pumping borehole, rather than the hydraulic properties of the media. This fact is also consistent with the literature review of tests in heterogeneous media. Thus, the designation *apparent* storativity is suggested in heterogeneous media.

As may be expected, virtually no correlation was found between the estimated apparent storativity of observation sections from interference tests and the estimated transmissivity of the sections from single-hole tests. This fact is likely to depend on the different representativity of the two parameters in heterogeneous rock, i.e. the transmissivity from short-time single-hole tests more represents the local conditions at the actual observation sections whereas the apparent storativity rather reflects their respective hydraulic connection to the pumping borehole.

A clear (positive) correlation between the estimated apparent hydraulic diffusivity T_o/S_o and connectivity Index 1, based on the response time of the observation section, was observed. The apparent hydraulic diffusivity increased with increasing Index 1, i.e. with increasing hydraulic connectivity between the pumping borehole and the observation sections. Thus, the estimated, apparent hydraulic diffusivity seems to be a good indicator of the hydraulic connection between the boreholes. As discussed above, this is also true for the estimated apparent storativity of the sections which is inversely correlated to the connectivity. Finally, good agreement was generally found between the estimated apparent hydraulic diffusivity from the hydraulic evaluation of the interference tests and that obtained from the analysis of response (lag) times of the observation sections. The conclusions from the diagnostic scatter plots presented above for the selected interference tests at Laxemar and Forsmark are consistent with the findings in the referenced papers in this report, see e.g Chapter 3.

6.3 Comparison of results fron Forsmark and Laxemar

The diagnostic scatter plots of estimated hydraulic parameters also indicated some general differences between the estimated parameter values at the two sites. However, the data material is too limited to make any firm conclusions of the results. The estimated transmissivities from the two tests at Forsmark were generally slightly higher than the transmissivities from Laxemar, also showing lower variability. In addition, the deviations between the estimated transmissivity of the observation sections from the interference tests and previous single-hole tests, respectively were slightly lower at Forsmark. Slightly lower storativities and higher apparent hydraulic diffusivities were estimated from Forsmark. However, it should be remembered that the selection of observation sections for transient analysis and the hydrogeological conditions differ at the two sites. In particular, the estimated values from Forsmark are likely to be reflected by the sub-horizontal deformation zones. In addition, the inherent hydraulic properties of the actual rock volumes tested during the selected interference tests may be different.

6.4 Proposal to test hydraulic tomography analysis on previous cross-hole tests

Based on the results of the case studies above, it is suggested to test the capability of hydraulic tomography for analysis of interference tests performed in crystalline rock at Forsmark or Oskarshamn, including Laxemar and the Hard Rock Laboratory (HRL) at Äspö. A proposal for suitable tests for application of hydraulic tomography at different test scales is presented in Part B of this report.

In hydraulic tomography analysis, data from several (and even mutually reciprocal) interference tests within the same observation borehole network is highly recommended. Thus, the large-scale hydraulic interference tests analysed in this report may, possibly, not be entirely suitable for hydraulic tomography analysis since only two tests were performed at each site at different locations and at different times with slightly different observation networks. Alternatively, previous interference tests from the Äspö Hard Rock Laboratory e.g. the True Block Scale project presented in Andersson et al. (2002) or TRUE-1 Completion in Nordqvist et al. (2014) would be good candidates for hydraulic tomography analysis, see Part B. Some potential problems for hydraulic tomography analysis of data from Äspö Hard Rock Laboratory would possibly be:

- High variability in estimated local T and S (or K and S_s) and high contrasts between hydraulic properties of deformation zones and adjacent wall rock. For example, single-hole tests in observation borehole sections have shown variations of 5–6 orders of magnitude or.
- Noise in the test data. Head data from interference tests are generally affected by both natural processes (e.g. precipitation, tidal effects, seawater level fluctuations etc) and external effects due to interference from other activities during the tests. This problem could possibly be overcome by selecting data sets with sufficiently high signal-to-noise ratios and compensate for tidal effects as discussed above by Xiang et al. (2009) in Case study 6 and Illman et al. (2009) in Case study 5.

As pointed out in the review of the case studies, cf. Chapter 5, it would be an advantage to include supporting data (including *soft information*) from other sources of information, eg. from single-hole hydraulic tests, tracer tests, groundwater flow measurements, flow logging and borehole geophysical surveys, including cross-hole radar and/or seismic data, in the hydraulic tomography, and not to mention existing integrated hydro-structural models of the area or its environs which could provide a useful *training map*.

References

SKB's (Svensk Kärnbränslehantering AB) publications can be found at www.skb.se/publications.

Andersson P, Byegård J, Dershowitz B, Doe T, Hermanson J, Meier P, Tullborg E-L, Winberg A (ed), 2002. Final report of the TRUE Block Scale project. 1. Characterisation and model development. SKB TR-02-13, Svensk Kärnbränslehantering AB.

Bohling G C, Butler J J, Zhan X, Knoll M D, 2007. A field assessment of the value of steady shape hydraulic tomography for characterization of aquifer heterogeneities. Water Resources Research 43. doi:10.1029/2006WR004932

Butler J J, 2008. Pumping tests for aquifer evaluation – time for a change? Ground Water 47, 615–617.

Butler J J, Liu W Z, 1993. Pumping tests in nonuniform aquifers: the radially asymmetric case. Water Resources Research 29, 259–269.

Dougherty D E, Babu D K, 1984. Flow to a partially penetrating well in a double-porosity reservoir. Water Resources Research 20, 1116–1122.

Enachescu C, Rahm N, 2007. Oskarshamn site investigation. Method evaluation of single-hole hydraulic injection tests at site investigations in Oskarshamn. SKB P-07-79. Svensk Kärnbränslehantering AB.

Gokall-Norman K, Ludvigson J-E, 2008. Forsmark site investigation. Large-scale interference test with borehole HFM14 used as pumping borehole, 2007. SKB P-07-228, Svensk Kärnbränslehantering AB.

Hantush M S, Jacob C E, 1955. Non-steady radial flow in an infinite leaky aquifer. American Geophysical Union Transactions 36, 95–100.

Hao Y, Yeh T-C J, Xiang J, Illman W A, Ando, K, Hsu K-C, Lee C-H, 2008. Hydraulic tomography for detecting fracture zone connectivity. Ground Water 46, 183–192.

Harrström J, Svensson T, Ludvigson J-E, 2007. Forsmark site investigation. Single-hole injection tests in borehole KFM12A. SKB P-07-121, Svensk Kärnbränslehantering AB.

Hjerne C, Nordqvist R, Harrström J, 2010. Compilation and analyses of results from cross-hole tracer tests with conservative tracers. SKB R-09-28, Svensk Kärnbränslehantering AB.

Illman W A, Liu X, Craig A, 2007. Steady-state hydraulic tomography in a laboratory aquifer with deterministic heterogeneity: multi-method and multiscale validation of hydraulic conductivity tomograms. Journal of Hydrology 341, 222–234.

Illman W A, Craig A J, Liu X, 2008. Practical issues in imaging hydraulic conductivity through hydraulic tomography. Ground Water 46, 120–132.

Illman W A, Liu X, Takeuchi S, Yeh T-C J, Ando K, Saegusa H, 2009. Hydraulic tomography in fractured granite: Mizunami Underground Research site, Japan. Water Resources Research 45. doi:10.1029/2007WR006715

Knudby C, Carrera J, 2006. On the use of apparent hydraulic diffusivity as an indicator of connectivity. Journal of Hydrology 329, 377–389.

Kruseman G P, de Ridder N A, 1990. Analysis and evaluation of pumping test data. Wageningen, The Netherlands: International Institute for Land Reclamation and Improvement.

Lindquist A, Hjerne C, Nordqvist R, Ludvigson J-E, Harrström J, Carlsten S, 2008a. Oskarshamn site investigation. Confirmatory hydraulic interference test and tracer test in Laxemar. SKB P-08-96, Svensk Kärnbränslehantering AB.

Lindquist A, Hjerne C, Nordqvist R, Byegård J, Walger E, Ludvigson J-E, Wass E, 2008b. Forsmark site investigation. Confirmatory hydraulic interference test and tracer test at drill site 2. SKB P-08-13, Svensk Kärnbränslehantering AB.

Lindquist A, Hjerne C, Nordqvist R, Wass E, 2008c. Forsmark site investigation. Large-scale confirmatory multiple-hole tracer test. SKB P-08-59, Svensk Kärnbränslehantering AB.

Ludvigson J-E, Hansson K, Rouhiainen P, 2002. Methodology study of Posiva difference flow meter in borehole KLX02 at Laxemar. SKB R-01-52, Svensk Kärnbränslehantering AB.

Ludvigson J-E, Jönsson S, Levén J, 2004. Forsmark site investigation. Hydraulic evaluation of pumping activities prior to hydro-geochemical sampling in borehole KFM03A – Comparison with results from difference flow logging. SKB P-04-96, Svensk Kärnbränslehantering AB.

Ludvigson J-E, Hansson K, Hjerne C, 2007. Forsmark site investigation. Method evaluation of single-hole hydraulic injection tests at site investigations in Forsmark. SKB P-07-80, Svensk Kärnbränslehantering AB.

Meier P M, Carrera J, Sánchez-Vila X, 1998. An evaluation of Jacob's method for the interpretation of pumping tests in heterogeneous formations. Water Resources Research 34, 1011–1025.

Moench A F, 1985. Transient flow to a large-diameter well in an aquifer with storative semiconfining layers. Water Resources Research 21, 1121–1131.

Ni C-F, Yeh T-C J, Chen J-S, 2009. Cost-effective hydraulic tomography surveys for predicting flow and transport in heterogeneous aquifers. Environmental Science & Technology 43, 3720–3727.

Nordqvist R, Byegård J, Hjerne C, 2014. Complementary tracer tests – SWIW, CEC and multi-hole reciprocal cross flow tests at the TRUE-1 site. TRUE-1 Continuation project. TRUE-1 Completion. SKB P-11-27, Svensk kärnbränslehantering AB.

Oliver D S, 1990. The averaging process in permeability estimations from well-test data. SPE Formation Evaluation 5, 319–324.

Oliver D S, 1993. The influence of nonuniform transmissivity and storativity on drawdown, Water Resources Research 29, 169–178.

Rouhiainen P, Sokolnicki M, 2005. Forsmark site investigation. Difference flow logging in borehole KFM06A. SKB P-05-15, Svensk Kärnbränslehantering AB.

Sánchez-Vila X, Meier P M, Carrera J, 1999. Pumping tests in heterogeneous aquifers: an analytical study of what can be obtained from their interpretation using Jacob's method. Water Resources Research 35, 943–952.

Straface S, Yeh T-C J, Zhu J, Troisi S, Lee C H, 2007. Sequential aquifer tests at a well field, Montalto Uffugo Scalo, Italy. Water Resources Research 43. doi:10.1029/2006WR005287

Streltsova T D, 1988. Well testing in heterogeneous formations. New York: Wiley.

Theis C V, 1935. The relation between lowering of the piezometric surface and the rate and duration of discharge of a well using groundwater storage. American Geophysical Union Transactions 16, 519–524.

Thur P, Jönsson S, Harrström J, Ludvigson J-E, 2009. Site investigation SFR. Hydraulic tests, flow logging and chemical sampling. Borehole HFR106. SKB P-09-54, Svensk Kärnbränslehantering AB.

Walger E, Jönsson S, Ludvigson J-E, 2007. Forsmark site investigation. Pumping tests and flow logging. Boreholes HFM36, HFM37 and HFM38. SKB P-07-22, Svensk Kärnbränslehantering AB.

Wu C-M, Yeh T-C J, Zhu J, Lee T H, Hsu N-S, Chen C-H, Sancho A F, 2005. Traditional analysis of aquifer tests: comparing apples to oranges? Water Resources Research 41. doi:10.1029/2004WR003717

Xiang J, Yeh T-C J, Lee C-H, Hsu K-C, Wen J-C, 2009. A simultaneous successive linear estimator and a guide for hydraulic tomography analysis. Water Resources Research 45. doi:10.1029/2008WR007180

Yeh T-C J, Gutjahr A L, Jin M, 1995. An iterative cokriging-like technique for ground-water flow modelling. Ground Water 33, 33–41.

Yeh T-C J, Liu S, 2000. Hydraulic tomography: development of a new aquifer test method. Water Resources Research 36, 2095–2105.

Yeh T-C J, Lee C-H, 2007. Time to change the way we collect and analyze data for aquifer characterization. Ground Water 45, 116–118.

Zhu J, Yeh T-C J, 2005. Characterization of aquifer heterogeneity using transient hydraulic tomography. Water Resources Research 41. doi:10.1029/2004WR003790

Appendix 1

Examples of transient evaluation of responses from the selected hydraulic interference tests

Descriptions of the test diagrams

In the test diagrams presented below the measured drawdown (blue) and its derivative (black) versus time in the pumping boreholes and a selected observation section is shown in log-log graphs for the interference tests in Forsmark and Laxemar. (For the test in HFM14 the drawdown derivative is green). In addition, the transient evaluation of the tests is shown by the red lines (simulated curves) of the drawdown and drawdown derivative. The estimated hydraulic parameters using the software AQTESOLV are shown besides the graphs.

For the test in HLX27 several drawdown curves with different type of drawdown responses (distinct and weak) in selected observation sections are shown in different colours.

Nomenclature in AQTESOLV:

T = transmissivity (m^2/s)

S = storativity (–)

K_Z/K_r = ratio of hydraulic conductivities in the vertical and radial direction (set to 1)

Sw = skin factor

r(w) = borehole radius (m)

r(c) = effective casing radius (m)

r/B = leakage coefficient (s^{-1})

b = thickness of formation (m)

A1.1 Interference test in HLX28

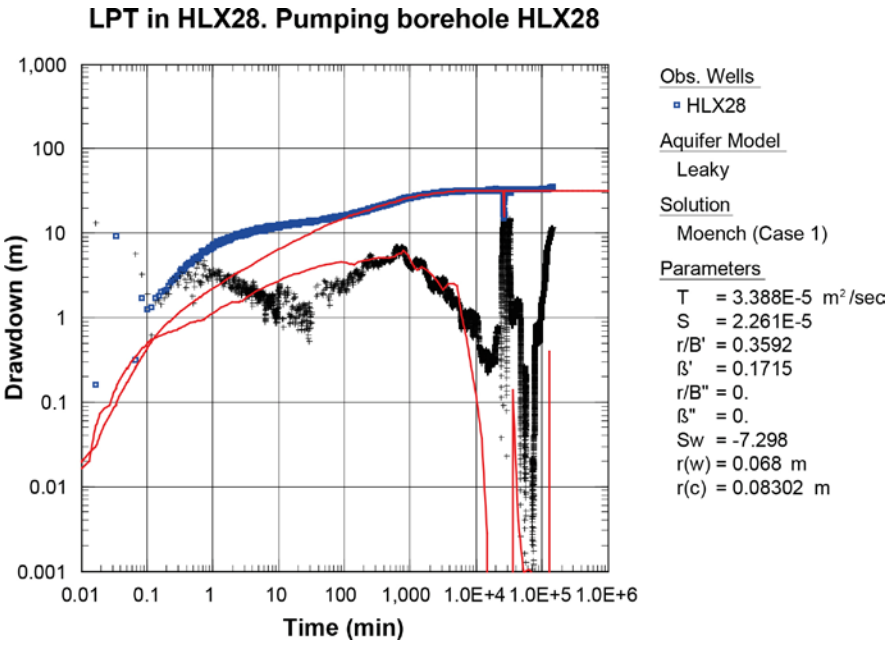

Figure A1-1. *Log-log plot of drawdown (indicated by symbols "▫") and drawdown derivative, ds/d(ln t) (indicated by symbols "+"), versus time in the pumping borehole HLX28 during the interference test in HLX28. Transient evaluation is based on the intermediate part of the flow period. From Thur et al. (2009).*

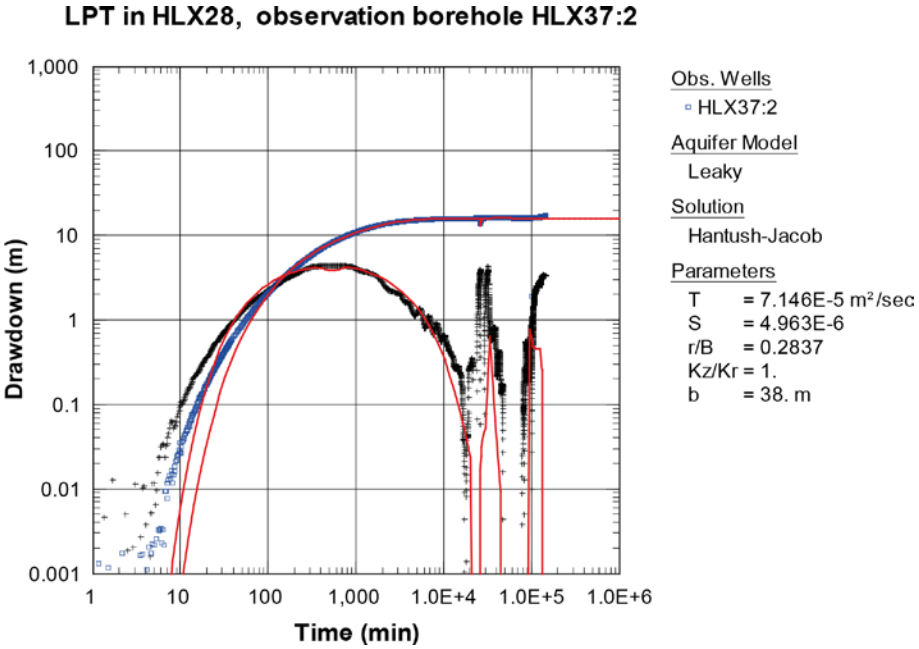

Figure A1-2. *Log-log plot of drawdown (indicated by symbols "▫") and drawdown derivative, ds/d(ln t) (indicated by symbols "+"), versus time in HLX37:2 (distance r_s = 501 m) during the interference test in HLX28. The transient evaluation is based on the first part of the flow period (up to t = 25,000 min). From Thur et al. (2009).*

A1-2 Interference test in HLX27

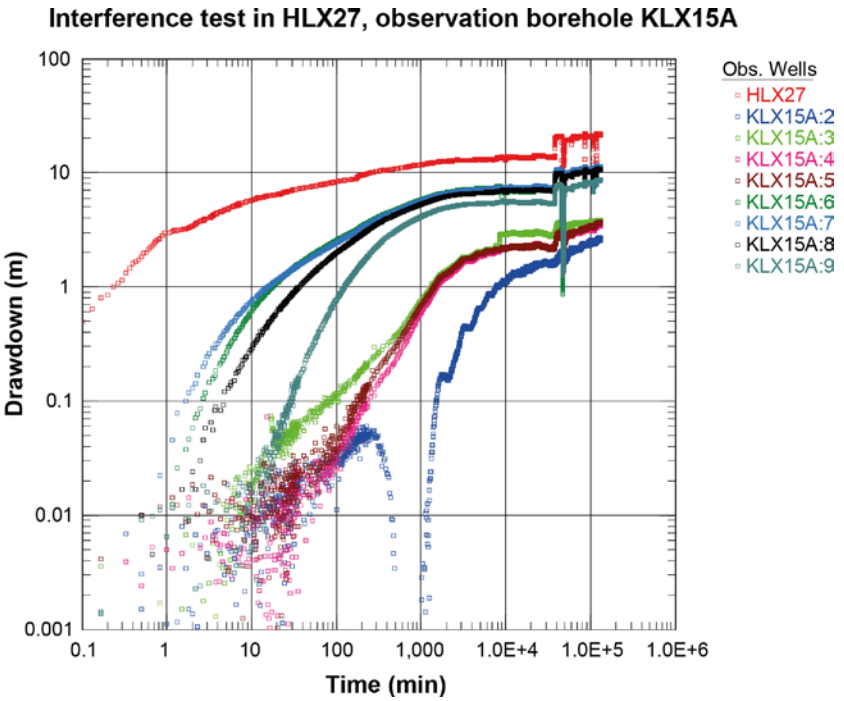

Figure A1-3. *Examples of distinct responses in observation borehole sections in KLX15A together with the response in the pumping borehole HLX27 during the interference test in HLX27. Logarithmic plot of drawdown versus time after start of pumping. The drawdown data have been compensated for the naturally decreasing trend. Some sections are affected by tidal effects. The distances to the observation sections in KLX15A range from 148 to 619 m. From Lindquist et al. (2008a).*

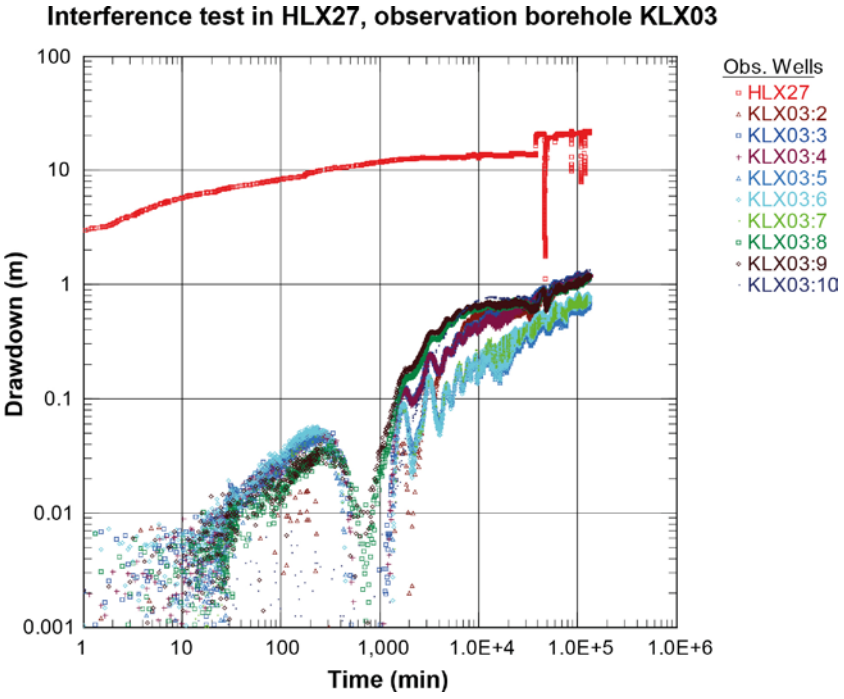

Figure A1-4. *Examples of subdued responses in observation borehole sections in KLX03 together with the response in the pumping borehole HLX27 (upper curve) during the interference test in HLX27. Log-log plot of drawdown versus time after start of pumping. The drawdown data have been compensated for the naturally decreasing trend. All sections are strongly affected by tidal effects. The distances to the observation sections in KLX03 range from 570 to 900 m. From Lindquist et al. (2008b).*

A1-3 Interference test in KFM02B

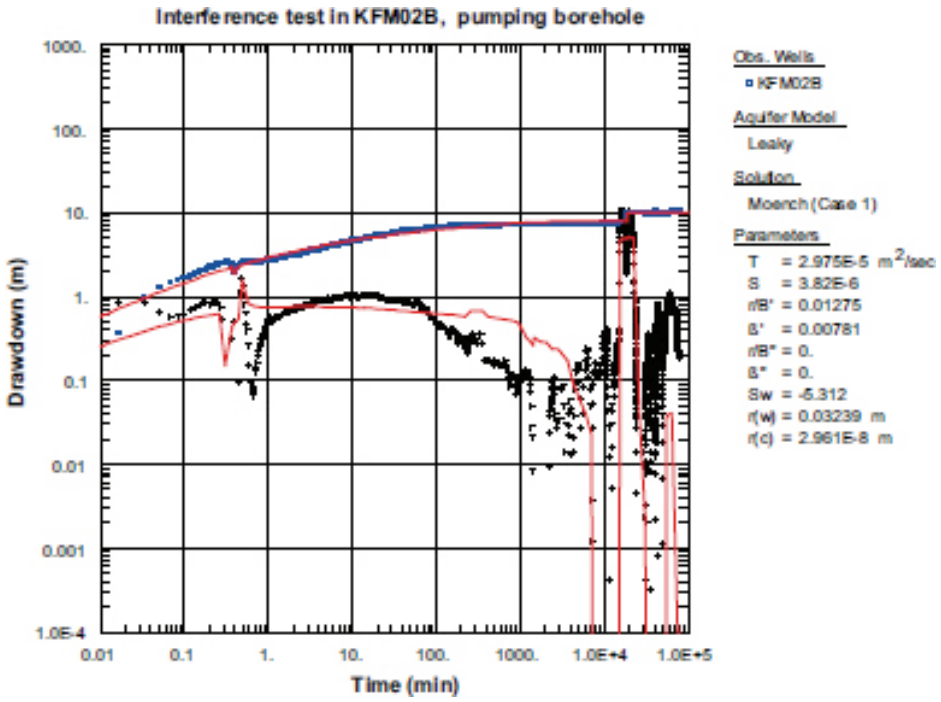

Figure A1-5. *Log-log plot of drawdown (indicated by symbols "▫") and drawdown derivative, ds/d(ln t) (indicated by symbols "+"), versus time in the pumping borehole section KFM02: 408.5–434.0 m, during the interference test in KFM02B.From Lindqvist et al. (2008b).*

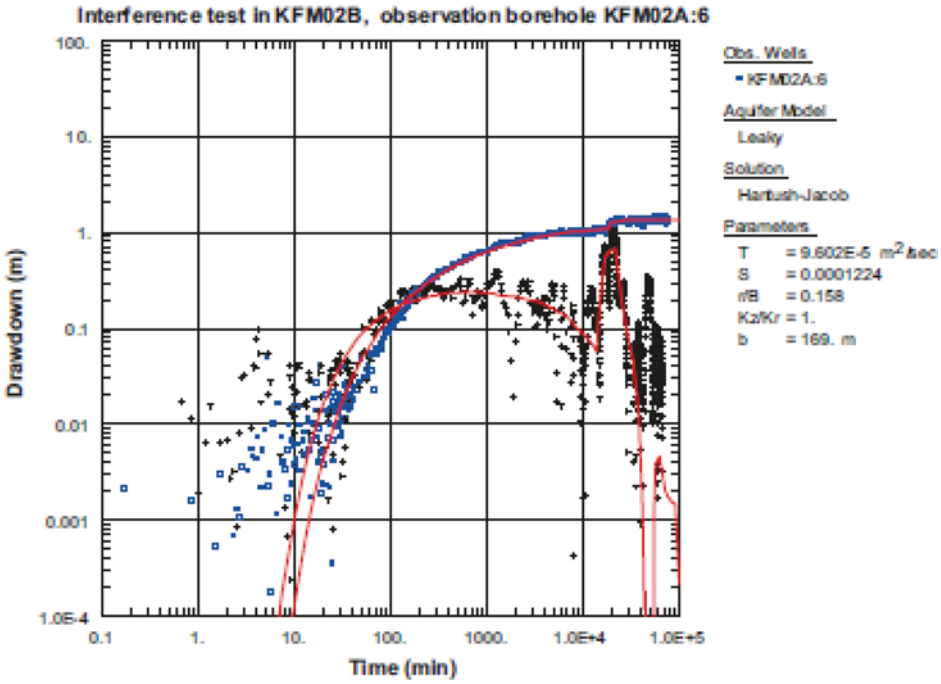

Figure A1-6. *Log-log plot of drawdown (indicated by symbols "▫") and drawdown derivative, ds/d(ln t) (indicated by symbols "+"), versus time in observation borehole section KFM02A:6 ($(r_s$ = 104 m) during the interference test in KFM02B. From Lindqvist et al. (2008b).*

A1-4 Interference test in HFM14

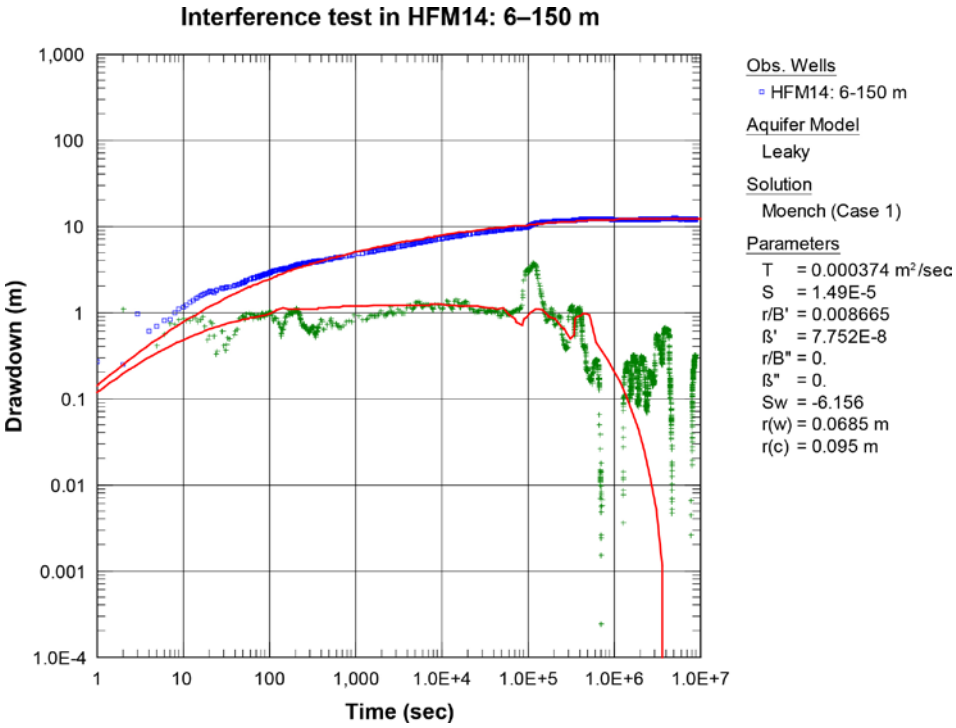

Figure A1-7. *Log-log plot of drawdown (indicated by symbols "▫") and drawdown derivative, ds/d(ln t) (indicated by symbols "+"), versus time in the pumping borehole HFM14 during the interference test in HFM14. From Gokall-Norman and Ludvigson (2008).*

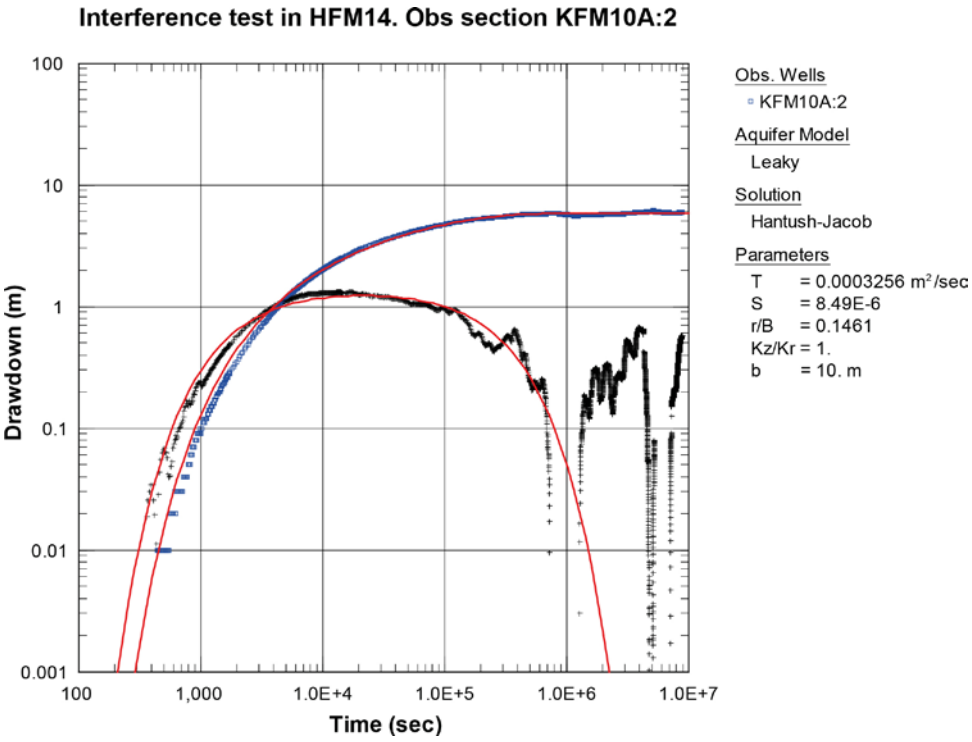

Figure A1-8. *Log-log plot of drawdown (indicated by symbols "▫") and drawdown derivative, ds/d(ln t) (indicated by symbols "+"), versus time in observation section KFM10A:2 (distance r_s = 493 m) during the interference test in HFM14. From Gokall-Norman and Ludvigson (2008).*

Appendix 2

Case studies of hydraulic tomography

This section includes summaries of a number of case studies regarding hydraulic tomography. Due to copyrights permissions and associated costs it is not possible to include figures and tables from the original articles in this section. Instead, the reader is referred to figures and tables that may be found in the original articles.

Case study A2-1: A field assessment of the value of steady shape hydraulic tomography for characterization of aquifer heterogeneities

Bohling et al. (2007) made a field assessment of hydraulic tomography for characterization of heterogeneities in a porous aquifer. The study was made in an alluvium aquifer consisting of sand and gravel overlain by silt and clay, i.e. a confined aquifer. Both steady shape and transient hydraulic tomography was performed in vertical cross-sections of the aquifer. Steady shape hydraulic tomography is similar to steady state tomography but utilizes drawdown data before the actual head values have reached a true steady state, i.e. when only the hydraulic gradients have become steady although drawdown is still increasing overall.

A steady shape drawdown, sometimes denoted a transient steady state (Kruseman and de Ridder 1990), is generally achieved long before an (eventual) true steady state is reached and before any effects of hydraulic boundaries significantly have affected the drawdown response and thus, in turn, the hydraulic tomography analysis. Steady shape hydraulic tomography significantly reduces the computational efforts compared to transient tomography. In addition, transient hydraulic tomography was performed.

The estimated hydraulic conductivity (K) fields from steady shape HT and transient hydraulic tomography were quite similar despite although with a much lower computational effort in the case of steady shape hydraulic tomography. The results were consistent with those from a tracer test and single-hole permeameter field tests. Cross-hole radar surveys were used to identify the different layers in the aquifer. The results of the hydraulic tomography indicated that the borehole radar surveys provided useful supporting information regarding the geometry (layer zonations) of the K field.

The study clearly demonstrated the advantages of hydraulic tomography analysis over conventional analysis of pumping (cross-hole) tests, which only provided large-scale averages, and also over single-hole hydraulic tests which do not provide connectivity information (e.g. high K-zones) within the aquifer, which may be important in e.g. contaminant studies.

Case study A2-2: Practical issues in imaging hydraulic conductivity through hydraulic tomography

Illman et al. (2008) estimated hydraulic conductivity (K) fields from steady-state hydraulic tomography using the SSLE estimator by Yeh and Liu (2000) from simulated pumping test data in a synthetic aquifer and from generated, real drawdown data in a sandbox in the laboratory. They investigated the sensitivity of various factors which may affect the results of hydraulic tomography. The factors studied were *i*) the influence of the signal-to-noise ratio of the drawdown data, *ii*) the order in which the data sets were included in the tomography and *iii*) the role of conditioning the K tomograms (i.e. maps of the distributions of the estimated K-fields from hydraulic tomography) with other data, i.e. core K data, K data from slug tests and K-data from other single hole hydraulic tests. The resulting K-tomograms were compared with reference K-tomograms. Finally, they proposed different ways to validate the estimated K-tomograms.

A larger signal-to-noise ratio can be achieved by increasing the pumping rate thus creating larger drawdowns and/or by decreasing the noise level of the data by filtering techniques. Illman et al. (2008) tested the effect of the signal-to-noise ratio by conducting pumping tests at two different rates. In the synthetic case it was concluded that the pumping rate had a little effect on the synthetic K tomogram. However, for the real case the pumping rate had a significant effect due to the larger noise level in the drawdown data for the lower rate.

The order in which the test data were included in the hydraulic tomography analysis had little effect on the synthetic K-tomogram. However, the order of data had a large impact on the real K-tomogram, due on the fact that some drawdown records from different pumping tests were noisier than others. It was found that including the cleanest data records with the highest signal-to-noise ratio first in the HT analysis and the noisier data records later tended to improve the results. This fact was found to be due to the performance of the SSLE estimator used in HT.

It was also found that conditioning the HT analysis with core K data (with a small support scale) dramatically improved the estimated K tomograms, both for the synthetic case and the real case. In particular, low K blocks on the bottom of the sandbox appeared more clearly in the latter case. However, conditioning on K data from both slug tests and single-hole tests (the latter obtained from transient analysis of the responses in the pumping wells) entailed a slight deterioration of the K tomograms, both for the synthetic and real case, i.e. the low K blocks appeared smoother in the K tomograms. This fact was attributed to the fact that the support volume of the K data from the slug tests was larger than the numerical grid in the computation of the K tomogram, thus smoothing the tomograms.

The K-tomograms were validated by simulating an additional pumping test in a well that was not used in the HT analysis. The simulated heads were then compared with the observed heads at the different observation points in a cross plot for the different cases described above. In the sandbox aquifer, the agreement between simulated and observed heads was very good, except for the simulated test with low pumping rate, i.e. with a low signal-to-noise ratio. In addition, the goodness of fit between the simulated and observed head was evaluated by two criteria; the average absolute error norm (L_1) and the mean-squared error norm (L_2), see Illman et al. (2008).

Case study A2-3: Sequential aquifer tests at a well field, Montalto Uffugo Scalo, Italy

Summary of approach (Straface et al.2007)

1. Drawdown data were obtained from 6 pumping tests in a real aquifer in an alluvial deposit mainly consisting of highly permeable sands and conglomerates.
2. Conventional time-drawdown, distance-drawdown and drawdown-time/distance analysis was made for all observation wells and pumping tests.
3. Transient hydraulic tomography analysis with drawdown data from all 6 pumping tests and 5 observation wells in each was performed using the Sequential Successive Linear Estimator (SSLE) by Zhu and Yeh (2005). The spatially varying T and S fields of the aquifer were estimated.
4. The results from the HT analysis were compared with estimated locations of in-homogeneities in the aquifer from the drawdown derivatives and with geological evaluations of the site.
5. Conclusions were drawn from the study.

Aquifer description and selection of data

The well field of the site includes an area of c. 35×60 m with highly heterogeneous layers consisting of sand and shale layers. Six wells were drilled to depths of 10 m and 40 m, i.e. into the shallow aquifer and the main aquifer, respectively. All wells were cased. The shallow wells were screened over a 2 m interval whereas the deep wells had a screened interval of 17 m. All wells have a diameter of 200 mm. Drawdown data from 5 observation wells from each of the 6 pumping tests were used in the HT analysis. The duration of the pumping tests was c. 24–43 h in the different wells.

Conventional aquifer analysis

Conventional time-drawdown, drawdown-distance and drawdown-distance/time analyses were performed for data from all 5 observation wells at each pumping test. The time-drawdown curves from the observation wells during each of the 6 pumping tests are shown in Figure 2 in Straface et al. (2007). The figure shows that the drawdown curves in a lin-log diagram do not exhibit straight lines at the end as would be expected in a homogeneous aquifer with infinite extent (according to Cooper-Jacob'

method). Instead, they exhibit a continuous, but different change in slope, indicating a heterogeneous aquifer with higher-permeability regions within or adjacent to lower-permeability regions. In addition, the response (lag) times due to pumping were different for each well and test.

The estimated T and S values varied with the location of the observation and pumping wells. Furthermore, the estimated T and S values changed with time, the T values tended to converge to a certain value at later times whereas the S values stabilized rather quickly to distinct values but were more scattered compared to the T values.

Finally, the distances to heterogeneities or hydraulic boundaries within the aquifer were estimated from the inflection points of the time-drawdown derivative curves using a formula by Oliver (1990) for each observation borehole and pumping test.

Hydraulic tomography analysis

First the T and S fields were estimated from data from the first pumping test. The estimated fields were then improved by incorporating another set of time-drawdown data from another well until the data sets from all 6 tests were utilized. A square modelled area of 100×100 m was selected and discretized into 50×50 elements with an element size of 2.0×2.0 m. The dimensions of the modelled domain were consistent with the estimated radius of influence from previous aquifer tests in the area.

The SSLE estimator requires initial input values of the spatial variability of the aquifer hydraulic properties, i.e. the mean, variance, correlation scales and the theoretical covariance model. A mean value of $T = 1.69 \cdot 10^{-4}$ m^2/s and $S = 7.2 \cdot 10^{-3}$ were used based on the classical drawdown-time-distance analysis. Three drawdown points from the time-drawdown curves (at early, intermediate and late times) were selected in the HT analysis. The times ranged from 1,800–108,000 s (0.5–30 h). In total, 87 drawdown measurements were used in the HT analysis.

The estimated T and S fields from HT are shown in Figure 6 and 7 in Straface et al. (2007), respectively. Figure 6 shows that the well field is located in a large isolated, permeable island surrounded by low-transmissive materials. There are some highly permeable patches within this island. The geometric means of T and S from the HT analysis are $3.26 \cdot 10^{-5}$ m^2/s and $2 \cdot 10^{-3}$, respectively. The variances of the estimated ln T and Ln S are 5.145 and 3.569, respectively.

The estimated distances to heterogeneities or hydraulic boundaries within the aquifer from the derivative, as described above, are included in Figure 6 in Straface et al. (2007) from the pumping test in well P7. According to the authors, the estimated locations of possible inhomogeneities in the aquifer were consistent with the estimated T field from the hydraulic tomography.

Conclusions (according to the authors)

All drawdown curves from the observation wells exhibited different behaviour and showed effects of heterogeneity. Analysis with standard methods (e.g. Theis' method) yielded different T and S values from each well and changed with time. The estimated T-values from standard analysis stabilized at large times and converged to slightly different values for different observation wells and pumping tests. The estimated S-values diverged more but stabilized to distinct values for each observation well and test. These results are consistent with the findings by Wu et al. (2005) regarding estimated T and S in heterogeneous media.

Based on the findings above, the validity of traditional aquifer test analysis was questioned for cross-hole tests in heterogeneous aquifers. However, the former methods are still important in aquifer characterization. For example, standard methods can be used to obtain first estimates of the aquifer properties and be used to plan further testing. In addition, the estimated T and S–values can be used as starting parameters for the hydraulic tomography analysis.

Finally, the study showed that hydraulic tomography analysis produced more information than classical aquifer tests at this well field although only data from five observation wells were included. The SSLE algorithm by Zhu and Yeh (2005) yielded reasonable estimates of the spatially varying T and S fields. The estimated fields reflected the possible pattern of inhomogeneities or changes in hydraulic properties within the aquifer and were considered to be consistent with the geological setting of the site. Yet, more confirmations of the results are needed.

Case study A2-4: Hydraulic tomography for detecting fracture zone connectivity

Summary of approach (Hao et al. 2008)

1. Drawdown data were obtained from simulated pumping tests in a synthetic, cross-sectional (2D) aquifer with prescribed constant hydraulic head boundaries around the aquifer. The aquifer included five vertical and two horizontal fracture zones embedded in a rock matrix.
2 Transient hydraulic tomography analysis of selected drawdown data from 9 simulated pumping tests were obtained using the Sequential Successive Linear Estimator (SSLE). The K and S_s fields and the connectivity of the aquifer were estimated in four different cases for transient HT and one case with steady-state HT.
3. Assessment of performance of the SSLE estimator was made.
4. Conclusions were drawn from the study.

Generation of drawdown data

The domain of the synthetic aquifer was 40×40 m with prescribed constant hydraulic head boundaries equaling 100 m around the domain, see Figure 1 in Hao et al. (2008). The domain was discretized into 40×40 elements of 1×1 m in size. Five vertical and 2 horizontal fracture zones of 1 m width embedded in the rock matrix were simulated. The fracture zones have constant (but different) hydraulic properties in the four cases. The properties of the rock matrix were assumed be constant in some cases and heterogeneous in others. Four inclined boreholes were assumed to penetrate the aquifer, see Figure 1 in Hao et al. (2008).

Pumping tests were simulated at nine (9) different locations at intersections between boreholes and fracture zones such that maximal pressure disturbances were obtained. Time-drawdown data were generated in 30, or alternatively 42 observation points, in four different cases for the hydraulic tomography analysis. Observation points were located at each intersection points between the boreholes and fracture zones and more sparsely along the borehole with no fracture zone intersections. The hydraulic conductivity and estimated specific storage values along the boreholes were assumed to be known from previous single-hole tests.

Hydraulic tomography analysis

From the simulated drawdown responses and assumed K and S_s of the boreholes together with given, although assumed, statistical input parameters as starting values, transient hydraulic tomography with the SSLE estimator was then performed to identify the detailed distributions of hydraulic conductivity and specific storativity of the aquifer. Selected drawdown data at t = 0.01, 0.05, 0.15, 0.30 and 0.5 min were used in the analysis. In addition, the extent, distribution and interconnectivity of the fracture zones were investigated.

Four different cases were investigated by hydraulic tomography analysis, based on the simulated drawdown responses. In case 1, the heterogeneous hydraulic conductivity field was estimated assuming that S_s in the fracture zones and rock matrix, respectively are homogeneous and known a priori. It was assumed that only pumping test data from Wells #1 and #2 was available for HT analysis. The hydraulic conductivity of the fracture zones was assumed to K = 10 m/min (0.17 m/s) while the hydraulic conductivity of the rock mass was assumed to be homogeneous with K = 0.5 m/min (0.0083 m/s). The specific storage of the fracture zones and rock matrix was assumed to $S_s = 1 \cdot 10^{-5}$ 1/m and $S_s = 2 \cdot 10^{-4}$ 1/m, respectively. Drawdown data from the tests in Wells #1 and #2 wells were used together with guessed mean, variance and correlation scales of the hydraulic conductivity field in the X- and Z-directions as input data to hydraulic tomography.

In case 2, both the K and S_s were assumed to be heterogeneous and their parameter distributions were estimated from HT using the same drawdown data (two tests) and input values of the K-field as in case 1 and assumed input values for the S_s distribution.

In case 3, the effects of the contrast of the K and S_s fields between fracture zones and rock matrix as well as the heterogeneity of the rock matrix on the estimated fields were investigated. The same drawdown data (two tests) were used as in case 2. The hydraulic conductivity of the fracture zones

was assumed to K = 10 m/min ($1.7 \cdot 10^{-1}$ m/s) while the hydraulic conductivity of the rock mass was s spatially varying with a mean of 0.1 m/min ($1.7 \cdot 10^{-3}$ m/s). The specific storage of the fracture zones and rock matrix was assumed to $S_s = 1 \cdot 10^{-5}$ 1/m and $S_s = 1 \cdot 10^{-3}$ 1/m, respectively. The spatial variability within these hydraulic units was considered to be negligible.

In case 4, for the same aquifer properties and input parameters as in case 3, the effects of increasing the number of observation points by adding drawdown data from two additional wells (Wells #3 and #4) were investigated. Finally, the K field of the aquifer was estimated from the simulated steady-state drawdown curves for the same input data as in case 4.The estimated hydraulic conductivity and specific storage fields from the hydraulic tomography analysis in case 4 are shown in Figure 6 and 7 in Hao et al. (2008), respectively. The estimated, overall K- and S_s-fields in these figures correspond well with the true fracture zone pattern although the estimated fields are smoother than the underlying true field Hao et al. (2008).

Evaluation of performance

The performance of the SSLE estimator used in the hydraulic tomography analysis was evaluated by statistical measures, i.e. the correlation coefficient between the true and estimated K and S_s-fields, the mean absolute error norm L1 and mean square error L2, see Hao et al. (2008). In addition, visual comparisons of the fields were made to evaluate the goodness of the estimated fields.

Conclusions by the authors

At an increased contrast (100) between the hydraulic properties of the fracture zones and the mean K of the rock matrix, the capability of the SSLE estimator decreases to provide information of the fracture zones. According to Hao et al. (2008) this fact may be attributed to that the degree of non-linearity between head and hydraulic properties becomes more significant as the contrast increases. However, the variability of the hydraulic conductivity of the rock matrix was found to be negligible on the estimated K field.

According to Hao et al. (2008), hydraulic tomography can satisfactorily map the high K zones (preferential flow paths) in fractured media although the estimated K and S_s fields are smoother than the true fields. As the number of cross-hole tests and observation points increases, the contrast between the estimated properties of the fracture zones and rock matrix becomes more evident and the fracture distribution and estimated hydraulic parameters will approach the assumed (true) values. The estimated K field was slightly improved by using simulated steady-state drawdown data instead of transient data.

Finally, the authors conclude that hydraulic tomography seems a viable technique for mapping of fracture zones and their connectivity in fractured rock but more field studies are needed to fully assess its capabilities. Inclusion of supporting data, e.g. from tracer and geophysical tomographic surveys, in hydraulic tomography studies are recommended in studies in fractured media.

Case study A2-5: Hydraulic tomography in fractured granite: Mizunami Underground Research site, Japan

Summary of approach (Illman et al. 2009).

1 Data selection and pre-processing of measured field test data.

2. Estimation of input parameters for hydraulic tomography.

3. Aquifer description and definition of model domain for hydraulic tomography.

4. Transient hydraulic tomography analysis of selected drawdown data from two cross-hole pumping tests using the Sequential Successive Linear Estimator (SSLE) by Zhu and Yeh (2005).

5. Evaluation of the results from the hydraulic tomography analysis.

6. Findings and conclusions drawn from the study.

Data selection and pre-processing of test data

Transient hydraulic head (drawdown) records from observation sections with preferably strong responses to the pumping and not too noisy data were selected from the cross-hole tests. However, sections with weaker responses in two boreholes were also included. Some head data were excluded to be used subsequently for validation purposes. The errors in the data were firstly reduced by accounting for pressure transducer drift and removal of data affected by skin effects.

In many observation sections, the responses were only c. 2 kPa (0.2 m). Prior to the analysis, the data were processed (filtered) to remove effects of earth tides and variations of the barometric pressure. An example is shown in Figure 3 in Illman et al. (2009).

Estimation of input parameters for hydraulic tomography

Input to the model for transient hydraulic tomography (THT) may include the following parameters:

- Initial guesses of the mean K and S_s-values of the rock.
- Estimates of the variances and correlation scales for K and S_s.
- Volumetric discharge for each pumping test.
- Available point (single-hole) measurements of K and S_s.
- Head (drawdown) data from selected observation sections.

In this case, point measurements of K and S_s were not used. The mean values of K and S_s may be estimated as the effective hydraulic conductivity (K_{eff}) and specific storage (S_{eff}) for an equivalent homogeneous medium. Alternatively, if small-scale data are available, the geometric mean of these data (core, slug and single-hole tests) can be calculated. The geometric mean values of equivalent K and S_s determined from the cross-hole tests were used in this case. These values were $K = 1.0 \cdot 10^{-2}$ m/d (c. $1.2 \cdot 10^{-7}$ m/s) and $S_s = 2.3 \cdot 10^{-6}$ m^{-1}.

The variance of K ($\sigma_{lnK}^2 = 2.0$) and S_s ($\sigma_{lnSs}^2 = 0.5$) were estimated from cross-hole test 1 and used as input to the THT analysis for both test 1 and 2. The correlation scales were approximated on the basis of observed lineaments to 50 m in both the horizontal and vertical direction, while an exponential model was used in the THT analysis. It was assumed that the uncertainties in both the estimated variances and correlation scales have a negligible effect on the THT analysis.

From the selected head records, transient drawdown curves were prepared from 24 observation intervals in cross-hole test 1 together with 11 intervals in test 2. Finally, 4 to 7 drawdown values were selected from each head record to represent the entire drawdown curve in the THT analysis. In total, 141 drawdown values were utilized in cross-hole test 1 and 77 values in test 2.

Aquifer description and definition of model domain

A rectangular domain of dimensions 884×392×1,054 m was selected for the THT analysis. It was discretized into 4,216 elements and 5,184 nodes with element dimensions of 52×49×34 m. The top boundary was set as a constant head boundary while all other boundaries were assumed as no-flow boundaries.

Results of the hydraulic tomography analysis

The estimated 3D tomogram for K (m/d) from the hydraulic tomography analysis of the two cross-hole tests is shown in Figure 4 in Illman et al. (2009). Pumping boreholes are indicated by solid white spheres while observation intervals are indicated by solid black squares. The estimated K-field shows several high K-zones which appear to be connected. Well connected fracture sets are referred to as the continuous high K region above a cut-off value of 0.1 m/d (shown in red in Figure 4 in Illman et al. (2009)).

The estimated 3D tomogram for S_s (m^{-1}) from the hydraulic tomography analysis of the two cross-hole tests is shown in Figure 6 in Illman et al. (2009). As before, pumping boreholes are indicated by solid white spheres while observation intervals are indicated by solid black squares. Figure 6 in Illman et al. (2009) indicates two regions of lower S_s, generally corresponding to the high K-zones. These regions may correspond to a fracture/fault zone as interpreted from geological investigations of the site. The estimated K and S_s tomograms are likely to be smoother than the true heterogeneity distribution within the site. The authors attribute the smoothness of the tomograms to the availability of data from only two cross-hole tests and only a limited number of observation intervals within the 0.36 km^3 block of fractured rock investigated.

Evaluation of the quality of results from hydraulic tomography

Three independent approaches to evaluate the quality of the estimated K and S_s-fields were presented:

- Comparison of simulated and observed drawdown records from observation intervals not included in the THT-analysis.
- Comparison of tomograms to known fault zones.
- Comparison of induced groundwater level responses during large earthquakes.

Figure 9 in Illman et al. (2009) shows observed (small dots) and simulated (curves) drawdown records versus time in 34 observation intervals during cross-hole test 1. Drawdown data used as input data to the THT analysis are indicated as open squares. In general, the simulated responses agree reasonably to the observed ones but to a varying degree, ranging from poor to excellent. This fact is explained by the inability of the THT-model to reproduce all drawdown records for the following reasons, Illman et al. (2009):

- The representation of the heterogeneous rock with a coarse grid.
- The conditional effective estimates from the THT inverse model.
- Discrepancies between the true and modelled initial and boundary conditions.
- The THT model disregards effects of borehole storage, skin and non-Darcy flow in fractures.
- To some extent, by disturbances from external signals such as earth tides and ambient groundwater flow.

By the correlation of the tomograms with the local geology at the site, the major fault zones were plotted into the tomograms to look for any correlation although the hydraulic properties of the fault zones were not known in detail, see Figure 11 in Illman et al. (2009). In general, the high K zones correspond to the major fault zones. In addition, continuous low-K zones, identified in the tomograms, may possibly correspond to low-conductive fault zones.

Conclusions by the authors

The following conclusions were drawn from the study by the authors:

- The THT analysis was able to image continuous high K and low S_s zones, which represent fast flow paths, and their connectivities.
- Reasonable agreement was obtained between simulated and observed drawdown records, including records not utilized in the THT analysis.
- The estimated tomograms are consistent with available geological records of the site.
- The estimated tomograms were consistent with observed co-seismic groundwater pressure changes from major earthquakes.
- More rigorous and quantitative means to evaluate the quality of the estimated K and S_s tomograms are needed. For example, an appropriate validation approach would be to predict drawdown fields, based on the estimated K and S_s fields, under different flow scenarios. Possibly, tracer tests and geophysical surveys may be used to support the results of the hydraulic tomography.

Case study A2-6: A simultaneous successive linear estimator and a guide for hydraulic tomography analysis

Summary of approach (Xiang et al. 2009)

1. Pre-processing of measured test data.
2. Examination of the signal-to noise ratio (SNR) of measured test data.
3. Estimation of effective hydraulic parameters (hydraulic conductivity K and specific storage S_s) of an equivalent homogeneous medium and spatial statistics of the heterogeneity of the formation.
4. Transient hydraulic tomography analysis using drawdown data from 4 simulated pumping tests (24 observation points) by the Simultaneous Successive Linear Estimator (SimSLE) in combination with a stopping criterion. The estimator was tested in a synthetic, cross-sectional (2D) aquifer with prescribed hierarchical heterogeneity and in a vertical sandbox with prearranged heterogeneity in the laboratory. The heterogeneous K and S_s fields of the aquifers were estimated in both cases.
5. In the synthetic cross-sectional aquifer the results from the hydraulic tomography were validated by visual comparison of the true heterogeneous K and S_s fields and the corresponding estimated fields together with analysis of the associated performance assessment statistics including similarity analysis.
6. In the sandbox experiment the true K and S_s fields are unknown and the performance metrics thus cannot be evaluated. Instead, in the estimated K and S_s fields an independent pumping test was simulated and the estimated heads at different times at 47 observation points were compared to the corresponding observed heads at the same positions. In addition, drawdowns were simulated using the estimated effective K and S_s fields corresponding to an equivalent homogeneous formation for comparison.
7. Conclusions drawn from the study.

Pre-processing of test data

The following pre-processing of measured test data was recommended:

a) Diagnosis of bias

As a first step, qualitative checks of any bias or inconsistencies in the data should be made, e.g. by visual inspection of plots of time-drawdown and contour maps of drawdown. In time-drawdown plots, the arrival (response) times in the observation wells should be checked and any outer boundary effects should be identified. Any bias or inconsistencies in the data should be examined and corrected (or data excluded from the analysis).

b) Wavelet de-noising

Perturbations of data caused by factors other than aquifer heterogeneity (e.g. earth tidal effects) should be eliminated before the hydraulic tomography analysis. A method based on wavelet analysis, similar to Fourier analysis is proposed for this purpose.

Signal-to-noise ratio of test data

The signal-to-noise ratio (SNR) was examined for all drawdown curves. It is defined as the ratio between the maximum drawdown of the de-noised drawdown curve and the standard deviation of the noise estimated from the previous wavelet de-noising procedure. It was found that drawdown curves with an average SNR of 7.13 or greater were effective in the synthetic case. Curves with lower SNR were discarded since it did not improve the estimates of the K and S_s fields. Drawdown curves with low SNR at early times can lead to erroneous estimates of the S_s field according to the authors.

Estimation of effective properties and variances

Effective values of K and S_s for an equivalent homogeneous aquifer were estimated by least square regression analysis of selected drawdown curves from all pumping tests together using a finite element model (VSAFT2). In addition, the sample variance of the observed heads and the variance of the hydraulic properties were estimated. The estimated, effective parameters K and S_s and variances were used as input to the subsequent hydraulic tomography analysis.

The estimated effective K was found to be slightly greater than the geometric mean of the K-values from the four units in Table 5-1 while the estimated effective S_s was in agreement with the arithmetic mean of the units.

Hydraulic tomography analysis

Hydraulic tomography was performed in a synthetic cross-sectional 2D aquifer and in a laboratory sandbox of the same physical dimensions. The two studies are summarised below.

a) Synthetic cross-sectional aquifer

The synthetic aquifer imitated a geologic formation of hierarchical heterogeneity, i.e. spatial variations of the hydraulic properties between the units as well as within the units. The aquifer consists of four heterogeneous units (1–4) with a bedding dip angle of 20°, see Figure 2a in Xiang et al. (2009). The true fields of K and S_s in the synthetic aquifer are shown in Figure 2a and 2e in Xiang et al. (2009), respectively. The Ln (K) and Ln (S_s) fields within each unit were assumed to be normally distributed random fields with different means and variances, see Table 1 in Xiang et al. (2009).

The synthetic aquifer had the same length and height as the sandbox used in the second HT analysis presented below. The sandbox was 193.0 cm in length, 82.6 cm in height and 10.2 cm in depth. Both sides of the aquifer had a constant head of 200 cm while the top and bottom boundaries were assumed to be no-flow boundaries. An exponential model with correlation scales of 200 cm in the bedding direction and 12 cm in the direction perpendicular to bedding was used to describe the spatial covariance functions of the field.

Totally 24 locations (black dots in Figure 7 in Xiang et al. (2009)) were used as observation points during simulated short pumping tests at four locations (open circles in Figure 7). The drawdown reached a steady-state in all tests due to the small size of the aquifer. The simulated drawdown data (hydrographs) were regarded as "noise-free" but a white noise was added to represent measurement errors ("noisy hydrographs"). Finally, the wavelet de-noising procedure was used to obtain "de-noised hydrographs". All 96 hydrographs (4×24) from the four pumping tests were included in the HT analysis since their SNR was much greater than 1.

In the HT analysis, drawdown data at 5 selected times (4 early times and 1 late time) during the tests were used. According to Wu et al. (2005) the drawdown at early times is highly correlated with the estimated S_s field but only weakly correlated to the K field. At large times the drawdown is correlated at various degrees to the K field within the radius of investigation but not to the S_s field.

The results of the HT analysis in the synthetic aquifer are shown in Figure 2b-h in Xiang et al. (2009). HT analysis was made with *i)* noise-free data (figures b and f), *ii)* noisy data (figures c and g) and *iii)* de-noised data (figures d and h) according to the definitions above. The true K and S_s fields are shown in figures (a and e). Figures (b–h) indicate that the SimSLE estimator in general reveals the spatial heterogeneity of both the K and S_s fields. The latter field is more sensitive to the quality of the drawdown data regarding noise.

b) Laboratory sandbox experiment

As described above, the laboratory sandbox aquifer had the physical dimensions of 193.0×82.6×10.2 cm, see Figure 7 in Xiang et al. (2009). The open rectangles represent low-permeability zones. Eight pumping tests were simulated in the sandbox at the open circles in the figure. Drawdown data were sampled from 47 observation points during each test, excluding the pumping point. The data were de-noised using the wavelet de-noising procedure described above before HT analysis. Data from two pumping tests which had low SNR's were discarded from the analysis. Estimated K and S_s values from an in-situ slug test at point 1 in Figure 7 were used as hard data to condition the HT analysis.

The effective K and S_s for an equivalent homogeneous aquifer (0.1268 cm/s and $8.73 \cdot 10^{-4}$ 1/cm, respectively) were estimated as described above for the synthetic aquifer. Similarly, the variances of Ln K and Ln S_s were estimated to 2.0 and 0.1, respectively. The correlation scales were subjectively estimated to 70 cm and 20 cm in the horizontal and vertical directions of the sandbox. As before, 5 head values at different times at each observation point during the six selected pumping tests were included in the HT analysis.

Figure 10 in Xiang et al. (2009) shows the estimated K and S_s fields in the sandbox experiment from the HT analysis. The figure shows that 6 of the 8 low-permeability zones were revealed in the K field. The two low-K zones close to the bottom were however fuzzy due to the presence of the no-flow

boundary at the bottom of the sandbox. The estimated S_s field does not reflect the pattern of the K-field but indicates decreasing S_s values towards the bottom, consistent with geological findings and results of hydraulic tests.

Since the true K and S_s fields are unknown in this case, no performance assessment statistics for validation of the HT analysis can be obtained. Instead, an independent pumping test was simulated at point 46 in Figure 10 in Xiang et al. (2009) using the estimated K and S_s fields from the HT analysis as input. Data from this observation point was not used in the HT analysis. The simulated and observed heads from all 47 observation points were compared at 4 selected test times, see Figure 11 in Xiang et al. (2009). The simulated and observed heads were in close agreement at all times except at 3.0 s which may be due to other factors.

For comparison, also simulated heads at point 46 using the effective values of K and S_s for an equivalent homogeneous aquifer (presented above) were included in the plots in Figure 11 in Xiang et al. (2009). The latter heads deviated, in varying degrees, from the observed heads at all times due to the heterogeneity of the aquifer.

Conclusions by the authors

According to Xiang et al. (2009), the following main conclusions can be made from the study:

- Hydraulic tomography reveals detailed hydraulic heterogeneity of aquifers, which can be used to predict different flow scenarios in contrast to standard analysis of pumping tests based on effective hydraulic parameters of an equivalent homogeneous aquifer.
- Simultaneous use of all drawdown curves from observation wells during pumping tests in the analysis (SimSLE) constitutes some advantages over the previous sequential approach (SSLE) but suffers from the need for large computational resources.
- If the head data are affected by noise, the SNR (Signal-to-Noise Ratio) is a useful measure of the quality of the data in the HT analysis. Wavelet de-noising is recommended to correct the data from such noice. In addition, use of a stop convergence criterion in SimSLE avoids over-interpretation of noisy data.
- In addition, the study shows that using the estimated hydraulic conductivity and specific storage fields of the sandbox, the classic groundwater flow model accurately predicts temporal and spatial distributions of drawdown induced by an independent pumping event in the sandbox. On the other hand, the classic groundwater flow model yields less satisfactory results when equivalent homogeneous properties of the sandbox are used.

Case study A2-7: Cost-effective hydraulic tomography surveys for predicting flow and transport in heterogeneous aquifers

Summary of approach (Ni et al. 2009)

1. Numerical simulations of flow and transport in a synthetic, cross-sectional (2D) confined aquifer with heterogeneous properties (only flow is reviewed here).
2. Different random fields of heterogeneity were generated of the aquifer. Steady-state flow fields were simulated for prescribed constant hydraulic head boundaries at the left and right sides in the aquifer.
3. Steady-state hydraulic tomography analysis was performed and the K fields of the aquifer were estimated in different cases from selected head data from 8 simulated cross-hole tests using the Sequential Successive Linear Estimator (SSLE). In addition to head data from the cross-hole tests, direct K-measurements from the different observation intervals (from well logs, single-hole tests etc) were used in the HT analysis. Simulated K-field was also prepared from kriging of the direct K-measurements. The estimated K-field from hydraulic tomography was compared with the corresponding K-field based on kriging.
4. Assessment of performance of the hydraulic tomography.
5. Based on the results from the HT analysis, strategies for cost-effective design of hydraulic tomography surveys regarding i) pumping strategy, ii) degree of aquifer heterogeneity and iii) use of direct K-measurements are proposed.
6. Conclusions drawn from the study.

Description of synthetic aquifer and generation of drawdown data

The domain of the synthetic 2D aquifer was 60×20 m, discretized into 1,200 elements of 1×1 m. The left and right sides of the aquifer had prescribed constant hydraulic head boundaries of 100.6 m and 100 m respectively. Figure 2 in Ni et al. (2009) shows a schematic diagram of the experimental setup with the locations of pumping, monitoring, and the concentration source zone. Only the flow predictions are discussed here, not the transport. The distributions of hydraulic conductivity, porosity, and longitudinal and transverse dispersivities of the aquifer were generated using an algorithm based on known means, variances, and correlation lengths in an exponential covariance model. These distributions are considered to account for the true fields.

Three observation wells, divided in 9 sections by packers, were simulated. Steady-state pumping tests were then independently simulated in 8 different sections and head data were collected at all observations sections in the wells (totally 3×9 sections) during each test. Direct K-measurements of all observation sections (27) were assumed to be known from well logs, single-hole tests etc. In addition, the tracer concentrations were measured at a few observation sections (but not reviewed here).

Hydraulic tomography analysis

From the simulated drawdown responses and the direct K-measurements, steady-state hydraulic tomography (HT) analysis was performed using the SSLE estimator to identify the detailed hydraulic conductivity K-fields of the aquifer for different cases. In addition, kriging of the K-fields based on the 27 direct K-measurements from the observation sections using an exponential semi-variogram model was made for comparison. Different from the kriging estimation, the HT analysis couples the direct *K* measurements with head values observed from different cross-hole pumping tests.

It was concluded that the estimated hydraulic conductivity K-field from hydraulic tomography analysis better agreed with the assumed true K-field than the field from kriging, see Figure 1 and Figure 3 in Ni et al. (2009). The latter gave a relatively smooth K-field. In addition, it was also concluded that the estimated steady-state flow fields from HT better agreed with the true field.

Assessment of performance of hydraulic tomography

The performance of the SSLE estimator used in the hydraulic tomography was evaluated quantitatively by statistical measures, i.e. the mean absolute error normal L1 and mean square error normal L2 between the true and estimated parameter values, see Ni et al. (2009). In addition, the correlations based on the estimated and true parameters were also calculated. Furthermore, cross plots of the estimated versus true K-fields were prepared, both from the HT analysis and kriging of the direct measurements of K, see Figure 5 in Ni et al. (2009) .

Figure 5b in Ni et al. (2009) indicates that the HT analysis and the associated SSLE model produced accurate estimations of K. However, the kriging algorithm provided biased estimations of K (see Figure 5a in Ni et al. (2009)), which can be caused by the origin of 27 direct K-measurements used in the kriging estimation. Most *K* measurements used for the kriging estimation are relatively high which resulted in bias towards high *K* values in the kriging estimation. The authors concluded that, in order to obtain a better estimation of *K* and velocity fields, the correlation between head and hydraulic conductivity must be considered simultaneously, which is accounted for in the HT analysis.

Sampling strategy for hydraulic tomography surveys

Based on the estimated K-field from hydraulic tomography for the synthetic aquifer described above, a variety of cases were studied to illustrate the accuracy of *K* field estimations from HT due to different pumping strategies, numbers of direct *K* measurements and degrees of *K* heterogeneity in the aquifer, respectively.

Pumping strategy: The following observations were made regarding the pumping strategy: 1) the pumping locations that provided higher head changes (higher pumping rates) resulted in more accurate estimation of *K* fields, 2) more pumping events will generally lead to a more accurate estimation of the *K* field; however, the appropriate number of pumping events depends on the pumping rate and the *K* distribution in an aquifer and 3) the pumping locations should be in high *K* zones (or layers)

of an aquifer to maximize the head information from the measurement points. On the basis of these observations it was concluded that the appropriate number of pumping locations for the actual aquifer is 2 to 3, positioned in the high *K* zones.

Degree of aquifer heterogeneity: K-fields were generated with different heterogeneity (i.e. variance and correlation length of K) using a random field generator. Based on the previous results of the pumping strategy, the assessment of the sampling strategy was based on a case with 3 pumping locations and pumping events (cross-hole tests). Each generated K-field was subsequently analysed by HT using head data from all 27 observation sections. The mean performance of the HT analyses was then assessed from the estimated L1 and L2 normals described above. These performance measures showed that the estimation accuracy decreased with increased variance of the K-values and improved with increasing correlation length. Based on these results, the study suggested that an appropriate distance of the observation wells to the pumping well should be less than one-third of the correlation length for ln(K) in the X-direction.

Effects of direct K-measurements: The effects on HT of the number of included direct K-measurements from the observation well sections (in addition to the head data from these wells) were studied for two of the cases (f and j) from previous simulations on the effect of the pumping strategy. The cases represent two (case f) and three pumping events (case j), respectively, for a decreasing number (from left to right) of direct K-values used in the HT analyses (from initially 27 to zero K-values). The same number of K-values was used in each of the three observation wells.

The results show that the estimation errors (represented by L1 and L2) increased gradually with decreasing numbers of direct *K*-measurements included in the HT analyses. However, the differences were not significant for small numbers of *K*-measurements such as three, one, and zero. The worst scenario is zero *K* measurements for each case. Under this scenario, *L*1 and *L*2 are 0.385 and 0.230 for case (f), while *L*1 and *L*2 are 0.352 and 0.192 for case (j). It was concluded that more pumping events (case j) will give better results, although no direct *K*-measurements are used for *K* estimations in HT.

Finally, it was concluded that the HT analyses results were significantly improved by including more pumping events (cross-hole tests) when no direct *K*-measurements are available. However, with a sufficient number of direct *K*-measurements, more pumping events had relatively minor impact on the final *K* estimation from HT.

Conclusions by the authors

The numerical assessments on the HT test strategy showed that more pumping events (cross-hole tests) will generally lead to more accurate estimations of *K* fields of the aquifer. However, with a sufficient number of direct *K*-measurements included as supporting data, more pumping events have relatively little impact on the final *K* estimation from HT.

Pumping locations which provided higher drawdown (higher pumping rates) resulted in more accurate estimation of *K* fields. Thus, the pumping locations should be located in high *K* zones in the aquifer to maximize the head information from observation wells.

It was concluded that the appropriate number of pumping events for the actual aquifer is 2–3, located in high *K* zones. Finally, the appropriate distances to observation wells are suggested to be less than one-third of the ln(*K*) correlation length in the X-direction.

PART B

Interference tests serving as potential candidates for hydraulic tomography analysis

1 Introduction

In this part an overview of data from selected, hydraulic interference tests and associated measurements during the SKB site investigations at Forsmark and Laxemar is presented. Selected interference tests from these two sites are discussed in Section 3 and 4 in Part A of this report. In addition, a summary of results from previous subsurface investigations at the Hard Rock Laboratory of Äspö is presented. The main aim is to propose 1–2 (series of) interference tests as potential candidates for hydraulic tomography analysis as suggested in Part A. The data material is focussed on hydraulic interference tests at different scales in heterogeneous, fractured rock, preferably in combination with tracer dilution tests and cross-hole tracer tests in selected observation borehole sections. In addition, data from e.g. single-hole hydraulic tests and borehole flow logging (including difference flow logging) are included.

Hydraulic tomography is based on simultaneous analysis of data from several interference tests with pumping boreholes at several locations within the same observation borehole network. Furthermore, supporting data from groundwater flow measurements in observation boreholes and cross-hole tracer tests may be used to further condition and constrain the hydraulic tomography analysis. The data material in this appendix is therefore focussed on previous interference tests in the TRUE and TRUE Block Scale projects in sub-surface boreholes at the Hard Rock Laboratory at Äspö. In these two projects a large number of hydraulic interference tests in different boreholes in combination with groundwater flow measurements and cross-hole tracer tests have been performed.

Hydraulic interference tests performed in other projects at the Äspö Hard Rock Laboratory (e.g. Prototype) have generally not been combined with tracer tests and groundwater flow measurements and are therefore not included in this report. Hydraulic interference tests in surface boreholes during the site investigations at Forsmark and Laxemar are only discussed briefly in this appendix since a synthesis of the results of interference tests combined with groundwater flow measurements and cross-hole tracer tests, as potential candidates for hydraulic tomography, are reported in Part A of this report.

The main aim of this appendix is to provide an overview of the scope and main results of combined hydraulic interference tests and associated measurements during different test campaigns of the selected SKB characterization projects. To get more detailed information of the actual tests the corresponding test reports must be consulted. Retrieval of test data and estimated parameters should be made from the Sicada data base. In the first part of this appendix the scope of testing in the different stages of the projects is described whereas in the second part the main results of the corresponding tests are presented in Appendices.

2 Selected hydraulic interference tests from the site investigations at Forsmark and Laxemar

In this section, a list of hydraulic interference tests performed during the site investigations in Forsmark and Laxemar of potential interest for hydraulic tomography is firstly presented, see Table 2-1. Only large-scale interference tests including a large number of observation boreholes in rock are included (no soil pipes). The results from four (4) selected interference tests from Forsmark and Laxemar are discussed in Chapter 3 and 4 in Part A of this report. Secondly, candidate interference tests for hydraulic tomography analysis are selected and discussed further.

The selected candidate interference tests for hydraulic tomography in Table 2-2 mainly correspond to the large-scale, confirmatory interference tests combined with cross-hole tracer tests and tracer dilution tests (for groundwater flow) listed in Table 2-1. A synthesis of the results from four confirmatory hydraulic interference tests and tracer tests at Forsmark and Laxemar is presented in Part A of this report. Thus, only a brief description of these tests is made here.

2.1 Forsmark site

Two large-scale hydraulic interference tests were carried out in HFM14 during the site investigations. The first test was performed during the summer of 2006. The second test was performed in 2007 in combination with cross-hole tracer tests and tracer dilution tests for groundwater flow measurements. The test layout was similar for the two interference tests but more boreholes were drilled and included in the later test. The locations of the boreholes in the Forsmark area, including the pumping borehole HFM14 and radii corresponding to distances of 500 m, 1,000 m and 2,000 m from HFM14, are shown in Figure 2-1.

A confirmatory hydraulic interference test and tracer test in the pumping borehole section KFM02B:408.5 –434.0 m. The objectives of the combined interference test and tracer test were to partially verify the hydrogeological model of the Forsmark candidate area and the transport characteristics previously determined from laboratory tests of drill cores. The pumping borehole KFM02B is located to the southeast of HFM1, see Figure 2-1. The flow rate and drawdown by the end of the flow period in the pumping borehole section in KFM02B are shown in Table 2-2. The subsequent pressure recovery periods of the tests was also recorded.

Another large-scale interference test was carried out in HFM33. The pumping borehole HFM33 is located to the northeast of HFM1, see Figure 2-1. However, no supporting measurements were made in this test.

2.2 Laxemar site

Two confirmatory, combined hydraulic interference tests and tracer tests were performed in HLX27 and HLX28 at Laxemar. The main aims of the tests were to verify the hydrogeological model of the Laxemar area and the transport properties of some major flow paths in the area previously determined from laboratory tests of drill cores and other investigations. The locations of the boreholes, including the pumping boreholes HLX27 and HLX28, are shown in Figure 2-2. Borehole HLX27 is located to the southeast of HLX28. The flow rates and drawdown in the pumping boreholes by the end of the flow period are shown in Table 2-2. The subsequent pressure recovery period of the tests was also recorded. In addition, a large number of hydraulic interference tests were performed in Laxemar. Since the latter tests were not combined with any supporting hydraulic measurements they are considered to be of less interest for hydraulic tomography. An exception would possibly be the interference tests in boreholes KLX09B-F and KLX11B-F which were combined with flow measurements (difference flow logging) in open observation boreholes while pumping in one of the other open boreholes (without using packers). The primary aim of the measurements was to determine the position and flow rate of conductive fractures and to establish the hydraulic connectivity between the boreholes.

Table 2-1. List of selected hydraulic interference tests at Forsmark and Laxemar during the site investigations of potential interest for hydraulic tomography.

Site	Pumping borehole	Year	Combined with the following measurements	SKB report
Forsmark	HFM14	2006	GW flow measurements in observation sections (tracer dilution tests)	P-06-196 P-06-188
Forsmark	HFM14	2006*	None	P-06-196
Forsmark	HFM14	2007	Cross-hole tracer test+GW flow measurements in observation sections (tracer dilution tests)	P-07-228
Forsmark	KFM02B**	2007	Cross-hole tracer test+GW flow measurements in observation sections (tracer dilution tests)	P-08-13
Forsmark	HFM33	2007	None	P-07-229
Laxemar	HLX27	2008	Cross-hole tracer test+GW flow measurements in observation sections (tracer dilution tests)	P-08-96
Laxemar	HLX28	2009	Cross-hole tracer test+GW flow measurements in observation sections (tracer dilution tests)	P-09-62
Laxemar	HLX27, HLX28, HLX32	2008	None	P-07-186
Laxemar	KLX19A-two sections	2008	None	P-08-15
Laxemar	KLX27A-two sections	2008	None	P-08-16
Laxemar	A large number of cored boreh.	2007	None	P-07-182
Laxemar	A large number of cored boreh.	2008	None	P-07-183
Laxemar	KLX27A-two sections	2008	None	P-08-16
Laxemar	KLX09B-F	2006	GW flow measurements in open observation boreholes (difference flow logging)	P-06-146
Laxemar	KLX11B-F	2007	GW flow measurements in open observation boreholes (difference flow logging)	P-07-65
Laxemar	KLX07A-five sections	2007	None	P-06-145
Laxemar	KLX08-three sections	2007	None	P-07-18
Laxemar	KLX20A-two sections	2007	None	P-07-39
Laxemar	HLX34, HLX37, HLX42	2007	None	P-07-185

* Same test as above but also including borehole KFM10A.
** Pumping was performed in an isolated borehole section.

Table 2-2. Selected candidate hydraulic interference tests at Forsmark and Laxemar during the site investigations for hydraulic tomography. Test data from the pumping boreholes together with estimated transmissivity T of the pumping boreholes/sections.

Site	Pumping borehole	Config. of pumping borehole	Flow rate (L/min)	Final drawdown[1)] (m)	T [2)] (m^2/s)	Duration[3)] (days)
Forsmark	HFM14	Open hole	349	c. 12	$5 \cdot 10^{-4}$	c. 105
Forsmark	KFM02B	Isolated section	20 → 25	c. 10	$3 \cdot 10^{-5}$	c. 55
Laxemar	HLX27	Open hole	50 → 75	c. 22	$3–5 \cdot 10^{-5}$	c. 90
Laxemar	HLX28	Open hole	350 → 300	c. 36	$3 \cdot 10^{-4}$	c. 126
Laxemar	KLX09B-F	Open hole	10–33	Varying[4)]	Varying[4)]	c. 2–4
Laxemar	KLX11B-F	Open hole	2.3–21.1	Varying[4)]	Varying[4)]	c. 4–5

[1)] Final drawdown in pumping borehole at stop of pumping.
[2)] Determined from transient evaluation of single-hole pumping tests before any outer boundary effects.
[3)] Duration of the flow period.
[4)] Varying in different borehole.

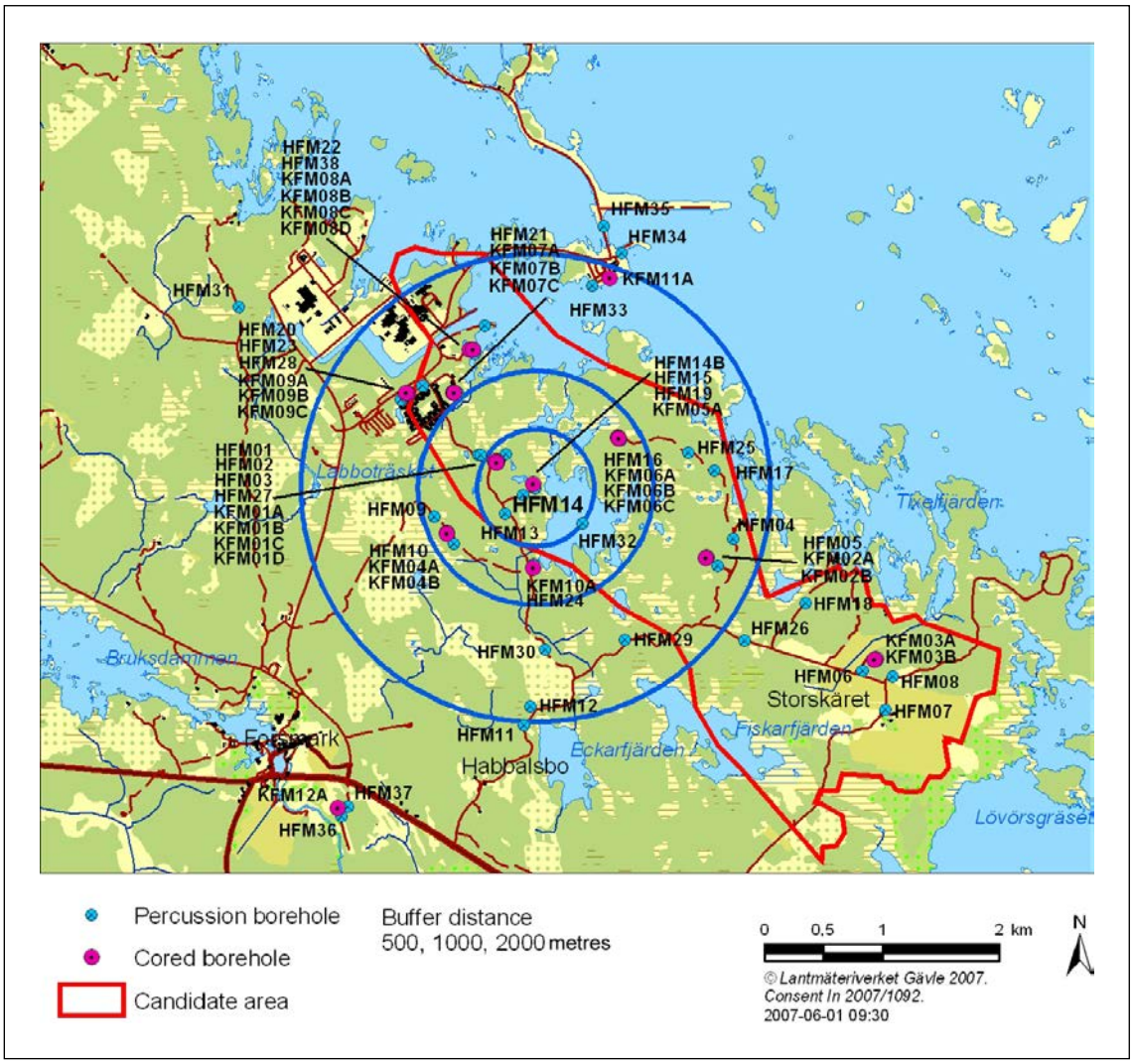

Figure 2-1. *The investigation area in Forsmark including part of the candidate area selected for more detailed investigations. The positions of the boreholes included in the interference test in HFM14 are displayed as well as the areas corresponding to radii of 500 m, 1,000 m and 2,000 m from HFM14, respectively. From Gokall-Norman and Ludvigson (2008b).*

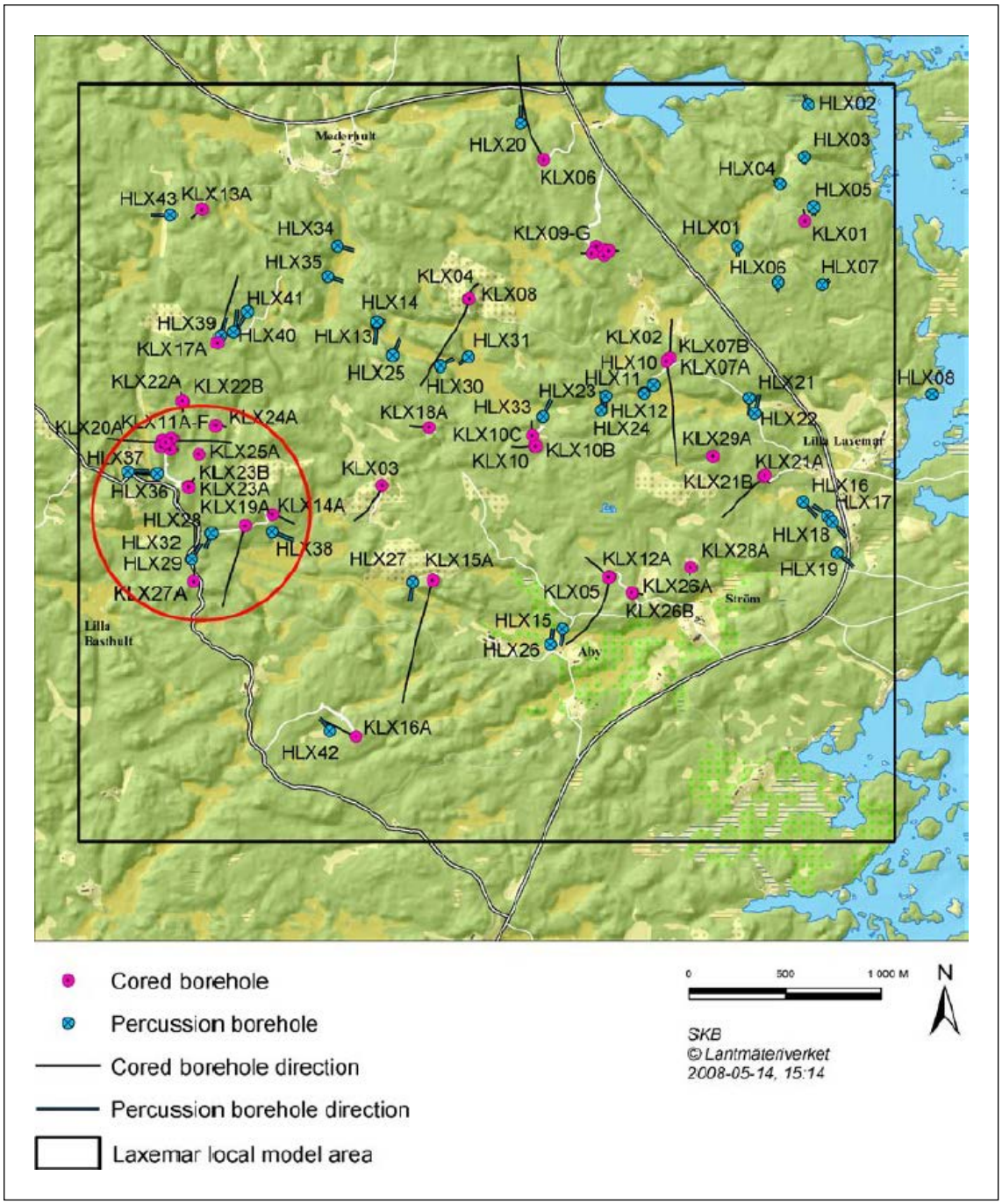

Figure 2-2. *The Laxemar area and the boreholes involved in the interference tests. The pumping boreholes HLX27 and HLX28 are located in the south-western part. From Thur et al. (2010).*

3 Combined hydraulic interference tests and tracer tests in TRUE project at Äspö

In this section the data available from selected cross-hole pressure interference tests and accompanying measurements previously performed in the TRUE project including TRUE-1, TRUE Continuation and TRUE Completion at the Hard Rock Laboratory at Äspö are presented. Several of the tests are combined with borehole flow (tracer dilution) tests, cross-hole tracer tests, flow logging, difference flow logging together with single-hole hydraulic tests (mainly flow- and pressure build-up tests).

3.1 TRUE-1

3.1.1 General

The first TRUE stage (TRUE-1) aimed at understanding tracer transport in a single fracture. An array of 5 boreholes (KXTT1-4 and KA3005A) penetrating interpreted hydraulic features in the TRUE-1 rock block was investigated, see Figure 3-1, on a detailed investigation scale (< 10 m). Four hydraulic features (Feature A–D) were identified within the borehole array. Feature A was primarily investigated together with its hydraulic interaction with its immediate surroundings. The boreholes were equipped with multi-packer systems with up to 5 test sections in each borehole. The packer configuration in the boreholes was changed (optimized to different purposes) during different stages of the TRUE-1 stage, see Appendix 1.

During TRUE-1, single-hole flow and pressure build-up tests, high resolution single packer flow logging and cross-hole interference tests were carried out. Continuous hydraulic head measurements were made in all borehole sections connected to the Äspö HRL Hydro Monitoring System (HMS) during the entire test period. The tests were carried out during 1995–2001. Furthermore, tracer dilution tests were performed in selected observation sections during the interference tests to quantify the groundwater flow through the borehole sections at natural and under flowing conditions, respectively. Finally, a few cross-hole tracer tests were carried out.

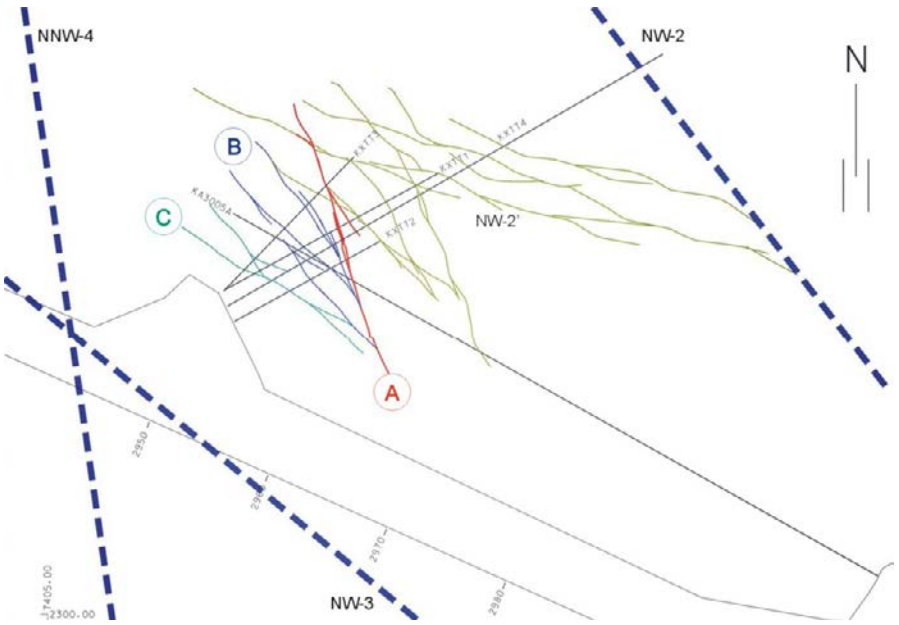

Figure 3-1. *Horizontal section at Z = –400 masl showing structural model based on identified conductive geological structures in the TRUE-1 rock volume. From Winberg et al. (2000).*

3.1.2 Cross-hole pressure interference tests

In total, 14 short cross-hole tests were carried out by individually flowing selected borehole sections in different hydraulic features, see Table 3-1. The flow rates varied from 0.14 to c. 52 L/min while the duration of the flow period ranged between 30–319 minutes. The pressure responses in adjacent boreholes were recorded by the HMS or by portable data loggers. An example of the pressure responses during a cross-hole pressure interference test is shown in a linear HMS-diagram in Figure 3-2.

Response analysis

Firstly, a response analysis was made based on response Index 1 and 2, defined in Section 3.2 in the Part A of this report, to get an overview of the pressure drawdown responses during the different interference tests. Time-drawdown plots were prepared for borehole sections showing a total drawdown of more than s = 0.1 m (1 kPa) at stop of the flow period. This threshold pressure drawdown was chosen with consideration of the amplitude of the tidal effects in the boreholes which may be in the order of 1–5 kPa, thus complicating the identification of responding observation sections during the tests. From these plots, the response times (tr) for each section were estimated. The response time is here defined as the time after start of flowing when a pressure drawdown (or recovery) of 1 kPa is observed (from logarithmic drawdown plots) in the observation sections.

The response times were normalised with respect to the straight-line distance R between the (midpoints of) the sink section and each observation section. The ratio (tr/R^2) is denoted response Index 1. This ratio is inversely related to the hydraulic diffusivity (T/S) of the rock, which indicates the speed of propagation of the pressure drawdown signal created in the sink section. The final drawdown at stop of pumping (s) in the observation sections was determined from the drawdown data. To account for the different flow rates used in the tests and to make pressure response plots comparable between tests, the final drawdown was normalised with respect to the final flow rate (Q). The ratio (s/Q) is denoted response Index 2.

From response plots of s/Q versus t_r/R^2 for each interference test, sections with anomalously fast response times (high hydraulic diffusivity) and large (normalised) drawdown can be identified. Such sections, showing primary responses, can be assumed to have a distinct hydraulic connection to the sink section and may be intersected by a single fracture, deformation zones or other conductive structures in the rock. On the other hand, sections with delayed and weak (secondary) responses may correspond to sections in the rock mass between such structures.

Table 3-1. Compilation of test data from the flowing boreholes during the cross-hole pressure interference tests in the TRUE-1 block. From Winberg et al. (2000)

Test #	Flowing borehole	Section ID code **	Flow (L/min)*	Flow period (min)	Hydraulic Feature
1	KXTT1	P2	0.28	78	A
2	KXTT1	P3	1.70	248	B
3	KXTT2	P1	0.14	73	A
4	KXTT2	P3	0.95	248	B
5	KXTT2	P2	0.34	70	B
6	KXTT3	P2	4.12	319	A
7	KXTT3	P3	0.40	70	B
8	KXTT4	P2	7.30	268	NW-2’
9	KXTT4	P4	0.40	61	B
10	KA3010A	P1+P2	25.40	218	NW-2
11	KA3005A	P4	0.65	67	A?
12	KA3005A	P2	0.90	188	A
13	KXTT1	P1–P4	52.20	232	NW-2
14	KXTT4	P3	0.48	30	A

* Flow at the end of flow period.
** The section ID codes are explained in Appendix 1.

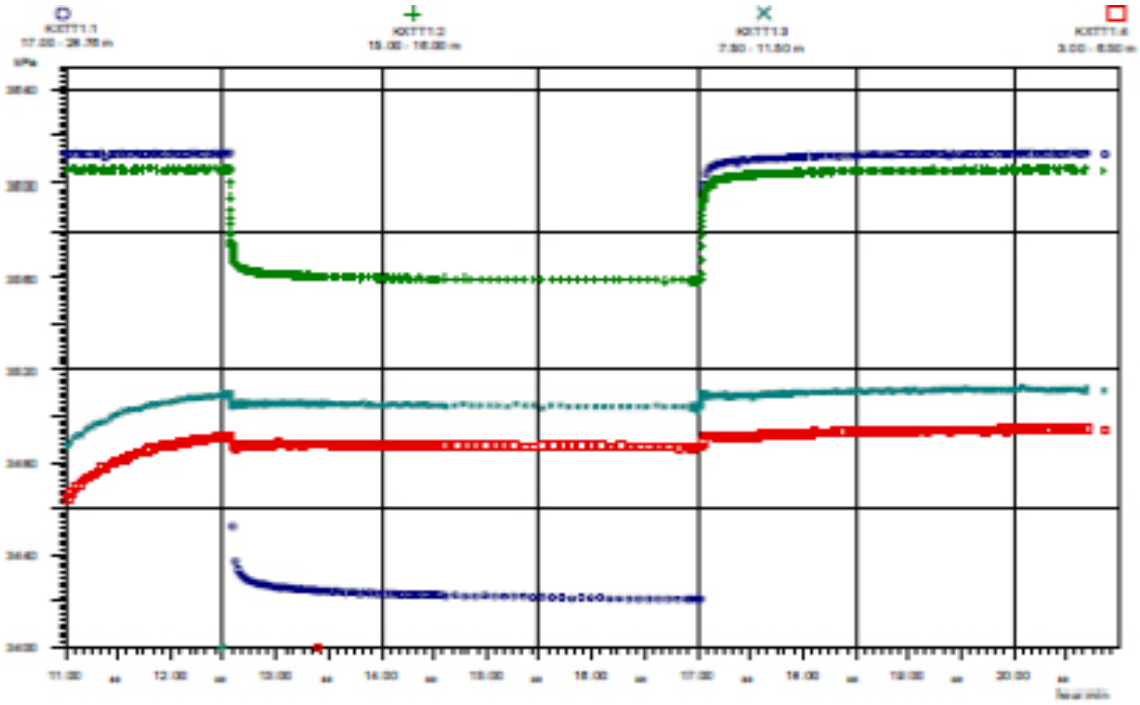

Figure 3-2. *Example of pressure responses in observation sections KXTT1:R1, KXTT1:R2 and KXTT1:R3 during the cross-hole pressure interference test in borehole section KXTT4:P2 (test #8). From Winberg et al. (2000).*

By classifying the response indices during each test a response matrix for all interference tests may be prepared. The response matrices of Index 1 and 2 during the interference tests in TRUE-1 are presented in Table A2-1a and 1b in Appendix 2, respectively. The definitions and classifications of the response indices 1 and 2 are shown in Table A2-1c. The response matrices show that, for the tests performed in Feature A, distinct responses were obtained in the observation sections in Feature A which reflects the relative hydraulic isolation of Feature A within the TRUE-1 rock block. The interference tests in Feature B and D show more complex response patterns.

Transient evaluation of pressure responses

The transient evaluation was concentrated on the pressure responses in observation sections located in Feature A (Tests #1, #3, #6, #12 and #14) and in zones NW-2 (Tests #10 and #13) and NW-2' (Test #8), see Table 3-1. However, only observation sections with the most distinct pressure responses (according to the previous response analysis) were evaluated for hydraulic parameters.

Since the interpreted dominating transient flow regime converged from pseudo-radial to pseudo-spherical in most observation sections, a standard model for a leaky aquifer in a porous medium (Hantush and Jacob 1955) was used in the transient evaluation of the pressure responses in the observation sections. The estimated transmissivity T, storativity S and leakage coefficient K'/b', which thus represent hydraulic parameters of an equivalent homogeneous porous medium, are shown in Table A2-2 in Appendix 2. In fractured rock like the TRUE-1 rock block, the tested target hydraulic feature may be assumed to represent the (leaky) aquifer whereas the confining layers may be represented by the adjacent rock between the hydraulic structures.

3.1.3 Tracer dilution tests

Tracer dilution tests under natural groundwater flow conditions in selected test sections in Features A and B were carried out during TRUE-1 in October, 1995 and April, 1997, see Table A2-3 in Appendix 2. It should be observed that the packer positions in the boreholes were slightly changed between the two series of measurements, see Appendix 1. The measured changes of flow were small between the two measurement series.

3.1.4 Cross-hole tracer tests

The TRUE-1 tracer test programme included 18 different test set ups performed during 1995–1998, see Table 3-2. In total, seven flow paths were tested in Feature A and one in Feature B over distances ranging from 2.6–9.6 m between injection and withdrawal points. Both conservative and sorbing tracers were used in the tracer tests. An example of the tracer breakthrough curve and estimated transport parameters for the flow path KXTT1:R2→KXTT3:R2 from simplified analytical interpretations are shown in Figure 3-3 and Table A2-4 in Appendix 2, respectively. The parameters shown in the latter table were determined for almost all TRUE-1 tracer tests.

3.1.5 Flow and pressure build-up tests

Estimated steady-state transmissivities (T_M) according to Moye's formula from single-hole flow- and pressure build-up tests in c. 2–4 m long sections in the boreholes in the TRUE-1 array are shown in Table A2-5 in Appendix 2. The lower and upper measurement limit of these tests were $T_{min} = 5 \cdot 10^{-10}$ and $2.8 \cdot 10^{-6}$ m^2/s respectively. For comparison, summed up transmissivities (T_F) from single-packer flow logging in consecutive 0.5–1 m sections corresponding to the measured borehole sections during the flow and pressure build-up tests are also presented in Table A2-5. The agreement of the results is generally good.

For the flow and pressure build-up tests in Feature A, also transient GRF (Generalized Radial Flow) and GTFM (Graph Theoretic Field Model)-analyses were performed. In addition, steady-state analysis of the responses in test sections in Feature A in the flowing boreholes during the cross-hole tests was made according to Thiem's equation. A typical range of the estimated transmissivity of Feature A is $T = 8 \cdot 10^{-9}$–$4 \cdot 10^{-7}$ m^2/s.

Table 3-2. Summary of cross-hole tracer tests performed within the TRUE-1 Project. From Winberg et al. (2000).

Test	Flow geometry	Flow path	Mass recovery (%)
PTT-1	Radially Converging	T1→T3 *)	95
		T3→T4 **)	92
RC-1	Radially Converging	T1→T3	93
		T2→T3	0
		T4→T3	100
		KA3005A→T3	0
DP-1	Dipole	T1→T3	88
DP-2	Dipole	T2→T1	56
DP-3	Dipole	T2→T1	45
DP-4	Dipole	T2→T4	30
RC-2	Radially Converging	T1→T4	5
DP-5	Dipole	T4→T3	28
DP-6	Dipole	T4→T3	70
PDT-1	Radially Converging	T1→T3	44
		T4→T3	74
PDT-2	Radially Converging	T1→T3	52
		T4→T3	99
PDT-3	Radially Converging	T4→T3	95
STT-1	Radially Converging	T4→T3	100
PDT-4	Radially Converging	T1→T3	100
STT-1b	Radially Converging	T1→T3	100
RC-3	Radially Converging	T2→T3	13
STT-2	Radially Converging	T4→T3	88

*) Test in Feature A (KXTT4:P3 → KXTT3:P2), cf. Appendix 2.
**) Test in Feature B (KXTT3:P3 → KXTT4:P4), cf. Appendix 2.

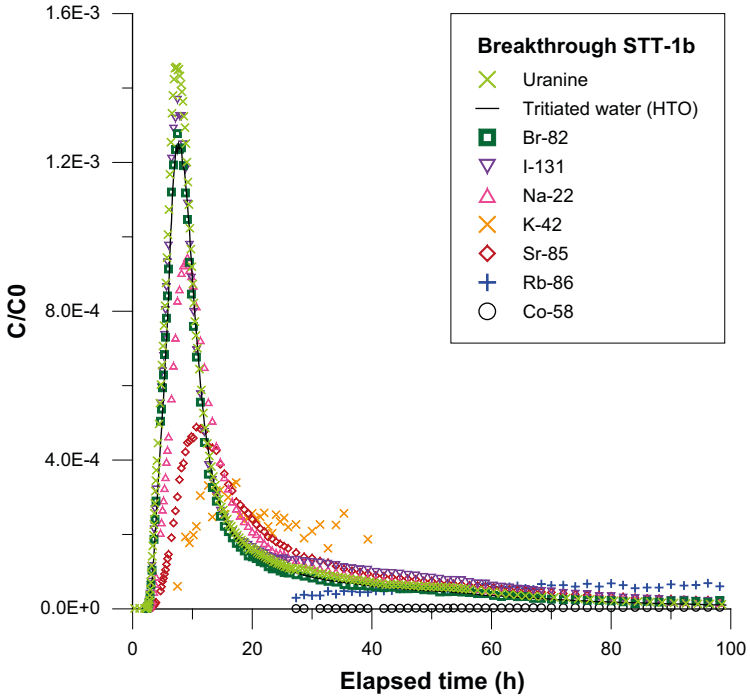

Figure 3-3. *Tracer breakthrough after 100 h in the pumping section KXTT3:R2 during test STT-1b (see Table A2-4 and A2-5). Concentrations are normalized to concentrations in the injection section at t = 2 h. From Winberg et al. (2000).*

3.1.6 Single-packer flow logging

Single-packer flow logging was made in 0.5 m steps to identify major inflow zones along the boreholes. The size of the flow anomalies were calculated from the difference of the cumulative flow between two consecutive flow measurements. The minimal detectable flow difference is c. 0.01 L/min. The results of the single packer flow logging are shown in Figure A2-1 in Appendix 2. The transmissivity of 0.5 m borehole sections were estimated from the total (steady-state) transmissivity (T_M) of the borehole estimated from a single-hole flow measurement and the fraction of flow from the 0.5 m section in relation to the total flow.

3.2 TRUE-1 Continuation

3.2.1 General

The project TRUE-1 Continuation involved complementary investigations at the TRUE-1 site with the aim of exploring some of the unresolved issues from previous hydraulic tests and tracer tests performed at the site. The purposes of the TRUE-1 Continuation tests were to obtain more information about the internal structure of the target structure (Feature A), in particular the reason for the dual-peak breakthrough obtained during previously performed tracer tests and the interaction between Feature A and the surrounding fracture network, in particular the interpreted Features B and NW-2. During TRUE-1 Continuation, a new borehole (KXTT5) was drilled and included in the tests. The intersection of KXTT5 with Feature A is shown in Figure 3-6.

The complementary investigations involved five different test set-ups, the three first (CX-1 to CX-3) involving tracer dilution tests combined with cross-hole interference tests and the last two (CX-4 and CX-5) including multiple-hole tracer tests, see Table 3-3. The flow and recovery phases of tests CX-1 to CX-3 were performed as conventional constant rate pressure interference tests implying that the pressures were monitored with a high measurement frequency by the Äspö Hydro Monitoring System (HMS). Flow rate data from the sink sections and the electrical conductivity of the withdrawal water were measured manually during the flow period.

Table 3-3. Sinks, flow rates (Q_2), duration of the flow period (t_p) and sources used for tracer injection during the tests in TRUE-1 Continuation. Section limits in all boreholes at the TRUE-1 site are given in Appendix 1. From Andersson et al. (2002a).

Test	Sink	Feature	Q_2 (L/min)	t_p (h)	Source	Feature	Comments
CX-1	KXTT4:S3	A	0.56	64	KXTT1:R2	A	TDT/interference test
CX-2	KXTT4:S4	B	0.44	64	KXTT1:R3	B	TDT/interference test
CX-3	KXTT3:R2	A	2.64	42	KXTT2:R2	A	TDT/interference test
					KXTT2:R3	B	
					KXTT3:R2	A	Test CX-1 and CX-2
					KXTT3:R3	B	
					KXTT4:S2	A´	
					KXTT4:S3	A	Test CX-2 and CX-3
					KXTT4:S4	B	Test CX-1 and CX-3
					KXTT5:P2	A	
					KA3005A:R2	B	
					KA3005A:R3	A	
					KA3010A:P2	NW-2	
CX-4	KXTT3:R2	A	0.2	c. 535	KXTT4:S2	A´	Tracer test (RC)
					KXTT4:S3	A	
CX-5	KXTT3:R2		2.97	c. 650	KXTT4:S4	B	Tracer test (RC)
					KXTT1:R3	B	
					KXTT4:S3	A	
					KXTT1:R2	A	

TDT = Tracer dilution test.
RC = Radially converging tracer test (during flowing at a constant flow rate).

Tests CX-4 and CX-5 were focused on conservative tracer transport. Both tests were performed in a radially converging flow field with a constant withdrawal rate in borehole section KXTT3:R2 (Feature A). During the entire test sequence, pressure measurements were made in the surrounding borehole sections by the HMS.

3.2.2 Cross-hole pressure interference tests

Three hydraulic interference tests (CX-1 to CX-3) were performed during TRUE-1 Continuation with sinks established in Features A and B, see Table 3-3. The tests were combined with tracer dilution tests in selected observation sections. The evaluation of the interference tests was mainly diagnostic, involving preparation of pressure response diagrams for each test and a common pressure response matrix for all three tests. The response analysis was made on data from the drawdown phase. Pressure data from the recovery phase were only used as supporting data. No transient evaluation was made of the pressure responses in the observation boreholes during the interference tests but hydraulic head data are available from HMS during the entire test period, see Figure A3-1 in Appendix 3.

From the calculated values of the response indices sp/Q2 (Index 1) and tR/R^2 (Index 2) for each observation section during each interference test, a common pressure response matrix as described in Section 3.1.2 showing the response patterns for all three tests was prepared, see Figure A3-2 in Appendix 3. The new borehole KXTT5 was included in these tests. The definitions and class limits of the response indices 1 and 2 are shown in Table A3-1. Slightly different notation of the response parameters was used here compared to the response analysis described in Section 3.1.2.

3.2.3 Tracer dilution tests

Tracer dilution tests were performed in selected sections during tests CX-1 to CX-3, both at natural and during flowing conditions respectively, see examples in Figure 3-4. The measured flows and flow differences ΔQ through the borehole sections due to flowing the sink sections are shown in Table A3-2 in Appendix 3. The new borehole KXTT5 was also used in the tracer dilution tests.

3.2.4 Cross-hole tracer tests

The tests CX-4 and CX-5 were performed as cross-hole tracer tests under radially converging conditions with a constant flow rate in the sink section. In test CX-4, tracers were injected in two borehole sections, see Table 3-3. In test CX-5, tracers were injected in four borehole sections. Examples of tracer breakthrough curves for two flow paths are shown in Figure 3-4. Tracer breakthrough was observed in two sections in each test. The breakthrough curves were analysed with a one-dimensional advection-dispersion model using an automated parameter estimation program (PARAST). The model simulations are shown in Figure 3-5. A summary of the estimated hydraulic and transport parameters for the tested flow paths in tests CX-4 and CX-5 is shown in Table A3-3 in Appendix 3.

3.2.5 Difference flow logging

Difference flow logging (PFL) was performed in the new borehole KXTT5 in TRUE Continuation.

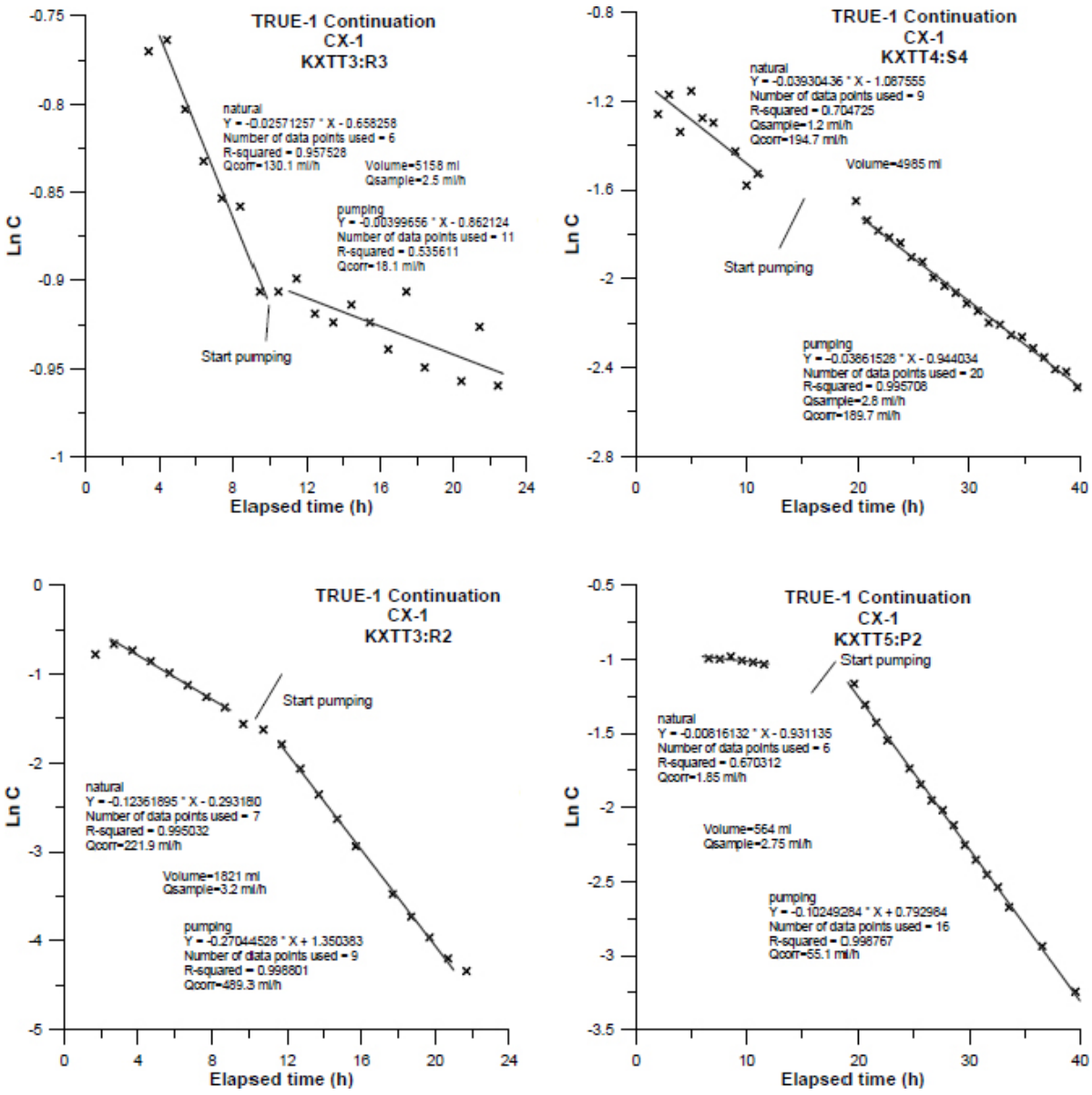

Figure 3-4. *Examples of tracer dilution graphs with LnC (Logarithm of concentration) versus time in sections KXTT3:R3 (Feature B), KXTT4:S4 (Feature B), KXTT3:R2 (Feature A) and KXTT5:P2 (Feature A) during test CX-1 in TRUE-1 Continuation. Steeper dip of the straight-line fit implies a higher flow rate. From Andersson et al. (2002a).*

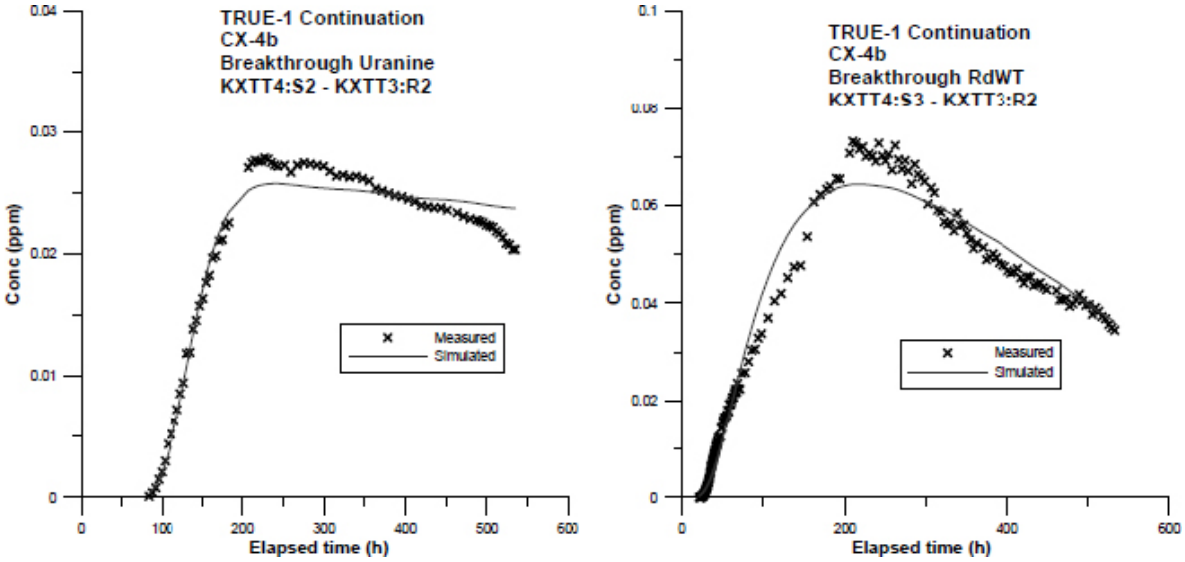

Figure 3-5. *Examples of model simulations of tracer breakthrough curves for two flow paths from test CX-4b in TRUE-1 Continuation. From Andersson et al. (2002a).*

3.3 TRUE-1 Completion

3.3.1 General

As a complement to the TRUE-1 Continuation experimental programme, TRUE-1 Completion was performed at the TRUE-1 site. The main activity within this project has been the injection of epoxy with subsequent over-coring of relevant parts of hydraulic Feature A. Furthermore, a number of complementary *in situ* experiments were performed in order to gather important additional information about Feature A and the TRUE-1 site before the epoxy injection and subsequent destruction (overcoring) of the site.

Three complementary *in situ* experiments, including pre-tests, were performed within TRUE-1 Completion: a SWIW test (Single-Well Injection-Withdrawal), a CEC test (Cation Exchange Capacity) and COM tests (multiple-hole reciprocal cross flow tests).The target structure for all these tests was the hydraulic Feature A at the TRUE-1 site. Six boreholes intercepting Feature A were used in the experiments. In this report the main results of the COM-tests together with the associated tracer dilution tests are presented.

The COM tests were performed for examining and evaluating effects of channelling in Feature A. The tests consist of a number of hydraulic interference tests with measurements of both pressure and flow responses in the observation borehole sections in Feature A. The flowing borehole was alternated in order to evaluate the pressure and flow interferences in several directions and to study whether the responses were reciprocal or not. The flow responses were measured by means of the tracer dilution test under both ambient and flowing conditions.

The COM tests resulted in an assessed hydraulic conductivity distribution and connectivity within Feature A. The approach of systematic alteration of flowing boreholes in combination with registration of both pressure and flow responses may provide a good basis for a detailed modelling of an individual hydraulic feature or a complete site.

3.3.2 Cross-hole pressure interference tests

During the COM tests, eight cross-hole hydraulic interference tests were performed with measurements of both flow and pressure responses in the observation borehole sections penetrating Feature A. Flow responses were measured by tracer dilution tests under both ambient and flowing conditions. Flowing was made in all six borehole sections penetrating Feature A in boreholes KXTT1, KXTT2, KXTT3, KXTT4, KXTT5 and KA3005A, see Figure 3-6. The actual borehole section intervals

including Feature A together with the flow rates used in each flowing borehole section are shown in Table 3-4. The upper and lower limits of all borehole sections during TRUE-1 Completion are shown in Appendix 1.

A response analysis of the pressure responses in the observation sections was made according to Section 3.1.2. The matrices of response indices 1 and 2 for all tests are shown in Table A4-1a and A4-1b. A response diagram for all the eight pressure interference tests in Table A2-3 and A2-4 is shown in Figure A4-1 in Appendix 4.

Steady-state analysis of transmissivity (T_{Th}) was made from the pressure responses in the observation sections in Feature A according to Thiem's method, see Table A4-2. In addition, the transmissivity of the flowing borehole sections (T_M) in Feature A was estimated by Moye's steady-state formula. No transient analysis was made of the COM tests.

Table 3-4. Upper and lower borehole section intervals (Secup and Seclow) of the flowing borehole sections penetrating Feature A together with the flow rates and duration of the flow period of the cross-hole interference tests in TRUE-1 Completion. After Nordqvist et al. (2014).

Flowing borehole section	Secup (m)	Seclow (m)	Q_{pump} (mL/min)	Duration[2)] (h)
KXTT1:R2	15.00[1)]	16.00	350	20.0
KXTT2:R2	14.55	15.55	190	20.8
KXTT3:S3	12.67	14.72	385	11.0
KXTT3:S3	12.67	14.72	2,800	10.1
KXTT4:T3	11.67	13.68	200	14.0
KXTT4:T3	11.67	13.68	600	24.2
KXTT5:P2	9.61	9.81	1,540	19.5
KA3005A:R3	44.78	45.78	870	21.3

[1)] 15.50 m according to Winberg et al. (2000).
[2)] Duration of flow period.

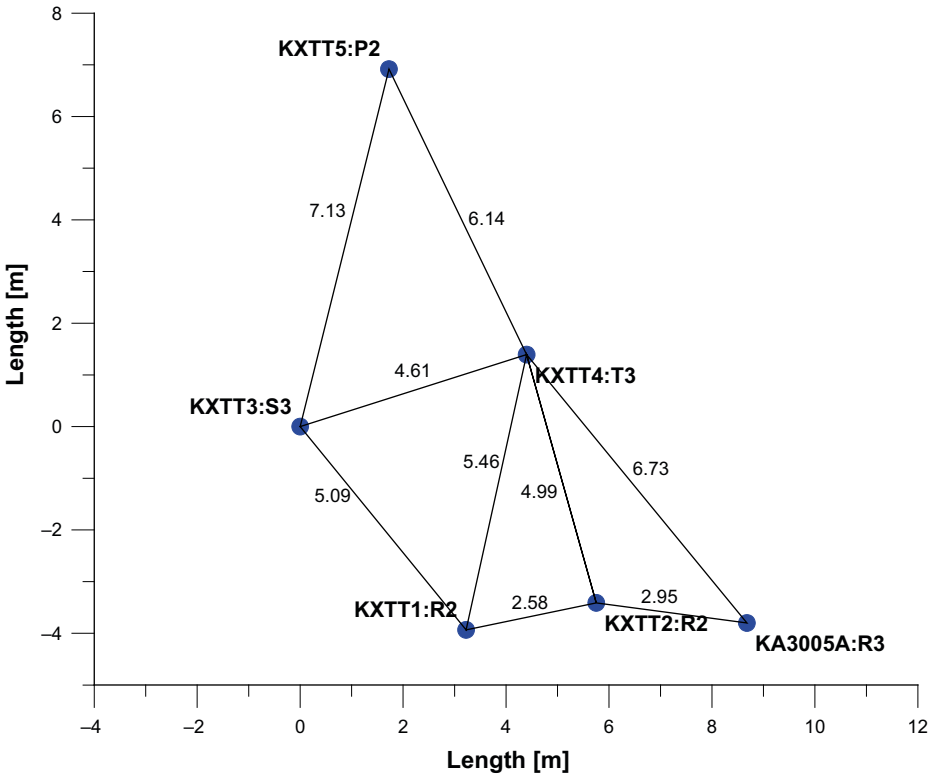

Figure 3-6. *Borehole intersection pattern with Feature A and distances between the actual borehole sections (planar view through Feature A). From Nordqvist et al. (2014).*

3.3.3 Tracer dilution tests

A number of dilution tests under natural and flowing conditions, respectively were performed within the SWIW, CEC and COM experiments, either as part of the main test or as a pre-test. The results of the dilution tests under natural and flowing conditions during the COM hydraulic interference tests are shown in Table A4-3a and A4-3b, respectively.

Finally, the measured flow through the observation sections from the tracer dilution tests (Q_{flow}) was compared by the corresponding flow that would be theoretically expected (Q_{theory}), based on the actual pumping flow rate and assuming radial flow in an equivalent homogeneous two-dimensional hydraulic feature. In most cases, the ratio Q_{flow}/Q_{theory}, was well below 1 which would indicate rather poor flow responses in the observation boreholes, indicating rather low hydraulic connectivity or long flow paths.

3.3.4 Cross-hole tracer tests

No cross-hole tracer tests were performed in TRUE-1 Completion.

4 Combined hydraulic interference tests and tracer tests in TRUE Block scale at Äspö

The TRUE Block Scale project at the Hard Rock Laboratory at Äspö consists of several stages; the Preliminary Characterization Stage (PCS), Detailed Characterization Stage (DCS), Tracer Test Stage (TTS) and TRUE Block Scale Continuation.

4.1 Preliminary characterization stage

4.1.1 General

One of the components of the TRUE Block Scale Preliminary Characterization Stage (PCS) was to conduct a combined interference and tracer test programme in the instrumented array within the Äspö HRL. In total, 19 short interference tests of different duration were performed, six of them with duration of 1–2 days and the rest with duration of only 30–60 minutes. The pressure responses were measured in a large number of observation borehole sections.

Flow measurements using the tracer dilution technique were performed simultaneously in 3–6 observation sections during the long-term interference tests. Furthermore, tracer injections were made in three observation sections during one of the tests as a cross-hole tracer test.

4.1.2 Cross-hole interference tests

A planar view of the TRUE Block Scale area including all boreholes used for pressure monitoring is shown in Figure 4-1. A summary of the test periods, sink sections and flow rates in the sink sections used during all 19 interference tests is given in Table 4-1. Both constant flow (CF) and constant head (CH) interference tests were performed, partly due to restrictions set by the equipment (not able to regulate flow rates above 5 L/min) and partly for practical reasons, cf. Table 4-1.

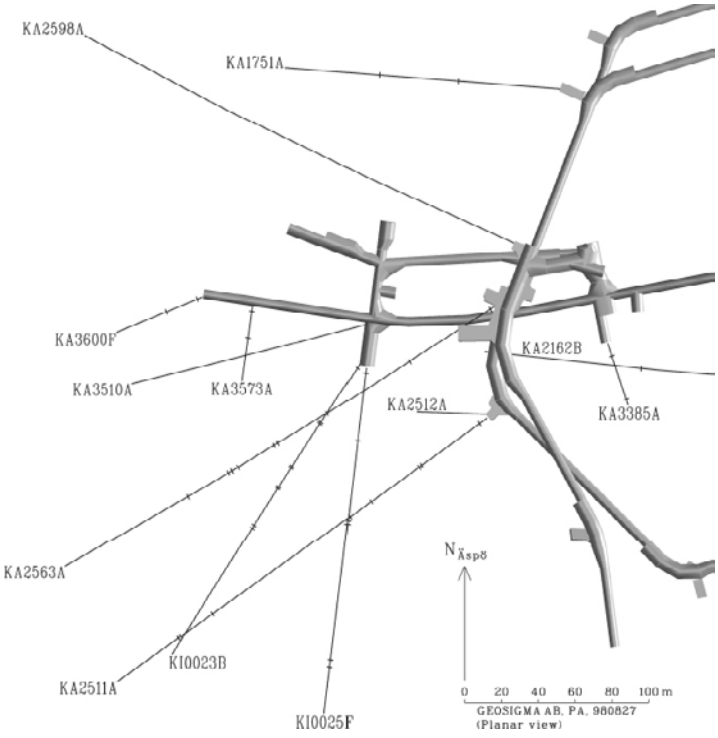

Figure 4-1. *Planar view of the TRUE Block Scale area including all boreholes used for pressure monitoring. The tics on the borehole projections represent packer positions valid at the time, cf. Appendix 5 and Figure A6-1a and A6-1b for the exact packer positions. From Andersson et al. (1998).*

Table 4-1. Summary of performed interference tests during TRUE Block Scale. Preliminary Characterization Stage. (CH = Constant head, CQ = Constant flow). Packer positions are given in Appendix 5. From Andersson et al. (1998).

Test #	Source section	Test type	Q* (l/min)	S_p ** (m)	Q/s_p (m^2/s)	Flow period (h)	Structure
ENW-2	KA2511A:S5	CQ	3.10	2.9	1.78E-05	48	#7
ENW-1	KA3573A:P2	CH	9.3	36.1	4.29E-06	48	#5
ESV-2	KI0023B:P8	CQ	4.14	7.86	8.78E-06	48	#7
ESV-1a	KA2563A:R5	CQ	1.55	18.9	1.37E-06	24	#20
ESV-1b	KI0025F:R4	CH	0.39	415	1.57E-08	24	#20
ESV-1c	KI0023B:P6	CQ	1.04	62	2.80E-07	384	#9
1	KI0023B:P4	CH	0.8	386	3.45E-08	0.5	#13
2	KA2512A:P1	CH	20	300	1.11E-06	1	#5
3	KA2598A:P1	CH	40	240	2.78E-06	3.5	#1, #8
4	KA2563A:R1	CH	0.23	309	1.24E-08	0.5	#9, #10
5	KA2563A:R4	CH	0.24	307	1.30E-08	0.5	#13, #18
6	KA2511A:S4	CH	3.4	35.8	1.58E-06	0.5	#6, #16
7	KI0025F:R3	CH	0.36	419	1.43E-08	0.5	?
8	KI0025F:R5	CH	0.63	410	2.56E-08	0.5	#6, #7
9	KI0025F:R2	CH	3.6	10.7	5.61E-06	0.5	#19
10	KI0023B:P7	CH	3.8	280	2.26E-07	0.5	#6, #20
11	KI0023B:P5	CH	0.43	414	1.73E-08	0.5	#18
12	KI0023B:P2	CH	1.9	236	1.34E-07	0.5	#19
13	KA3573A:P1	CH	1.2	216	9.26E-08	0.5	#15

* Flow at the end of pumping period
** Drawdown at the end of the pumping period

The evolution of packer configurations in the boreholes during different stages at the TRUE Block Scale site is shown in Appendix 5. The boreholes used for monitoring of pressure responses in the cross-hole pressure interference tests are shown in Figure A6-1a and A6-1b in Appendix 6. In total, 42 borehole sections were monitored for pressure of which 19 were used as sink sections.

Analysis of the pressure responses in the observation sections was made according to Section 3.1.2. The response matrix for the first 9 interference tests (test ENW-2 to 3) according to Table 4-1 is shown in Figure A6-1a and for the last 10 interference tests (test 4–15) in Figure A6-1b. In addition, transient analysis was made of the pressure responses in selected observation sections. The main purpose of the transient analysis of the interference tests in this study was to estimate the hydraulic parameters and the hydraulic characteristics (eg transient flow regimes) of the most significant pressure responses in the observation sections during each test.

The transmissivity, storativity, hydraulic diffusivity, and in appropriate cases also the leakage coefficient K'/b', were estimated from the tests by standard methods, see Table A6-2 in Appendix 6. As standard interpretation model, Hantush model (Hantush and Jacob 1955) for constant flow rate tests in a leaky aquifer with no aquitard storage was used. The model selection was based on the diagnostic analysis of the dominating transient flow regime(s) during the tests. The distances between the sink sections and the observation sections during each interference test in the Preliminary Characterization Stage are shown in Table A6-1 in Appendix 6.

4.1.3 Tracer dilution tests

The flow rates in three to six selected observation sections during each interference test were determined by tracer dilution tests to serve as guide for selection of suitable tracer injection sections. The dilution tests were performed both under natural gradient and under stressed conditions (flowing during interference tests). Thus, it was possible to simultaneously measure both flow and pressure changes due to flowing of the section. The duration of each tracer dilution test was about 20–24 hours. Tracer dilution tests were carried out in seven observation sections during selected interference tests. In total, 51 flow measurements were performed. The results of the tracer dilution tests are shown in Table A6-3 in Appendix 6.

The results in Table A6-3 show that only two sections responded significantly to flowing, i.e. sections KA2563A:R5 and KI0023B:P6 intersected by structures #20 and #9, respectively. A response was also indicated in section KI0023B:P4 (test ESV-1b) but this response was judged as highly uncertain due to a very scattered data set.

4.1.4 Cross-hole tracer test

Interference test ESV-1c also involved a radially converging cross-hole tracer test with tracer injections in three sections, two in the same structure (Structure #20), KI0025F:R4 and KA2563A:R5, and one in the newly identified Structure #13, in section KI0023B:P4. The tracer injections were performed as decaying pulse injections and sampling was performed in the water withdrawn from the source section, KI0023B:P6 (Structure #9). The tracers used were three different fluorescent dyes, Uranine (KI0025F:R4), Rhodamine WT (KA25623A:R5) and Amino G Acid (KI0023B:P4).

Tracer breakthrough could only be detected from the injection of Rhodamine WT in KA2563A:R5. The breakthrough curve showed one distinct peak after 30 hours of elapsed time. There were no visible signs of transport in multiple pathways although this may be hidden in the tailing of the curve. The one-dimensional advection–dispersion model described above, could not fit the tail of the breakthrough curve very well. This may be explained by the presence of multiple pathways, but also by other phenomena, e.g. diffusion or sorption.

A summary of the estimated hydraulic and transport parameters is shown in Table A6-4. The transport parameters derived from the numerical modelling and the analytical expressions described in Appendix 3 (Table A3-3) are very similar to those obtained for Feature A in the TRUE-1 tracer tests, cf. Table A2-4.

4.2 Detailed characterization stage

4.2.1 General

One of the components of the TRUE Block Scale Detailed Characterisation Stage (DCS) was to conduct a combined pressure interference and tracer test programme (pre-tests) in the instrumented Block Scale array. The overall objectives of the pre-tests (PT-1 to PT-4) were to test the current deterministic structural model (March 99 model) and to test the possibility to conduct cross-hole tracer tests with injection of tracer in points belonging to the network of deterministic (discrete) structures.

In total, four hydraulic interference tests (PT-1 to PT-4) were performed with duration of 1 to 28 days. Flow measurements using the tracer dilution technique were performed simultaneously in 6 to 12 observation sections during the long-term interference tests. The test cycle for PT-1 to PT-3 was similar to the one used in the combined interference and tracer dilution tests in the Preliminary Characterisation Stage (PCS) whereas PT-4 was performed as a radially converging tracer test. Table 4-2 summarises the test set-ups including the expected flow rates through the borehole sections under naturally conditions and the distances to the sink sections.

Table 4-2. Test set-ups for the pre-tests PT-1 to PT-4 during the Detailed Characterization Stage of TRUE Block Scale. The structural interpretation refers to the March 1999 model. From Andersson et al. (1999).

Test #	Sink	Structure #	Test sections	Structure #	Est. nat. flow* (mL/h)	Euclidean distance (m)
PT-1	KI0023B:P4	13	KA2563A:S3	13	?	21
			KI0025F02:P3	13	14	27
			KI0025F02:P5	20	5	22
			KA2563A:S4	20	500	26
			KI0025F:R4	20	2	41
			KI0023B:P6	21	2	15
PT-2	KI0023B:P6	21	KI0025F02:P5	20	5	20
			KA2563A:S4	20	500	16
			KI0025F:R4	20	2	42
			KI0023B:P4	13	1	15
			KI0025F02:P3	13, 21	14	36
			KA2563A:S3	13	?	21
			KI0025F02:P8	6	30	23
			KI0025F02:P6	22	?	18
			KI0023B:P7	6, 20	?	14
			KI0025F02:P7	?	?	20
			KI0023B:P5	?	?	7
			KA2563A:S1	19	?	40
PT-3	KI0025F02:P5	20	KI0023B:P6	21	2	20
			KA2563A:S4	20, 20	500	35
			KI0025F:R4	13	2	24
			KI0023B:P4	13, 21	1	22
			KI0025F02:P3	13	14	24
			KA2563A:S3	6	?	38
			KI0025F02:P8	22	30	21
			KI0025F02:P6	6, 20	?	7
			KI0023B:P7	?	?	26
			KI0023B:P5	?	?	20
			KI0025F02:P7	19	?	15
			KI0023B:P2		?	43
PT-4	KI0023B:P6	21	KA2563A:S1	19	?	40
			KA2563A:S4	20	500	16
			KI0025F02:P3	13, 21	14	36
			KI0025F02:P6	22	?	18

* Estimated based on earlier measurements.

The position of the sink section and tracer dilution test sections during pre-test *PT-1* are shown in Figure 4-2. Tracer injections were made in four borehole sections during the last test (PT-4). Tracer breakthrough was obtained from all four injection points.

4.2.2 Cross-hole interference tests

The flow tests in the sink sections were performed as conventional constant head drawdown tests implying that the flow rate was slightly decaying during the tests. The pressures in all observation borehole sections were monitored with a high measurement frequency to enable transient evaluation of pressure data. The flow rate from the flowing sections together with the electrical conductivity of the discharged water was measured manually during the pumping period. A summary of the sink sections together with flow rate, drawdown, specific capacity and duration of the flow period during the interference tests is shown in Table 4-3.

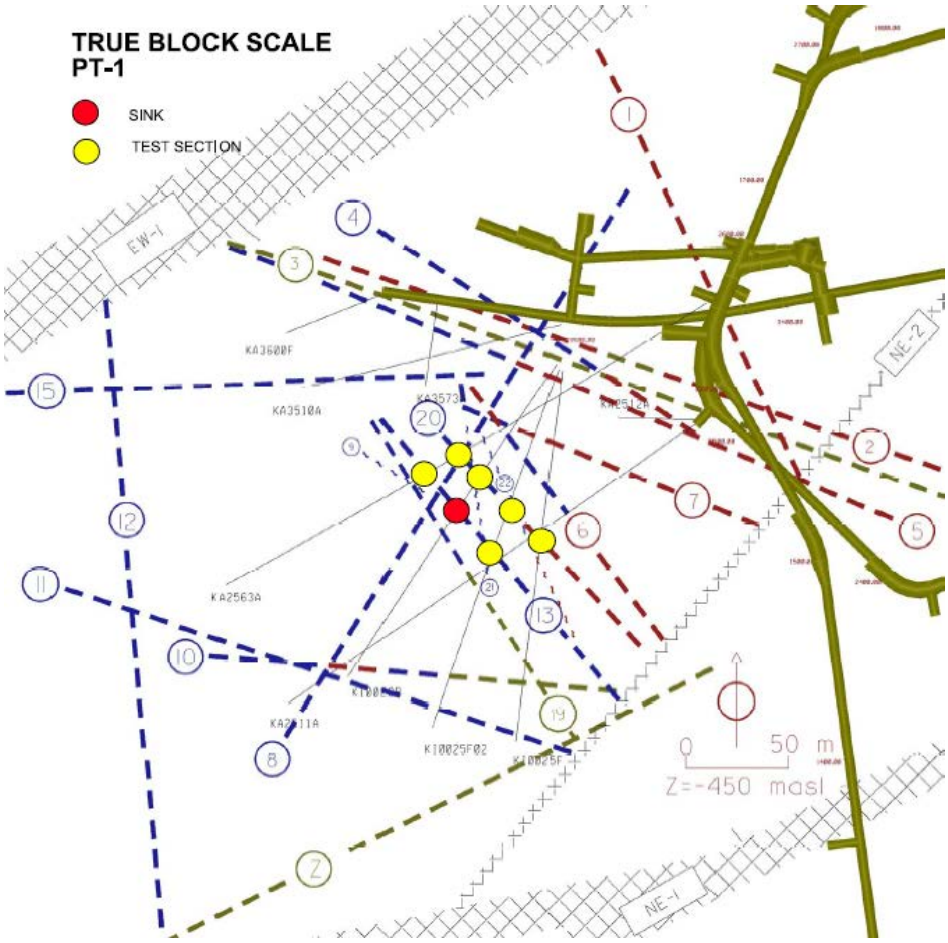

Figure 4-2. *Position of sink and dilution test sections during the TRUE Block Scale pre-test PT-1. The positions of the structures are based on the March 1999 structural model. Z = –450 masl. From Andersson et al. (1999).*

Table 4-3. Sink sections and hydraulic structures together with flow rate (Q), final drawdown (s_p), specific capacity (Q/s_p) and duration of the flow period during the interference tests (pre-tests) in TRUE Block Scale, Detailed Characterization Stage. Packer positions in the boreholes are given in Appendix 5. From Andersson et al. (1999).

Test #	Sink	Structure	Q* (L/min)	s_p ** (m)	Q/s_p (m^2/s)	Flow period (h)
PT-1	KI0023B:P4	13	0.675	389	$2.9 \cdot 10^{-8}$	24
PT-2	KI0023B:P6	21	2.55	225	$1.9 \cdot 10^{-7}$	48
PT-3	KI0025F02:P5	20	4.70	72	$1.1 \cdot 10^{-6}$	93
PT-4	KI0023B:P6	21	2.40	209***	–	663

* Flow rate at the end of the flow period.
** Drawdown at the end of the flow period.
*** Affected by “global” pressure variations.

Analysis of the pressure responses in the observation sections was made according to Section 3.1.2. The pressure response matrix for PT-1 to PT-3 is shown in Figure A7-1 in Appendix 7. The matrix is based on the responses during the flow period. For PT-1 and PT-3 the drawdown pattern at the end of the flow period is shown whereas for test PT-2 the data during the flow period were truncated at t = 1,140 min due to external disturbances. Figure A7-1 shows that pressure responses were obtained in 15 observation borehole sections during PT-1, 40 sections during PT-2 and 46 sections during PT-3.

Transient analysis was made for the pressure responses in selected observation sections. The transmissivity, storativity and hydraulic diffusivity, and in appropriate cases also the leakage coefficient, were estimated from the tests by standard methods, see Table A7-1. The distances between the sink sections and the observation sections during each interference test are shown in Table A6-1.

4.2.3 Tracer dilution tests

Tracer dilution tests were performed both under natural gradient and under stressed conditions (i.e. pumping during interference tests). Thus, it was possible to simultaneously measure both flow and pressure changes due to pumping in the selected observation sections. The duration of each tracer dilution test in tests PT-1 to PT-3 was 24–93 hours, see Table 4-3. The results of the tracer dilution tests are shown in Table A7-2 in Appendix 7.

4.2.4 Cross-hole tracer tests

The fourth pre-test, PT-4, was focused on tracer transport. Based on the many good flow responses observed during PT-2 the same set-up was decided for use in PT-4. Flowing was done in KI0023B:P6 with the same flow rate as in PT-2 and four primary injection sections were chosen. Tracer breakthrough was measured in 4 sections during PT-4. The breakthrough curves from PT-4 were evaluated using numerical modelling (PAREST) and the one-dimensional advection-dispersion model described in Appendix 3. The estimated transport parameters are presented in Table A7-3.

4.3 Tracer test stage

4.3.1 General

Phase A of the TRUE Block Scale Tracer Test Stage (TTS) included four large-scale pressure interference tests combined with tracer dilution tests (Tests A-1 to A-4) and cross-hole tracer tests (A-4 and A-5) in two different flow geometries. The main objective of the tests in Phase A was to test the connectivity of the target area to serve as a basis for selecting suitable flow geometry for the planned tracer tests in Phase B and C of the project, the latter involving injection of radioactive sorbing tracers.

4.3.2 Cross-hole interference tests

The test cycles for tests A-1 to A-4 were similar to the one used in the combined interference- and tracer tests performed in the Preliminary Characterisation Stage (PCS). Test A-4 and A-5 were focused on tracer transport and performed in radially converging flow geometry. A summary of the test set-ups is shown in Table 4-4 together with the expected flow rates through the borehole sections under naturally conditions together with the distances to the sink sections. The position of the sink section and tracer dilution test sections during test A-1 are shown in Figure 4-3.

The flow tests in the sink sections were performed as conventional constant head drawdown tests implying that the flow rate was slightly decaying during the tests. The pressures in all observation borehole sections were monitored with a high measurement frequency to enable transient evaluation of pressure data. The flow rate from the flowing sections together with the electrical conductivity of the discharged water was measured manually during the pumping period. The flow rates and drawdown in the sink sections together with the specific capacity and duration of the flow period is shown In Table 4-5.

Table 4-4. Test set-ups for TRUE Block Scale Tracer Test Stage (TTS), Phase A, tests A-1 to A-5. The structural interpretation and notation refers to the reconciled March 99 model. From Andersson et al. (2000).

Test #	Sink	Structure #	Observation sections	Structure #	Ambient flow (mL/h)	Euclidean distance (m)	Distance along structures
A-1	KI0025F03:P5	20	KI0025F02:P5	20	50	11	
			KA2563A:S4	20	100	29	
			KI0023B:P7	6, 20	10,000	22	
			KI0025F02:P6	22	100	12	
			KI0023B:P4	13	20	18	
			KI0025F02:P3	13, 21	40	26	
			KI0023F03:P3	13	?	18	
			KI0023B:P6	21	3	14	
			KI0025F03:P4	21	?	14	
			KA2563A:S3	13	1	31	
			KI0025F03:P6	22	?	12	
			KI0025F02:P7	23	10	17	
			KA2563A:S1	19	100	52	
			KI0025F:R4	20, 22	1	40	
			KI0023B:P2	19	14	41	
			KI0023B:P5	18	?	15	
			KI0025F03:P7	23	?	26	
			KI0025F02:P8	6	30	23	
A-2	KI0025F03:P4	21	KI0025F02:P5	20	50	17	
			KI0023B:P6	21	3	24	
			KI0023B:P7	6, 20	10,000	36	
			KA2563A:S4	20	100	38	
			KI0023B:P4	13	20	17	
			KI0025F02:P3	13, 21	40	16	
			KI0025F03:P3	13	?	4	
			KA2563A:S3	13	1	33	
			KI0025F03:P6	22	?	26	
			KI0025F02:P6	22	100	23	
			KI0025F03:P5	20	?	14	
			KI0025F02:P7	23	10	30	
			KA2563A:S1	19	100	50	
			KI0023B:P2	19	14	29	
			KI0025F:R4	20, 22	1	34	
			KI0023B:P5	18	?	19	
			KI0025F03:P7	23	?	30	
			KI0025F02:P8	6	30	37	
A-3	KI0025F02:P5	20	KA2563A:S3	13	1	39	200
			KI0025F:R4	20, 22	1	23	26
			KI0023B:P4	13	20	22	54
			KI0023B:P5	18	?	20	?
			KI0023B:P7	6, 20	10,000	27	27
			KI0025F02:P3	13, 21	40	21	43
			KI0025F02:P7	23	10	16	?
			KI0025F03:P3	13	?	20	
			KI0025F03:P4	21	?	17	11
			KI0025F03:P5	20	?	11	
			KI0025F03:P6	22	?	17	
			KI0025F03:P7	23	?	21	
A-4	KI0023B:P6	21	KI0025F03:P3	13	?	27	
			KI0025F03:P4	21	?	24	
			KI0025F03:P5	20	?	14	
			KI0025F03:P6	22	?	15	
			KI0025F03:P7	23	?	17	
A-5	Best Sink A-1 to A-3	?	?	?	?	?	

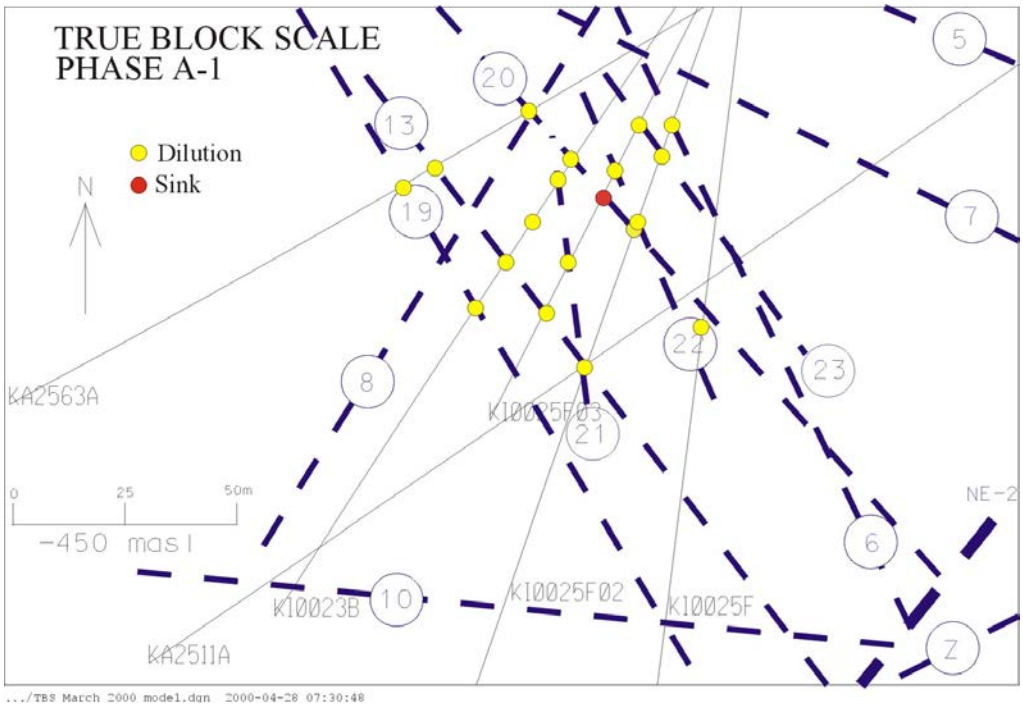

Figure 4-3. *Position of sink and dilution test sections during test A-1 during the Tracer Test Stage of TRUE Block Scale. The positions of the structures are based on the reconciled March 1999 structural model. Z = –450 masl. From Andersson et al. (2000).*

Table 4-5. Summary of test data in the sinks for combined interference tests A-1 to A-5 in the Tracer Test Stage of TRUE Block Scale. After Andersson et al. (2000).

Test #	Sink	Structure #	Q_1 (L/min)	Q_2 (L/min)	s_p (m)	Q_2/s_p (m^2/s)	Flow period (h)
A-1	KI0025F03:P5	20	2.05	2.65	249	$1.8 \cdot 10^{-7}$	67
A-2	KI0025F03:P4	21	1.00	1.18	361	$5.4 \cdot 10^{-8}$	71
A-3	KI0025F02:P5	20	3.60	4.10	45.2	$1.5 \cdot 10^{-6}$	46.4
A-4	KI0023B:P6	21	2.05	2.30	190	$2.0 \cdot 10^{-7}$	289.5
A-5	KI0025F03:P5	20	2.60	2.60	237	$1.8 \cdot 10^{-7}$	906

Q_1 = Flow rate during step1 (0–5 h), for test A-3: 0–4 h.
Q_2 = Flow rate during step2 (at the end of the flow period)s_p = Drawdown at the end of the test.
Q_2/s_p = Specific capacity.

Analysis of the pressure responses in the observation sections was made according to Section 3.1.2. The pressure response matrix for tests A-1 to A-4 is shown in Figure A8-1 in Appendix 8. The matrix is based on the responses at the end of the flow period. Figure A8-1 shows that pressure responses were obtained in 45 observation borehole sections during test A-1, in 18 sections during test A-2, in 41 sections during test A-3 and in 52 sections during test A-4.

Transient analysis was made of the pressure responses in selected observation sections with the most distinct responses. The transmissivity, storativity and hydraulic diffusivity, and when appropriate also the leakage coefficient, were estimated from the tests by standard methods, see Table A8-1. In addition, the dominating transient flow regimes during the tests were interpreted. The Euclidian distances R between the sink sections and the observation sections are shown in Table 4-4. An example of a drawdown versus time/distance (t/R^2)-diagram during test A-1 is shown in Figure 4-4.

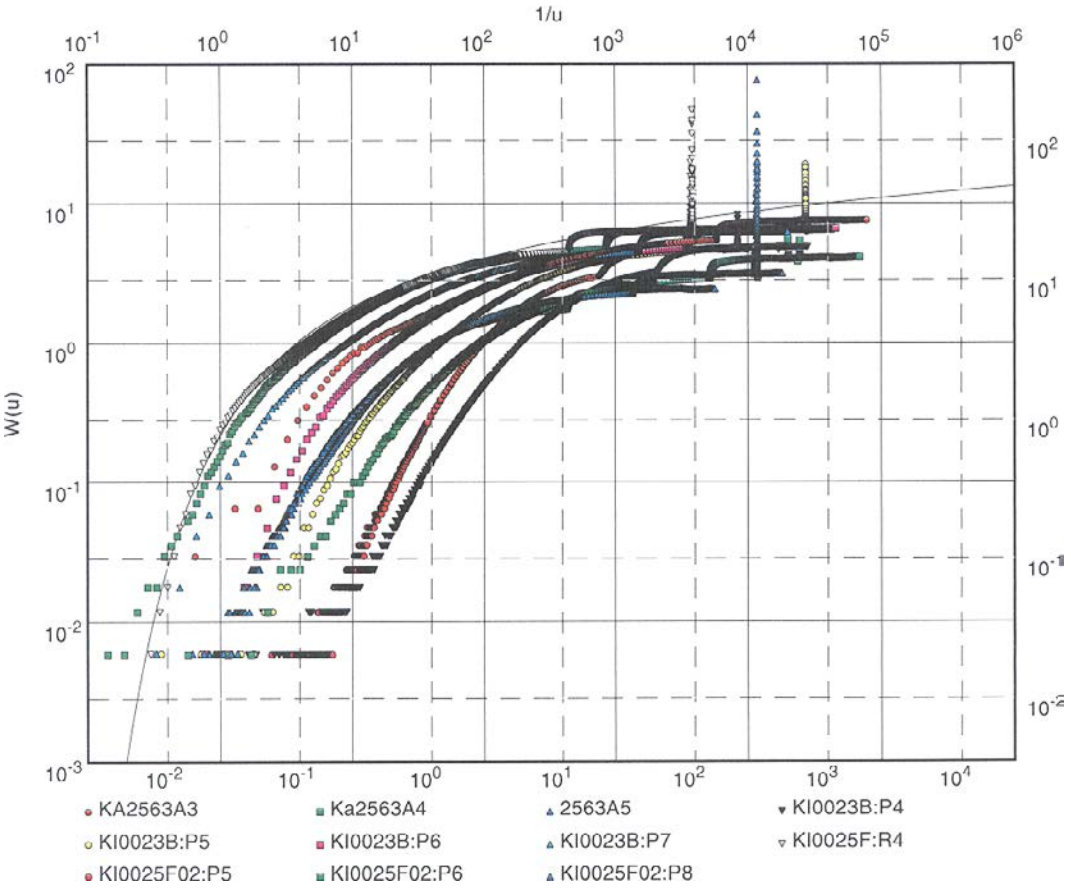

Figure 4-4. *Drawdown versus t/R^2-diagram for test A-1 in the Tracer Test Stage of TRUE Block Scale. The line represents the Theis' curve for section KI0025F:R4. Evaluated parameters; T = 7.6E–7 m^2/s, S = 7.7E–8. From Andersson et al. (2000).*

4.3.3 Tracer dilution tests

Tracer dilution tests were performed both under natural gradient and under stressed conditions (i.e. flowing during the pressure interference tests). Thus, it was possible to simultaneously measure both flow and pressure changes due to pumping in the selected observation sections. The duration of the flow period for the tracer dilution tests in A-1 to A-3 are shown in Table 4-5 whereas the duration of the flow period for the tracer dilution tests in A-4 was 24 hours. The results of the tracer dilution tests are shown in Table A8-2 in Appendix 8.

4.3.4 Cross-hole tracer tests

Tests A-4 and A-5 were focused on tracer transport in radially converging flow geometry. In test A-4 tracer injections were made in three sections (KI0025F03:P5, KI0025F03:P6 and KI0025F03:P7) with pumping in section KI0023B:P6. In test A-5 the same set-up as in A-1 was used, based on several good flow responses observed during test A-1. Tracer injections were made in five sections (KI0025F02:P3, KI0025F02:P5, KI0025F02:P6, KI0025F03:P6 and KA2563A:S4) with flowing in section KI0025F03:P5 with the same flow rate as in test A-1. The tracer injections were performed as decaying pulses and samples were continuously withdrawn from the source sections. In one injection, the tracer solution was exchanged with non-traced water in order to obtain a well-defined finite pulse injection (source term), and thus, shorten the tail of the breakthrough curve.

The breakthrough curves were evaluated using numerical modelling (PAREST) and the one-dimensional advection-dispersion model described in Section 3.1.2. The estimated transport parameters from test A-4 and A-5 are presented in Table A8-3 and A8-4 respectively.

4.4 True Block Scale Continuation

4.4.1 General

A series of pre-tests were performed in the TRUE Block Scale Continuation Project (BS2B). The pre-tests included a combination of flow and pressure interference tests and tracer tests with non-sorbing tracers. The tests involved six different test set-ups, the three first (CPT-1 to CPT-3) comprised tracer dilution tests combined with pumping tests and the three last (CPT-4a to CPT-4c) included multiple-hole tracer tests. A summary of the sink sections and source sections for the tracer dilution tests during the pre-tests is given in Table 4-6. The packer positions in the boreholes are given in Subappendix 5. The position of the sink sections and the tracer dilution source sections during pre-tests CPT-1 through CPT-3 are shown in Figure 4-5. The flow rates by the end of the flow period and the duration of the flow period for the tests is shown in Table 4-7. The cross-hole tracer test CPT-4 lasted from 20031022–20040227.

The measured hydraulic head distribution in Structures #19 and #25 during the entire test period are shown in Figure A9-1 in Appendix 9. The influences of the flowing in different sections are clearly seen. A slowly decreasing pressure trend in the sink KI0025F03:R3 is also clearly seen, possibly indicating restrictions in the flow system (i.e. apparent no-flow hydraulic boundary). The low pressure in section KI0025F02:R2 in January 2004 is due to a water sampling campaign.

Table 4-6. Sink sections for pumping and source sections for tracer injection during pre-tests CPT-1 through CPT-4 in TRUE Block Scale Continuation. After Andersson et al. (2004).

Test	Sink	Structure	Tracer Source	Structure	Comments
CPT-1	KI0025F:R2	#19	KI0025F02:R3	#19	Interference test+TDT
			KI0025F03:R3	#19	
			KI0023B:P2	#19	
			KA2563A:S1	#19	
			KI0025F02:R2	#25	
			KI0025F03:R2	#25	
			KI0025F02:R5	#13, 21	
CPT-2	KI0025F02:R3	#19	KI0025F:R2	#19	Interference test+TDT
			KI0025F03:R3	#19	
			KI0023B:P2	#19	
			KA2563A:S1	#19	
			KI0025F02:R2	#25	
			KI0025F03:R2	#25	
			KI0025F03:R5	#13	
			KI0025F02:R5	#13, 21	
CPT-3	KI0025F03:R3	#19	KI0025F:R2	#19	Interference test+TDT
			KI0025F02:R3	#19	
			KI0023B:P2	#19	
			KA2563A:S1	#19	
			KI0025F02:R2	#25	
			KI0025F03:R2	#25	
			KI0025F03:R5	#13	
			KI0025F02:R5	#13, 21	Contaminated
CPT-4a	KI0025F03:R3	#19	KI0025F:R2	#19	Tracer test (rad. conv.)
			KI0025F02:R3	#19	
			KI0023B:P2	#19	
CPT-4b	KI0025F03:R3	#19	KA2563A:S1	#19	Tracer test (dipole, RC)
			KA2563A:S2	#19	
			KI0025F02:R2	#25	
CPT-4c	KI0025F03:R3	#19	KI0025F02:R3	#19	Tracer test (weak dipole)
			KI0023B:P2	#19	
			KI0025F02:R2	#25	

TDT = Tracer dilution test.
RC = Radially converging.

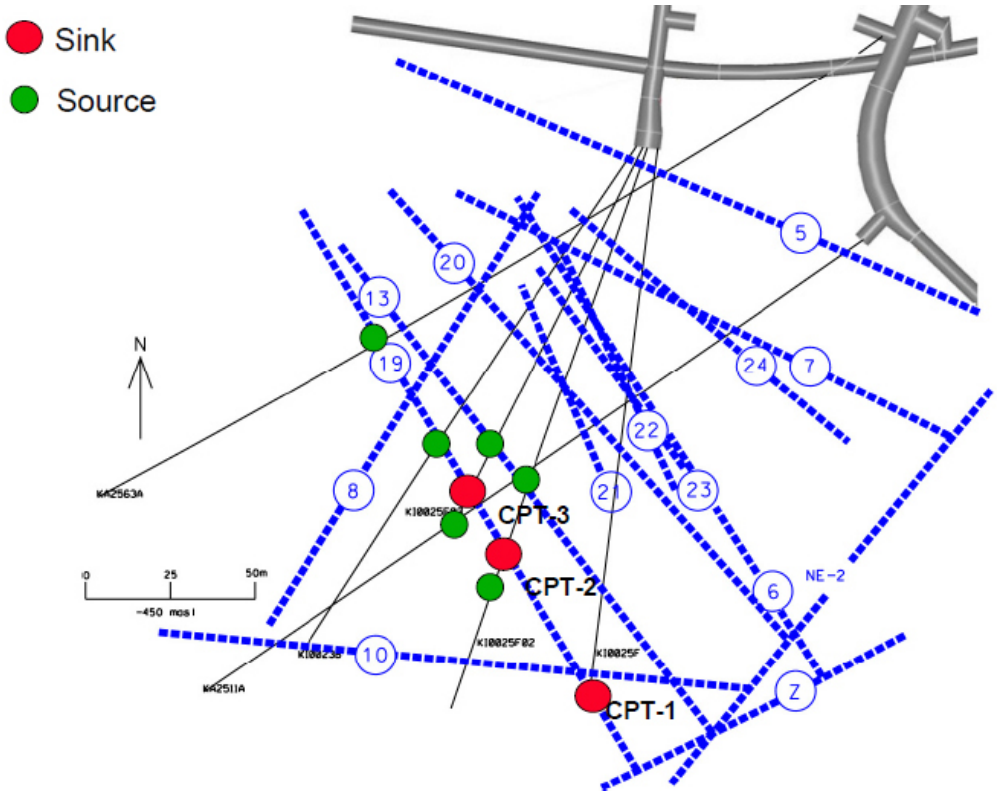

Figure 4-5. *Sink sections and source sections for tracer dilution tests in the cross-hole interference tests during pre-tests CPT-1 through CPT-3 in True Block Scale Continuation. From Andersson et al. (2004).*

Table 4-7. Summary of test data in the sinks for pre- tests CPT-1 to CPT-4 in TRUE Block Scale Continuation. After Andersson et al. (2004).

Test #	Sink	Structure #	Q_p (L/min)	Flow period (h)
CPT-1	KI0025F:R2	19	3.4	48
CPT-2	KI0025F02:R3	19	1.6	48
CPT-3	KI0025F03:R3	19	2.8	48
CPT-4	KI0025F03:R3	19	2.6	c. 3,072

Q_p = Flow rate by the end of the flow period.

4.4.2 Cross-hole interference tests

The test cycle for CPT-1 to CPT-3 was similar to the one used in the combined interference and tracer dilution tests in the TRUE-1 Continuation pre-tests CX-1 to CX-3, see Section 3.2.2, and in the TRUE Block Scale pre-tests PT-1 to PT-4 (Section 4.2.2). The cross-hole interference tests were performed as conventional constant rate drawdown tests. The flow rate was established by using the maximum sustainable flow (2.6–2.8 L/min) regarding the dimension of the flow lines and the transmissivity of the sink sections. The pressure was monitored in all observation borehole sections with a high measurement frequency by the HMS. The flow rate from the sink sections together with the electrical conductivity of the discharged water was measured manually during the flow period.

Analysis of the pressure responses in the observation sections was made according to Section 3.1.2 using standard methods. The pressure response matrix for pre-tests CPT-1 to CPT-3 is shown in Figure A9-2 in Appendix 9. The matrix is based on the pressure responses by the end of the flow period. Figure A9-2 shows that pressure responses were obtained in 46 observation borehole sections during CPT-1, 20 sections during CPT-2 and 28 sections during CPT-3. No analysis of the pressure responses in the observation sections was made in this stage.

4.4.3 Tracer dilution tests

Tracer dilution tests were performed both under natural gradient and under stressed conditions (i.e. flowing during the interference tests) in pre-tests CPT-1 to CPT-3. Thus, it was possible to simultaneously measure both flow and pressure changes in the selected (source) observation sections. The duration of the flow period in each tracer dilution test was 24 hours. The results of the tracer dilution tests are shown in Table A9-1 in Appendix 9.

4.4.4 Cross-hole tracer tests

The fourth pre-test, CPT-4, was focused on tracer transport. Test CPT-4 was divided into three separate batches of tracer injections including three injections in each batch (CPT-4a–c). The last batch of injections, CPT-4c, included reruns in three of the earlier tested flow paths but with partly changed flow geometry. The tests were performed as cross-hole tracer tests using KI0025F03:R3 (Structure #19) as sink. The selection of sink was based on the results of CPT-1 through CPT-3 where the selected section gave the best hydraulic and flow responses and also the best possibilities to use different geometries.

The tests were performed in a radially converging flow field with a withdrawal rate of Q = 2.8 L/min at start of CPT-4a in September 2004 and slowly decreasing to Q = 2.6 L/min until stop of CPT-4c in February/March 2004. Some of the injections were also accompanied by net fluid injections into the injection section in order to avoid excessive tailing of the injection function. Breakthrough was monitored in KI0025F03:R3 from all three injection points in test CPT-4a. Breakthrough was also monitored from all three injection points in CPT-4b and CPT-4c. The breakthrough curves were evaluated using numerical modelling (PAREST) and one-dimensional advection-dispersion models assuming one (AD-1), two (AD-2) flow paths, respectively and for a single flow path with matrix diffusion (MD). The estimated parameter values from the models are shown in Table A9-2 in Appendix 9.

The model fits were generally fairly good for all of the nine breakthrough curves. In most of the cases, the AD-1 model (Advection-Dispersion, single flow path) appears to be inadequate for explaining the later parts of the curves, while the AD-2 (Advection-Dispersion, two flow paths) and MD (Advection-Dispersion-Matrix diffusion, single flow path) models in those cases usually provide a better fit. However, the AD-2 and MD models in many cases also show systematic model errors in the later parts of the curves. In three of the curves (Uranine and Amino G Acid in CPT-4a; Uranine in CPT-4b), high concentrations remain at later parts of the curve that neither the AD-2 model nor the MD model could reproduce.

4.5 Additional measurements

During different phases of the True Block Scale project a number of additional hydraulic measurements and tests were performed, i.e. single-hole pressure build-up tests and borehole flow logging including difference flow logging. A summary of these measurements is presented below.

4.5.1 Single-hole hydraulic tests

Selective single-hole tests have been performed in most of the boreholes involved in the TRUE Block Scale project. Borehole KA2511A was drilled prior to start of the Block Scale project and boreholes KA2563A and KA3510A during the Scoping Stage of the Block Scale project. Boreholes KI0025F and KI0023B were drilled during the Preliminary Characterisation Stage, borehole KI0025F02 during the Detailed Characterisation Stage and borehole KI0025F03 during the Tracer Test Stage.

The type of the single-hole hydraulic tests in these boreholes together with additional information is listed in Table 4-8. In boreholes KI0023B, KI0025F02 and KI0025F03 some of the single-hole tests were combined with short-time pressure interference tests with c. 0.5 h flow period. After shut-in, the pressure recovery was measured in the borehole sections. In KI0023B and KI0025F02, tracer dilution tests were also performed in a few selected observation sections during the short-time interference tests.

Table 4-8. Selected borehole intervals for single-hole hydraulic tests (SHT) in TRUE Block Scale. Some of the tests were combined with short-time interference tests and tracer dilution tests.

Borehole	Type of SHT	Number of sections tested (m)	Section length (m)	Total T-range for all PBUT (m^2/s)	SHT combined with:		SKB-Report
					INTER	TDT	
KA2511A*	PBUT-DP PBUT-SP	32** 1	3 0–156.25	c. $1{\cdot}10^{-11}$–c. $3{\cdot}10^{-5}$ *** $6.3{\cdot}10^{-5}$	No No	No No	HRL PR-25-94-14
KA2563A*	PBUT-SP	2	0–99 0–105	$1.5{\cdot}10^{-5}$ $3.2{\cdot}10^{-5}$	Yes Yes	No No	
KA3510A*	PBUT-SP	1	0–47	n.a.	Yes	No	ITD-00-02
KI0025F	PBUT PBUT	5 1	1 7.8	$1.8{\cdot}10^{-7}$–$5.7{\cdot}10^{-6}$“	No	No	IPR-01-58 IPR-01-45
KI0023B	PBUT PBUT CHT	16 3 1 (P6)	1 0.5	$1.8{\cdot}10^{-10}$–$1.8{\cdot}10^{-5}$“	No	No	IPR-01-43
KI0025F02	CHT+PBUT CHT+PBUT CHT	11 10 9 (P1–P3, P5–P10)	4 1	$2{\cdot}10^{-12}$–$2{\cdot}10^{-6}$“ $7.9{\cdot}10^{-7}$–$1.3{\cdot}10^{-5}$	Yes Yes	Yes No	IPR-01-56 ITD-00-02
KI0025F03	CRT+PBUT CHT+PBUT	13 5	2 3.5–7.5	$3.3{\cdot}10^{-10}$–$1.3{\cdot}10^{-6}$ $1.8{\cdot}10^{-8}$–$3.3{\cdot}10^{-7}$ ****	Yes Yes	No No	IPR-01-58 IPR-00-28

* Tested before TRUE Block Scale Project.
** Only borehole interval 172–265 m was measured in 3 m sections.
*** The transmissivity may be overestimated due to leakage in the packer system (Olsson et al. 1994).
**** Specific capacity Q_p/s_p.
n.a. = not evaluated.

PBUT-DP = Pressure build-up test with double packers.
PBUT-SP = Pressure build-up test with single packer.
INTER = Interference test.
TDT = Tracer dilution test.
CRT+PBUT = Constant rate interference test in combination with pressure build-up test.
CHT+PBUT = Constant head interference test in combination with pressure build-up test.

The single-hole hydraulic tests were evaluated by standard steady-state and transient methods including wellbore storage and skin. The interference tests in conjunction with the single-hole tests in KI0025F02 and KI0025F03 (during CRT) were analysed in the same way as described above for the longer interference tests by standard methods.

A pressure response matrix was prepared for the interference tests together with transient evaluation of the most distinct responses in the observation borehole sections. However, only qualitative evaluation was made for the short-term interference tests in KI0025F03 in conjunction with the CHT. The tracer dilution tests in conjunction with the interference tests in KI0025F02 were analysed by the same methods as described above for the longer interference tests.

The estimated transmissivity of the deterministic structures included in the TRUE Block Scale hydrostructural model from the single-hole hydraulic tests is shown in Appendix 10.

4.5.2 Borehole flow logging

Three flow logging methods were used in the True Block Scale project. The techniques used were (1) double packer flow logging, (2) ultrasonic current meter (UCM) flow logging and (3) heat-pulse difference flow logging (PFL). Table 4-9 presents some of the characteristics of the flow logging methods and in which boreholes the methods were utilised. Packer flow logging and UCM flow logging were used first. PFL (Posiva flow logging) was introduced later in the project. Portions of boreholes KA2563A and KA2511A were re-logged with PFL.

From the PFL logging, discrete single fractures can be identified and their transmissivity estimated by steady-state methods. From the packer flow logging the transmissivity of short sections was estimated. The UCM flow logging was mainly used to identify horizons of changing water flow along the borehole indicating conductive zones. The results of the flow logging are presented in the associated test reports shown in Table 4-9.

4.5.3 Other investigations

Several other types of measurements were made in the boreholes in the TRUE Block Scale Project, e.g. borehole radar, cross-hole seismic measurements, core logging investigations, borehole television surveys, measurements of pressure responses in other boreholes during drilling and hydro-geochemical investigations. The results of these measurements are described in Andersson et al. (2002b).

Table 4-9. Characteristics of the flow logging methods used in the TRUE Block Scale Project together with references to the test reports. X = not applied in the borehole. From Andersson et al. (2002b).

	Packer Flow Log	UCM Ultrasonic Current Meter Flow Log	Posiva (DIFF) Heat Pulse Flow Log
Spatial Resolution	1 to 5 m	1 m	0.1 m
Flow Range	0.0003–>45 l/m	0.044–132 l/m (76 mm hole)	0.002–5.0 l/m
Cumulative		Yes	
Discrete	Yes		Yes
KA2511A	/Gentzschein, 1997/		/Rouhiainen and Heikkinen, 1999a/
KA2563A	X	X	/Rouhiainen and Heikkinen, 1999a/
KI0025F	/Gentzschein, 1997/	X	
KI0023B	X	X	
KI0025F02		X	/Rouhiainen and Heikkinen, 1998/
KI0025F03			/Rouhiainen and Heikkinen, 1999b/

5 Compilation of tests and data availability

In this chapter, compilations of the hydraulic interference tests and associated measurements in the different stages of the TRUE and TRUE Block Scale projects at the Hard Rock Laboratory at Äspö are presented in Table 5-1 and 5-2, respectively. In addition, the availability of the corresponding test data files and associated result tables of interpreted parameters in the Sicada database for the different test activities in the projects are listed. If the data are not available in Sicada, other available storage media (e.g. CD) for the data are listed in the tables. Note that the data availability reflect the situation 2010, but now 2014 additional data may be available in Sicada database. In addition, pressure measurements from all tests can be retrieved from the HydroMonoringSystem (HMS) at Äspö.

Table 5-1. Compilation of tests and availability of test data and calculated parameters from the test activities in the TRUE-1 Project at the Äspö Laboratory. CHPIT = cross-hole pressure interference test, TDT = tracer dilution test, CHTT = cross-hole tracer test, CH-PBUT = constant head drawdown and pressure build-up test, SPFL = single-packer flow logging.

Phase	Test type	Number of tests	Test data	Sicada Act. code	Data on other digital media	Calculated parameters	Sicada Act. code	Results on other digital media
TRUE-1	CHPIT	14 short-time cross-hole tests	Pressure vs time in observation borehole sections	[1]	CD, HMS	Response matrix. Calc. T, S, T/S, K'/b' for selected observation sections	–	CD
TRUE-1	TDT	10 obs-sections	Tracer concentration versus time in obs-sections	TR026	CD	Calc. flow through borehole sections	TR026	
TRUE-1	CHTT	17 cross-hole tracer tests [2]	Rad. Conv Tests Dipole tests	TR001 TR010		Calculated hydraulic& transport parameters	TR001 TR010	
TRUE-1	CH-PBUT		Pressure p and flow Q in active borehole sections	HY040		Calc. T in 2–4 m long borehole sections	HY040	
TRUE-1	SPFL		Flow versus borehole length	HY085		Calc. T in 0.5–1 m borehole sections	HY085	
TRUE-1 Continuation	CHPIT	3 cross-hole tests CX-1 to CX-3	Pressure vs time in observation borehole sections	HY088		Response matrix. No hydraulic parameters were calculated	–	
TRUE-1 Continuation	TDT	36 obs-sections CX-1 to CX-3	Tracer concentration versus time in obs-sections	–	CD	Calc. flow through borehole sections	TR026 [3]	CD
TRUE-1 Continuation	CHTT	6 obs-sections CX-4 to CX-5	Tracer concentration versus time in obs-sections	TR001 [4]	CD	Calculated hydraulic& transport parameters	–	CD
TRUE-1 Completion	CHPIT	8 cross-hole tests in Feature A	Pressure vs time in observation borehole sections in Feature A	HY088		Response parameters. Transmissivity T_{Th} in observation sections and T_M in pumped sections	Not completely reported	CD
TRUE-1 Completion	TDT	8+5 tests (pumping + undisturbed cond's)	Tracer concentration versus time in obs-sections in Feature A	–	CD	Calc. flow through obs-borehole sections in Feature A	Not completely reported	CD

[1] Data only available after 951206.
[2] Radially converging tracer tests and Dipole tracer tests.
[3] Incomplete data block.
[4] Only data from the tracer test in borehole KXTT1.
HMS = hydro-Monitoring System at Äspö.

Table 5-2. Compilation of tests and availability of test data and calculated parameters from the test activities in the TRUE Block Scale Project at the Äspö Laboratory. CHPIT = cross-hole pressure interference test, TDT = tracer dilution test, CHTT = cross-hole tracer test, CH-PBUT = constant head drawdown and pressure build-up test, SPFL = single-packer flow logging.

Phase	Test type	Number of tests	Test data	Sicada Activity code	Test data on other digital media	Calculated parameters	Sicada Activity code	Calc. param. on other digital media
Prel. Char. Stage (PCS)	CHPIT	6 long+13 short time tests	Pressure vs time in observation borehole sections	HY180		Response matrix. Calc. T, S, T/S, K'/b' for selected observation sections	HY180	
Prel. Char. Stage (PCS)	TDT	7 obs-sections	Tracer concentration versus time in obs-sections	TR026		Calc. flow through selected borehole sections	TR026	
Prel. Char. Stage (PCS)	CHTT	1 tracer test (RCV)	Tracer concentration versus time in obs-sections	–	CD	Calc. hydraulic& transport parameters for selected obs-sections	TR001	
Det. Char. Stage (DCS)	CHPIT	3 cross-hole tests PT-1 to PT-3	Pressure vs time in observation borehole sections	–	CD, HMS	Response matrix. Calc. T, S, T/S, K'/b' for selected observation sections	HY180	
Det. Char. Stage (DCS)	TDT	30 obs-sections PT-1 to PT-3	Tracer concentration versus time in obs-sections	TR026		Calc. flow through selected borehole sections	TR026	
Det. Char. Stage (DCS)	CHTT	1 tracer test PT-4 RCV)	Tracer concentration versus time in obs-sections	TR001 [1)]	CD	Calc. hydraulic& transport parameters for selected obs-sections	–	CD
Tracer Test Stage (TTS)	CHPIT	4 cross-hole tests A-1 to A-4	Pressure vs time in observation borehole sections	HY088		Response matrix. Calc. T, S, T/S, K'/b' for selected observation sections	HY180	
Tracer Test Stage (TTS)	TDT	52 obs-sections A-1 to A-4	Tracer concentration versus time in obs-sections	TR026		Calc. flow through selected borehole sections	TR026	
Tracer Test Stage (TTS)	CHTT	2 tracer tests A-4 to A-5	Tracer concentration versus time in obs-sections	TR001 [2)]	CD	Calc. hydraulic& transport parameters for selected obs-sections	TR001	
Block Scale Continuation	CHPIT	3 cross-hole tests CPT-1 to CPT-3	Pressure vs time in observation borehole sections	–	CD, HMS	Response matrix. No hydraulic parameters were calculated	–	CD
Block Scale Continuation	TDT	23 obs-sections CPT-1 to CPT-3	Tracer concentration versus time in obs-sections	–	CD	Calc. flow through selected borehole sections	–	CD
Block Scale Continuation	CHTT	3 tracer tests CPT-4a to CPT-4c	Tracer concentration versus time in obs-sections	–	CD	Calc. hydraulic& transport parameters for selected obs-sections	–	CD
Block Scale	Single Hole Hydraulic Tests		Pressure p and flow Q in active borehole sections	HY180		Calc. Transmissivity of selected test sections	HY180	
Block Scale	Double packer Flow Logging		Flow Q in 5 m sections along the borehole	HY086		Transmissivity of 5 m sections	HY086	
Block Scale	Borehole Flow Logging (UCM)		Cum-Q versus bh. length (only from UCM-logging)	HY080		Transmissivity was not calculated	–	–
Block Scale	Difference Flow Logging (PFL)		Q of identified flow anomalies versus borehole length	HY070–HY071		Calc. Transmissivity of identified flow anomalies	3)	

[1)] Incomplete data block.
[2)] Only data from the tracer test in KI0023B:P6 (test A-4).
[3)] to be stored in Sicada during the autumn 2010.

6 Overview of tests and proposed interference tests for hydraulic tomography

As discussed in Part A of this report the major problem in standard analysis of hydraulic interference tests is the assumption of an equivalent isotropic, homogeneous porous medium by the evaluation. This means that the flow rate in the active borehole (sink) is assumed to be evenly (radially) distributed from the sink in all directions of the rock. Clearly, this is not the case in heterogeneous rock. The porous medium assumption leads to rather uniform, apparent values of transmissivity from the transient evaluation of the pressure responses in observation borehole sections by standard analysis methods. In addition, the estimated, apparent storativity more represents the degree of hydraulic interconnection between the sink and the actual observation section rather than the true hydraulic properties of the rock.

One way to improve the standard analysis of hydraulic interference tests would, possibly, be to include the estimated flow through the actual observation sections under non-pumping and pumping conditions, respectively in the test evaluation. During most of the cross-hole interference tests in the TRUE and TRUE Block Scale Projects in the Hard Rock Laboratory at Äspö, tracer dilution tests have been performed in several observation sections. This means that a combined evaluation of both the pressure and flow rate responses may be possible in these observation sections. This fact might possibly lead to more representative values of the hydraulic parameters (T and S) of the rock between the sink and the observation sections. In addition, supporting data from associated cross-hole tracer tests might further improve the analysis of pressure interference tests.

Thus, it is proposed to select hydraulic interference tests which are combined with flow measurements from tracer dilution tests in several observation test sections. From Table 5-1 and 5-2 it can be seen that a large number of tracer dilution tests (TDT) were performed in TRUE-1 Continuation (36 observation sections), in TRUE-1 Completion (5 observation sections) and in the Tracer Test Stage during TRUE Block Scale (52 observation sections) in conjunction with pressure interference tests. Both pressure responses and flow responses were thus measured in these sections.

The main difference between the hydraulic interference tests in these projects is the measurement scale. In TRUE-1, a detailed scale was investigated (1–10 m) representing single hydraulically conductive fractures or features whereas a larger scale in the fractured rock was investigated in the TRUE Block Scale (5–50 m). Thus, a higher degree of heterogeneity of the rock can be expected in the latter project.

In order to test the proposed new analysis technique of hydraulic tomography (including both pressure and flow measurements) on a detailed scale of individual hydraulic features and fracture planes it is firstly proposed to select the combined hydraulic interference tests and tracer dilution tests, performed in the COM tests in TRUE-1 Completion.

A possible, qualitative interpretation of the hydraulic conductivity distribution in Feature A, based on the COM tests is shown in Figure 6-1. It should be observed that this interpretation is not unambiguous as pointed out by Nordqvist et al. (2014). The interpreted conductivity distribution in Feature A may be compared with e.g. hydraulic tomography analysis.

From Table 6-1 it is shown that only steady-state analysis (Thiem's method) was made on the pressure responses in the observation borehole sections in Feature A together with steady-state analysis (Moye's formula) in the pumping boreholes. It is proposed to also make complementary standard transient analysis on the measured pressure responses in observation sections in Feature A for comparison with results from e.g. hydraulic tomography.

Transient analysis could also be made of pressure responses in adjacent observation borehole sections not intersected by Feature A in order to extend the analysis to a larger volume of rock including several hydraulic structures and increased heterogeneity. In addition, distance-drawdown or time/distance-drawdown analysis of data from the observation sections may be performed.

Secondly, in order to test hydraulic tomography under real heterogeneous conditions in heterogeneous fractured rock at a rock block scale, the combined hydraulic interference tests and tracer dilution tests in the Tracer Test Stage of TRUE Block Scale are proposed. The associated cross-hole tracer tests may be used as supporting data. From Table 6-1 it is seen that four cross-hole interference tests were performed and a large number of observation sections were monitored for both changes in pressure and flow during flowing conditions in the Tracer Test Stage of TRUE Block Scale project. The number of observation sections analysed by standard methods for hydraulic parameters (mainly T and S) from the pressure responses are however relatively few. It is thus proposed to extend the standard transient analysis to include measured pressure responses in additional observation sections for comparison with results from hydraulic tomography. In addition, extended distance-drawdown or time/distance-drawdown analysis of data from observation sections is suggested.

Finally, the large-scale hydraulic interference tests in surface boreholes during the site investigations at Forsmark and Laxemar represent a much larger test scale (c. 50 – c. 1,500 m) within a larger investigation area. Thus, the pumping boreholes during the hydraulic interference tests were more separated in space compared to tests performed at Äspö Hard Rock Laboratory. Besides, the tests at Forsmark and Laxemar had partly deviating observation borehole networks during the tests due to additional drilling. In addition, the number of such interference tests is less than in the interference tests made at the Äspö Hard Rock Laboratory. Although these tests thus may not be entirely suited for hydraulic tomography analysis they (few tests and slightly different observation borehole networks) are yet considered as potential candidates to test hydraulic tomography in highly heterogeneous rock on a large scale.

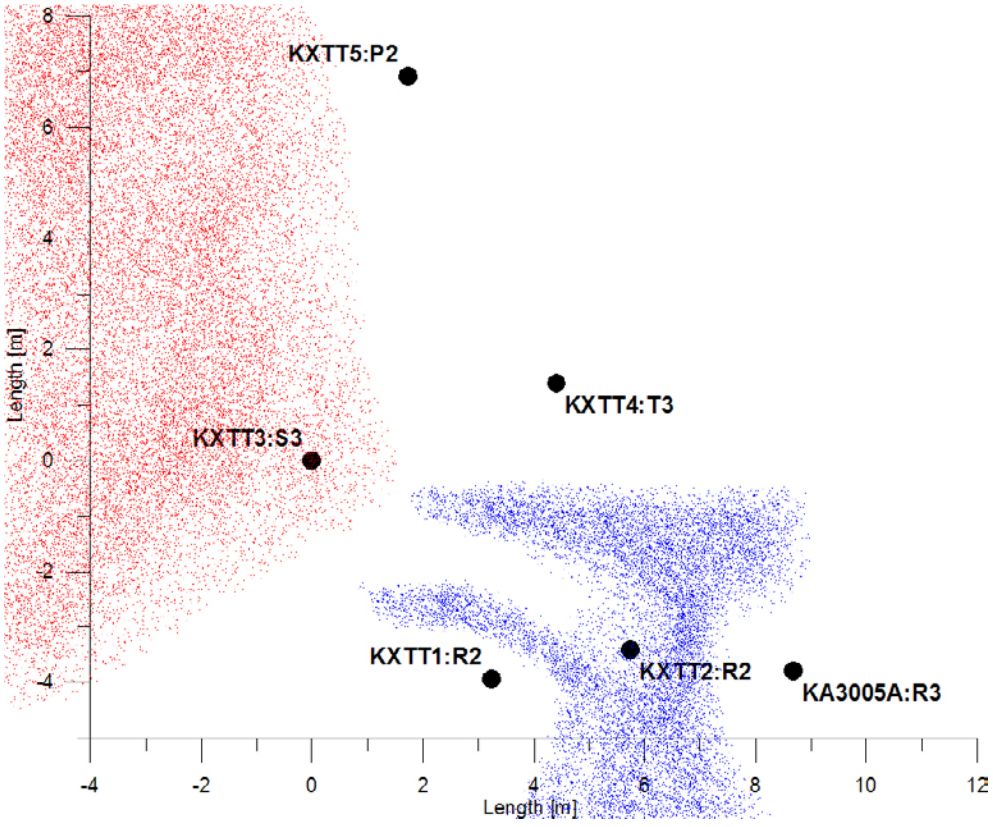

Figure 6-1. *Interpretation of the hydraulic conductivity distribution of Feature A based on the COM-test results. Red colour indicates high conductivity, white, medium and blue, low conductivity. From Nordqvist et al. (2014).*

Table 6-1. Overview of measured and analysed pressure responses in the observation borehole sections during the cross-hole interference tests (CHPIT) in the TRUE and TRUE Block Scale Projects at the Äspö Laboratory.

Project	Phase	Number of cross-hole tests performed	Total number of pressure monitored observation sections (for all tests)	Approximate distance range (sink to obs-sections (m)	Total number of responding observation sections	Total number of evaluated observation sections for T and S	Response analysis and calculated hydraulic parameters
TRUE	TRUE-1	14 short-time interference tests	536	1–10	248	20 (transient analysis)	Response matrix. Calc. T, S, T/S, K'/b' for selected observation sections**
TRUE	TRUE-1 Continuation	3 interference tests CX-1 to CX-3	126	1–10	94	0	Response matrix. No hydraulic parameters were calculated from the CHPIT
TRUE	TRUE-1 Completion	8 short interference tests in Feature A	40	1–10	40	40 (Only T, from steady-state analysis)	Response parameters. Calc. T for observation sections in Feature A
TRUE Block Scale	Prel. Char. Stage (PCS)	6 long+13 short- time interference tests	760	5–50	148	40* (transient analysis)	Response matrix. Calc. T, S, T/S, K'/b' for selected observation sections**
TRUE Block Scale	Det. Char. Stage (DCS)	3 interference tests PT-1 to PT-3	138	5–50	99	37 (transient analysis)	Response matrix. Calc. T, S, T/S, K'/b' for selected observation sections**
TRUE Block Scale	Tracer Test Stage (TTS)	4 interference tests A-1 to A-4	212	5–50	156	20 (transient analysis)	Response matrix. Calc. T, S, T/S, K'/b' for selected observation sections**
TRUE Block Scale	Block Scale Continuation	3 interference tests CPT-1 to CPT-3	147	5–50	95	0	Response matrix. No hydraulic parameters were calculated from the CHPIT

* only selected observation sections from the 6 longer interference tests were evaluated for hydraulic parameters.
** only observation sections with the most distinct responses were selected for calculation of hydraulic parameters.

References

SKB's (Svensk Kärnbränslehantering AB) publications can be found at www.skb.se/publications.

Adams J, 1998. Äspö Hard Rock Laboratory. TRUE Block Scale experiment. Preliminary results of selective pressure build-up tests in borehole KI0023B. SKB IPR-01-43, Svensk Kärnbränslehantering AB.

Adams J, Andersson P, Meier P M, 1999. Äspö Hard Rock Laboratory. TRUE Block Scale Project. Preliminary Results of Selective pressure build-up tests in borehole KI0025F02. SKB IPR-01-56, Svensk Kärnbränslehantering AB.

Andersson P, Ludvigson, 1999. Äspö Hard Rock Laboratory. TRUE Block Scale Project. Tracer dilution tests during pumping in borehole KI0023B and short-term interference tests in KI0025F02 and KA3510A. SKB ITD-00-02, Svensk Kärnbränslehantering AB.

Andersson P, Ludvigson J-E, Wass E, 1998. Äspö Hard Rock Laboratory. TRUE Block Scale Project. Preliminary characterization stage. Combined interference tests and tracer tests. Performance and preliminary evaluation. SKB IPR-01-44, Svensk Kärnbränslehantering AB.

Andersson P, Ludvigson J-E, Wass E, Holmqvist M, 1999. Äspö Hard Rock Laboratory. TRUE Block Scale. Detailed characterisation stage. Interference tests and tracer tests PT-1 – PT-4. SKB IPR-01-52, Svensk Kärnbränslehantering AB.

Andersson P, Ludvigson J-E, Wass E, Holmqvist M, 2000. Äspö Hard Rock Laboratory. TRUE Block Scale Project. Tracer test stage. Interference tests, dilution tests and tracer tests. SKB IPR-00-28, Svensk Kärnbränslehantering AB.

Andersson P, Wass E, Gröhn S, Holmqvist M, 2002a. Äspö Hard Rock Laboratory. TRUE-1 Continuation project. Complementary investigations at the TRUE-1 site – Crosshole interference, dilution and tracer tests, CX-1–CX-5. SKB IPR-02-47, Svensk Kärnbränslehantering AB.

Andersson P, Byegård J, Dershowitz B, Doe T, Hermanson J, Meier P, Tullborg E-L, Winberg A (ed), 2002b. Final report of the TRUE Block Scale project. 1. Characterisation and model development. SKB TR-02-13, Svensk Kärnbränslehantering AB.

Andersson P, Gröhn S, Nordqvist R, Wass E, 2004. Äspö Hard Rock Laboratory. TRUE Block Scale Continuation project. BS2B pretests. Crosshole interference, dilution and tracer tests, CPT-1–CPT-4. SKB IPR-04-25, Svensk Kärnbränslehantering AB.

Enachescu C, Böhner J, Rohs S, 2007a. Oskarshamn site investigation. Hydraulic interference tests, pumping borehole KLX07A Subarea Laxemar. SKB P-06-145, Svensk Kärnbränslehantering AB.

Enachescu C, Wolf P, Rohs S, van der Wall R, 2007b. Oskarshamn site investigation. Hydraulic interference tests, pumping borehole KLX08 Subarea Laxemar. SKB P-07-18, Svensk Kärnbränslehantering AB.

Enachescu C, Rohs S, Wolf P, 2007c. Oskarshamn site investigation. Hydraulic interference tests, pumping borehole KLX20A Subarea Laxemar. SKB P-07-39, Svensk Kärnbränslehantering AB.

Enachescu C, Rohs S, van der Wall R, 2008a. Oskarshamn site investigation. Evaluation of hydraulic interference tests, pumping borehole KLX19A. Subarea Laxemar. SKB P-08-15, Svensk Kärnbränslehantering AB.

Enachescu C, Rohs S, van der Wall R, Wolf P, Morosini M, 2008b. Oskarshamn site investigation. Evaluation of hydraulic interference tests, pumping borehole KLX27A. Subarea Laxemar. SKB P-08-16, Svensk Kärnbränslehantering AB.

Gentzschein B, 1997. Äspö Hard Rock Laboratory. TRUE Block Scale experiment. Detailed flow logging of core boreholes KA2511A, KI0025F and KA3510A using a double packer system. SKB IPR-01-69, Svensk Kärnbränslehantering AB.

Gentzschein B, Ludvigson J-E, 1999. Äspö Hard Rock Laboratory. Single-hole hydraulic tests and short-term interference tests in KI0025F03. SKB IPR-01-58, Svensk Kärnbränslehantering AB.

Gentzschein B, Morosini M, 1998. Äspö Hard Rock Laboratory. TRUE Block Scale Project. Selective pressure build-up tests in borehole KI0025F. SKB IPR-01-45, Svensk Kärnbränslehantering AB.

Gokall-Norman K, Ludvigson J-E, 2007. Forsmark site investigation. Hydraulic interference test in borehole HFM14. SKB P-06-196, Svensk Kärnbränslehantering AB.

Gokall-Norman K, Ludvigson J-E, 2008a. Forsmark site investigation. Hydraulic interference test with borehole HFM33 used as pumping borehole, November of 2007. SKB P-07-229, Svensk Kärnbränslehantering AB.

Gokall-Norman K, Ludvigson J-E, 2008b. Forsmark site investigation. Large-scale interference test with borehole HFM14 used as pumping borehole, 2007. SKB P-07-228, Svensk Kärnbränslehantering AB.

Hantush M S, Jacob C E, 1955. Non-steady radial flow in an infinite leaky aquifer. American Geophysical Union Transactions 36, 95–100.

Harrström J, Walger E, Ludvigson J-E, Morosini M, 2008. Oskarshamn site investigation. Hydraulic interference tests of HLX27, HLX28, HLX32 and single hole pumping test of KLX27A. Subarea Laxemar. SKB P-07-186, Svensk Kärnbränslehantering AB.

Lindquist A, Wass E, 2006. Forsmark site investigation. Groundwater flow measurements in conjunction with the interference test with pumping in HFM14. SKB P-06-188, Svensk Kärnbränslehantering AB.

Lindquist A, Hjerne C, Nordqvist R, Byegård J, Walger E, Ludvigson J-E, Wass E, 2008a. Forsmark site investigation. Confirmatory hydraulic interference test and tracer test at drill site 2. SKB P-08-13, Svensk Kärnbränslehantering AB.

Lindquist A, Hjerne C, Nordqvist R, Ludvigson J-E, Harrström J, Carlsten S, 2008b. Oskarshamn site investigation. Confirmatory hydraulic interference test and tracer test in Laxemar. SKB P-08-96, Svensk Kärnbränslehantering AB.

Morosini M, Jönsson S, 2007. Oskarshamn site investigation. Pump- and interference testing of percussion drilled section of cored boreholes KLX09, KLX11A, KLX12A, KLX13A, KLX18A, KLX19A and KLX39. Subarea Laxemar. SKB P-07-182, Svensk Kärnbränslehantering AB.

Moye D G, 1967. Diamond drilling for foundation exploration. Civil Engineering Transactions, Institute of Engineers (Australia), April, 95–100.

Nordqvist R, Byegård J, Hjerne C, 2014. Complementary tracer tests – SWIW, CEC and multi-hole reciprocal cross flow tests at the TRUE-1 site. TRUE-1 Continuation project. TRUE-1 Completion. SKB P-11-27, Svensk Kärnbränslehantering AB.

Olsson O, Stanfors R, Ramqvist G, Rhén I, 1994. Äspö Hard Rock Laboratory Localization of experimental sites and layout of turn 2 – Results of investigations. SKB HRL Progress Report PR 25-94-14, Svensk Kärnbränslehantering AB.

Rouhiainen P, Heikkinen P, 1998. Äspö Hard Rock Laboratory. TRUE Block Scale Project. Difference flow measurements in borehole KI0025F02 at the Äspö HRL. SKB IPR-01-46, Svensk Kärnbränslehantering AB.

Rouhiainen P, Heikkinen P, 1999a. Äspö Hard Rock Laboratory. TRUE Block Scale Project. Difference flow measurements in boreholes K2563A and KA2511A at the Äspö HRL. SKB IPR-01-48, Svensk Kärnbränslehantering AB.

Rouhiainen P, Heikkinen P, 1999b. Äspö Hard Rock Laboratory. TRUE Block Scale Project. Difference flow measurement in borehole KI0025F03 at the Äspö HRL. SKB IPR-01-55, Svensk Kärnbränslehantering AB.

Sokolnicki M, Pöllänen J, 2007a. Oskarshamn site investigation. Interference difference flow logging of boreholes KLX09B-F Subarea Laxemar. SKB P-06-146, Svensk Kärnbränslehantering AB.

Sokolnicki M, Kristiansson S, 2007b. Oskarshamn site investigation. Interference difference flow logging of boreholes KLX11B-F Subarea Laxemar. SKB P-07-65, Svensk Kärnbränslehantering AB.

Thur P, Walger E, Ludvigson J-E, Mansueto M, 2007. Oskarshamn site investigation. Hydraulic interference tests in HLX34, HLX37 and HLX42 Laxemar Subarea. SKB P-07-185, Svensk Kärnbränslehantering AB.

Thur, P, Hjerne C, Ludvigson J-E, Svensson T, Nordqvist R, 2010. Oskarshamn site investigation. HLX28 large-scale confirmatory multiple-hole tracer test and hydraulic interference test. SKB P-09-62, Svensk Kärnbränslehantering AB.

Walger E, Ludvigson J-E, Svensson T, Thur P, Harrström J, Morosini M, 2008. Oskarshamn site investigation. Hydraulic interference tests in boreholes KLX06, KLX14A, KLX15A, KLX16A, KLX17A, KLX18A, KLX19A, KLX21A, KLX22A, KLX22B, KLX23A, KLX23B, KLX26A and KLX26B. Subarea Laxemar. SKB P-07-183, Svensk Kärnbränslehantering AB.

Winberg A (ed), Andersson P, Hermanson J, Byegård J, Cvetkovic V, Birgersson L, 2000. Äspö Hard Rock Laboratory. Final report of the first stage of the tracer retention understanding experiments. SKB TR-00-07, Svensk Kärnbränslehantering AB.

Appendix 1

Borehole instrumentation at the TRUE-1 site

Table A1-1. Evolution of packer configurations in boreholes at the TRUE-1 site with time showing the designations (Sec) and the upper and lower delimiters (Secup and Seclow) of the borehole sections. From Nordqvist et al. (2014).

		Secup	Seclow	Date YYMMDD			Secup	Seclow	Date YYMMDD			Secup	Seclow	Date YYMMDD			Secup	Seclow	Date YYMMDD	
Borehole	Sec	[m]	[m]	Start	Stop	Sec	[m]	[m]	Start	Stop	Sec	[m]	[m]	Start	Stop	Sec	[m]	[m]	Start	Stop
KXTT1	P1	17.00	28.76	950707	951211 [1)]	R1 [2)]	17.00	28.76	951211											
	P2	15.00	16.00	950707	951211 [1)]	R2 [2)]	15.00[3)]	16.00	951211											
	P3	8.50	10.50	950707	951211 [1)]	R3 [2)]	7.50	11.50	951211											
	P4	3.00	7.50	950707	951211 [1)]	R4 [2)]	3.00	6.50	951211											
KXTT2	P1	14.30	18.30	950708	951206	R1	16.55	18.3	951206 [4)]											
	P2	11.30	13.30	950708	951206	R2	14.55	15.55	951206 [4)]											
	P3	8.80 [5)]	10.30	950708	951206	R3	11.55	13.55	951206 [4)]											
	P4	3.05	7.80	950708	951206	R4	7.55	10.55	951206 [4)]											
						R5	3.05	6.55	951206 [4)]											
KXTT3	P1	15.42	17.43	950708	951211 [6)]	R1 [2)]	15.42	17.43	951211	051025	S1	15.77	17.43	051026	070410					
	P2	10.92 [7)]	14.42	950708	951211 [6)]	R2 [2)]	12.42	14.42	951211	051025	S2	14.97	15.52	051026	070410					
	P3	8.92	9.92	950708	951211 [6)]	R3 [2)]	8.92	11.42	951211	051025	S3	12.67	14.72	051026	070410					
	P4	3.17	7.92	950708	951211 [6)]	R4 [2)]	3.17	7.92	951211	051025	S4	8.92	11.67	051026						
											S5	3.17	7.92	051026						
KXTT4	P1	24.42	49.31	950718	951211 [6)]	R1 [2)]	24.42	49.31	951211	991214	S1	14.92	49.31	991214 [6)]	051027	T1	15.77	49.31	051027	070410
	P2	14.92	23.42	950718	951211 [6)]	R2 [2)]	14.92	23.42	951211	991214	S2	12.92	13.92	991214 [6)]	051027	T2	13.93	15.52	051027	070410
	P3	11.42	13.92	950718	951211 [6)]	R3 [2)]	11.42	13.92	951211	991214	S3	11.92	12.42	991214 [6)]	051027	T3	11.67	13.68	051027	070410
	P4	8.42	10.42	950718	951211 [6)]	R4 [2)]	8.42	10.42	951211	991214	S4	8.42	10.92	991214 [6)]	051027	T4	8.42	10.67	051027	
	P5	3.17	7.42	950718	951211 [6)]	R5 [2)]	3.17	7.42	951211	991214						T5	3.17	7.42	051027	
KXTT5	P1	10.81	25.85	991214																
	P2	9.61	9.81	991214																
	P3	6.11	8.61	991214																
	P4	3.11	5.11	991214																
KA3005A	P1	46.43	58.11	950227	951101	1	0	58.11	951101	951207	R1	51.03	58.11	951207						
	P2	44.43	45.43	950227	951101						R2	46.78 [8)]	50.03	951207						
	P3	38.93	43.43	950227	951101						R3	44.78	45.78	951207						
	P4	36.93	37.93	950227	951101						R4	39.03	43.78	951207						
	P5	6.53	35.93	950227	951101						R5	6.53	38.03	951207						

[1)] No stop date in Sicada.
[2)] Installation missing in Sicada.
[3)] 15.50 m according to Winberg et al. (2000).
[4)] Other date in the HMS manual.
[5)] 8.30 m according to Sicada.
[6)] Other date according to Sicada.
[7)] 10.93 m according to Winberg et al. (2000).
[8)] 46.93 m according to Winberg et al. (2000).

Results of the TRUE-1 stage

Table A2-1a. TRUE-1 Interference tests – Connectivity matrix of indexed response measure II (log (s/Q). From Winberg et al. (2000).

SOURCE		RECEIVER	KXTT1 P1	P2	P3	P4	KXTT2 P1	P2	P3	P4	KXTT3 P1	P2	P3	P4	KXTT4 P1	P2	P3	P4	P5	KA2858A P2	KA2862A P1	KA3005A P1	P2	P3	P4	KA3010A P2	KA3067A P1	P2	P3	P4	KA3105A P1	P2	P3	P4	KA3110A P1	P2	SA2880A P1	SA3045A P1	KA2050A P1	P2	P3	HA1960A P1
KXTT1	P1-4						3	4	4	4	3	2	4	4	1	4	2	4	4	0	0	3	2	2	2	0	0	0	0	0	0	0	0	0	0	0	0	0	0	0	0
	P2		1		0	0	1	0	0	0	3	4	0	0	0	1	3	0	0			1	1	1	1	0	0	0	0	0	0	0	0	0	0	0	0	0	0	0	0	0
	P3		1	1		7	3	7	7	7	1	1	7	7	0	1	2	7	7			5	4	4	3	0	0	0	0	0	0	0	0	0	0	0	0	0	0	0	0	0
KXTT2	P1		2	3	3	3		3	2	3	3	4	3	5	2	0	3	3	2			5	5	5	4	0	0	0	0	0	0	0	0	0	0	0	0	0	0	0	0	0
	P2		1	2	7	6	3		6	6	0	2	6	6	0	1	3	6	6	0	1	5	4	4	3	1	0	1	1	0	0	0	0	1	0	1	0	0	0	0	0
	P3		1	0	6	7	3	7		7	1	1	6	7	1	0	2	6	7			5	4	4	3	0	0	0	0	0	0	0	0	0	0	0	0	0	0	0	0	0
KXTT3	P2		2	4	1	1	6	2	1	1	2		2	2	1	2	3	2	1	0	0	2	3	3	3	0	0	0	0	0	0	0	0	0	0	0	0	0	0	0	0
	P3		0	1	6	6	3	6	6	6	0	1		6	0	0	1	7	6	0	0	5	3	3	2	0	0	0	0	0	0	0	0	0	0	0	0	0	0	0	0
KXTT4	P2		3	2	0	0	2	0	0	0	3	2	0	0	1		2	0	0	0	0	1	2	2	2	0	0	0	0	0	0	0	0	0	0	0	0	0	0	0	0
	P3		2	2	2	1	3	2	0	1	2	3	2	1	0	2		1	2	0	0	2	4	4	4	0	0	0	0	0	0	0	0	0	0	0	0	0	0	0	0
	P4		0	1	6	6	3	6	6	6	1	2	7	6	1	1	2		6	1	0	5	3	3	2	1	0	1	1	1	0	1	0	0	0	0	0	0	0	0	0
KA3005A	P2		2	2	4	4	5	5	4	4	2	3	4	4	1	2	5	4	4	0	0	5		7	6	0	1	0	0	0	0	0	0	0	0	0	0	0	0	0	0	0
	P4		1	2	3	3	4	3	3	3	2	3	2	3	0	2	4	3	3	0	0	3	6	7		0	0	0	0	0	0	0	0	0	0	0	0	0	0	0	0	0
KA3010A	P1-2		0	0	0	0	0	0	0	0	0	0	0	0	1	0	0	0	0	0	0	0	0	0	0		1	1	1	1	1	0	0	0	0	0	0	1	1	1	1	0

Note: Light shade (yellow) = Interpreted primary responses induced by tests in Feature A Dark shade (green) = Interpreted primary responses induced by tests in Feature B .

Table A2-1b. TRUE-1 Interference tests – Connectivity matrix of indexed response measure I (t_r(s = 0.1 m)/R^2). From Winberg et al. (2000).

SOURCE		RECEIVER	KXTT1 P1	P2	P3	P4	KXTT2 P1	P2	P3	P4	KXTT3 P1	P2	P3	P4	KXTT4 P1	P2	P3	P4	P5	KA2858A P2	KA2862A P1	KA3005A P1	P2	P3	P4	KA3010A P2	KA3067A P1	P2	P3	P4	KA3105A P1	P2	P3	P4	KA3110A P1	P2	SA2880A P1	SA3045A P1	KA2050A P1	P2	P3	HA1960A P1
KXTT1	P1-4						3	4	4	4	3	2	4	4	1	4	2	4	4	0	0	3	2	2	2	0	0	0	0	0	0	0	0	0	0	0	0	0	0	0	0
	P2		1		0	0	1	0	0	0	3	4	0	0	0	1	3	0	0			1	1	1	1	0	0	0	0	0	0	0	0	0	0	0	0	0	0	0	0	0
	P3		1	1		7	3	7	7	7	1	1	7	7	0	1	2	7	7			5	4	4	3	0	0	0	0	0	0	0	0	0	0	0	0	0	0	0	0	0
KXTT2	P1		2	3	3	3		3	2	3	3	4	3	5	2	0	3	3	2			5	5	5	4	0	0	0	0	0	0	0	0	0	0	0	0	0	0	0	0	0
	P2		1	2	7	6	3		6	6	0	2	6	6	0	1	3	6	6	0	1	5	4	4	3	1	0	1	1	0	0	0	0	1	0	1	0	0	0	0	0
	P3		1	0	6	7	3	7		7	1	1	6	7	1	0	2	6	7			5	4	4	3	0	0	0	0	0	0	0	0	0	0	0	0	0	0	0	0	0
KXTT3	P2		2	4	1	1	6	2	1	1	2		2	2	1	2	3	2	1	0	0	2	3	3	3	0	0	0	0	0	0	0	0	0	0	0	0	0	0	0	0
	P3		0	1	6	6	3	6	6	6	0	1		6	0	0	1	7	6	0	0	5	3	3	2	0	0	0	0	0	0	0	0	0	0	0	0	0	0	0	0
KXTT4	P2		3	2	0	0	2	0	0	0	3	2	0	0	1		2	0	0	0	0	1	2	2	2	0	0	0	0	0	0	0	0	0	0	0	0	0	0	0	0
	P3		2	2	2	1	3	2	0	1	2	3	2	1	0	2		1	2	0	0	2	4	4	4	0	0	0	0	0	0	0	0	0	0	0	0	0	0	0	0
	P4		0	1	6	6	3	6	6	6	1	2	7	6	1	1	2		6	1	0	5	3	3	2	1	0	1	1	1	0	1	0	0	0	0	0	0	0	0	0
KA3005A	P2		2	2	4	4	5	5	4	4	2	3	4	4	1	2	5	4	4	0	0	5		7	6	0	1	0	0	0	0	0	0	0	0	0	0	0	0	0	0	0
	P4		1	2	3	3	4	3	3	3	2	3	2	3	0	2	4	3	3	0	0	3	6	7		0	0	0	0	0	0	0	0	0	0	0	0	0	0	0	0	0
KA3010A	P1-2		0	0	0	0	0	0	0	0	0	0	0	0	1	0	0	0	0	0	0	0	0	0	0		1	1	1	1	1	0	0	0	0	0	0	1	1	1	1	0

Note: Light shade (yellow) = Interpreted primary responses induced by tests in Feature A Dark shade (green) = Interpreted primary responses induced by tests in Feature B.

Table A2-1c. Definition of response measures and their indexing. From Winberg et al. (2000).

A. Indexing used for the normalised response time ratio I: $t_r(s = 0.1m)/R^2$.

$t_r(s = 0.1m)/R^2$	Index I	Comment
< 0.005	7	Excellent
0.005–0.01	6	Almost excellent
0.01–0.05	5	Very good
0.05–0.10	4	Good
0.10–0.50	3	Rather good
0.50–1.0	2	Rather poor
> 1.0	1	Poor
no response	0	None

B. Indexing of the normalised drawdown ratio II: log(s/Q).

log(s/Q)	Index II	Comment
> 3.0	7	Excellent
2.5–3.0	6	Almost excellent
2.0–2.5	5	Very good
1.5–2.0	4	Good
1.0–1.5	3	Rather good
0.5–1.0	2	Rather poor
0.0–0.5	1	Poor
< 0	0	None

I: Normalised response time ratio; $t_r(s = 0.1m)/R^2$.
II: Normalised drawdown ratio; log(s/Q).

where:
$t_r(s = 0.1\ m)$ = time (min) at which drawdown s in a given observation section is 0.1m.
s = drawdown in a given observation section due to pumping (m).
Q = measured flow from source section during interference test.
R = Straight line distance between source and receiver section mid points.

Table A2-2. Results of cross-hole pressure interference tests in TRUE-1. Estimated hydraulic parameters for the sink sections (S) and selected observation sections in Feature A. The estimated transmissivities of the borehole sections from single-packer flow logging (T_F) are also included for comparison. From Winberg et al. (2000).

Test#	Section	T (m^2/s)	S	K'/b' (s^{-1})	T_F (m^2/s)
1	KXTT1:P2 **(S)**	$1.3\cdot10^{-8}$	–	–	$1.2\cdot10^{-8}$
	KXTT2:P1	$5.8\cdot10^{-7}$	$5.9\cdot10^{-6}$	$3.2\cdot10^{-8}$	$9.7\cdot10^{-9}$
	KXTT3:P2	$3.4\cdot10^{-7}$	$2.0\cdot10^{-7}$	$1.1\cdot10^{-8}$	$3.6\cdot10^{-7}$
	KXTT4:P3	$1.3\cdot10^{-6}$	$1.6\cdot10^{-6}$	$5.6\cdot10^{-8}$	$3.1\cdot10^{-8}$
	KA3005A:P2	$6.2\cdot10^{-6}$	$1.4\cdot10^{-5}$	$8.1\cdot10^{-9}$	$5.0\cdot10^{-8}$
3	KXTT1:P2	$1.5\cdot10^{-6}$	$7.0\cdot10^{-6}$	$9.0\cdot10^{-9}$	$1.2\cdot10^{-8}$
	KXTT2:P1 **(S)**	$6.6\cdot10^{-9}$	–	–	$9.7\cdot10^{-9}$
	KXTT3:P2	$2.7\cdot10^{-7}$	$3.8\cdot10^{-7}$	$1.7\cdot10^{-9}$	$3.6\cdot10^{-7}$
	KXTT4:P3	$6.8\cdot10^{-7}$	$6.8\cdot10^{-7}$	$3.5\cdot10^{-9}$	$3.1\cdot10^{-8}$
	KA3005A:P2	$2.3A10^{-7}$	$4.8\cdot10^{-6}$	$3.4\cdot10^{-9}$	$5.0\cdot10^{-8}$
6	KXTT1:P2	$4.5\cdot10^{-7}$	$5.7\cdot10^{-8}$	$3.7\cdot10^{-9}$	$1.2\cdot10^{-8}$
	KXTT2:P1	$6.4\cdot10^{-8}$	$9.6\cdot10^{-8}$	$4.0\cdot10^{-10}$	$9.7\cdot10^{-9}$
	KXTT3:P2 **(S)**	$3.4\cdot10^{-7}$	–	–	$3.6\cdot10^{-7}$
	KXTT4:P3	$1.1\cdot10^{-7}$	$2.1\cdot10^{-7}$	$6.3\cdot10^{-10}$	$3.1\cdot10^{-8}$
	KA3005A:P2	$1.6\cdot10^{-6}$	$3.6\cdot10^{-6}$	$1.6\cdot10^{-9}$	$5.0\cdot10^{-8}$
12	KXTT1:P2	$4.4\cdot10^{-6}$	$2.4\cdot10^{-5}$	$1.3\cdot10^{-8}$	$1.2\cdot10^{-8}$
	KXTT2:P1	$9.9\cdot10^{-8}$	$2.9\cdot10^{-6}$	$2.3\cdot10^{-9}$	$9.7\cdot10^{-9}$
	KXTT3:P2	$2.0\cdot10^{-6}$	$5.5\cdot10^{-6}$	$34\cdot10^{-9}$	$3.6\cdot10^{-7}$
	KXTT4:P3	$2.6\cdot10^{-6}$	$1.3\cdot10^{-5}$	$9.4\cdot10^{-9}$	$3.1\cdot10^{-8}$
	KA3005A:P2 **(S)**	$4.8\cdot10^{-8}$	–	–	$5.0\cdot10^{-8}$
14	KXTT1:P2	$5.7\cdot10^{-6}$	$1.3\cdot10^{-6}$	$9.9\cdot10^{-9}$	$1.2\cdot10^{-8}$
	KXTT2:P1	$1.9\cdot10^{-6}$	$8.0\cdot10^{-7}$	$1.3\cdot10^{-9}$	$9.7\cdot10^{-9}$
	KXTT3:P2	$3.3\cdot10^{-6}$	$1.4\cdot10^{-6}$	$8.6\cdot10^{-9}$	$3.6\cdot10^{-7}$
	KXTT4:P3 **(S)**	$2.2\cdot10^{-8}$	–	–	$3.1\cdot10^{-8}$
	KA3005A:P2	$4.5\cdot10^{-7}$	$2.3\cdot10^{-6}$	$4.1\cdot10^{-10}$	$5.0\cdot10^{-8}$

Table A2-3. Natural groundwater flow. Comparison of tracer dilution tests performed in October 1995 and April 1997 respectively. The section identification codes (Id codes) are explained in Subappendix 1. From Winberg et al. (2000).

Borehole	Section Id code	Volume (mL)	$Flow_{1997}$ (mL/min)	$Flow_{1995}$ (mL/min)	Comments
KXTT1	R2	1,560	0.08	0.1	
	R3	8,275	1.10	1.8	Section increased 2.0 m
KXTT2	R2	1,548	0.01	*)	
	R3	4,299	0.33	0.3	Section moved 0.25 m
KXTT3	R2	1,915	1.67	1.4	Section decreased 1.5 m
	R3	5,252	0.11	0.1	Section increased 1.5 m
KXTT4	R3	1,898	0.01	*)	
	R4	5,210	2.81	5.0	Section increased 0.5 m
KA3005A	R2	7,945	0.40	*)	
	R3	2,285	0.18	0.2	Section moved 0.35 m

Table A2-4. Summary of estimated flow and transport parameters determined for the flow path KXTT1:R2 → KXTT3:R2 (distance 5.03 m) in Feature A in TRUE-1. From Winberg et al. (2000).

Test*	Q (L/min)	Δh (m)	R (%)	D/v (m)	K_{fr} (m/s)	$2b$ (m)	θ_k
PTT-1	0.87	24	95	(0.6)***	$3.5 \cdot 10^{-4}$	$1.4 \cdot 10^{-3}$	$1.0 \cdot 10^{-3}$
RC-1	0.2 (0.4)**	2.5 (5.6)**	93	0.24	$5.0 \cdot 10^{-4}$	$2.2 \cdot 10^{-3}$	$0.7 \cdot 10^{-3}$
DP-1	0.1	5.8	88	0.40	$2.8 \cdot 10^{-4}$	–	$1.2 \cdot 10^{-3}$
PDT-1	0.1	0.6	44	1.3	$11 \cdot 10^{-4}$	$2.1 \cdot 10^{-3}$	$0.4 \cdot 10^{-3}$
PDT-2	0.2	1.9	52	1.0	$5.6 \cdot 10^{-4}$	$2.6 \cdot 10^{-3}$	$0.7 \cdot 10^{-3}$
PDT-4	0.4	9.3	100	–	–	–	–
STT-1b	0.4	9.3–12.8	100	0.55	$1.8 \cdot 10^{-4}$	$1.8 \cdot 10^{-3}$	$1.1 \cdot 10^{-3}$

* See Table 3-2 in main report.
** Pumping increased during the experiment.
*** Uncertain value due to transport in equipment.

Definitions:

- Tracer travel times, t_5, t_{50} and t_{95}, defined as the times when 5, 50 and 95% of the recovered mass had arrived, respectively based on the injected mass at t_{inj}.
- Fracture conductivity, K_{fr} (m/s), assuming radial flow and validity of Darcy's law. Calculated based on the mean travel times, t_m, determined from the parameter estimation of the conservative tracers.
- Equivalent fracture aperture (transport aperture), $2b$ (m).
- Flow porosity, Θ_k (estimated as $\Theta_k = K/K_{fr}$), where K is the steady state hydraulic conductivity for the packed-off section containing Feature A. It should be acknowledged that the term flow porosity may be misleading to use for discrete fractures, as it is defined for a porous medium. However, it is often used in fractured media as a scaling factor for transport, but then defined over a finite thickness which, in his case, is defined as the length of the packed-off borehole section in the pumping borehole.

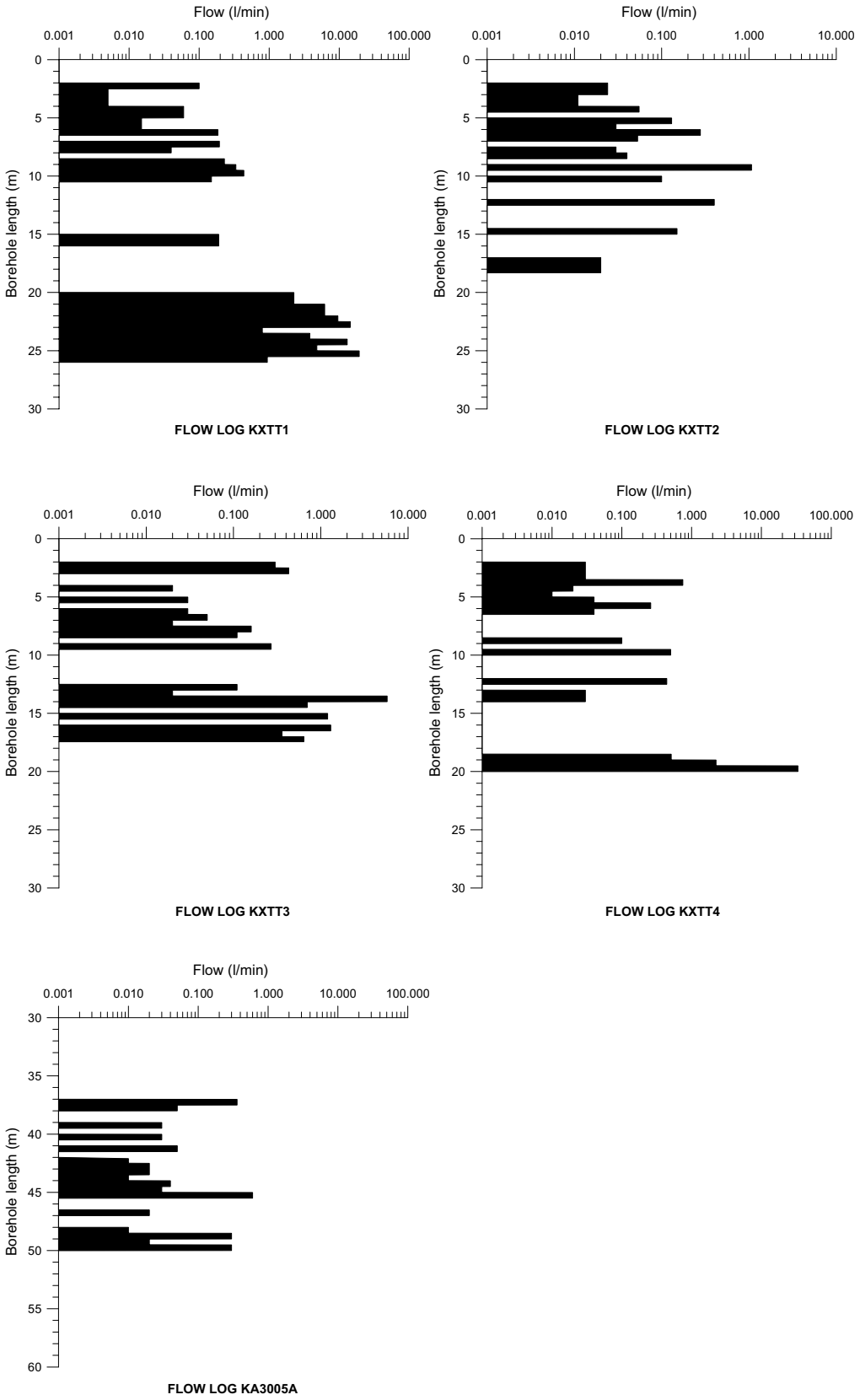

Figure A2-1. *Results of the single-packer flow logging with 0.5–1 m section length in boreholes within the TRUE-1 rock block. In boreholes KXTT1, KXTT4 and KA3005A the flow logs are truncated along depth to exclude long measurement sections in the bottom of the boreholes. From Winberg et al. (2000).*

Table A2-5. Comparison between transmissivities evaluated from single hole flow logging (T_F) and from flow and pressure build-up tests (T_M) in TRUE-1. Evaluation is made using Moye's formula. From Winberg et al. (2000).

Borehole	Test section (m)	L (m)	T_M (m^2/s)	T_F (m^2/s)	Comments
KXTT1	2.0–4.0	2.0	–	6.1 E–9	Casing 0–2.0 m
	4.0–7.0	3.0	8.1 E–8	1.5 E–8	D
	7.0–10.0	3.0	1.5 E–7	7.2 E–8	B, D
	10.0–13.0	3.0	2.0 E–7	8.7 E–9	
	13.0–16.0	3.0	1.0 E–8	1.1 E–8	A, C
	16.0–20.0	4.0	–	< E–9	
	20.0–23.0	3.0	3.0 E–6	1.9 E–6	NW-2'
	23.0–26.0	3.0	2.0 E–6	2.5 E–6	NW-2'
	26.0–28.8	2.8	–	3.5 E–9	
KXTT2	2.0–3.5	1.5	–	2.0 E–9	Casing 0–2.0 m
	3.5–6.5	3.0	7.2 E–8	2.8 E–8	D
	6.5–9.5	3.0	8.4 E–8	6.8 E–8	B, D
	9.5–12.5	3.0	2.0 E–8	2.8 E–8	B
	12.5–15.5	3.0	1.0 E–8	8.5 E–9	A, C
	15.5–18.3	3.2	–	1.1 E–9	
KXTT3	2.0–4.0	2.0	–	4.0 E–8	Casing 0–2.0 m
	4.0–7.0	3.0	5.1 E–9	7.1 E–9	D. Below measurement limit, test was interrupted.
	7.0–10.0	3.0	5.9 E–8	3.1 E–8	B
	10.0–12.0	0.0	–	< E–9	
	12.0–15.0	3.0	3.3 E–7	3.6 E–7	A
	15.0–17.4	2.4	3.1 E–7	1.9 E–7	NW-2'. Possibly flow around packers.
KXTT4	2.0–3.5	1.5	–	1.8 E–9	Casing 0–2.0 m
	3.5–6.5	3.0	2.1 E–7	6.9 E–8	D
	6.5–9.5	3.0	2.0 E–8	6.1 E–9	B
	9.5–12.5	3.0	6.6 E–8	5.8 E–8	A, B
	12.5–15.5	3.0	< 5 E–9?	> 3.7 E–9	No flow.
	15.5–18.5	3.0	–	< E–9	
	18.5–21.5	3.0	2.8 E–6	> 2.2 E–6	NW-2'
	21.5–27.5	6.0	–	2.2 E–7	NW-2', T_F = 20.5–28.5 m
	27.5–30.5	3.0	8.7 E–7	> 7.6 E–7	
	30.5–33.5	3.0	1.3 E–6	1.3 E–6	
	33.5–49.8	16.3	–	5.7 E–7	NW-2
KA3005A	2.0–37.0	35.0	–	< E–9	Casing 0-2.0 m
	36.9–37.9	1.0	2.5 E–8	2.4 E–8	Main flow at 36.9-37.4m
KA3005A	37.4–43.5	6.1	–	1.4 E–8	
	43.5–44.5	1.0	5.0 E–11	3.3 E–9	
	44.5–45.5	1.0	4.2 E–8	4.2 E–8	A. Main flow at 45.0–45.25m.
	45.5–46.5	1.0	6.1 E–11	< E–09	
	46.5–48.4	1.9	–	2.0 E–9	
	48.4–49.4	1.0	2.8 E–8	2.1 E–8	B
	49.4–58.1	8.7	–	2.0 E–8	

Appendix 3

TRUE-1 Continuation stage

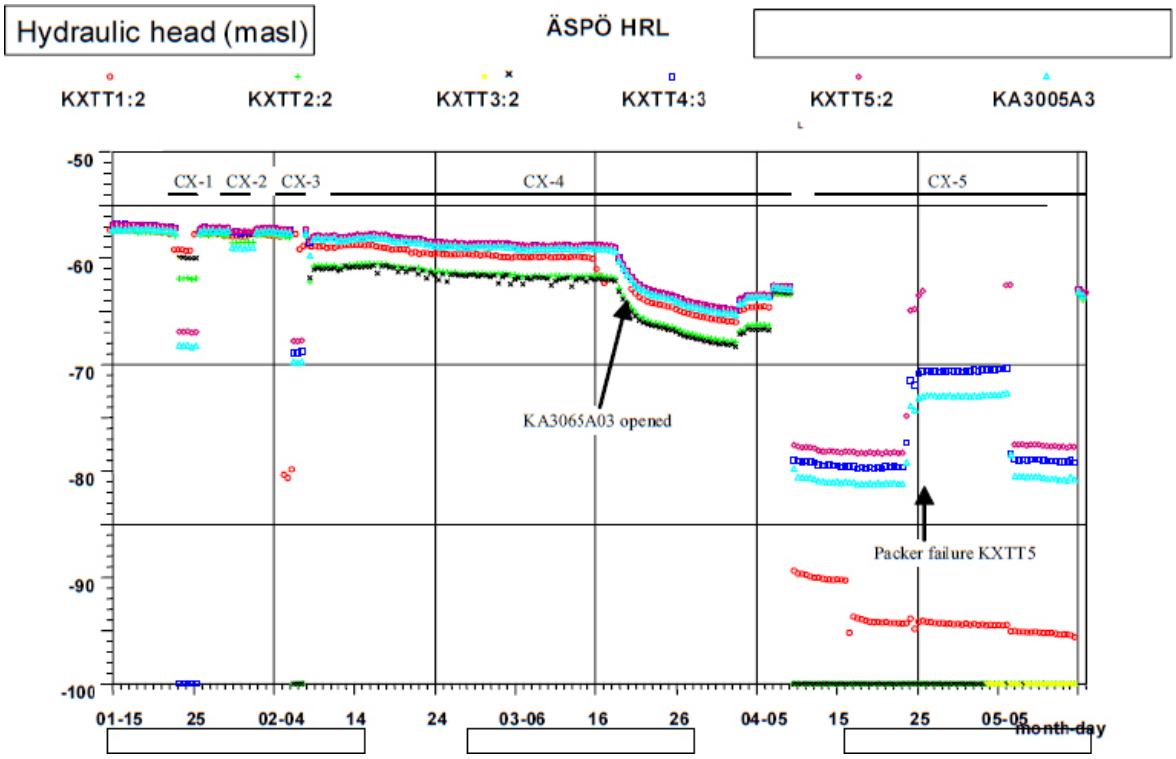

Figure A3-1. *Hydraulic head in Feature A during TRUE-1 Continuation tests CX-1–CX-5, January 15th to May 15th, 2002. From Andersson et al. (2002a).*

Table A3-1. Definition and class limits of response Index 1 and 2. From TR-02-47.

Index 1 (sp/Q_2)	
$sp/Q2 > 1 \cdot 10^5$ s/m^2	Excellent (Red)
$3 \cdot 10^4 < sp/Q_2 \leq 1 \cdot 10^5$ s/m^2	High (Yellow)
$1 \cdot 10^4 < sp/Q_2 \leq 3 \cdot 10^4$ s/m^2	Medium (Green)
$sp/Q_2 \leq 1 \cdot 10^4$ s/m^2	Low (Blue)

For response Index 2 the following class limits and associated response characteristics were used:

Index 2 (tR/R^2)	
$tR/R^2 < 0.01$ s/m^2	Excellent (E)
$0.01 \leq tR/R^2 < 0.1$ s/m^2	Good (G)
$0.1 \leq tR/R^2 < 0.3$ s/m^2	Medium (M)
$tR/R^2 \geq 0.3$ s/m^2	Bad (B)

$t_R(s = 0.1m)$ = time (s) at which drawdown s in a given observation section is 0.1m (1 kPa).
s_p = drawdown in a given observation section by the end of the flow period (m).
Q_2 = measured flow rate from sink section by the end of the flow period (m^3/s).
R = straight line (spherical) distance between sink and mid-point of observation section (m).

Sink in Feature		A	B	A	
Borehole	Interval (m)	CX-1	CX-2	CX-3	Structure
KXTT1:R1	17.00-28.76	B	B	M	NW-2´
KXTT1:R2	15.00-16.00	E	B	G	A
KXTT1:R3	7.50-11.50	B	G	M	B
KXTT1:R4	3.00-6.50	B	G	B	D
KXTT2:R1	16.55-18.30	B	M	M	?
KXTT2:R2	14.55-15.55	M	M	M	A
KXTT2:R3	11.55-13.55	B	M	B	B
KXTT2:R4	7.55-10.55	B	B	M	B
KXTT2:R5	3.05-6.55	G	M	G	D
KXTT3:R1	15.42-17.43	M	B	B	NW-2´
KXTT3:R2	12.42-14.42	M	B	S	A
KXTT3:R3	8.92-11.42	B	G	B	B
KXTT3:R4	3.17-7.92	B	G	B	B+D
KXTT4:S1	14.92-49.31	B	B	G	NW-2
KXTT4:S2	12.92-13.92	B	G	B	A´
KXTT4:S3	11.92-12.42	S	G	B	A
KXTT4:S4	8.42-10.92	B	S	M	B
KXTT4:S5	3.17-7.42	B	G	M	B+D
KXTT5:P1	10.81-25.85	B	B	M	NW-2
KXTT5:P2	9.61-9.81	G	M	M	A
KXTT5:P3	6.11-8.61	B	M	B	B
KXTT5:P4	3.11-5.11	B	M	B	D
KA3005A:R2	46.78-50.03	B	B	M	B
KA3005A:R3	44.78-45.78	G	B	G	A
KA3005A:R4	39.03-43.78	M	B	M	A?
KA3005A:R5	6.53-38.03	B	B	G	?
KA3010A:P2	8.56-15.06			B	NW-2
KA3067A:1	34.55-40.05			M	?
KA3067A:2	30.55-33.55			M	?
KA3067A:3	28.05-29.55			G	NW-2?
KA3067A:4	6.55-27.05			M	NW-3
KA3105A:P1	53.01-68.95			B	
KA3105A:P2	25.51-52.01			B	
KA3105A:P3	22.51-24.51			B	
KA3105A:P4	17.01-19.51			B	
KA3110A:P1	20.05-28.63			B	NNW-4
KA3110A:P2	6.55-19.05			B	
KA2050A:P1	155-211.57			M	
KA2050A:P2	102-154			M	NW-2?
KA2050A:P3	6-101			B	
KA2862A:P1	7.37-15.98			B	NW-3
HA1960A:P1	4-32			B	NNW-4

INDEX 1=Sp/Q
EXCELLENT
HIGH
MEDIUM
LOW

INDEX 2=tR/R2
E=EXCELLENT
G=GOOD
M=MEDIUM
B=BAD

S=SINK

Figure A3-2. *Pressure response matrix for the combined cross-hole interference tests and tracer dilution tests CX-1 through CX-3 in TRUE-1 Continuation tests. From Andersson et al. (2002a).*

Table A3-2. Results of tracer dilution tests during tests CX-1 to CX-3 in TRUE-1 continuation. From Andersson et al. (2002a).

Test	Test section	Feature	Section vol. (mL)	$Q_{natural}$ (mL/h)	Q_{pump} (mL/h)	$\Delta Q = Q_{pump} - Q_{natural}$ (mL/h)
CX-1	KXTT1:R2	A	1,466	2	9	+7
	KXTT1:R3	B	8,181	122	107	–15
	KXTT2:R2	A	1,455	16	7	–9
	KXTT2:R3	B	4,205	31	13	–18
	KXTT3:R2	A	1,821	222	489	+267
	KXTT3:R3	B	5,158	130	18	–112
	KXTT4:S2	A’	1,414	7	4	–3
	KXTT4:S3	**A**	**1,156**		**SINK**	
	KXTT4:S4	B	4,985	195	190	–5
	KXTT5:P2	A	564	2	55	+53
	KA3005A:R2	B	7,852	?	19	?
	KA3005A:R3	A	2,192	10	4	–6
	KA3010A:P2	NW-2	13,742	831	828	–3
CX-2	KXTT1:R2	A	1,466	2	6	+4
	KXTT1:R3	B	8,181	122	2,050	+1,928
	KXTT2:R2	A	1,455	2	4	+2
	KXTT2:R3	B	4,205	31	104?	+73
	KXTT3:R2	A	1,821	148	376	+228
	KXTT3:R3	B	5,158	16	483	+467
	KXTT4:S2	A’	1,414	3	4	+1
	KXTT4:S3	A	1,156	3	2	–1
	KXTT4:S4	**B**	**4,985**		**SINK**	
	KXTT5:P2	A	564	2	5	+3
	KA3005A:R2	B	7,852	23	50	+27
	KA3005A:R3	A	2,192	0.2	2	+1.8
	KA3010A:P2	NW-2	13,742	831	211?	–620
CX-3	KXTT1:R2	A	1,466	2?	574	+572
	KXTT1:R3	B	8,181	129	97	–32
	KXTT2:R2	A	1,455	7	25	+18
	KXTT2:R3	B	4,205	36	14	–22
	KXTT3:R2	**A**	**1,821**		**SINK**	
	KXTT3:R3	B	5,158	17	28	+11
	KXTT4:S2	A’	1,414	2	0.2	–1.8
	KXTT4:S3	A	1,156	4	14	+10
	KXTT4:S4	B	4,985	292	196	–96
	KXTT5:P2	A	564	1	44	+43
	KA3005A:R2	B	7,852	41	14	–27
	KA3005A:R3	A	2,192	0.8	1.3	+0.5
	KA3010A:P2	NW-2	13,742	882	1,084	+202

Table A3-3. Summary of hydraulic and transport parameters for the flow paths tested in CX-4b and CX-5 using KXTT3:R2 as sink. Values within brackets are standard errors in percent. From Andersson et al. (2002a).

Parameter	Test CX-4b KXTT4:S2	Test CX-4b KXTT4:S3	Test CX-5 KXTT1:R2	Test CX-5 KXTT4:S3	Source
Euclidian distance, L (m)	4.68	4.68	5.03	4.68	Geometry
Withdrawal rate, Q (l/min)	0.2	0.2	2.97	2.97	Measured
Mean head difference, Δh (m)	2.8	3.2	134.4	149.1	HMS
Inj. flow rate (ml/h)	0.2	0.6	727	21	Injection curve
Mean travel time, t_m (h)	140	97.5	0.34	1.6	PAREST
Mean velocity, v (m/s)	$9.26\cdot10^{-6}$ (1)	$1.33\cdot10^{-5}$ (1)	$4.10\cdot10^{-3}$ (2)	$8.01\cdot10^{-4}$ (3)	PAREST
First arrival, t_a (h)	90	23	0.3	1.6	BTC*
Peclet number, Pe	33	4.0	29	5.1	PAREST
Dispersivity, D/v (m)	0.14 (11)	1.16 (6)	0.17 (23)	0.92 (21)	PAREST
Fracture conductivity, K_{fr} (m/s)	$3.9\cdot10^{-5}$	$4.9\cdot10^{-5}$	$4.0\cdot10^{-4}$	$6.4\cdot10^{-5}$	
Equivalent fracture aperture, b (m)	$2.4\cdot10^{-2}$	$1.7\cdot10^{-2}$	$7.6\cdot10^{-4}$	$4.2\cdot10^{-3}$	
Flow porosity, θ_k (2 m thickness)	$3.5\cdot10^{-3}$	$2.8\cdot10^{-3}$	$2.6\cdot10^{-4}$	$1.6\cdot10^{-3}$	
Mass recovery, R (%)	31	27	79	56	BTC*

* BTC = Breakthrough curve.

Based on the mean travel times, t_m, determined from the parameter estimation, the hydraulic fracture conductivity, K_{fr} (m/s), was calculated assuming radial flow and validity of Darcy's law:

$$K_{fr} = \ln (r/r_w) (r^{22}–r_w^2)/2\cdot t_m\cdot\Delta h$$

where:

r = travel distance (m)

r_w = borehole radius (m)

t_m = mean travel time of tracer (s)

Δh = head difference (m)

The equivalent fracture aperture, b (m), was calculated from:

$$b = Q\cdot t_m/\pi\cdot(r^2–r_w^2)$$

where Q (m^3/s), is the mean flow rate.

Flow porosity, θ_k, was calculated using:

$$\theta_k = K/K_{fr}$$

where K is the average hydraulic conductivity of the borehole section determined from steady-state evaluation (Moye 1967) assuming a porous medium:

$$K = (Q/\Delta h\cdot L)\cdot((1+\ln L/2r_w)/2\pi)$$

where L (m) is the length of the section.

It should be noted that the term flow porosity might be misleading to use in a fractured heterogeneous rock as it is defined for a porous medium. However, it is often used in fractured medium as a scaling factor for transport, but then defined over a finite thickness which, in this case, is defined as the length of the packed-off borehole section (L = 2.0 m).

TRUE-1 Completion stage

Table A4-1a. Time response matrix of Index 1 ($t_R/r2$) for the complementary multiple-hole reciprocal cross flow tests in TRUE-1 Completion. The colours represent the speed of the response. From Nordqvist et al. (2014).

Pumping hole	Q_{pump} [ml/min]	Observation hole					
		KXTT1	KXTT2	KXTT3	KXTT4	KXTT5	KA3005A
KXTT1	350		0.60	0.08	0.13	0.03	2.62
KXTT2	190	0.90		0.09	0.24	0.07	1.15
KXTT3	385	0.08	0.09		0.09	0.04	0.65
KXTT3	2,800	0.15	0.09		0.19	0.08	0.16
KXTT4	200	0.20	0.40	0.19		0.05	0.31
KXTT4	600	0.13	0.24	0.09		0.05	0.13
KXTT5	1,540	0.03	0.05	0.04	0.05		0.04
KA3005A	870	0.54	0.69	0.11	0.13	0.01	

$t_R/r^2 < 0.1$ s/m^2	Good
$0.1 \le t_R r^2 < 0.3$ s/m^2	Medium
$t_R/r^2 \ge 0.3$ s/m^2	Bad

Table A4-1b. Drawdown response matrix of Index 2 (s_p/Q_{pump}) for the complementary multiple-hole reciprocal cross flow tests in TRUE-1 Completion. The colours represent the strength of the response. From Nordqvist et al. (2014).

Pumping hole	Q_{pump} [ml/min]	Observation hole					
		KXTT1	KXTT2	KXTT3	KXTT4	KXTT5	KA3005A
KXTT1	350		4.76E+05	4.67E+05	1.93E+05	1.96E+05	1.89E+05
KXTT2	190	3.77E+05		7.42E+05	4.08E+05	3.55E+05	8.01E+05
KXTT3	385	4.53E+05	9.79E+05		2.96E+05	2.69E+05	3.08E+05
KXTT3	2,800	5.37E+05	2.13E+06		2.92E+05	2.58E+05	2.83E+05
KXTT4	200	2.51E+05	4.70E+05	3.43E+05		8.93E+05	1.01E+06
KXTT4	600	2.09E+05	4.76E+05	3.18E+05		1.10E+06	1.05E+06
KXTT5	1,540	2.20E+05	5.12E+05	3.35E+05	1.52E+06		1.39E+06
KA3005A	870	2.06E+05	1.14E+06	3.11E+05	1.10E+06	9.35E+05	

$s_p/Q_{pump} \ge 1 \cdot 10^6$ s/m^2	Excellent
$3 \cdot 10^5 \le s_p/Q_{pump} < 1 \cdot 10^6$ s/m^2	High
$1 \cdot 10^5 \le s_p/Q_{pump} < 3 \cdot 10^5$ s/m^2	Medium
$s_p/Q_{pump} < 1 \cdot 10^5$ s/m^2	Low

Table A4-2. Estimated transmissivity, T_M and T_Th, for the flowing borehole sections and observation sections in Feature A, respectively during the complementary multiple-hole reciprocal cross flow tests in TRUE-1 Completion. From Nordqvist et al. (2014).

Flowing borehole	Q_{pump} [mL/min]	T_M [m^2/s]	T_{Th} [m^2/s] for observation borehole sections					
			KXTT1	KXTT2	KXTT3	KXTT4	KXTT5	KA3005A
KXTT1	350	1.2E–08	x	1.4E–08	1.6E–08	1.6E–08	1.8E–08	1.6E–08
KXTT2	190	6.2E–09	7.2E–09	x	8.8E–09	8.3E–09	9.6E–09	7.5E–09
KXTT3	385	6.0E–07	9.0E–07	2.4E–06	x	8.9E–07	9.6E–07	1.0E–06
KXTT3	2,800	2.7E–07	3.7E–07	1.4E–06	x	3.3E–07	3.6E–07	3.8E–07
KXTT4	200	5.7E–08	6.5E–08	6.6E–08	6.5E–08	x	7.3E–08	7.5E–08
KXTT4	600	2.4E–08	2.8E–08	2.8E–08	2.7E–08	x	2.9E–08	3.0E–08
KXTT5	1,540	5.3E–08	1.6E–07	1.7E–07	1.5E–07	1.8E–07	x	2.0E–07
KA3005A	870	3.7E–08	3.9E–08	3.6E–08	4.3E–08	4.2E–08	4.7E–08	x

TableA4-3a. Measured flow rates (Q_{flo}w) in mL/min in the observation borehole sections in Feature A from tracer dilution tests during the cross-hole interference tests in TRUE-1 Completion. After Nordqvist et al. (2014).

Pumping hole	Q_{pump} [mL/min]	Observation hole					
		KXTT1	KXTT2	KXTT3	KXTT4	KXTT5	KA3005A
KXTT1	350	x	0.06	8.00	0.11	0.68	–0.03
KXTT2	190	0.32	x	0.79[1)]	0.13	0.49	0.17
KXTT3	385	1.31	0.27	x	0.87	1.14	0.21[2)]
KXTT3	2,800	15.95	0.42	x	3.67	3.19	0.20[2)]
KXTT4	200	0.08	0.16	3.73	x	0.78	–0.11[2)]
KXTT4	600	0.21	0.15	0.12[1)]	x	2.25	–0.11[2)]
KXTT5	1,540	0.75	0.26	22.98	3.52	x	–0.07
KA3005A	870	0.30	1.10	13.38	1.05	6.83	x

[1)] Uncertain evaluation due to low tracer concentration.
[2)] Uncertain evaluation due to scattered data.

TableA4-3b. Measured flow rates (mL/min) in the observation borehole sections in Feature A from tracer dilution tests during undisturbed periods in connection to the cross-hole interference tests in TRUE-1 Completion. After Nordqvist et al. (2014).

Undisturbed period	Observation hole					
	KXTT1	KXTT2	KXTT3	KXTT4	KXTT5	KA3005A
2	0.27[1)]	0.09	x	–0.04	0.38	0.01
3	x	0.09	3.42	0.00	0.69	–0.01
4	0.15	0.07	0.94[1)]	0.06	x	0.03
5	0.08	x	3.51	0.02	0.06	–0.04[2)]
6	0.07	0.06	3.18	x	–0.01	–0.03[2)]

[1)] Uncertain evaluation due to low tracer concentration.
[2)] Uncertain evaluation due to scattered data.

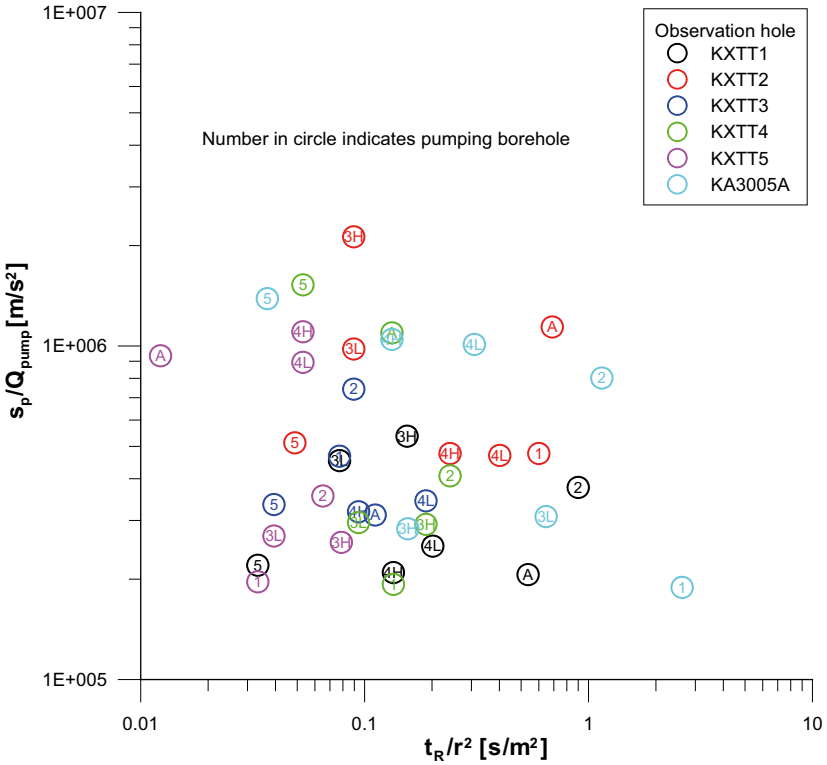

Figure A4-1. *Diagnostic plot of pressure response indices 1 and 2 during TRUE-1 Completion. The colours in the legend represent the observation boreholes while the numbers indicate the flowing boreholes. From Nordqvist et al. (2014).*

Appendix 5

Borehole instrumentation at the TRUE Block Scale site

Table A5-1. Evolution with time of packer configurations in boreholes in the True Block Scale project with time. The test section intervals are given in metres. From Andersson et al. (2002b).

Ceneration code:	P	R	S	T
Idcode	to 970429	to 980209	to 990201	present
KA2511A : 8				6 - 64
KA2511A : 7				65 - 95
KA2511A : 6		6 - 63		96-102
KA2511A : 5		64 - 91	52 - 54	103 - 110
KA2511A : 4	6- 30	92 - 138	92 - 109	111 - 138
KA2511A : 3	31 - 80	139 - 170	110 - 216	139 - 170
KA2511A : 2	81 - 170	171 - 230	217 - 241	171 - 238
KA2511A : 1	171 - 293	231 - 293	242 - 244	239 - 293
Idcode	to 980218	to 990120	present	
KA2563A : 7	6 - 75	76 - 145		
KA2563A : 6	76 - 112	146 - 186		
KA2563A : 5	113 - 145	187 - 190	146 - 186	
KA2563A : 4	146 - 186	191 - 219	187 - 190	
KA2563A : 3	187 - 196	220 - 224	206 - 208	
KA2563A : 2	197 - 265	225 - 228	236 - 241	
KA2563A : 1	266 - 362	262 - 362	242 - 246	
Idcode	present			
KI0023B : 9	4,6 - 40,45			
KI0023B : 8	41,45 - 42,45			
KI0023B : 7	43,45 - 69,95			
KI0023B : 6	70,95 - 71,95			
KI0023B : 5	72,95 - 83,75			
KI0023B : 4	84,75 - 86,20			
KI0023B : 3	87,2 - 110,25			
KI0023B : 2	111,25 - 112,70			
KI0023B : 1	113,7 - 200,71			
Idcode	to 980225	to 990728	present	
KI0025F : 8	0 - 2,5			
KI0025F : 7	3,5 - 40			
KI0025F : 6	41 - 85	3,5 - 40	5 - 41,5	
KI0025F : 5	86 - 88	41 - 85	42,5 - 86,5	
KI0025F : 4	89 - 151	86 - 88	87,5 - 89,5	
KI0025F : 3	152 - 157	89 - 163	90,5 - 164,5	
KI0025F : 2	158 - 168	164 - 168	165,5 - 169,5	
KI0025F :1	169 - 193.7	169 - 193.7	170,5 - 193,7	
Idcode	present			
KI0025F02 : 10	3,4 - 37,50			
KI0025F02 . 9	38,5 - 50,70			
KI0025F02 : 8	51,7 - 55,10			
KI0025F02 : 7	56,1 - 63,00			
KI0025F02 : 6	64 - 72,30			
KI0025F02 : 5	73,3 - 77,25			
KI0025F02 : 4	78,25 - 92,35			
KI0025F02 : 3	93,35 - 99,25			
KI0025F02 : 2	100,25 - 134,15			
KI0025F02 : 1	135,15 - 204,18			
Idcode	present			
KI0025F03 : 9	3,58 - 50,58			
KI0025F03 : 8	51,58 - 54,08			
KI0025F03 : 7	55,08 - 58,58			
KI0025F03 : 6	59,58 - 65,58			
KI0025F03 : 5	66,58 - 74,08			
KI0025F03 : 4	85,08 - 88,08			
KI0025F03 : 3	89,08 - 92,58			
KI0025F03 : 2	93,58 - 100,08			
KI0025F03 : 1	101,08 - 141,72			

Appendix 6

TRUE Block Scale-Preliminary characterization stage

Table A6-1. Distances between the sink sections and observation sections during the interference tests in the preliminary characterization stage of True Block Scale. Black = sink. From Andersson et al. (1998).

Borehole	ENW-2	ENW-1	ESV-2	ESV-1a	ESV-1b	ESV-1c	1	2	3	4	5	6	7	8	9	10	11	12	13
KA2511A:S1	190	170	136	114	110	109	243	221	277	99	105	143	92	125	89	123	103	73	152
KA2511A:S2	176	161	125	105	99	99	229	207	263	105	96	129	83	114	85	112	93	65	143
KA2511A:S3	110	129	86	76	67	71	163	142	199	149	79	63	72	74	95	78	68	67	112
KA2511A:S4	48	126	87	94	86	92	101	82	141	201	106		108	80	138	89	95	113	115
KA2511A:S5		144	114	129	122	128	53	41	100	245	143	47	147	111	178	120	132	156	137
KA2563A:R1	245	163	147	124	140	122	294	271	310		108	201	133	148	139	135	116	92	150
KA2563A:R2	163	90	62	38	70	39	211	188	225	86	22	124	87	70	115	50	34	32	74
KA2563A:R3	159	87	58	34	68	35	207	184	221	90	18	120	86	67	116	46	31	32	71
KA2563A:R4	143	75	41	17	60	21	190	167	203	108		106	85	54	119	29	19	39	59
KA2563A:R5	129	67	27		57	16	174	152	187	124	17	94	88	45	124	16	20	50	51
KA2563A:R6	109	61	14	23	61	30	153	131	165	146	39	80	96	42	135	18	36	69	48
KA2563A:R7	71	79	58	79	96	83	103	83	112	202	95	69	132	74	171	70	90	121	76
KI0025F:R1	191	206	148	139	95	125	114	230	264	144	133	151	55	118	15	136	119	97	190
KI0025F:R2	178	192	133	124	79	110	100	217	250	139	119	138	40	103		121	105	84	175
KI0025F:R3	147	155	93	88	39	73	65	185	216	133	85	108		63	40	82	69	58	139
KI0025F:R4	122	120	65	57		42	41	157	184	139	60	86	39	24	79	47	41	52	106
KI0025F:R5	111	101	35	45	24	33	41	142	166	148	54	80	63		103	31	37	62	89
KI0025F:R6	101	74	25	51	65	52	66	123	140	171	66	84	104	41	144	38	59	92	68
KI0023B:P1	195	158	120	99	91	91	77	227	271	71	86	149	74	108	75	106	84	50	141
KI0023B:P2	156	114	70	50	52	41	27	186	225	92	39	113	58	62	84	56	34		97
KI0023B:P3	146	103	57	38	45	28	14	176	213	100	28	105	60	51	91	43	21	13	87
KI0023B:P4	137	92	44	26	41	15		165	201	111	21	98	65	41	100	29	7	27	76
KI0023B:P5	133	87	36	20	41	7.3	7	160	194	116	19	95	69	37	105	22		34	71
KI0023B:P6	128	82	29	16	42		15	155	188	122	21	92	73	33	110	14	7	41	67
KI0023B:P7	120	73	15	16	47	15	29	145	175	135	29	89	82	31	121		22	56	59
KI0023B:P8	114	66		27	56	29	44	137	163	147	41	87	93	35	133	14	36	70	55
KI0023B:P9	107	61	20	44	71	48	63	126	147	165	59	89	109	47	149	34	56	90	55
KA3510A:P1	164	43	58	53	104	65	72	178	201	130	54	139	134	88	170	58	68	91	39
KA3573A:P1	137	18	55	51	106	67	76	147	183	150	59	115	139	89	175	59	71	97	
KA3573A:P2	144		66	67	120	82	90	150	180	163	75	126	154	101	191	73	87	114	18
KA3600F:P1	188	59	112	100	157	115	119	192	235	150	99	164	183	143	215	113	117	131	60
KA3600F:P2	175	39	99	92	149	108	114	178	215	159	94	155	179	133	213	130	111	130	45
KA1751A:P1	245	245	285	297	332	309	321	207	219	402	310	274	367	310	404	297	315	343	256
KA2162B:P1	95	194	174	197	190	197	209	82	23	319	213	140	219	174	251	185	203	231	195
KA2162B:P2	158	265	240	263	247	261	273	148	87	382	279	201	271	234	299	250	267	293	267
KA2162B:P3	215	325	297	321	301	318	329	207	147	438	336	258	322	290	346	308	323	350	326
KA2162B:P4	265	376	347	371	348	367	377	257	197	486	386	306	367	338	389	357	372	397	377
KA3385A:P1	144	209	167	192	167	186	196	158	98	298	205	166	190	156	218	176	191	216	208
KA3385A:P2	144	202	164	190	168	185	196	155	90	297	203	166	194	156	224	174	190	217	203
KA2512A	41	150	150	152	157	155	165		88	283	178	90	190	148	222	145	160	186	147
KA2598A	100	180	163	187	184	188	201	88		310	203	141	216	166	250	175	194	225	183
Source =																			

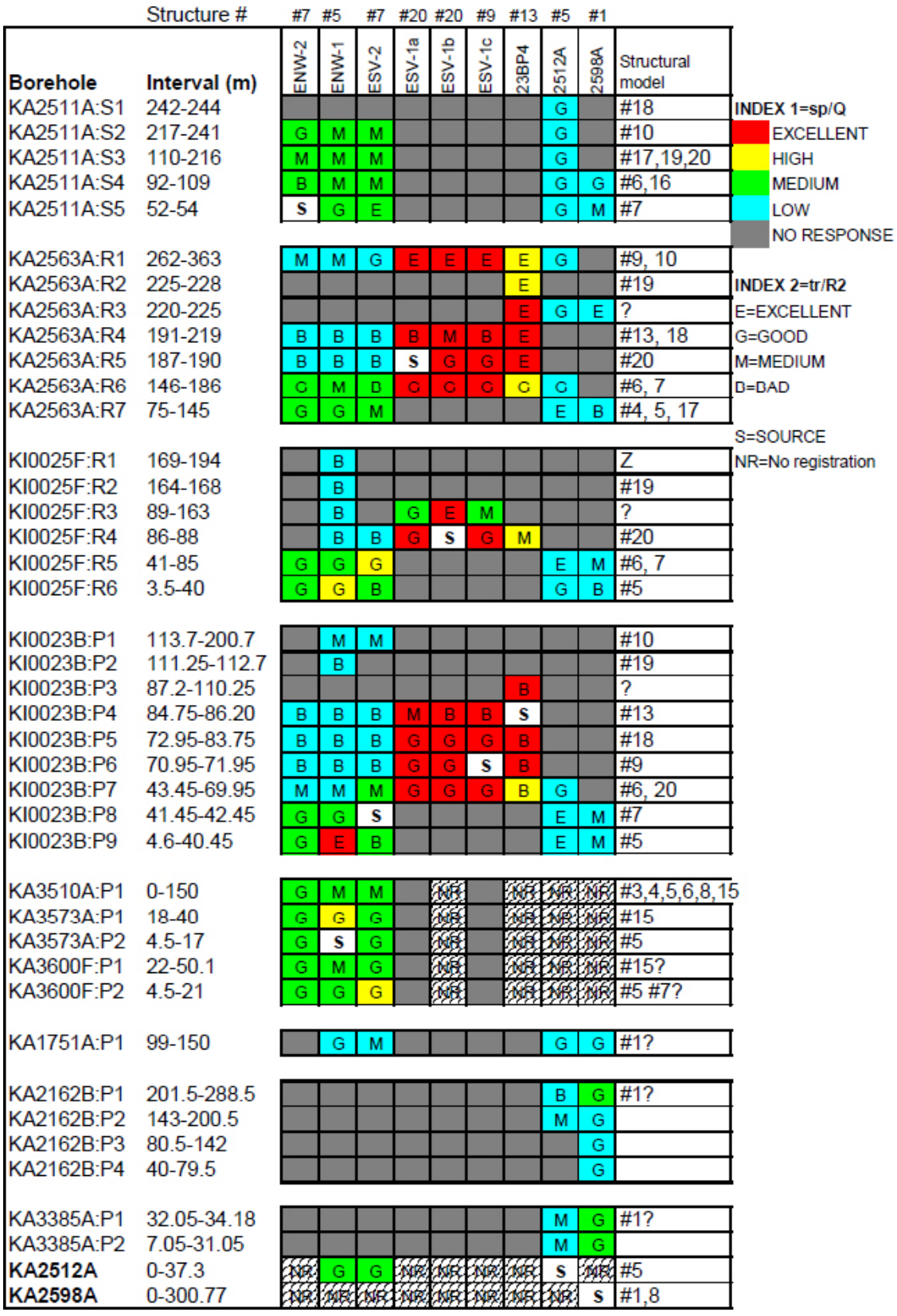

Figure A6-1a. *Response matrix for TRUE Block Scale Interference Tests ENW-1–2, ESV-2, ESV1a–c) and # 1–3 during the Preliminary Characterization Stage. From Andersson et al. (1998).*

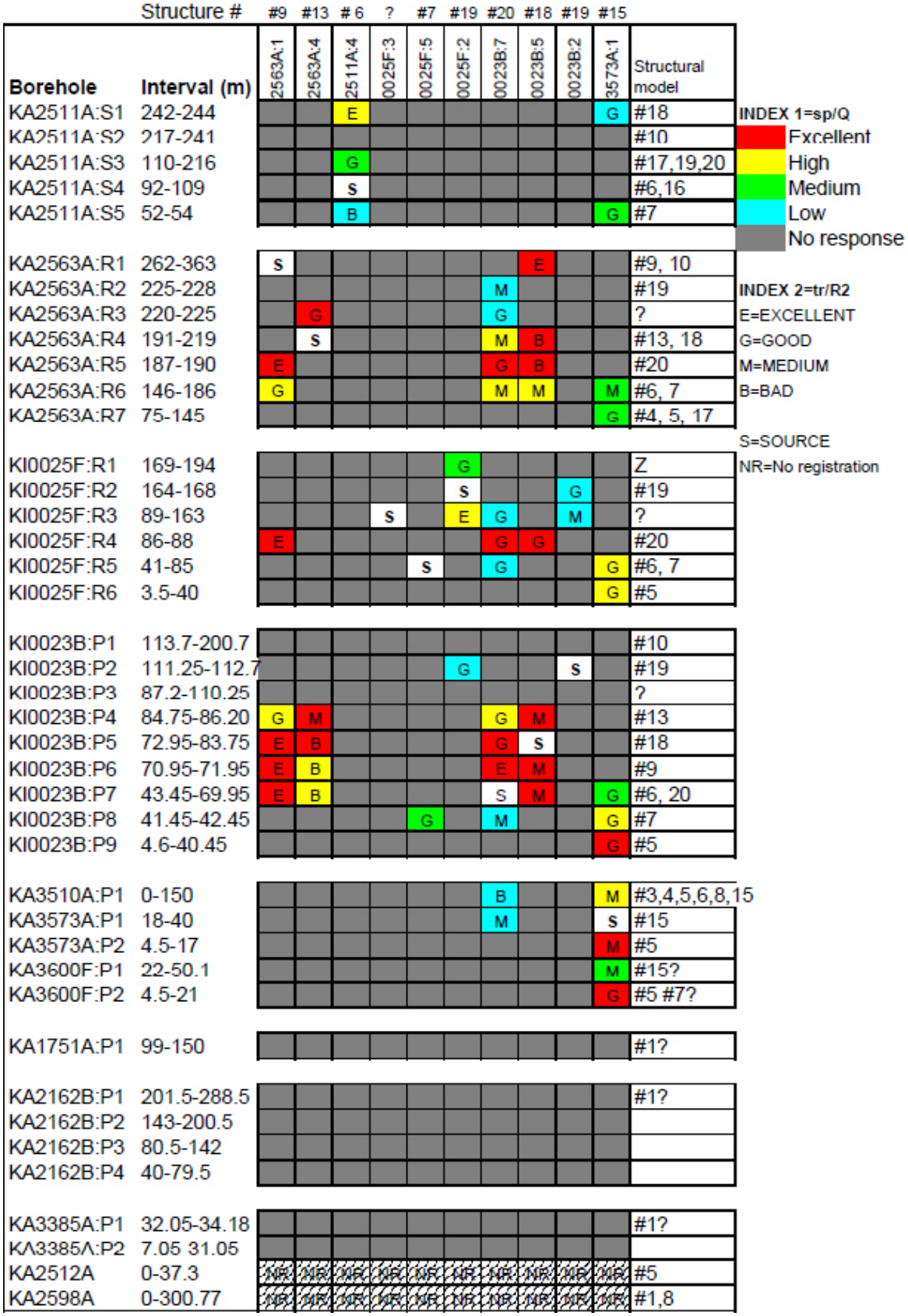

Figure A6-1b. *Response matrix for TRUE Block Scale Interference Tests # 4–13 during the Preliminary Characterization Stage. From Andersson et al. (1998).*

Table A6-2. Summary of estimated hydraulic parameters for the most significant response sections during the longer interference tests. Rad = Radial, Leaky = pseudo-spherical, NFB = Apparent no-flow hydraulic boundary. From Andersson et al. (1998).

Borehole section	Interval (m)	T (m^2/s)	S	T/S (m^2/s)	K'/b' (s^{-1})	Dom. Flow geometry
Test ENW-2. Source: KA2511A:S5. Structure #7						
KA2563A:R6	146–186	$3.3\cdot10^{-5}$	$3.1\cdot10^{-6}$	10.6	–	Rad
KI0025F:R5	41–85	$2.1\cdot10^{-5}$	$1.9\cdot10^{-6}$	11.0	–	Rad
KI0023B:P8	41.45–42.45	$2.3\cdot10^{-5}$	$1.6\cdot10^{-6}$	14.5	–	Rad
KA3510A:P1	0–150	$3.2\cdot10^{-5}$	$2.6\cdot10^{-6}$	12.2	–	Rad
KA3573A:P1	18–40	$2.9\cdot10^{-5}$	$9.8\cdot10^{-7}$	29.6	–	Rad
KA3573A:P2	4.5–17	$2.9\cdot10^{-5}$	$1.4\cdot10^{-6}$	20.5	–	Rad
KA3600F:P1	22–50.1	$2.3\cdot10^{-5}$	$1.0\cdot10^{-6}$	22.2	–	Rad
KA3600F:P2	4.5–21	$2.3\cdot10^{-5}$	$1.2\cdot10^{-6}$	20.0	–	Rad
Test ENW-1. Source: KA3573A:P2. Structure #5						
KA2511A:S5	52–54	$2.9\cdot10^{-5}$	$3.2\cdot10^{-6}$	8.9	–	Rad→NFB
KA2563A:R7	75–145	$2.8\cdot10^{-5}$	$4.9\cdot10^{-6}$	5.7	–	Rad→NFB
KI0025F:R5	41–85	$3.1\cdot10^{-5}$	$3.2\cdot10^{-6}$	9.6	–	Rad→NFB
KI0025F:R6	3.5–40	$1.9\cdot10^{-5}$	$6.8\cdot10^{-8}$	279		Rad
KI0023B:P8	41.45–42.45	$3.0\cdot10^{-5}$	$7.8\cdot10^{-6}$	3.8	–	Radi→NFB
KI0023B:P9	4.5–40.45	$2.6\cdot10^{-6}$	$1.2\cdot10^{-7}$	22.0	$3.9\cdot10^{-11}$	Leaky
KA3573A:P1	18–40	($5.7\cdot10^{-6}$)	($3.4\cdot10^{-6}$)	(1.7)	($8.1\cdot10^{-10}$)	Leaky
KA3600F:P2	4.5–21	$2.3\cdot10^{-5}$	$4.6\cdot10^{-6}$	5.0	–	Rad
KA1751A:P1	99–150	$2.8\cdot10^{-5}$	$9.2\cdot10^{-6}$	3.1	–	Rad
KA2512A	0–37.3	$1.9\cdot10^{-5}$	$3.1\cdot10^{-6}$	6.2	–	Rad
Test ESV-2. Source: KI0023B:P8. Structure #7						
KA2511A:S5	52–54	$3.5\cdot10^{-5}$	$1.5\cdot10^{-6}$	22.6	–	Rad→NFB
KI0025F:R5	41–85	$4.3\cdot10^{-5}$	–	–	–	Rad→NFB
KA3573A:P1	18–40	$4.9\cdot10^{-5}$	$1.0\cdot10^{-6}$	47.9	–	Rad→NFB
KA3573A:P2	4.5–17	$3.5\cdot10^{-5}$	$4.0\cdot10^{-6}$	8.7	–	Rad→NFB
KA3600F:P1	22–50.1	$3.9\cdot10^{-5}$	$2.2\cdot10^{-6}$	17.6	–	Rad→NFB
KA3600F:P2	4.5–21	$4.9\cdot10^{-5}$	$2.0\cdot10^{-7}$	247	–	Rad→NFB
KA2512A	0–37.3	$3.1\cdot10^{-5}$	$1.7\cdot10^{-6}$	17.8	–	Rad→NFB
Test ESV-1a. Source: KA2563A:R5. Structure #20						
KA2563A:R1	262–363	($1.0\cdot10^{-6}$)	($4.9\cdot10^{-10}$)	(2,040)	($6.0\cdot10^{-14}$)	Rad→Leaky
KI0025F:R4	86–88	$9.6\cdot10^{-7}$	$5.7\cdot10^{-8}$	16.8	$5.6\cdot10^{-12}$	Rad→Leaky
KI0023B:P5	72.4–84	$7.4\cdot10^{-7}$	$5.1\cdot10^{-7}$	1.4	$4.5\cdot10^{-12}$	Rad→Leaky
KI0023B:P6	70.4–71.4	$8.3\cdot10^{-7}$	$2.6\cdot10^{-7}$	3.1	$5.6\cdot10^{-11}$	Rad→Leaky
KI0023B:P7	43.45–69.4	$9.5\cdot10^{-7}$	$2.9\cdot10^{-7}$	3.2	$3.4\cdot10^{-11}$	Rad→Leaky
Test ESV-1b. Source: KI0025F:R4. Structure #20						
KA2563A:R1	262–363	$1.0\cdot10^{-6}$	$1.2\cdot10^{-8}$	86.4	$2.1\cdot10^{-12}$	Rad→Leaky
KA2563A:R5	187–190	$8.1\cdot10^{-7}$	$5.0\cdot10^{-8}$	16.4	$9.9\cdot10^{-12}$	Rad→Leaky
KI0025F:R3	89–163	$8.1\cdot10^{-7}$	$6.0\cdot10^{-8}$	13.5	$2.1\cdot10^{-11}$	Rad→Leaky
KI0023B:P6	70.4–71.4	$7.3\cdot10^{-7}$	$8.2\cdot10^{-8}$	8.8	$1.6\cdot10^{-11}$	Rad→Leaky
KI0023B:P7	43.45–69.4	$9.1\cdot10^{-7}$	$7.3\cdot10^{-8}$	12.6	$1.6\cdot10^{-11}$	Rad→Leaky
Test ESV-1c. Source: KI0023B:P6. Structure #9						
KA2563A:R1	262–363	$1.2\cdot10^{-6}$	$4.2\cdot10^{-9}$	294	$5.3\cdot10^{-13}$	Rad→Leaky
KA2563A:R5	187–190	$8.7\cdot10^{-7}$	$1.9\cdot10^{-7}$	4.5	$3.4\cdot10^{-11}$	Rad→Leaky
KI0025F:R4	86–88	$7.7\cdot10^{-7}$	$1.1\cdot10^{-7}$	7.0	$1.7\cdot10^{-11}$	Rad→Leaky
KI0023B:P5	72.4–84	$7.7\cdot10^{-7}$	$4.1\cdot10^{-7}$	1.9	$3.6\cdot10^{-11}$	Rad→Leaky
KI0023B:P7	43.45–69.4	$1.2\cdot10^{-6}$	$2.1\cdot10^{-7}$	5.9	$1.5\cdot10^{-11}$	Rad→Leaky

Table A6-3. Results of flow measurements (using tracer dilution tests) performed during TRUE Block Scale Interference Tests during the Preliminary Characterisation Stage. From Andersson et al. (1998).

Test#	Pumped Structure	Measured Borehole	Structure	Q (natural) (mL/h)	Q (pump) (mL/h)
ENW-2	#7	KA2511A:S4	#6, 16	1,100	1,100
ENW-1	#5			1,100	950
ESV-2	#7			1,150	1,100
ESV-1a	#20			1,200	1,050
ENW-2	#7	KA2563A:R5	#20		550
ENW-1	#5			540	560
ESV-2	#7			560	610
ESV-1b	#20			540	715
ESV-1c	#9			590	1,420
ENW-2	#7	KI0023B:P8	#6,7	< 1	< 1
ENW-1	#5	KI0023B:P6	#9	< 1	< 1
ESV-2	#7			3	
ESV-1a	#20			2	7
ESV-1b	#20			4	6
ENW-2	#7	KI0023B:P4	#13	< 1	< 1
ENW-1	#5			< 1	< 1
ESV-2	#7			< 1	< 1
ESV-1b	#20			1	4
ESV-1c	#9			< 1	< 1
ENW-2	#7	KI0025F:R2	#19	6	2
ENW-1	#5			16	6
ESV-2	#7			18	18
ENW-2	#7	KI0025F:R4	#20	7	5
ENW-1	#5			5	5
ESV-2	#7			4	
ESV-1a	#20			2	2
ESV-1c	#9			2	2

Table A6-4. Summary of estimated hydraulic and transport parameters for flow path KA2563A:R5–KI0023B:P6 during TRUE Block Scale Interference Tests during the Preliminary Characterisation Stage. From Andersson et al. (1998).

Parameter	Value	Source
Travel distance, L (m)	15.9 m	Geometry
Mean head difference, Δh (m)	54 m	HMS
Mean velocity, v (m/s)	$1.9 \cdot 10^{-4}$ m/s	PAREST
Mean travel time, t_m (h)	23.5 h	PAREST
First arrival, t_a (h)	10.8 h	Breakthrough curve
Dispersivity, D/v (m)	1.6 m	PAREST
Peclet number, Pe	10	
Fracture conductivity, K_{fr} (m/s)	$1.7 \cdot 10^{-4}$ m/s	Table A2 A3-3
Equivalent fracture aperture, b (m)	$1.9 \cdot 10^{-3}$ m	Table A2 A3-3
Flow porosity	$2.3 \cdot 10^{-3}$	Table A2 A3-3
Mass recovery, R (%)	44%	Breakthrough curve

TRUE Block Scale-Detailed characterization stage

Borehole	Interval (m)	#13 PT-1	#21 PT-2	#20 PT-3	Structure
KA2511A:T1	239-293		B	B	#10,11,18
KA2511A:T2	171-238		B	B	#19
KA2511A:T3	139-170		B	B	# ?
KA2511A:T4	111-138		B	B	#20
KA2511A:T5	103-110		B	B	#16
KA2511A:T6	96-102		B	B	#6
KA2511A:T7	65-95		B	B	# ?
KA2511A:T8	6-64		B	B	#4,7
KA2563A:S1	242-246	M	B	B	#19
KA2563A:S2	236-241		B	B	#19
KA2563A:S3	206-208	M	M	G	#13
KA2563A:S4	107-190	M	E	E	#20
KA2563A:S5	146-186	M	G	G	#6,7
KI0025F:R1	169-194		B	B	Z
KI0025F:R2	164-168		B	B	#19
KI0025F:R3	89-163		M	B	?
KI0025F:R4	86-88	M	G	G	# 20
KI0025F:R5	41-85		B	B	#6
KI0025F:R6	3.5-40		B	B	# 5
KI0023B:P1	113.7-200.7		B	B	#10
KI0023B:P2	111.25-112.7		B	B	#19
KI0023B:P3	87.20-110.25	E	E	G	?
KI0023B:P4	84.75-86.20	S	E	M	#13
KI0023B:P5	72.95-83.75	G	G	G	#18
KI0023B:P6	70.95-71.95	B	S	G	#21
KI0023B:P7	43.45-69.95	M	E	E	#6, 20
KI0023B:P8	41.45-42.45		B	M	#7
KI0023B:P9	4.5-40.45			B	#5
KI0025F02:P1	135.15-204		B	B	#?
KI0025F02:P2	100.25-134.15		B	B	#19
KI0025F02:P3	93.40-99.25	B	M	B	#13,21
KI0025F02:P4	78.25-92.4	B	B	B	#?
KI0025F02:P5	73.3-77.25	B	G	S	#20
KI0025F02:P6	64.0-72.3	B	M	M	#22
KI0025F02:P7	56.1-63.0	B	B	M	#?
KI0025F02:P8	51.7-55.1	M	G	G	#6
KI0025F02:P9	38.5-50.7		B	M	#7
KI0025F02:P10	3.4-37.5		B	B	#5
KA3510A:P1	122.02-150				#3,4,5,6,8
KA3510A:P2	114.02-121.02		B	M	#15
KA3510A:P3	4.52-113.02			B	#?
KA3548A01:P1	15-30			B	#?
KA3548A01:P2	10-14			B	#?
KA3573A:P1	18-40		B	B	#15
KA3573A:P2	4.5-17			B	#5
KA3600F:P1	22-50.1			B	#?
KA3600F:P2	4.5-21		B	B	#5, 7?

INDEX 1=sp/Q
EXCELLENT
HIGH
MEDIUM
LOW
NO RESPONS

INDEX 2=tr/R2
E=EXCELLENT
G=GOOD
M=MEDIUM
B=BAD

S=SOURCE

Figure A7-1. *Pressure response matrix) for pre-tests PT-1 to PT-3 during the Block Scale Detailed Characterization. From Andersson et al. (1999).*

Table A7-1. Summary of estimated hydraulic parameters and dominating flow regimes for the most significant response sections during the interference tests in PT-1 to PT-3 in the Detailed Characterization Stage in TRUE Block Scale. Leaky = pseudo-spherical, CHB = Apparent Constant head boundary. From Andersson et al. (1999).

Borehole Section	Structure #	T (m^2/s)	Storativity	T/S (m^2/s)	K'/b' (s^{-1})	Dom. Flow Geometry
PT-1						
KA2563A:S1	19	$3.7\cdot10^{-6}$ *	$1.8\cdot10^{-6}$ *	2.0 *	$5.7\cdot10^{-11}$ *	Leaky→CHB
KA2563A:S3	13	$4.5\cdot10^{-8}$	$8.6\cdot10^{-8}$	0.5	$1.2\cdot10^{-11}$	Leaky
KA2563A:S4	20	$6.9\cdot10^{-7}$	$1.3\cdot10^{-6}$	0.5	$1.1\cdot10^{-10}$	Leaky
KA2563A:S5	6, 7	$1.8\cdot10^{-6}$ *	$1.8\cdot10^{-6}$ *	1.0 *	$1.1\cdot10^{-10}$ *	Leaky→CHB
KI0025F:R4	20	$6.7\cdot10^{-7}$	$8.0\cdot10^{-7}$	0.8	$6.2\cdot10^{-11}$	Leaky
KI0023B:P4 (SINK)	13	$3.2\cdot10^{-7}$	–	–	–	Leaky→CHB
KI0023B:P5	18?	$2.4\cdot10^{-7}$ *	$3.4\cdot10^{-6}$ *	0.07 *	$6.9\cdot10^{-10}$ *	Irregular
KI0023B:P6	21	$6.9\cdot10^{-7}$ *	$3.6\cdot10^{-6}$ *	0.07 *	$2.5\cdot10^{-10}$ *	Leaky
KI0023B:P7	6, 20	$7.5\cdot10^{-7}$ *	$1.1\cdot10^{-6}$ *	0.7 *	$1.4\cdot10^{-10}$ *	Leaky
KI0025F02:P3	13, 21	$6.3\cdot10^{-6}$ *	$1.3\cdot10^{-5}$ *	0.5 *	$1.3\cdot10^{-9}$ *	Leaky→CHB
KI0025F02:P5	20	$7.3\cdot10^{-7}$	$2.0\cdot10^{-6}$	0.4	$2.1\cdot10^{-10}$	Leaky
KI0025F02:P6	22	$1.2\cdot10^{-6}$ *	$2.9\cdot10^{-6}$ *	0.4 *	$2.5\cdot10^{-10}$ *	Leaky
KI0025F02:P8	6	$1.5\cdot10^{-6}$ *	$1.6\cdot10^{-6}$ *	0.9 *	$1.6\cdot10^{-10}$ *	Leaky
PT-2						
KA2563A:S1	19	$2.4\cdot10^{-5}$ *	1.7·10–5 *	1.4 *	–	Radial→Tidal
KA2563A:S3	13	$6.0\cdot10^{-7}$	2.3·10–6	0.3	1.6·10–10	Leaky
KA2563A:S4	20	$7.4\cdot10^{-7}$	2.0·10–7	3.6	2.7·10–11	Leaky
KA2563A:S5	6, 7	$1.5\cdot10^{-6}$ *	8.9·10–7 *	1.7 *	1.8·10–10 *	Leaky
KI0025F:R4	20	$8.1\cdot10^{-7}$	1.1·10–7	7.5	8.7·10–12	Leaky
KI0023B:P4	13	$6.0\cdot10^{-7}$ *	3.8·10–6 *	0.2 *	2.1·10–10 *	Leaky
KI0023B:P5	18	$4.7\cdot10^{-7}$ *	1.3·10–6 *	0.4 *	1.2·10–10 *	Leaky
KI0023B:P6 (SINK)	21	$1.2\cdot10^{-6}$	–	–	–	Leaky→CHB
KI0023B:P7	6, 20	$7.9\cdot10^{-7}$ *	2.4·10–7 *	3.3 *	2.4·10–11 *	Leaky
KI0025F02:P3	13, 21	$1.0\cdot10^{-5}$ *	3.8·10–6 *	2.7 *	2.1·10–10 *	Leaky→CHB
KI0025F02:P5	20	$7.7\cdot10^{-7}$	1.9·10–7	4.0	2.9·10–11	Leaky
KI0025F02:P6	22	$1.1\cdot10^{-6}$	7.4·10–7	1.5	1.5·10–10	Leaky
KI0025F02:P7	?	$1.2\cdot10^{-6}$	3.6·10–6	0.3	4.4·10–10	Leaky
KI0025F02:P8	6	$1.4\cdot10^{-6}$	3.8·10–7	3.7	7.6·10–11	Leaky
PT-3						
KA2563A:S3	13	$6.0\cdot10^{-7}$	$9.5\cdot10^{-7}$	0.6	$4.8\cdot10^{-11}$	Leaky→NFB
KA2563A:S4	20	$7.0\cdot10^{-7}$	$7.4\cdot10^{-8}$	9.5	$8.3\cdot10^{-12}$	Leaky→NFB
KA2563A:S5	6, 7	$1.4\cdot10^{-6}$	$5.5\cdot10^{-7}$	2.6	$5.5\cdot10^{-11}$	Leaky→NFB
KI0025F:R4	20	$6.5\cdot10^{-7}$	$2.1\cdot10^{-7}$	3.1	$6.6\cdot10^{-12}$	Leaky→NFB
KI0023B:P4	13	$6.3\cdot10^{-7}$	$2.2\cdot10^{-6}$	0.3	$1.2\cdot10^{-10}$	Leaky→NFB
KI0023B:P5	18	$6.5\cdot10^{-7}$	$5.4\cdot10^{-7}$	1.2	$3.7\cdot10^{-11}$	Leaky→NFB
KI0023B:P6	21	$7.3\cdot10^{-7}$	$2.1\cdot10^{-7}$	3.4	$2.7\cdot10^{-11}$	Leaky→NFB
KI0023B:P7	6, 20	$7.8\cdot10^{-7}$	$1.2\cdot10^{-7}$	6.7	$9.8\cdot10^{-12}$	Leaky→NFB
KI0025F02:P3	13, 21	$1.0\cdot10^{-5}$ *	$1.3\cdot10^{-5}$ *	0.8 *	$1.5\cdot10^{-9}$ *	Leaky→NFB
KI0025F02:P5 (SINK)	20	$6.9\cdot10^{-7}$	–	–	–	Leaky→NFB
KI0025F02:P6	22	$1.0\cdot10^{-6}$ *	$2.2\cdot10^{-6}$ *	0.4 *	$2.0\cdot10^{-10}$ *	Leaky→NFB
KI0025F02:P7	?	$1.3\cdot10^{-6}$ *	$5.1\cdot10^{-6}$ *	0.2 *	$5.6\cdot10^{-10}$ *	Leaky→NFB
KI0025F02:P8	6	$1.5\cdot10^{-6}$ *	$5.8\cdot10^{-7}$ *	2.6 *	$6.1\cdot10^{-11}$ *	Leaky→NFB

* = Uncertain value, see discussion above.

Table A7-3. Results of the tracer dilution tests during PT-1 to PT-3 in the Detailed Characterization Stage in TRUE Block Scale. From Andersson et al. (1999).

Test	Test section	Structure	$Q_{natural}$ (mL/h)	Q_{pump} (mL/h)	ΔQ (mL/h)
PT-1	KA2563A:S3	13	1	16	+15
	KA2563A:S4	20	120	280	+160
	KI0023B:P6	21	36	40	+4
	KI0025F:R4	20	1	1	± 0
	KI0025F02:P3	13, 21	38	130	+92
	KI0025F02:P5	20	49	58	+9
PT-2	KA2563A:S3	13	14	11	–3
	KA2563A:S4	20	130	610	+480
	KA2563A:S1	19	115	400	+285
	KI0023B:P4	13	18	16	– 2
	KI0023B:P5	?	2	122	+120
	KI0023B:P7	6, 20	10,120	2,490	–7,630
	KI0025F:R4	20	3	1	–2
	KI0025F02:P3	13, 21	25	140	+115
	KI0025F02:P5	20	50	111	+61
	KI0025F02:P6	22	230	460	+230
	KI0025F02:P7	?	7	18	+11
	KI0025F02:P8	6	21	13	–8
PT-3	KA2563A:S3	13	?	15	?
	KA2563A:S4	20	80	950	+870
	KI0023B:P2	19	14	14	±0
	KI0023B:P4	13	?	?	?
	KI0023B:P5	?	(390)	(90)	–300
	KI0023B:P6	21	3	12	+9
	KI0023B:P7	6, 20	?	?	?
	KI0025F:R4	20	3	5	+2
	KI0025F02:P3	13, 21	?	250	+200?
	KI0025F02:P6	22	100	1,500	+1,400
	KI0025F02:P7	?	?	?	?
	KI0025F02:P8	6	33	39	+6

Table A7-4. Summary of estimated hydraulic and transport parameters for the flow paths KA2563A:S4–KI0023B:P6, KI0025F02:P3–KI0023B:P6 and KI0025F02:P6–KI0023B:P6 in PT-4. Values within brackets are standard errors in percent. From Andersson et al. (1999).

Parameter	KA2563A:S4–KI0023B:P6	KI0025F02:P3–KI0023B:P6	KI0025F02:P6–KI0023B:P6	Source
Travel distance, L (m)	16	36	18	Geometry
Mean head difference, Δh (m)	190	214.5	203.5	HMS
Mean velocity, v (m/s)	$3.9 \cdot 10^{-4}$ (1)	$7.1 \cdot 10^{-5}$ (0.5)	$4.5 \cdot 10^{-5}$ (0.5)	PAREST
Mean travel time, t_m (h)	11.5 (1)	140.3 (0.5)	98.3 (0.5)	PAREST
First arrival, t_a (h)	4	85	19	Breakthrough curve
Dispersivity, D/v (m)	5.3 (3.6)	2.9 (4.1)	5.0 (1)	PAREST
Peclet number, Pe	3.0	12.6	3.6	PAREST
Fracture conductivity, K_{fr} (m/s)	$9.8 \cdot 10^{-5}$	$4.1 \cdot 10^{-5}$	$1.4 \cdot 10^{-5}$	Table A3-3
Equivalent fracture aperture, b (m)	$2.2 \cdot 10^{-3}$	$5.2 \cdot 10^{-3}$	$1.4 \cdot 10^{-2}$	Table A3-3
Flow porosity (1 m thickness)	$1.1 \cdot 10^{-3}$	$2.7 \cdot 10^{-3}$	$8.0 \cdot 10^{-3}$	Table A3-3
Mass recovery, R (%)	51	75	80	Breakthrough curve

Appendix 8

TRUE Block Scale-Tracer test stage

Sink in Structure		#20	#21	#20	#21	
Borehole	Interval (m)	A-1	A-2	A-3	A-4	Structure
KA2511A:T1	239-293	B		B	B	#10,11,18
KA2511A:T2	171-238	B		B	B	#19
KA2511A:T3	139-170	B		B	B	# ?
KA2511A:T4	111-138	B		B	B	#20
KA2511A:T5	103-110	B		B	B	#16
KA2511A:T6	96-102	B		B	B	#6
KA2511A:T7	65-95	B		B	B	# ?
KA2511A:T8	6-64	B		B	B	#4,7
KA2563A:S1	242-246	B		B	B	#19
KA2563A:S2	236-241	B		B	B	#19
KA2563A:S3	206-208	M	B	G	M	#13
KA2563A:S4	187-190	E	G	E	G	#20
KA2563A:S5	146-186	G	M	G	G	#6,7
KI0025F:R1	169-194			B	B	Z
KI0025F:R2	164-168	B		B	B	#19
KI0025F:R3	89-163	B		B	B	?
KI0025F:R4	86-88	G	M	G	E	#20,22
KI0025F:R5	41-85	B		B	B	#7
KI0025F:R6	3.5-40	B			B	# 5
KI0023B:P1	113.7-200.7				B	#10
KI0023B:P2	111.25-112.7	B		B	B	#19
KI0023B:P3	87.20-110.25	Uncertain				?
KI0023B:P4	84.75-86.20	B	B	M	B	#13
KI0023B:P5	72.95-83.75	G	B	G	E	#18
KI0023B:P6	70.95-71.95	G	M	G	S	#21
KI0023B:P7	43.45-69.95	G	G	E	E	#6, 20
KI0023B:P8	41.45-42.45	B		B	B	#7
KI0023B:P9	4.5-40.45	B			B	#5
KI0025F02:P1	135.15-204				B	#?
KI0025F02:P2	100.25-134.15	B			B	#19
KI0025F02:P3	93.40-99.25	B	B	B	M	#13,21
KI0025F02:P4	78.25-92.4	Tight				#?
KI0025F02:P5	73.3-77.25	G	B	S	G	#20
KI0025F02:P6	64.0-72.3	M	B	M	M	#22
KI0025F02:P7	56.1-63.0	B	B	M	B	#23
KI0025F02:P8	51.7-55.1	G	M	G	G	#6
KI0025F02:P9	38.5-50.7	B		B	B	#7
KI0025F02:P10	3.4-37.5	B			B	#5
KI0025F03:P1	101.0-141.7	B		B	B	#19
KI0025F03:P2	93.5-100.0	B		B	B	?
KI0025F03:P3	89.0-92.5	B	B	B	B	#13
KI0025F03:P4	85.0-88.0	M	S	M	G	#21
KI0025F03:P5	66.5-74.0	S	B	E	G	#20
KI0025F03:P6	59.5-65.5	B	B	M	M	#22
KI0025F03:P7	55.0-58.5	M	B	M	M	#23
KI0025F03:P8	51.5-54.0	G	M	G	G	#6
KI0025F03:P9	3.5-50.5	B		B	B	#5, 7
KA3510A:P1	122.02-150					#?
KA3510A:P2	114.02-121.02	B		B	B	#15
KA3510A:P3	4.52-113.02	B			B	#3,4,5,6,8
KA3548A01:P1	15-30				B	#?
KA3548A01:P2	10-14				B	#?
KA3573A:P1	18-40				B	#15
KA3573A:P2	4.5-17				B	#5
KA3600F:P1	22-50.1	B		B	B	#?
KA3600F:P2	4.5-21	B		B	B	#5, 7?

INDEX 1=sp/Q
EXCELLENT
HIGH
MEDIUM
LOW
NO RESPONSE

INDEX 2=tr/R2
E=EXCELLENT
G=GOOD
M=MEDIUM
B=BAD

S=SINK

Figure A8-1. *Pressure response matrix for tests A-1 to A-4 in the Tracer Test Stage of TRUE Block Scale. From Andersson et al. (2000).*

Table A8-1. Summary of estimated hydraulic parameters and dominating flow regimes from the most significant response sections during interference tests A-1 to A-4 in the Tracer Test Stage of TRUE Block Scale. S = Sink, Rad = Radial, Leaky = pseudo-spherical, SS = steady-state flow. From Andersson et al. (2000).

Test #	Observation borehole section	Structure #	T (m^2/s)	S	T/S (m^2/s)	K'/b' (s^{-1})	Dom. flow regime
A-1	KA2563A:S4	20	$7.6\cdot10^{-7}$	$9.6\cdot10^{-8}$	8.0	$9.1\cdot10^{-12}$	Leaky→SS
	KI0025F:R4	20	$7.5\cdot10^{-7}$	$9.1\cdot10^{-8}$	8.2	$6.9\cdot10^{-12}$	Leaky→SS
	KI0023B:P5	18	$6.8\cdot10^{-7}$	$8.2\cdot10^{-7}$	0.8	$6.9\cdot10^{-11}$	Leaky→SS
	KI0023B:P6	21	$7.6\cdot10^{-7}$	$3.8\cdot10^{-7}$	2.0	$5.2\cdot10^{-11}$	Leaky→SS
	KI0023B:P7	6, 20	$8.6\cdot10^{-7}$	$1.5\cdot10^{-7}$	5.7	$1.4\cdot10^{-11}$	Leaky→SS
	KI0025F02:P5	20	$7.6\cdot10^{-7}$	$3.6\cdot10^{-7}$	2.1	$4.0\cdot10^{-11}$	Leaky→SS
	KI0025F03:P5 (S)	20	$6.4\cdot10^{-7}$	–	–	–	Leaky→SS
A-2	KA2563A:S3	13	$2.1\cdot10^{-7}$	$4.1\cdot10^{-7}$	0.5	$2.6\cdot10^{-11}$	Leaky→SS
	KA2563A:S4	20	$7.4\cdot10^{-7}$	$4.6\cdot10^{-7}$	1.6	$1.2\cdot10^{-11}$	Leaky→SS
	KI0025F:R4	20	$5.2\cdot10^{-7}$	$8.6\cdot10^{-7}$	0.6	$2.8\cdot10^{-11}$	Leaky→SS
	KI0023B:P4	13	$2.0\cdot10^{-7}$	$8.2\cdot10^{-7}$	0.2	$3.9\cdot10^{-11}$	Leaky→SS
	KI0023B:P6	21	$7.3\cdot10^{-7}$	$1.1\cdot10^{-6}$	0.7	$1.3\cdot10^{-11}$	Leaky→SS
	KI0023B:P7	6, 20	$7.8\cdot10^{-7}$	$5.2\cdot10^{-7}$	1.5	$1.1\cdot10^{-11}$	Leaky→SS
	KI0025F03:P4 (S)	21	$3.0\cdot10^{-8}$	–	–	–	Leaky→SS
A-3	KA2563A:S4	20	$7.6\cdot10^{-7}$	$7.2\cdot10^{-8}$	10.6	$8.9\cdot10^{-12}$	Leaky→SS
	KI0025F:R4	20	$6.9\cdot10^{-7}$	$2.2\cdot10^{-7}$	3.1	$1.3\cdot10^{-11}$	Leaky→SS
	KI0023B:P6	21	$7.3\cdot10^{-7}$	$2.4\cdot10^{-7}$	3.0	$1.5\cdot10^{-11}$	Leaky→SS
	KI0023B:P7	6, 20	$8.1\cdot10^{-7}$	$1.3\cdot10^{-7}$	6.4	$1.3\cdot10^{-11}$	Leaky→SS
	KI0025F02:P5 (S)	20	$7.5\cdot10^{-7}$	–	–	–	Leaky→SS
	KI0025F03:P5	20	$7.4\cdot10^{-7}$	$3.7\cdot10^{-7}$	2.0	$2.2\cdot10^{-11}$	Leaky→SS
A-4	KI0023B:P6 (S)	21	$5.4\cdot10^{-7}$	–	–	–	Leaky→SS
	KI0025F03:P4	21	$7.6\cdot10^{-7}$	$8.3\cdot10^{-7}$	0.9	$3.3\cdot10^{-11}$	Leaky→SS
	KI0025F03:P5	20	$7.9\cdot10^{-7}$	$4.1\cdot10^{-7}$	1.9	$5.2\cdot10^{-11}$	Leaky→SS
	KI0025F03:P8	6	$1.5\cdot10^{-6}$	$8.4\cdot10^{-7}$	1.8	$5.7\cdot10^{-10}$	Leaky→SS

Table A8-2. Results of the tracer dilution tests during test A-1 to A-4 in the Tracer Test Stage of TRUE Block Scale. Q_{pump1} is for the 5-hour period of flowing with reduced flow rate, Q_{pump2} is for the period of flowing with maximum flow rate. After Andersson et al. (2000).

Test #	Test section	Structure	$Q_{natural}$ (mL/h)	Q_{pump1} (mL/h)	Q_{pump2} (mL/h)	ΔQ (mL/h)
A-1	KA2563A:S1	19	73		48	–25
	KA2563A:S3	13	4		9	+5
	KA2563A:S4	20	199	511	604	+405
	KI0025F:R4	20, 22	6		9	+3
	KI0023B:P2	19	20		19	–1
	KI0023B:P4	13	2		4	+2
	KI0023B:P5	18	5		10	+5
	KI0023B:P6	21	21		19	–2
	KI0023B:P7	6, 20	11,070		420	–10,650
	KI0025F02:P3	13, 21	46		143	+97
	KI0025F02:P5	20	22		625	+603
	KI0025F02:P6	22	270		728	+458
	KI0025F02:P7	23	44		21	–23
	KI0025F02:P8	6	6		22	+16
	KI0025F03:P3	13	17		16	–1
	KI0025F03:P4	21	16		15	–1
	KI0025F03:P6	22	64	307	378	+314
	KI0025F03:P7	23	27		32	+5
A-2	KA2563A:S1	19	21		87	+66
	KA2563A:S3	13	5		9	+4
	KA2563A:S4	20	201		100	–101
	KI0025F:R4	20, 22	2		3	+1
	KI0023B:P2	19	16		13	–3
	KI0023B:P4	13	5		8	+3
	KI0023B:P5	18	5		120	+115
	KI0023B:P6	21	4		13	+9
	KI0023B:P7	6, 20	11,030		677	–10,353
	KI0025F02:P3	13, 21	25		562	+537
	KI0025F02:P5	20	11		21	+10
	KI0025F02:P6	22	138		485	+347
	KI0025F02:P7	23	10		10	± 0
	KI0025F02:P8	6	8		9	+1
	KI0025F03:P3	13	9		15	+6
	KI0025F03:P5	20	0		5	+5
	KI0025F03:P6	22	78	162	196	+118
	KI0025F03:P7	23	22		23	+1
A-3	KA2563A:S3	13	10		0	–10
	KI0025F:R4	20, 22	3		6	+3
	KI0023B:P4	13	4		6	+2
	KI0023B:P5	18	5		11	+6
	KI0023B:P7	6, 20	11,550		350	–11,200
	KI0025F02:P3	13, 21	30		205	+175
	KI0025F02:P7	23	9		9	± 0
	KI0025F03:P3	13	0		6	+6
	KI0025F03:P4	21	6		14	+8
	KI0025F03:P5	20	5		36	+31
	KI0025F03:P6	22	75		685	+610
	KI0025F03:P7	23	25		28	+3
A-4	KI0025F03:P3	13	4		10	+6
	KI0025F03:P4	21	1		10	+9
	KI0025F03:P5	20	2		35	+33
	KI0025F03:P6	22	90		410	+320
	KI0025F03:P7	23	32		39	+7

Table A8-3. Summary of estimated hydraulic and transport parameters for the flow paths in test A-4 in the Tracer Test Stage of TRUE Block Scale using KI0023B:P6 as sink. Values within brackets are standard errors in percent. After Andersson et al. (2000).

Parameter	KI0025F03:P5–KI0023B:P6	KI0025F03:P6–KI0023B:P6	Source
Distance along fractures (m)	16	73	Geometry
Euclidean distance, L (m)	14	15	Geometry
Mean head difference, Δh (m)	177.4	193.7	HMS
Injection flow rate (mL/h)	31	341	Injection curve
Mean velocity, v (m/s)	$5.01 \cdot 10^{-5}$ (1)	$3.83 \cdot 10^{-5}$ (1)	PAREST
Mean travel time, t_m (h)	77.7 (1)	108.8 (1)	PAREST
First arrival, t_a (h)	20	48	Breakthrough curve
Dispersivity, D/v (m)	3.1 (2)	1.2 (3)	PAREST
Peclet number, Pe	4.5	12.6	PAREST
Fracture conductivity, K_{fr} (m/s)	$1.2 \cdot 10^{-5}$	$8.9 \cdot 10^{-6}$	Table A2 A3-3
Equivalent fracture aperture, b (m)	$1.7 \cdot 10^{-2}$	$2.1 \cdot 10^{-2}$	Table A2 A3-3
Flow porosity (1 m thickness)	$9.4 \cdot 10^{-3}$	$12 \cdot 10^{-3}$	Table A2 A3-3
Mass recovery, R (%)	> 31	> 44 (> 34*)	Breakthrough curve

* = Recovery calculated by weighing.

Table A8-4. Summary of estimated hydraulic and transport parameters for the flow paths in test A-5 in the Tracer Test Stage of TRUE Block Scale using KI0025F03:P5 as sink. Values within brackets are standard errors in percent. After Andersson et al. (2000).

Parameter	25F02:P5–25F03:P5	25F02:P6–25F03:P5	25F03:P6–25F03:P5	2563A:S4–25F03:P5	Source
Distance along fractures (m)	9	57	65	27	Geometry
Euclidean distance, L (m)	11	12	12	29	Geometry
Mean head difference, Δh (m)	214.4	227.9	236.8	217.5	HMS
Inj. flow rate (mL/h)	536	1,090	327	570	Injection curve
Mean velocity, v (m/s)	$2.13 \cdot 10^{-3}$ (1)	$7.91 \cdot 10^{-5}$ (1)	$2.64 \cdot 10^{-5}$ (1)	$3.32 \cdot 10^{-4}$ (1)	PAREST
Mean travel time, t_m (h)	1.4 (1)	42.2 (1)	126.4 (1)	24.2 (1)	PAREST
First arrival, t_a (h)	1	8	60	10	Breakthrough curve
Dispersivity, D/v (m)	0.63 (11)	4.4 (1)	0.95 (4)	3.7 (4)	PAREST
Peclet number, Pe	17.5	2.7	12.7	7.8	PAREST
Fracture conductivity, K_{fr} (m/s)	$3.1 \cdot 10^{-4}$	$1.2 \cdot 10^{-5}$	$3.8 \cdot 10^{-6}$	$1.5 \cdot 10^{-4}$	Table A2 A3-3
Equivalent fracture aperture, b (m)	$5.9 \cdot 10^{-4}$	$1.5 \cdot 10^{-2}$	$4.4 \cdot 10^{-2}$	$1.4 \cdot 10^{-3}$	Table A2 A3-3
Flow porosity (7.5 m thickness)	$6.9 \cdot 10^{-5}$	$1.8 \cdot 10^{-3}$	$5.5 \cdot 10^{-3}$	$1.5 \cdot 10^{-4}$	Table A2 A3-3
Mass recovery, R (%)	125 (97*)	> 40 (> 27*)	84 (57*)	64 (47*)	Breakthrough curve

* = Recovery calculated by weighing.

Appendix 9

TRUE Block Scale-Continuation

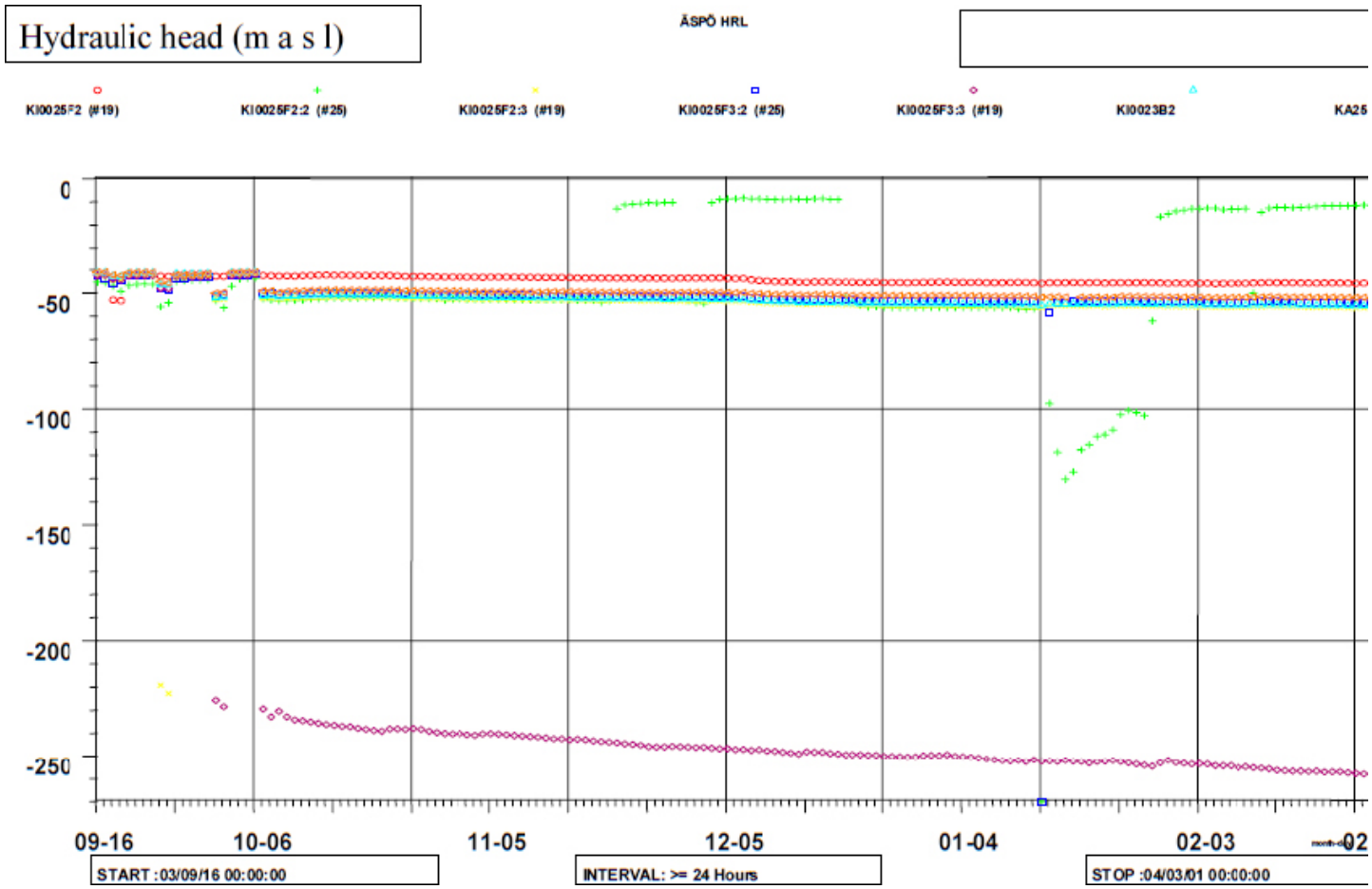

Figure A9-1. *Hydraulic head in Structures #19and #25 during TRUE Block Scale Continuation pre-tests CPT-1–CPT-4. From Andersson et al. (2004).*

Sink in Structure		# 19	# 19	# 19	
Borehole	Interval (m)	CPT-1	CPT-2	CPT-3	Structure
KA2511A:T1	239-293	B			# 10,11,18
KA2511A:T2	171-238	B			# 19
KA2511A:T3	139-170	B			# ?
KA2511A:T4	111-138	B			# 20
KA2511A:T5	103-110	B			# 16
KA2511A:T6	96-102	B			# 6
KA2511A:T7	65-95	B			# ?
KA2511A:T8	6-64	B			# 4, 7
KA2563A:S1	242-246	G	G	G	# 19
KA2563A:S2	236-241	G	G	G	# 19
KA2563A:S3	206-208	B	B	B	# 13
KA2563A:S4	187-190	B		B	# 20
KA2563A:S5	146-186	B			# 6, 7
KI0025F:R1	170.5-193.66	B	M	M	Z
KI0025F:R2	165.5-169.5	S	G	G	# 19
KI0025F:R3	90.5-164.5	E	B	M	?
KI0025F:R4	87.5-89.5	B	B	B	# 20, 22
KI0025F:R5	42.5-86.5	B			# 6, 7
KI0025F:R6	5-41.5	B			# 5
KI0023B:P1	113.7-200.7	B			# 10
KI0023B:P2	111.25-112.7	G	E	E	# 19
KI0023B:P3	87.20-110.25	B	G	G	?
KI0023B:P4	84.75-86.20	B	B	B	# 13
KI0023B:P5	72.95-83.75	B	B	B	# 18
KI0023B:P6	70.95-71.95	B	B	B	# 21
KI0023B:P7	43.45-69.95	B	B	B	# 6, 20
KI0023B:P8	41.45-42.45	B			# 7
KI0023B:P9	4.6-40.45	B			# 5
KI0025F02:R1	140.05-204.18	B		B	# ?
KI0025F02:R2	135.1-139.05	B	B	B	# 25
KI0025F02:R3	129.2-134.1	G	S	E	# 19
KI0025F02:R4	100.25-128.2	Tight			
KI0025F02:R5	93.35-99.25	B	B	B	# 13, 21
KI0025F02:R6	78.25-92.35	Tight			
KI0025F02:R7	73.3-77.25	B		B	# 20
KI0025F02:R8	64.0-72.3	B	B	B	# 22
KI0025F02:R9	56.1-63.0			B	# 23
KI0025F02:R10	3.4-55.1	B			# 5, 6, 7
KI0025F03:R1	135.03-141.72	B	M	G	# ?
KI0025F03:R2	129.03-134.03	B		B	# 25
KI0025F03:R3	123.03-128.03	G	G	S	# 19
KI0025F03:R4	93.53-122.03	B		B	# ?
KI0025F03:R5	89.03-92.53	B	B	B	# 13
KI0025F03:R6	75.03-88.03	B		B	# 21
KI0025F03:R7	66.53-74.03	B		B	# 20
KI0025F03:R8	59.53-65.53	B	B	B	# 22
KI0025F03:R9	55.03-58.53				# 23
KA3510A:R1	125-150.06				# ?
KA3510A:R2	110-124	B			# 15
KA3510A:R3	75-109	B			# ?
KA3510A:R4	51-74	B			# 6, 8
KA3510A:R5	4.5-50	B			# 3, 4, 5

INDEX 1=sp/Q
EXCELLENT
HIGH
MEDIUM
LOW
NO RESPONSE

INDEX 2=tr/R2
E=EXCELLENT
G=GOOD
M=MEDIUM
B=BAD

S=SINK

Figure A9-2. *Pressure response matrix for pre-tests CPT-1 through CPT-3 during TRUE Block Scale Continuation. From Andersson et al. (2004).*

Table A9-1. Results of the tracer dilution tests during CPT-1 to CPT-3. Figures in italics in CPT-2 are somewhat uncertain due to disturbed sampling caused by a power failure. After Andersson et al. (2004).

Test section	Structure #	Section volume (mL/h)	Qnatural (mL/h)	Qstressed (mL/h)	ΔQ (mL/h)
CPT-1. Sink: KI0025F:R2 (Structure #19)					
KA2563A:S1	19	8,814	17	12	–5
KI0023B:P2	19	3,621	26	30	+4
KI0025F:R2	19	7,210		**SINK**	
KI0025F02:R2	25	7,141	40	44	+4
KI0025F02:R3	19	7,747	11	9	–2
KI0025F02:R5	13, 21	7,856	9	8	–1
KI0025F03:R2	25	6,519	23	10	–13
KI0025F03:R3	19	6,343	3	61	+58
CPT-2. Sink: KI0025F02:R3 (Structure #19)					
KA2563A:S1	19	8,814	5	14	+9
KI0023B:P2	19	3,621	23	33	+10
KI0025F:R2	19	7,210	22	69	+47
KI0025F02:R2	25	7,141	35	51	+16
KI0025F02:R3	19	7,747		**SINK**	
KI0025F02:R5	13, 21	7,856	18	18	±0
KI0025F03:R2	25	6,519	7	8	+1
KI0025F03:R3	19	6,343	3	423	+420
KI0025F03:R5	13	4,912	9	2	–7
CPT-3. Sink: KI0025F03:R3 (Structure #19)					
KA2563A:S1	19	8,814	4	27	+23
KI0023B:P2	19	3,621	18	31	+13
KI0025F:R2	19	7,210	22	85	+63
KI0025F02:R2	25	7,141	42	42	± 0
KI0025F02:R3	19	7,747	18	76	+58
KI0025F02:R5	13, 21	7,856	30	18	–12
KI0025F03:R2	25	6,519	6	9	+3
KI0025F03:R3	19	6,343		**SINK**	
KI0025F03:R5	13	4,912	4	6	+2

Table A9-2. Summary of estimated parameter values from pre-tests CPT-4a to CPT-4c (estimation standard errors in percent of estimated value are given in parentheses). From Andersson et al. (2004).

	Model	AD-1			AD-2						MD			
		Parameter			Parameter						Parameter			
#	Tracer	t_0 (hour)	a_L (m)	pf	t_{01} (hour)	a_{L1} (m)	pf_1	t_{02} (hour)	a_{L2} (m)	Pf_2	t_0 (hour)	a_L (m)	Pf	A ($s^{½}$)
4a	RdWT	148 (1.1)	23.3 (3.9)	$2.04 \cdot 10^{-4}$ (1.1)	97.6 (1.2)	5.59 (27)	$8.64 \cdot 10^{-5}$ (42)	234 (25)	22.6 (73)	$1.35 \cdot 10^{-4}$ (28)	80.9 (4.9)	4.73 (11)	$2.79 \cdot 10^{-4}$ (1.2)	448 (7.8)
	AminoG	13.4 (1.6)	13.0 (7.0)	$2.69 \cdot 10^{-4}$ (0.8)	–	–	–	–	–	–	15.3 (12)	6.57 (18)	$2.95 \cdot 10^{-4}$ (1.7)	511 (28.2)
	Uranine	38.4 (1.8)	3.78 (10)	$1.25 \cdot 10^{-4}$ (1.6)	35.3 (1.1)	2.50 (6.2)	$1.14 \cdot 10^{-4}$ (1.4)	43.0 (15)	4.63 (41)	$4.52 \cdot 10^{-5}$ (25)	19.9 (3.6)	0.11 (73)	$1.48 \cdot 10^{-4}$ (1.2)	261 (7.2)
4b	RdWT	751 (1.0)	2.24 (6.7)	$7.12 \cdot 10^{-2}$ (2.8)	–	–	–	–	–	–	–	–	–	–
	AminoG	178 (0.7)	6.41 (2.7)	$4.39 \cdot 10^{-4}$ (0.8)	–	–	–	–	–	–	174 (6.7)	3.92 (11)	$5.20 \cdot 10^{-4}$ (2.7)	1,682 (23)
	Uranine	361 (1.3)	8.45 (6.8)	$1.01 \cdot 10^{-4}$ (1.5)	736 (38)	60.7 (30)	$7.78 \cdot 10^{-5}$ (21)	334 (1.4)	3.11 (18)	$5.70 \cdot 10^{-5}$ (13)	279 (8.8)	3.47 (22)	$1.32 \cdot 10^{-4}$ (4.1)	1,372 (23)
4c	RdWT	29.5 (1.2)	3.83 (6.2)	$8.47 \cdot 10^{-4}$ (1.8)	25.9 (2.4)	2.22 (9.9)	$6.32 \cdot 10^{-4}$ (20)	78.4 (34)	9.24 (121)	$3.78 \cdot 10^{-4}$ (38)	17.9 (3.6)	0.89 (12)	$1.22 \cdot 10^{-3}$ (1.4)	234 (7.1)
	AminoG	209 (0.5)	1.81 (2.4)	$5.74 \cdot 10^{-4}$ (1.1)	190 (1.5)	1.27 (3.3)	$4.56 \cdot 10^{-4}$ (4.3)	437 (3.6)	1.42 (29)	$1.73 \cdot 10^{-4}$ (14)	142 (1.5)	0.80 (4.0)	$7.77 \cdot 10^{-4}$ (4.7)	1,032 (4.7)
	Uranine	11.1 (2.9)	5.29 (15)	$1.44 \cdot 10^{-3}$ (2.3)	10.2 (4.8)	2.94 (29)	$1.10 \cdot 10^{-3}$ (11)	46.7 (105)	111 (185)	$9.26 \cdot 10^{-4}$ (40)	10.0 (14)	2.71 (31)	$1.64 \cdot 10^{-3}$ (3.6)	397 (41)

Appendix 10

Additional hydraulic measurements

Table A10-1. Transmissivity data for the deterministic structures.

Structure	KI0025F			KI0025F02			KI0025F03			KI0023B			KA2563A		
	PBU	PTT	PTSS	PBU	PTT	PTSS	PBU	PTT	PTSS	PBU	PTT	PTSS	PBU	PTT	PTSS
7	1.3E-05	3.7E-05	6.2E-08	1.7E-06	1.8E-06	>1.6E-07	x	x	6.3E-08	1.8E-05	1.6E-05	x	x	2.1E-05	x
6	x	x	x	1.5E-08	1.5E-08	1.1E-08	6.8E-08	1.1E-07	2.1E-07	4.0E-07	3.3E-08	1.7E-06	x	x	2.2E-08
24	x	x	x	x	x	x	x	x	3.0E-08	x	x	x	x	x	x
23	x	x	x	5.3E-09	1.1E-08	5.4E-09	1.5E-08	1.3E-08	2.0E-08	x	x	x	x	x	x
22				2.6E-07	3.3E-07	>1.0E-07	8.3E-09	x	3.5E-08	x	x	x	x	x	x
20	5.1E-07	8.5E-07	4.4E-08	6.5E-07	1.1E-06	>1.2E-07	6.1E-07	6.1E-07	7.5E-08	9.6E-07	1.4E-07	8.9E-08	x	8.7E-07	>1.9E-07
21	x	x	x	9.6E-09	5.0E-08	2.8E-08	3.9E-09	9.6E-09	2.1E-08	8.1E-07	6.9E-07	1.5E-07	x	x	6.8E-09
13	x	x	x	1.5E-09	4.6E-09	3.9E-09	3.8E-08	4.4E-08	6.7E-08	5.8E-08	9.8E-08	3.3E-08	x	4.5E-08	2.7E-08
19	2.9E-05	x	8.9E-07	1.7E-06	1.1E-07	>1.1E-07	1.3E-06	x	1.2E-07	3.9E-06	1.2E-06	1.2E-07	x	x	9.4E-08
10	x	x	x	5.3E-08	5.3E-08	3.3E-08	x	x	x	4.5E-06	2.7E-06	2.2E-07	x	x	x

PBU = Pressure Build-Up tests (transient evaluation, Cooper-Jacob)
PTT = Pump Test (Transient evaluation, Cooper-Jacob)
PTSS= Pump Test (packer flow log or Posiva flow log) (Steady State evaluation, Moye)